Synthesis of Heterogeneous Catalysts for the Transformation of Glycerol

Thesis Submitted in fulfillment of the requirement of the degree of

Doctor of Philosophy
By

Avneet Kaur
(Regn. No. 901409013)

Under the supervision of
Dr. Amjad Ali
Professor

SCHOOL OF CHEMISTRY AND BIOCHEMISTRY
Thapar Institute of Engineering and Technology
Patiala-147004, Punjab
India
July, 2021

DEDICATED

TO MY

DAUGHTER

GURNAAZ

ACKNOWLEDGEMENTS

*I would express my deepest gratitude to the **ALMIGHTY** for blessing me with good health throughout my research work.*

*I would express my deepest appreciation and respect to my supervisor **Dr. Amjad Ali**, for providing me this opportunity to work under his guidance. I acknowledge the freedom provided to me for planning and executing my research independently. His receptive attitude always inspires me to thrive for more. It is a privilege to get a chance to work and learn from him.*

*I am grateful to the Director, Thapar Institute of Engineering and Technology; Dean (Research and Sponsored Projects), and Head of School of Chemistry and Biochemistry for granting me the opportunity to undertake my doctoral research. I extend my thankfulness to my doctoral committee **Dr. Manmohan Chhibber, Dr. Ranjana Prakash,** and **Dr. H. Bhunia** for their healthy discussions, motivations, and constructive criticism. I extend my thanks to **Mr. Mukesh Aggarwal**, Lab In-charge SAI labs for his amiable attitude while operating the NMR facility. My sincere thanks to **Mr. Chander Thakur** and office staff **Mr. Mayank Sharma,** for their cooperation.*

I am grateful to the Department of Science and Technology (DST), New Delhi for providing me the financial support in the form of INSPIRE Fellowship throughout my Ph.D. work.

*A special thanks to my fellows **Himmat Singh, KM Abida, Sidharth Sharma** for their assistance in my experimental work and research discussions. This journey would have been different without my colleagues and friends. I am grateful to **Dr. Gurjit Kaur**, Dr. Ramandeep Kaur, Dr. Manpreet Kaur, Priyanka Gautam, Meenakshi Bhudhiraja, Priya, Param, and Pooja for their cheerful and motivating*

attitude. I extend my thanks to all the teaching and non-teaching staff members of the department for their generous help.

I am extremely grateful to a special person, my husband ***Mr. Maninder Singh*** *for his support and encouragement throughout my research journey. I will always be indebted to my both families for their love, patience, and support that made the completion of the degree possible.*

I am equally thankful to all the persons who could not be mentioned here but knowingly unknowingly helped me in the completion of my thesis.

Avneet Kaur

Certificate

This is to certify that thesis entitled "**Synthesis of Heterogeneous Catalysts for the Transformation of Glycerol**", being submitted by **Avneet Kaur**, School of Chemistry and Biochemistry, Thapar Institute of Engineering and Technology, Patiala for the award of degree Doctor of Philosophy, is a record bonafide of the research work carried out by her. Ms. Avneet Kaur has worked under my guidance and supervision and has fulfilled the requirements for the submission of the thesis, which to my knowledge has reached the requisite standard.

The results embodied in the thesis have not been submitted in a part or full to any other University or Institute for the award of any degree or diploma.

(Supervisor)

Dr. Amjad Ali

Professor
School of Chemistry and Biochemistry
Thapar Institute of Engineering and Technology, Patiala
Punjab (INDIA)

(Head)

Dr. Satnam Singh

22/4/22

Professor and Head
School of Chemistry and Biochemistry
Thapar Institute of Engineering and Technology, Patiala
Punjab (INDIA)

Candidate's Declaration

I, hereby declare that the work presented in the thesis entitled "**Synthesis of Heterogeneous Catalysts for the Transformation of Glycerol**" in the fulfillment of the requirement for the award of the degree of Philosophy, School of Chemistry and Biochemistry, Thapar Institute of Engineering and Technology, Patiala is an authentic record of my work carried out under the supervision of **Dr. Amjad Ali**, Professor, School of Chemistry and Biochemistry, Thapar Institute of Engineering and Technology, Patiala, India. The matter embodied in the thesis has not been submitted in part or full to any other University or Institute for the award of any degree in India or abroad.

Avneet Kaur

TABLE OF CONTENTS

LIST OF ABBREVIATIONS

Abbreviation	*Description*
GL	Glycerol
GLC	Glycerol Carbonate
DMC	Dimethyl Carbonate
DEC	Diethyl Carbonate
BD	Biodiesel
DMC-BioD	Dimethyl carbonate-Biodiesel
GLD	Glycidol
GDC	Glycerol Dicarbonate
DMF	Dimethylformamide
XRD	X-Ray Diffraction
XPS	X-Ray Photoelectron Spectroscopy
FT-IR	Fourier Transform Infra Red
SEM	Scanning Electron Microscopy
HRTEM	High Resolution Transmission Electron Microscopy
SAED	Selected Area Electron Diffraction
EDS	Energy Dispersive X-ray Spectroscopy
BET	Brunauer-Emmett-Teller
BJH	Barret-Joyner-Halenda
CO_2-TPD	Carbon dioxide Temperature Programmed Desorption
FT-NMR	Fourier Transform-Nuclear Magnetic Resonance
^{1}H-NMR	Proton Nuclear Magnetic Resonance
qHNMR	Quantitative Proton Nuclear Magnetic Resonance
GC	Gas Chromatography
HPLC	High Performance Liquid Chromatography
MP-AES	Microwave plasma-Atomic Emission Spectroscopy
CHNS	Carbon Hydrogen Nitrogen Sulphur
TMS	Trimethyl Silane
TOF	Turn Over Frequency
JCPDS	Joint Committee for Powder Diffraction Standards
D_2O	Deuterium oxide

DMSO	Dimethylsulfoxide
$KMnO_4$	Potassium Permaganate
% C_{GLC}	Conversion of Glycerol Carbonate
% C_{GL}	Conversion of Glycerol
TLC	Thin Layer Chromatography
Ppm	Parts per million
m^2/g	Metre square per gram
cm^{-1}	Inverse centimetre
Mol	Mole
mmol/g	Millimole per gram
kJ mol^{-1}	Kilo joule per mole
kJ mol^{-1} K^{-1}	Kilo Joule per mole per kelvin
$JK^{-1}mol^{-1}$	Joule per Kelvin per mole
$M^{-1}s^{-1}$	Moles per litre per second
Js	Joule second
JK^{-1}	Joule per Kelvin
min^{-1}	Per minute
h^{-1}	Per hour
mL	Millilitre
µL	Microlitre
Mg	Milligram
Nm	Nanometre
Mm	Millimeter
MHz	MegaHertz
eV	Electron volt
wt %	Weight percent
v/v	Volume by volume
NR	Not reported
RI	Refractive Index
B.E	Binding Energy
SD	Standard Deviation

LIST OF SYMBOLS

Symbols	Description
$^{\circ}A$	Angstrom
A	Pre-exponential factor
C	Celsius
E_a	Activation energy
R	Gas constant
K	Rate constant
T	Temperature
$\Delta H^{\ddagger}$	Enthalpy of reaction
$\Delta S^{\ddagger}$	Entropy of reaction
$\Delta G^{\ddagger}$	Gibb's free energy
k_B	Boltzmann constant
H	Planck constant
f_m	Active sites
G	Gram
○	Degree
Λ	Wavelength
Min	Minute
H	Hour
S	Second
%	Percentage
Y	Yield
C	Conversion
S	Selectivity
d1	Relaxation delay
T1	Longest relaxation time
K	Kelvin
I	Integration

LIST OF FIGURES

LIST OF TABLES

LIST OF SCHEMES

ABSTRACT

In the present thesis, three different heterogeneous catalysts Li/ZrO_2, modified CaO, and K/ZIF-8, were prepared to transform glycerol, the side product of the biodiesel industry, into glycerol carbonate. Out of all the literature-reported pathways, the transesterification route of dimethyl carbonate with glycerol was adopted to carry out glycerol carbonate synthesis. All the catalysts were prepared by the simple wet impregnation method. The structural properties of the prepared catalysts were analyzed by XRD, FTIR, and XPS techniques. Catalysts morphology and their surface properties were studied via SEM, HRTEM, and BET techniques. The basicity of all the prepared catalysts was determined through the CO_2-TPD experiment.

Considering the merits of the quantitative ^{1}H-NMR technique, the same was applied for the first time to quantify glycerol carbonate. Two quantification equations were proposed based on the ^{1}H-NMR spectra obtained from the analysis of mixtures having varied molar ratios of glycerol and glycerol carbonate (GLC). The results obtained from both the quantification equations were in agreement with the actual molar ratios of the glycerol carbonate taken. Moreover, the results attained from the qHNMR technique were in line with that of the HPLC technique. Nevertheless, the quantification formula applied to the real sample provided promising results.

In view of the requirement of the basic catalyst for the transesterification reaction of dimethyl carbonate (DMC) with glycerol (GL), basic properties of the alkali and alkaline earth metals (Li, Na, K, Ca, and Mg) and thermal stability of the ZrO_2 were tuned together by the wet impregnation method forming metal impregnated ZrO_2 catalysts. The application of the prepared catalysts for the glycerol carbonate synthesis revealed that 100 % GLC selectivity was achieved with all the prepared catalysts; however, 20 wt% Li-loaded ZrO_2 catalysts provided better GLC yield (91 %). The better catalytic activity of 20-Li/ZrO_2 catalyst was attributed to the formation of a single active Li_2ZrO_3 phase which was dependent upon the calcination temperature and LiOH concentration employed for the catalyst preparation. A decline in the catalytic activity during reusability was observed owing to the structural changes but selectivity remained unchanged. Besides determining the catalytic activity, a kinetic study was also conducted, revealing that the transesterification reaction followed second-order kinetic equation.

To find out the solution to the active site poisoning of the CaO by atmospheric moisture, attempt was made to make its surface hydrophobic. Various organic modifiers (aliphatic and aromatic) were grafted over the CaO surface to restrain its moisture sensitivity. Besides imparting stability to the native CaO, the surface modification also increased the basic strength of the native catalyst. Besides providing a good glycerol conversion level (82 %), the benzyl bromide modified CaO catalyst was found to impart better moisture resistance up to 5 wt% H_2O content in the glycerol. Even though the catalytic activity of the modified CaO catalyst got reduced upon repeated use, but was better than native CaO in every catalytic cycle.

Further efforts were made to enhance the reusability and moisture resistibility of the catalyst without sacrificing its activity. For this purpose, the stable crystalline framework and hydrophobic properties of ZIF-8 were explored. The basicity of ZIF-8 was improved by loading KOH onto its surface following the wet impregnation method. Prepared K/ZIF-8 catalyst demonstrated high catalytic activity towards the transesterification reaction of DMC with GL (95 % glycerol conversion) and stability up to 3 consecutive reaction cycles.

Keywords: Glycerol Carbonate, Quantification, Transesterification, Moisture resistant, Quantitative proton nuclear magnetic resonance.

Introduction and Literature Review

Abstract

Glycerol is a prevalent molecule called 'Jacks Of All Trades' ascribed to its countless applications in the food industry, cosmetics, polymer, and pharmaceutics. It is obtained as a by-product of three distinct reactions of natural fats and oils: hydrolysis, saponification, and transesterification. In the recent past, the flourishing biodiesel industry has resulted in the accumulation of the by-product glycerol. This surplus glycerol, regarded as a waste in the biodiesel industry, has choked the glycerol market globally. In the era of a greener environment, the utilization of waste into valuable products is highly recommended. However, the crude glycerol obtained from the biodiesel industry being contaminated with methanol, left out catalyst, and other organic residues could not be consumed directly in the food and pharmaceutical industries. Another alternative is to derive non-food and fuel additives from this surplus glycerol. In this regard, glycerol carbonate has emerged as promising candidate offering services in the food, polymer, electrolytic, and pharmaceutical industries. Out of the three preparation routes, the base-catalyzed transesterification route employing glycerol and dimethyl carbonate as the reactant is preferred due to the mild reaction conditions, high yield, and product selectivity. Homogeneous catalysts are refrained due to their separation issues.

Among heterogeneous catalysts, alkali and alkaline-based mixed metal oxide, hydrotalcite, metal-organic framework, mesoporous, basic catalyst were employed for conducting the glycerol carbonate synthesis. Even though significant glycerol conversion is obtained, poor selectivity and stability of these catalysts are a matter of concern. Apart from deriving chemical intermediate from excess glycerol, another alternative is to develop fuel additives such as solketal. The acid-catalyzed reaction of glycerol with acetone resulted in the solketal formation. Heteropolyacids, zeolites, resins, and silica-supported catalysts are broadly applied acid catalysts for the acetalization reaction. Requirement of the hydrophobic catalyst, use of entrainer, poor solketal selectivity are few things that need to be resolved. In another approach, glycerol production could be avoided during the triglyceride transesterification by using dimethyl carbonate instead of methanol as transmethylating agent. However, few basic catalysts are utilized in this field and much more needed to be explored.

1.1 Introduction

Glycerol (1,2,3-propanetriol), commercially known as glycerin, is a versatile compound known to mankind so far. The Greek derived name glycerol is coined by the chemist Michel Eugene Chevreul [1] for this sweet flavored liquid explored during the reaction of natural oil with lead oxide [2]. This colorless, non-toxic, eco-friendly liquid could be derived from both natural and petrochemical feedstocks. Naturally, it is produced by microbial fermentation utilizing various microorganisms such as yeast, algae, and bacteria [3]. However, in industry, glycerol (GL) could be produced either chemically employing propene as starting material (**Figure 1.1**) [4] or from fats or oils availing diverse routes namely: a) hydrolysis, b) saponification, and c) transesterification of fats and oils (**Figure 1.2**) [5].

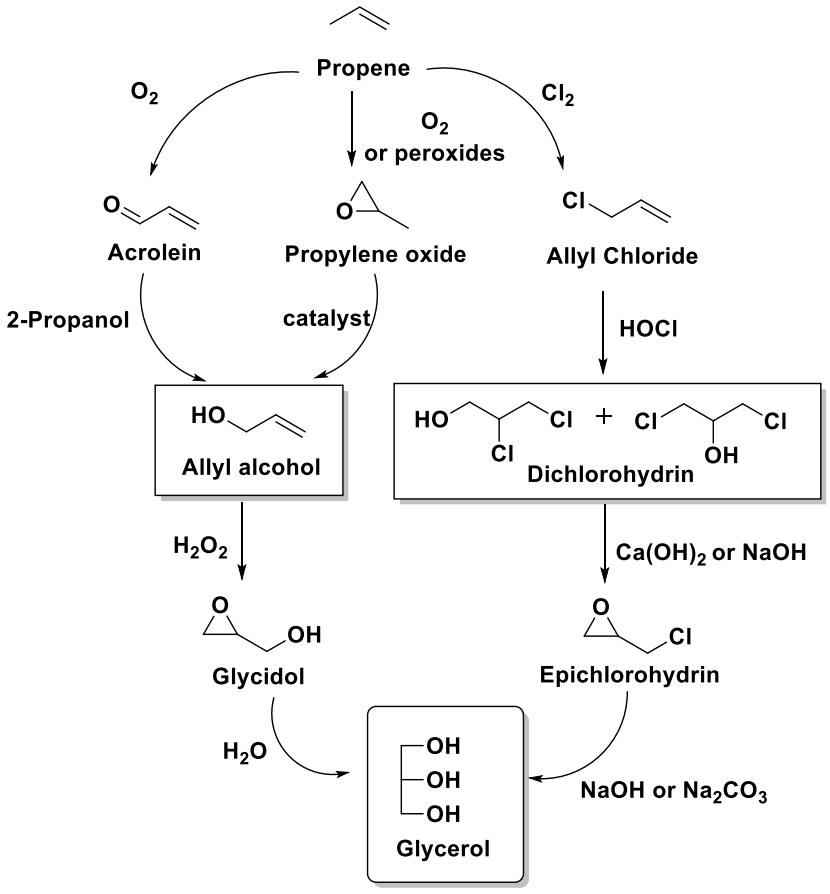

Figure 1.1 Glycerol preparation route from propene [4].

The presence of three hydroxyl groups in the GL is held accountable for its hygroscopic character, high viscosity, and solubility in the polar solvents [6]. These distinguishing features are responsible for the versatile applications of GL, due to which it could be called 'Jacks of all trades'. Due to its emollient property, it is used in the field of cosmetics as a moisturizer, emulsifier in water-based sunscreen [6]. Its demulcent property has made it an essential ingredient in numerable pharmaceutical preparations e.g., in preparing tinctures, expectorants, elixirs like theophylline to cure respiratory disorders [7]. As it imparted humidity and viscosity to the drugs, it has been used as a levigating agent [8] in the drug industry for the delivery of antibiotics and capsules [9] and plasticizer in the paper industry [10]. Other applications include its use as a humectant in ointments, toothpaste, and creams, as a water-absorbing agent to prepare adhesives and glues [11]. It has been used as a sweetener, solvent for food colors and beverage manufacturing, softening agent [10], and filler for low-fat food products in the food industry [12]. Apart from this, glycerol served as a potential feedstock for preparing polyhydroxyalkanoates (PHAs), offering wide application in the bio-medical, textile, and photographic industry [13].

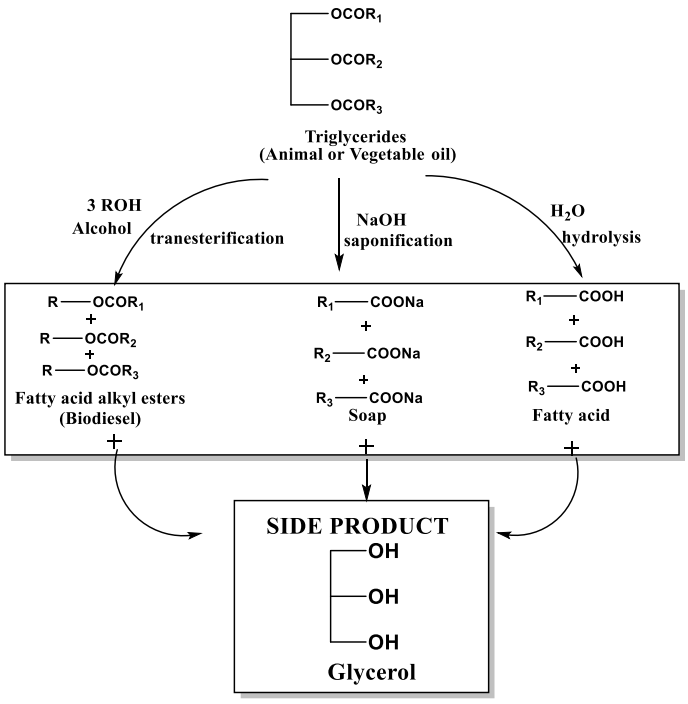

Figure 1.2 Industrial routes of GL production (where R_1, R_2 and R_3 represents the straight hydrocarbon chain with varied number of carbon atoms (14-20).

Due to its vast applications, GL production is already carried out on a large scale. Apart from the GL industries, GL is further added up from natural fats and oils as a side product (**Figure 1.3**). With ever-increasing concern towards the rapidly depleting fossil sources, global warming and environmental pollution has fuelled the interest to look for eco-friendly renewable bio-based alternatives for maintaining the sustainability of the society. As a part of this transition to renewable feedstock, biodiesel has emerged as an alternative fuel to the traditionally used petroleum [14]. Produced generally from the transesterification reaction of the vegetable oil with alcohol, biodiesel (BD) is often accompanied by the unavoidable side product glycerol (GL) [15]. For every 3 mole of triglyceride, 1 mole of GL is obtained to make approximately 10 wt% of the total BD production [16].

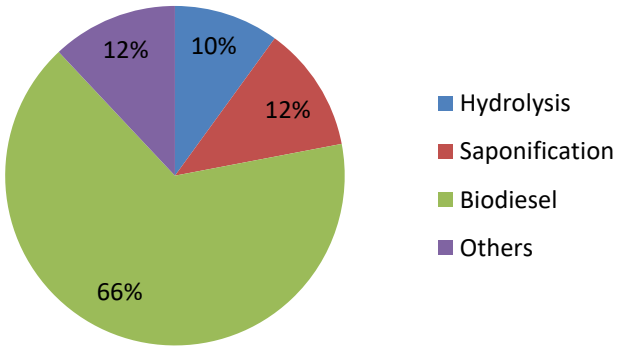

Figure 1.3 Statics showing the contribution of various reactions of fats and oils towards GL production [5].

It is estimated that in the future, BD production would grow by around 4.5% annually, reaching 41 Mm^3 in 2022 [17]. Although GL has diverse routes of effective utilization, an increased surge in the BD production has resulted in the surplus accumulation of GL, causing an imbalance in the existing steadiness of supply and demand of the GL market globally. Besides impacting the GL industry, this surplus GL also lead to the curtailment of the economic viability of the biofuel industry, hampering the adoption of biofuels worldwide.

This surplus stock of GL from the BD industry has forced to look out for new alternatives as the traditional routes are not sufficient to absorb the ever-growing production of GL. Thus

even for the BD industry sustainability, there is a need of the hour to develop strategies to utilize the excess of glycerol by transforming it into various value-added products such as fuel additives and chemical intermediates. It would not only improve the glycerol market but would also turn down the biodiesel production cost.

1.2 Application of Glycerol

Various pathways could be carved out for the effective utilization of the surplus GL as discussed below.

1.2.1 Food and Drug Industry

Various pathways for the synthesis of variety of chemical intermediates, detergents, fuel additives, polymers etc. [16] could be carved out from GL. It could be selectively transformed into various food-additives like monoglyceride [18], diglyceride [19], omega-3 fatty acids like docosahexaenoic acid [20] and eicosapentaenoic acid [21], propionic acid by fermentation, oxidation products like tartronic acid [22], etc. which are having a wide number of applications in food and pharmaceutical industry as depicted on **Figure 1.4**.

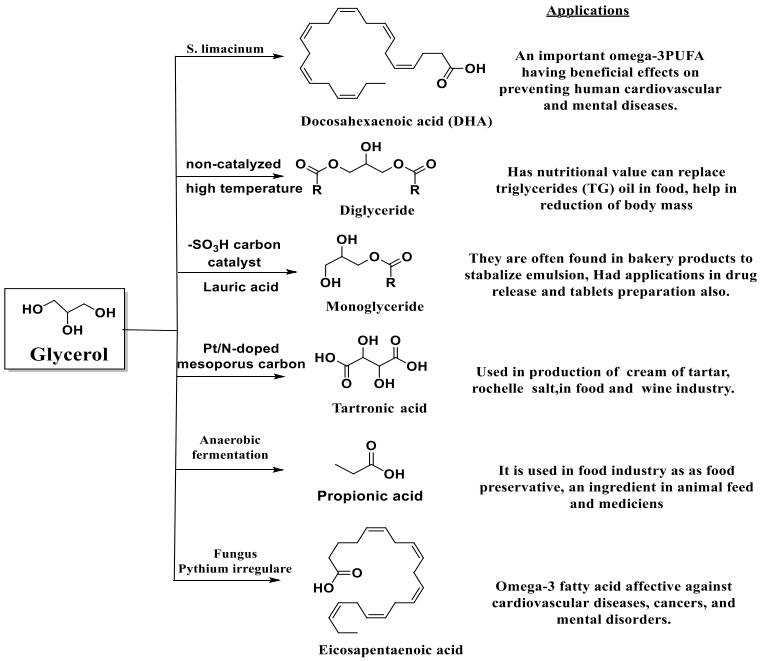

Figure 1.4 Few food additives derived from glycerol.

1.2.2 Non-Food Additives

The purity of the crude GL obtained from BD is dependent upon numerous factors such as the reaction efficiency, type of the catalyst involved, BD recovery from the reaction, and procedure adopted to recover the catalyst [23]. Furthermore, the refining process of GL involved removing impurities such as moisture, soap, left out catalyst, organic residue, and methanol, which made it a costly affair, affecting the BD production cost [24]. Thus instead of refining the GL for food additives, it is much easier and appropriate to utilize the crude GL for the synthesis of non-food additives such as polyglycerols [25], dihydroxy acetone [26], hydrogen [27], epichlorohydrin [28], glyceraldehydes [29], glyceric acid [30], hydroxyl pyruvic acid [31], succinic acid [32], propylene glycol [33], acrolein [34], 1,3-propandiol [35], mono alkyl glycerol ethers [36], glycerol carbonate (GLC) [37], solketal [17] and glycidol [38] (**Figure 1.5**). These derivatives have a wide range of applications in the pharmaceutical industry, polymer synthesis, cosmetics, paints, detergents, fibers, fuel cells, etc.

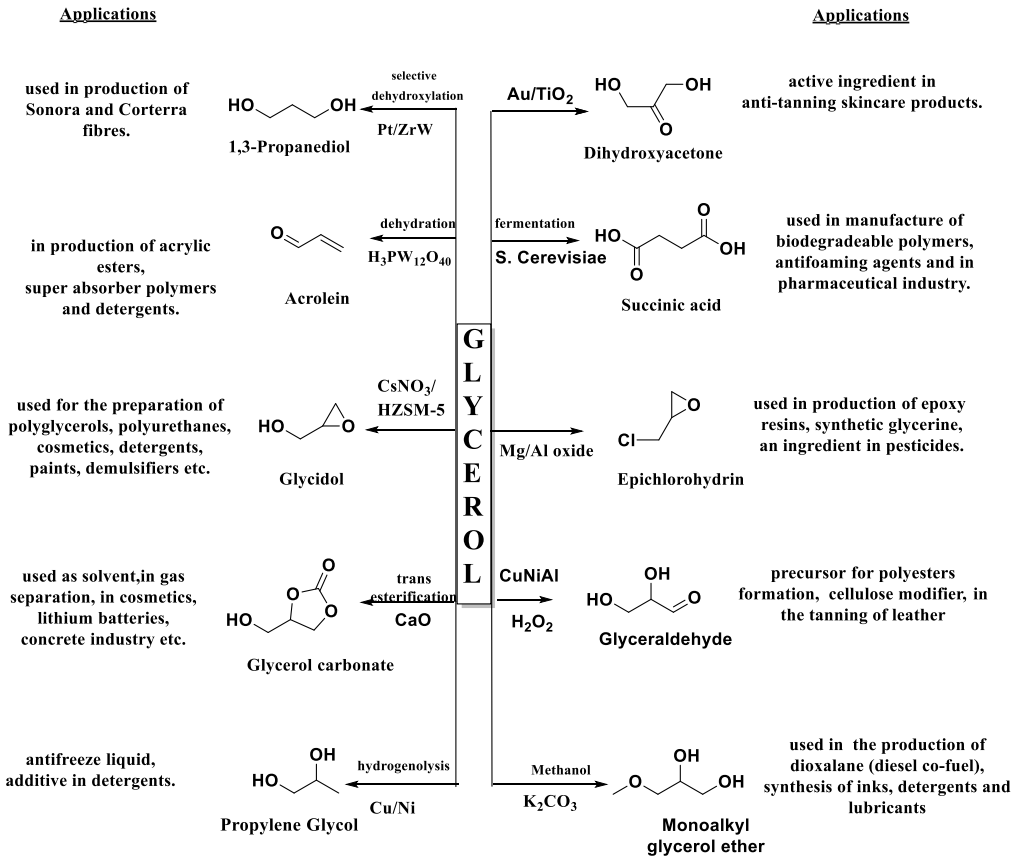

Figure 1.5 Illustration of few glycerol-derived non-food additives.

1.3 Glycerol Derivative: Glycerol Carbonate

Out of these described glycerol derivatives, Glycerol carbonate (4-hydroxymethyl-1,3-dioxolan-2-one) is a novel component offering its enormous potential in the synthesis area. Because of its low toxicity, high stability, low flammability and high boiling point, it is considered a new "green" solvent [39]. Glycerol carbonate provided the best bio-based alternative to organic solvents in various applications as an ionic liquids substitute [40]. Its dual functionality (dioxolane group and hydroxyl group) has opened up a broad spectrum of applications [41] such as electrolyte ingredient and liquid carrier in lithium-based batteries, in cosmetics as an emulsifier [42], curing agent in cement and concrete industry, glycerol precursor in detergent synthesis, for the synthesis of agricultural fertilizer [41], potential solvent for gas separation [43] and for acidic treatment of biomass [44], plasticizing agent [45,46] and precursor for polymers synthesis such as polyesters, polyamides [47]. GLC reacted with fatty acid anhydrides to furnish 1,3-*sn*-diglyceride, which are used as an ingredient in bakery products, eatables like chips, and fries [48] and as drug carriers [49]. It could also be used as a valuable intermediate to synthesize resins and plastics, polymers like polyglycerol esters exhibiting surfactant properties.

1.3.1 Pathways for Glycerol Carbonate Synthesis

A variety of routes has been opted in literature for GLC synthesis from GL (**Figure 1.6**). One of them is the direct carbonation using CO_2 and other indirect methods included glycerolysis by urea and transesterification with cyclic carbonates or dialkyl carbonates.

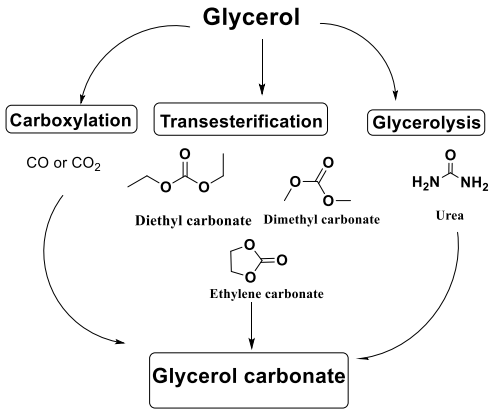

Figure 1.6 Various routes of glycerol carbonate synthesis.

1.3.1.1 Synthesis from Glycerol and CO_2

Carbon dioxide is a cheap, abundant greenhouse gas produced as a by-product in coal power stations [50]. Over the decades, this cheaply available waste product served as a potential feedstock for producing a variety of industrial chemicals such as urea, cyclic carbonates, salicylic acid, and polycarbonates [51]. Direct carbonation of the glycerol for the synthesis of the glycerol carbonate would further help in recycling the waste CO_2 hence reducing global warming. Thermodynamic studies conducted for the direct carbonation reaction of glycerol with CO_2 revealed that reaction is thermodynamically limited [52] and some dehydrating agent should be employed to get rid of the thermodynamic constrain with the removal of the H_2O produced (**Figure 1.7**).

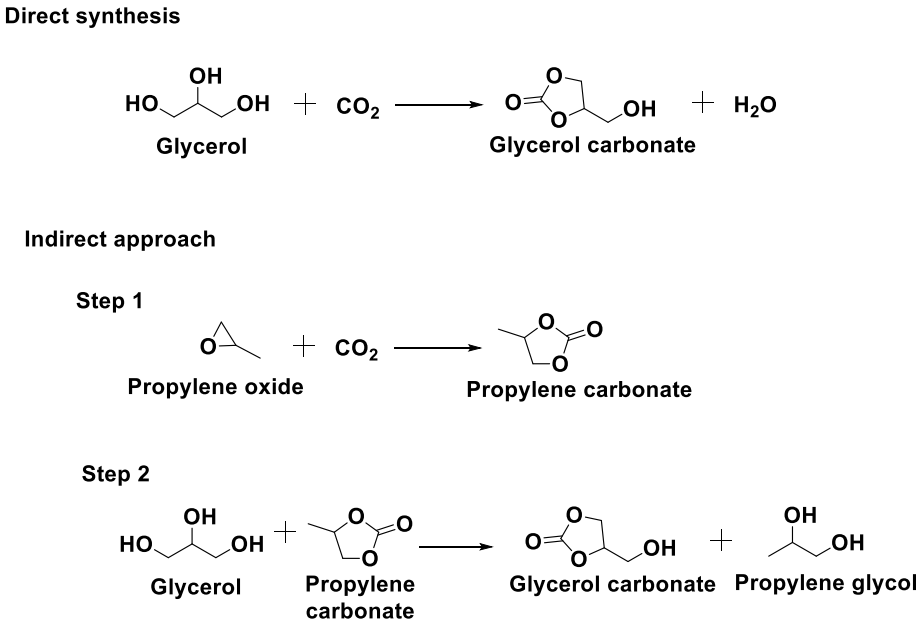

Figure 1.7 Glycerol carbonate synthesis from CO_2 [53].

Due to their surface adsorption properties, metal oxides were employed for carrying out the direct carbonation reaction of glycerol. Liu et al. found the catalytic activity of CeO_2 towards glycerol carbonate formation was significantly affected by its redox properties [54]. The activity of CeO_2 was also influenced by the choice of dehydrating agent and solvent. They demonstrated that among the acetonitrile, benzonitrile, valeronitrile, phenylacetonitrile and 2-cyanopyridine dehydrating agents; 2-cyanopyridine outshined all the others to assist the CeO_2 catalyzed

carbonation reaction due to its strong alkalinity. Along with 2-cyanopyridine, the use of DMF as solvent further enhanced the CeO_2 activity as it offered better dissolution of the CO_2, raising its concentration on the catalyst, providing glycerol carbonate yield of 21% at 4 MPa, 150 $^{\circ}$C in 5 h [54]. To enhance the CeO_2 catalytic activity, Ce-Zr mixed metal oxides with varied doping of Zr have also been employed for carrying out the reaction of glycerol with CO_2. It was found that doping of 0.02-mole fraction of Zr on CeO_2 considerably enhanced the glycerol conversion (41%) and glycerol carbonate yield (36.3 %). The better performance of the catalyst is explained in terms of the improvement in the acid-base properties of the catalyst as Lewis acidic and basic sites favored the activation and adsorption of the OH group of glycerol and CO_2, respectively [55]. Lately, CaC_2 has also been applied as a dehydrating agent for conducting the direct carboxylation of GL [56]. In the presence of 1-methyl-2-pyrrolidinone solvent and CaC_2, a combination of $Zn(OTf)_2$ catalyst and 1,10-phenanthroline ligand provided a GLC yield of 88% but with a longer reaction time (16 h). Su et al. have conducted metal catalyst-free conversion of CO_2 and GL only by employing a dehydrating agent, 2-cyanopyridine [57]. With 2-cyanopyridine, they obtained GLC conversion (18.5% at 180 $^{\circ}$C and 15MPa) comparable to that obtained using metal oxides. Comparison of the activity of 3-cyanopyridine and 4-cyanopyridine revealed that the stereo-structure of the dehydrating agent played a significant role in the reaction. The superiority of 2-cyanopyridine towards the carbonation reaction was attributed to the easy activation of the CO_2 by simultaneous interaction with N site of pyridine as well as of cyano group resulting in the formation of five-membered ring intermediate, which readily underwent a nucleophilic attack by the activated hydroxyl group of GL; producing GLC (**Figure 1.8**).

Recently carbonaceous material, biochar obtained from various feedstocks, has been used as a catalyst for carrying out direct synthesis of GLC from GL and CO_2, taking acetonitrile as dehydrating agent [58]. It was observed that instead of the surface area and porosity, the composition of the catalyst also influenced the overall catalytic activity. Biochar with more ash and carbon content contributed actively towards GLC formation (0.0482 mol L^{-1}, with rice husk biochar). Comparison of the untreated and demineralized biochar samples revealed that potassium content also played a significant role in the catalytic activity. Biochar obtained from

oil seed rape with more K content (17.1 at. %) provided a higher GLC yield (0.0340 mol L^{-1}). In the absence of K, GLC production decreased dramatically in all the catalysts.

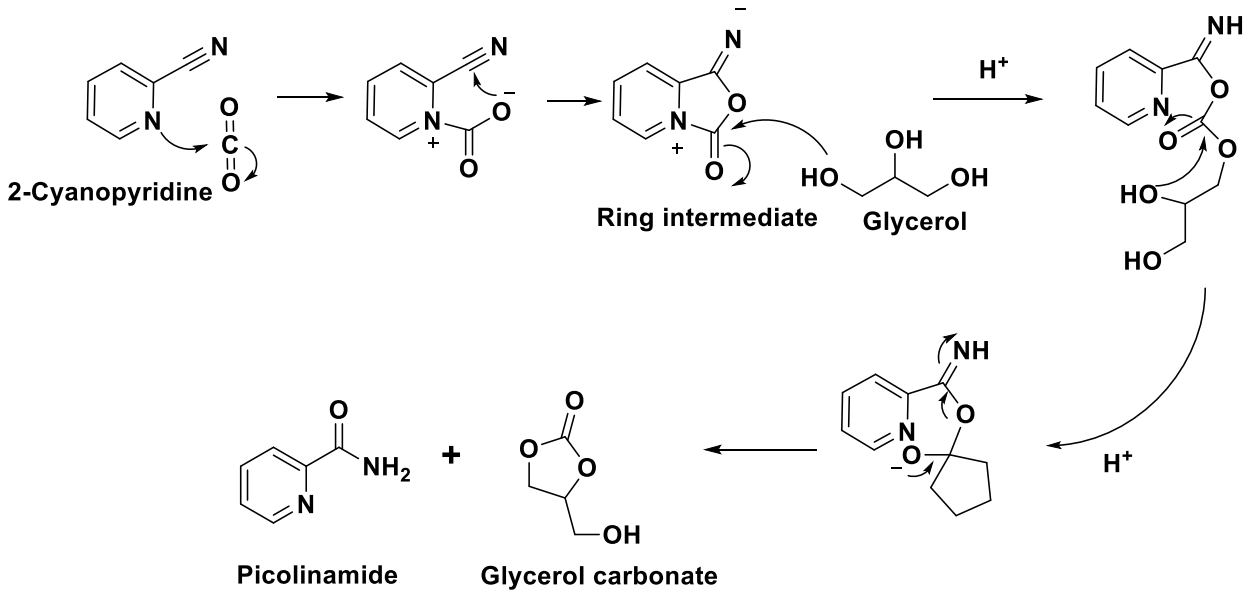

Figure 1.8 Reaction mechanism of 2-cyanopyridine catalyzed carbonation reaction of glycerol [57].

To overcome the thermodynamic limitations of the direct carbonation reaction, indirect approach is adopted where an epoxide is used as a coupling reagent in the reaction. The reaction proceeded in two steps: (1) cycloaddition reaction of the epoxide with CO_2 forming carbonate and (2) transesterification reaction of the glycerol with the prepared carbonate (**Figure 1.7**). Both the reactions were thermodynamically favorable and this would help in overcoming the thermodynamic limitations of the direct carbonation reaction of glycerol, providing good GLC yield [45]. Ma et al. found that nucleophilicity and leaving ability of the alkali halide played an important role in catalyzing the reaction [53]. Song et al. have utilized imidazole based ionic liquids grafted on DVB based polymer as heterogeneous catalysts for carrying out this two-step carbonation reaction of glycerol. They established that the catalytic performance was greatly affected by the mode of the catalyst preparation. Among the prepared catalysts, P-DVB-(vIm-BuBr), possessing more ionic liquid groups on its surface, provided the highest GLC yield of 81% at 100 $^{\circ}$C, 2 MPa in 4 h [59]. High catalytic activity and good stability (up to 5 cycles) of this catalyst opened the way for its industrial implementation. Similarly, 3-chloro-1,2-

propanediol was also utilized as starting material for the GLC formation, but the unexplained formation of glycerol was a concern [50,60].

Apart from the above-described catalysts, Zn, La, and Al-based catalyst: $La_2O_2CO_3$/ZnO [61], Zn/La/Al, and Zn/Al/La/M, Sn-based catalysts: Bu_2SnO [62], n-$Bu_2Sn(OMe)_2$ [63], Cu based catalysts Cu/MgO [64] and Cu/La_2O_3 [65] have also been reported for conducting the GLC synthesis from the CO_2 route (**Table 1.1**).

Even though this direct reaction of glycerol and CO_2 made the best use of the biobased and industry-based by-product from the ecological point of view, but few parameters are still needed to be optimized to make this route suitable for its industrial implementation. Requirement of the organic solvents such as nitrobenzene, dimethyl sulfoxide (DMSO) or N,N-dimethyl formamide (DMF), and methanol (MeOH), non-recoverable homogeneous catalysts, high pressure, and long heating time at elevated temperatures are the few factors having negative ecological impacts that need to be addressed.

Table 1.1 Tabulated view of various catalysts employed for the preparation of glycerol carbonate (GLC) from CO_2.

Direct Approach

Catalyst	Reaction conditions	Catalyst amount (wt%)	Dehydrating agent	% GL Conversion	% Yield/ Selectivity GLC %	Reference
10%W-Zn	5.0 MPa, 150 °C, 6 h	54	DMF	6.5	6.5/ 100	[66]
Al_2O_3	10 MPa, 170 ^{o}C, 12 h	7.3	2-cyanopyridine	34.5	10.5/ 30.4	[57]
ZnO	10 MPa, 170 ^{o}C, 12 h	7.3	2-cyanopyridine	41.3	11.9/ 28.8	[57]
Zn/Al/La	4.0 MPa, 170 °C, 12 h	3	CH_3CN	30.4	13.3/ 43.8	[67]
Zn/Al/La/Li	4.0 MPa, 170 °C, 14 h	3	CH_3CN	39.5	18.7/ 47.3	[67]
Zn/Al/La/Cl	4.0 MPa, 170 °C, 12 h	3	CH_3CN	35.5	16/ 45.2	[68]
Cu/La_2O_3	7.0 MPa, 150 ^{o}C, 3 h	1.73	CH_3CN	8.9	2.6/ 29.3	[64]
Cu/MgO	7.0 MPa, 150 ^{o}C, 3 h	1.73	CH_3CN	8.6	2.2/ 26.1	[64]
$2.3\%Cu/La_2O_3$	7.0 MPa, 150 ^{o}C, 12 h	5	CH_3CN	33.4	15.2/ 45.4	[65]
$La_2O_2CO_3/ZnO$	4.0 MPa, 170 ^{o}C, 12 h	5	CH_3CN	30.3	14.3/ 47.3	[61]

Indirect Approach

Catalyst	Reaction conditions	Catalyst amount	Coupling agent	% GL Conversion	% Yield/ Selectivity GLC	Reference
KI	2 MPa, 115 ^{o}C, 1.5 h	5	Propylene oxide	78	75/ 96.15	[53]
Triethylamine (TEA)	2.5 MPa, 100 ^{o}C, 1h	TEA/CPD=1.5	3-chloro-1,2-propanediol (CPD)	100	90/90	[50]
$KHCO_3$	80 ^{o}C,1.3 h	CPD/$KHCO_3$= 3:1	3-chloro-1,2-propanediol (CPD)	NR	60/NR	[60]

1.3.1.2 Synthesis from Glycerol and Urea

Urea, produced from CO_2 and ammonia, is a bio-based reactant having CO_2 in the activated form [57]. The easy availability, low cost, and non-toxicity of urea have made this indirect carbonation route for GLC production more economical. The glycerolysis of urea was generally carried out at reduced pressure and high temperature for pushing the chemical equilibrium in the forward direction with the elimination of by-product ammonia [52]. Various Zn-based homogeneous catalysts viz., $ZnCl_2$, $ZnBr_2$, ZnO, $Zn(NO_3)_2 \cdot 6H_2O$, and $Zn(OAc)_2 \cdot 2H_2O$ have been applied for the glycerolysis reaction [69]. However, besides good conversion, the homogeneity of the catalysts remained an issue. These drawbacks shifted the focus to discover heterogeneous catalysts for the glycerolysis reaction. Looking into the mechanism of the GLC formation employing urea, it was observed that an adequate amount of both Lewis acidic and basic sites was required for the effective conversion [70]. Lewis acidic sites helped in the activation of the urea, and basic sites activated the GL through its hydroxyl group (**Figure 1.9**). The cyclization of the formed intermediate glycerol urethane lead to the formation of GLC with the removal of ammonia molecule [71]. Park et al. also supported this fact as they have isolated $Zn(NH_3)_2Cl_2$ and $Zn(C_3H_6O_3)$ intermediate species which actively participated in the reaction as Lewis base and Lewis acid, respectively [69].

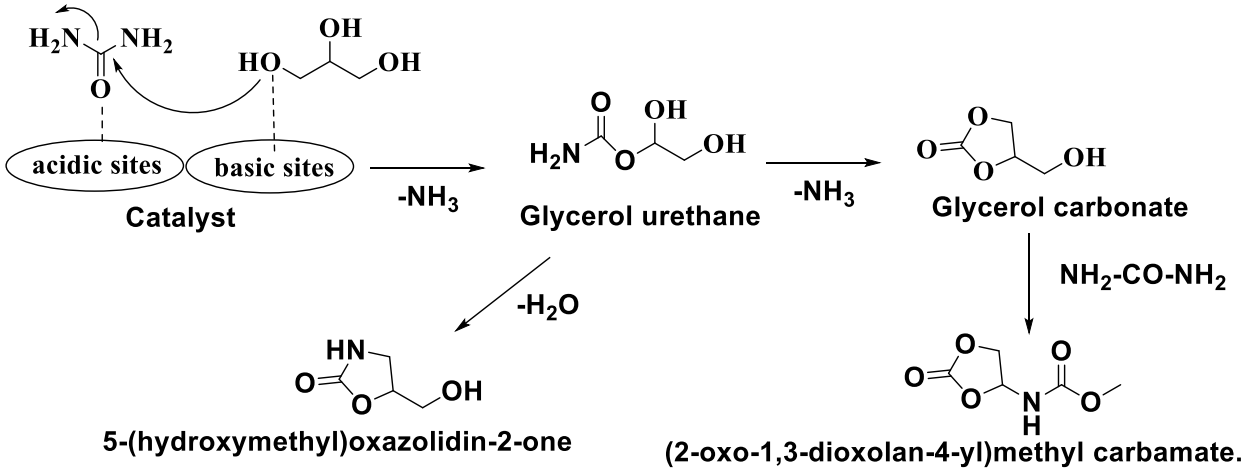

Figure 1.9 Proposed mechanism for the catalyst-assisted GLC synthesis from urea [71].

Marcos et al. observed that the catalytic properties of the Zn-supported Co_3O_4 catalysts were remarkably affected by the preparation method and the thermal treatment adopted [71].

Co_3O_4/Zn catalyst prepared by a dry nano-dispersion method was found to be more selective towards GLC (97%) due to the greater dispersion of the Co_3O_4 active sites on the catalyst interface. However, calcination of the catalyst at 500 °C expedited the formation of the spinel $Zn_{0.20}Co_{0.80}Co_2O_4$ inactive species [72]. Further, Liu et al. formed highly porous Co_3O_4/ZnO nanocage catalysts using thermolysis of the heterometallic metal-organic framework (MOF)-template [73]. They also established that the activity of the catalysts was correlated with the number of hetero-interfaces present on the surface along with the presence of Co_3O_4 and ZnO oxides. At 150 °C, 91% GLC selectivity was achieved with $Co_{50}Zn_{50}$-350 catalyst, but the loss of the catalyst during the recovery process lead to a decline in the glycerol conversion (70%).

Wang et al. have studied the effect of the Zr on the catalytic performance of the Mg-Al hydrotalcite towards the formation of glycerol carbonate [74]. They discovered that acidic sites of the Zr helped in enhancing the catalytic selectivity towards GLC but excess of the same lead to the urea poisoning. The basic sites of the catalyst were responsible for the production of the side products of the glycerol carbonate reaction, 4-(hydroxymethyl) oxazolidin-2-one (**Figure 1.9**) and glycidol. They also concluded that a well-balanced combination of the acidic and basic sites was required for achieving maximum GLC yield (87.8%) from urea.

In addition, heteropolyacids (HPAs) owing to their strong acidic strength, redox activity and unusual thermal and hydrolytic have been widely put to use for carrying out GLC synthesis. Ta_xHPA [75], Sn/CsPW [76], Zn incorporated heteropolytungstate [77], and Sm exchanged heteropolytungstate [78] has also been applied for the glycerol carbonate synthesis from glycerol and urea (**Table 1.2**). However, their good catalytic activity was also associated with the formation of by-products such as glycidol and glycerol urethane, poor reusability, and longer reaction time.

Apart from these catalysts, ionic liquids are also adopted for carrying out the glycerolysis of urea. Among the acidic, basic, and neutral ionic liquids, neutral ionic liquids performed better than others because of their well-balanced acid–base properties which played an important role in enhancing the catalytic activity [79]. The difficulty of the separation of the homogeneous ionic liquids from the reaction mixture could be solved by immobilizing them on various supports, thus converting them into heterogeneous ones. Kim et al. determined that Merrifield peptide resin-based ionic liquids (MPR-ILs) having longer alkyl chains of more electron donating ability

and counteranions of less steric hindrance showed better catalytic behavior towards the GLC synthesis (80.9% glycerol carbonate selectivity) [80]. They also studied the effect of different metals (Cu, Zn, and Mg) and anionic nucleophilicity on the catalytic properties of polystyrene-supported ionic liquids [81]. It was determined that Zn metal-based IL, PS-$(Im)_2ZnI_2$ with greater anionic nucleophilicity and well-balanced Lewis acid-base sites afforded good GL conversion but in longer reaction time (6 h).

The indirect route of GLC formation has the advantage of utilizing bio-based reactants GL and urea. The GLC formation could be made more effective by employing higher temperature and lower pressure. However, difficulty to manage the ammonia released in the reaction, formation of by-products, harsh reaction conditions, and longer reaction time are the few shortcomings that limited its application.

Table 1.2 Tabulated view of various catalysts employed for the preparation of glycerol carbonate (GLC) from urea.

Catalyst	Reaction conditions	Catalyst loading	% GL Conversion	% Yield/ Selectivity GLC	Reusability (cycles)	Reference
MoO_3/SnO_2	GL:Urea: 3; Dry N_2, 4 h; 150 °C	10 wt %	69.2	67/97.1	4	[82]
Zn2CrO	GL:Urea: 1; 3 kPa, 3 h; 140 °C	5 wt %	76	57/NR	NR	[83]
$Sn(OH)_2$	GL:Urea : 1; Air Flux; 4 h; 140 °C	4.9 mol %	87	NR/85	NR	[84]
Zn/MCM-41	GL:Urea : 1; N_2 flow ; 5 h; 140 °C	5 wt %	78	NR/98	NR	[70]
15 % WO_3/TiO_2	GL:Urea : 1; reduced pressure; 4 h; 140 °C	10 wt %	73	73/100	3	[85]
Sn/CsPW	GL: Urea: 1; reduced pressure; 4 h; 140 °C	0.1 wt%	91	83/91	NR	[76]
$Ta_{0.4}HPA$	GL: Urea: 1; vaccum pump; 4 h; 150 °C	0.1 wt%	71	71/100	3	[75]
$LaCl_3$	GL: Urea: 1; 5 kPa 3 h; 150 °C	1 mmol	95.4	95.4/99.9	NR	[86]
F-IRMOF-3(BuI)	GL:Urea: 1; Vaccum (14.7 kPa); 3 h; 140 °C	5 wt %	71	67.8/95.5	3	[87]
Sn-W mixed oxide	GL:Urea : 1; reduced pressure; 4 h; 140 °C	10 wt %	52	NR/95	3	[88]
$La_2Cu_{0.5}Fe_{0.5}O_4$	GL: Urea: 1; N_2 flow; 4 h; 150 °C	5 wt %	49.0	40.1/89.1	6	[89]
Zn_xTPA	GL: Urea:1; Reduced pressure; 4 h; 140 °C	10 wt %	69.2	68.8/99.4	3	[77]
1wt%AuPd/MgO	GL: Urea: 1.5; N_2 flow; 4 h; 150 °C	1.8 wt%	87	67/77	NR	[90]
2.5wt%Au/MgO	GL: Urea: 1.5; N_2 flow; 4 h; 150 °C	1.8 wt%	81	56/68	10	[91]
ϒ-Zirconium Phosphate	GL:Urea : 1; 20 Pa ; 3 h; 140 °C	1 wt %	80	80/100	5	[92]

1.3.1.3 Synthesis from Glycerol and Cyclic or Dialkyl Carbonates

One of the widely studied pathways for glycerol carbonate formation is the transesterification reaction of either cyclic carbonates such as ethylene carbonate, propylene carbonate, or dialkyl carbonates as dimethyl carbonate (DMC), or diethyl carbonate (DEC) with glycerol. The advantages offered by this method such as a) evading the release of toxic side products, b) employment of the non-toxic reagents, c) simple and environment-friendly reaction conditions, and d) greater selectivity [37] has made this pathway more feasible economically [93]. This method is usually carried out without the requirement of any solvent. However, due to the reversible nature of the transesterification reaction, excess of DMC was added to push the reaction in the forward direction. Thermodynamic studies also revealed that this pathway is thermodynamically favorable when high dialkyl carbonate to glycerol molar ratio was taken [52].

Catalysts for the Transesterification Reaction

Homogeneous acidic catalysts

The acidic catalysts like H_2SO_4, *p*-toulenesulphonic acid were not suitable, as they showed poor catalytic activity (10.6% and 19% GL conversion, respectively) for transesterification [94]. In addition, corrosion on reactors and pipelines and the difficulty to separate them from the reaction mixture were the demerits of the homogeneous acid catalysts.

Heterogeneous acidic catalysts

Acidic heterogeneous catalysts, due to their lesser activity, were seldom explored for the GLC production. Ti-silica-based catalysts having mild acidic properties were employed for the GLC production [95]. The presence of weak Lewis acidic sites attributed to the Ti^{4+} ions was the main driving force in activating the carbonyl group of DMC and the hydroxyl group of GL was activated by a weak conjugate base represented by silica oxygen framework (Si-O-Ti). A regression model established that temperature has the most considerable effect on the GL (94%) conversion along with GLC selectivity. Nevertheless, loss in the activity after 3 catalytic cycles was attributed to the condensed silica frameworks resulting in the closure of the active sites.

Homogeneous basic catalysts

Homogeneous alkali catalysts like K_2CO_3, KOH, NaOH have been primarily employed for the glycerol carbonate synthesis [94] due to high conversion under relatively mild reaction conditions. However, catalyst neutralization and separation remained a challenging task after the completion of the reaction as water could not be employed to get rid of the alkali-hydroxide due to the miscibility of GLC with water.

Heterogeneous basic catalysts

Despite good GL conversions, separation and neutralization issues associated with the homogeneous catalysts limit down their applicability at a large scale. These shortcomings shifted the focus towards the heterogeneous catalysts; the applicability of few reported catalysts are discussed below.

Alkaline earth metals

Due to the easy availability, high basicity, and non-toxic nature of the alkaline earth metals, the same have been applied widely employed in the field of catalysis. The O^{2-} centers of their respective oxides act as strong Lewis basic sites for executing the transesterification reaction. Ochoa-Gomez et al. [94] concluded that basic strength of the catalyst and catalytic activity are part and parcel of each other. They have proposed a reaction mechanism revealing that that strong basic strength was needed for carrying out the initial step of the reaction i.e., proton abstraction from the primary hydroxyl group of GL forming glyceroxide anion (**Figure 1.10**). The nucleophilic attack on the carbonyl group of DMC and the elimination of one methanol molecule gave rise to an intermediate. The formed intermediate with intramolecular nucleophilic substitution furnished GLC as the end product with the release of another methanol molecule [96].

Among the alkaline earth metals, CaO and MgO were widely considered for the GLC production on account of their non-toxicity, cheap and easy availability. In most of the reported studies, basic sites of the CaO easily got contaminated with atmospheric CO_2 and H_2O adsorption, affecting its catalytic activity [97,98]. Moreover, the GL procured from the biodiesel industry retained traces of water during the refining process. Therefore, besides imparting stability to the catalyst, moisture-resistant properties of the catalyst should also be improved.

Ca/La mixed oxides exhibited good stability but their moisture-resistant properties are not studied [99]. KNO_3 loaded CaO [100] and CaO/Al_2O_3(polya,3) [101] catalyst strengthened up the moisture resistance of CaO up to the presence of 5wt% and 2% water content in GL respectively. For improving the water tolerance of the CaO, Kaur et al. adopted a hydrophobic functionalization approach to modify the CaO surface [102] with different alkyl or benzyl bromide groups. Amidst all, 0.5 wt% benzyl bromide modified CaO catalyst displayed 100% selectivity towards GLC along with providing resistance up to 5 wt% of H_2O content in the reaction owing to the presence of the aromatic hydrophobic layer on the CaO surface. In order to make the transesterification pathway more economical, cockle shell-derived CaO catalyst employed for GLC synthesis demonstrated 92.1% GLC yield at 80 $^{\circ}$C attributed to its high basicity and surface area [103]. In further continuation, Algoufi and Hameed have utilized natural dolomite as a precursor for the preparation of CaO-MgO mixed oxides. Formation of a mesoporous network with greater surface active sites afforded 94% GLC yield at 75 °C in 90 min [104]. Despite that, all the above reported CaO based catalysts; observed a decline in the catalytic activity on repeated use owing to the formation of $CaCO_3$.

Manikandan and Sangeetha have prepared MgO nanoparticles employing starch as bio-template and applied the same for the DMC transesterification reaction. They found that choice of calcination temperature play a deciding role for acquiring MgO nanoparticles with high surface area and basicity. Moreover the presence of an adequate amount of Lewis basic sites in the catalyst is held responsible for the excellent GLC selectivity of 93% [105]. However, Bai et al. discovered the fact that trapezoidal MgO, despite of its lower surface area, pore-volume, and weaker basicity, performed considerably well, providing 99% GLC yield suggesting that physiochemical properties and morphology played a crucial role in determining the catalyst activity [106].

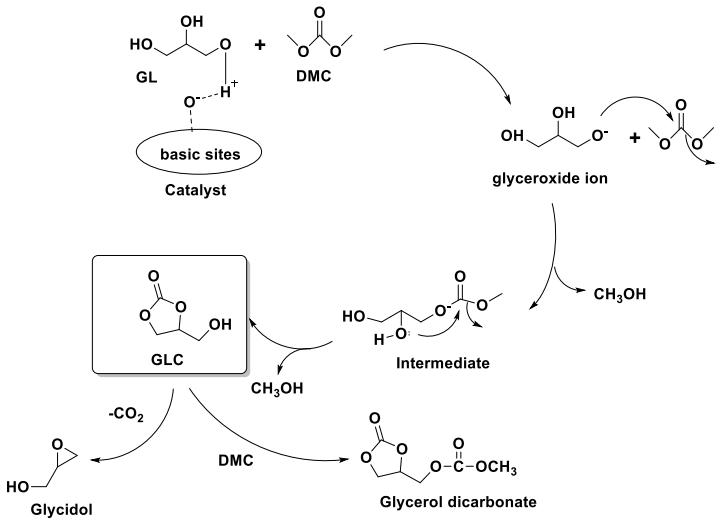

Figure 1.10 Reaction mechanism depicting the base catalyzed synthesis of GLC from GL and DMC.

Mixed metal oxides

With the aim of achieving maximum stability and boosting up the basicity of the catalyst, doping as well mixing of the metal oxides is adopted, forming mixed metal oxide catalysts.

Mixed metal oxides, perovskite represented with formula ABO_3 [107] (where A=lanthanide/alkali element and B= transition metal) with their thermal stability and oxidative ability showed good catalytic properties [108]. Utilizing these properties, crystalline La and Co-based perovskite [109] with higher percentage of the La_2O_3 phase displayed 98% GL conversion but with lower GLC selectivity (77%). The combined synergic effect of the basic sites of metal oxides and perovskite was held responsible for forming side product glycidol (22% selectivity). Pattanaik et al. also revealed that a particular combination of acidic and basic sites was required to attain maximum GLC yield [110]. With Fe-La mixed oxides having $LaFeO_3$ perovskite as a major phase, 71% GLC yield was obtained. Pradhan et al. observed that a combination of Lewis acidic sites of ZnO and basic sites of MgO in Mg/ZnO catalyst offered good GL conversion (98.4%) with 96.89% GLC selectivity in 2h at DMC/GL molar ratio of 4 [39]. A prompt decline in the GL conversion after the 5^{th} catalytic cycle was attributed to the leaching of the active basic sites of the catalyst.

Zirconia has been utilized widely as catalyst support owing to its thermal stability, amphoteric character, and high specific surface area [111]. In the mesoporous Ca-ZrO_2 catalyst [112], the substitution of the Zr^{4+} with the Ca^{2+} ion (lattice Ca^{2+}:Zr^{4+} atomic ratio up to 0.6) resulted in the formation of a stable solid solution with high dispersion of the Ca^{2+} ion. The higher basic strength of the Ca-ZrO_2 catalyst favored the GL conversion but extended the catalyst selectivity towards glycidol formation. The possible reason mentioned for this was the adsorption of the GLC on the surface basic sites favoring the decarboxylation reaction. Thus an appropriate balance of the catalyst basic sites was necessary for attaining good GLC selectivity. Likewise, nanocrystalline mesoporous Mg-ZrO_2 catalyst provided 88% GLC yield but at the cost of high catalyst amount (15 wt%), reaction time (3h), and glycidol formation [113]. Lately, Kaur et al. [114] impregnated LiOH on the ZrO_2 matrix and found that solid-state interactions among the both lead to the formation of active Li_2ZrO_3 phase. The prepared catalyst exhibited 100% selectivity towards GLC along with 91% GL conversion under mild reaction conditions. For the first time, they reported the quantification of the produced GLC via ^{1}H-NMR technique [115]. Although a decline in the catalytic activity was observed upon reuse but selectivity remained unaltered.

Miscellaneous catalysts

Industrial waste

To make the transesterification pathway greener and environment-friendly, industrial waste materials were utilized as heterogeneous basic catalysts. Das and Mohanty found that a high concentration of $NaAlO_2$, $Ca_2(SiO_4)$ and $Na_8Al_6(SiO_4)_6Cl_2$ phases in the red mud catalyst were responsible for its high surface area and active basic sites. Apart from good GL conversion (95.21%) and GLC selectivity (96.64%), RM-500 catalyst also showed better stability towards the presence of impurities in the GL as only 5.01% decrease in GLC yield was observed when the reaction was carried out in the presence of 3 wt% of water and methanol. However, RM-500 catalyst exhibited poor reusability because of the leaching of the active components from the catalyst [116]. The incorporation of K onto the red mud surface improved its stability as 78.09% GL conversion was attained during fourth catalytic cycle [117] owing to its stronger interaction with the components of the red mud.

Calcined silicate

Alkali calcined silicate, Na_2SiO_3 with high basicity but lower BET surface area provided maximum GL conversion (97.8%) and GLC selectivity (97.6%) indicating that catalytic activity was subject to the basicity of the catalyst rather than surface area. The structural study revealed that phase transformation of the silicate during calcination and formation of crater structures facilitated the accessibility of GL and DMC to the active sites favoring more GL conversion [118]**.** Similarly, Ca and Al-based hydrocalumite-type compound, HC2USR24 with lower surface area, provided 79% GL conversion but only 60% selectivity towards GLC [119]. Reduction in the crystallinity of the Ca-Al LDH phase, formation of $CaCO_3$ phase, and withholding of the reactant species onto the basic centers of the catalysts were the few reasons quoted for the drop in the catalyst activity during the reusability experiment.

Metal-Organic Frameworks (MOFs)

Zeolitic imidazolate frameworks (ZIFs) are the sub-class of MOFs that have gained attention in the recent decade in the field of catalysis with their high surface area, hydrophobicity crystallinity, porosity, and thermal stability [120]. The structural and basic properties of the MOF could be tuned according to the choice of metal centres and organic ligands [120]. Chang and co-workers have prepared MgO-loaded ZIF-8 catalyst through wet-impregnation and calcination method [47]. High dispersion of MgO was attained while preserving the crystallinity and micro-porosity of ZIF-8. They have proposed an acid-base bifunctional model explaining the synergistic effect among basic sites of MgO and acidic sites of ZIF-8 that enhanced the GLC formation (70% yield at DMC: GL molar ratio of 4). Despite the good catalytic activity, the reusability of the catalyst was not studied.

Furthermore, $BaCO_3$/C composites [121], Mg/La mixed oxides [122], KF loaded HAP [123], K_2CO_3/MgO [124], Zn/La mixed oxides [125], $Mg_{1.2}Ca_{0.8}O_2$ [126], Mg/Al/Zr [127], Mg/Zr/Sr [128], Ionic liquids [129,130], hydrotalcites like Mg/Al [131], Rehydrated Mg/Al [132], HTC-Ni [133], $LiNO_3$/Mg-Al catalysts [134] are also applied for the GLC formation as summarized in **Table 1.3**.

The transesterification route for the GLC synthesis is widely explored owed to its easy experimental requirements. However, in most of the reported catalysts, good GLC selectivity and

GL conversion seemed to be different sides of the same coin as one achieved at the expense of later. Apart from that, practicing high DMC/GL ratio and catalyst amount to achieve good conversion, formation of side products, catalyst poisoning, stability, and reusability are the few factors that required further attention.

Table 1.3 Tabulated view of various catalysts employed for the preparation of glycerol carbonate (GLC) from GL and DMC.

Catalyst	Reaction conditions	Catalyst loading	% GL Conversion	% Yield/ Selectivity GLC	Reusability (cycles) (GLC yield %)	Reference
Cu/Al hydrotalcite	GL:DMC:1:4; 90 °C; 1.5 h	0.22 g	96	86/89.5	4 (78%)	[135]
$NaAlO_2$	GL:DMC: 1:4;70 °C; 2 h	30 wt %	85	85/100	5 (69)	[136]
3.50Li-La_2O_3	GL:DMC: 1:3 85°C, 3 h	3.3 wt %	94.4	93.7/92.1	4 (81.5)	[137]
0.3KF/La-Zr	GL:DMC: 1:2 80°C, 1 h	1 wt %	91.77	91.77/100	3 (54.14)	[96]
BaO	GL:DMC: 1:3; 120 °C , 1.5 h, DMF	5 wt %	98	68.6 /70	NR	[138]
Sr-Al	GL:DMC: 1:2 70°C, 1 h	3 wt %	99.4	99.4/100	5 (96)	[139]
Li/ZnO	GL:DMC: 1:2 95°C, 2 h	5 wt %	96.12	93.76/97.54	4 (46.95)	[140]
Trisodium phosphate	GL:DMC: 1:2 70°C, 1 h	3 wt %	99.5	99.5/100	9 (90)	[141]
3CaLa	GL:DMC: 1:5 90°C, 1.5 h	10 wt %	94	74/78.7	4 (67)	[99]
KNO_3/CaO	GL:DMC: 1:3 70°C, 2 h	10 wt %	99.23	85.85/85.19	4 (94.95)	[100]
$LiNO_3/Mg_4Al_{5.5}$	GL:DMC: 1:3 80°C, 1.5 h	4 wt %	100	96.3/96.3	NR	[134]
[p-DABCO]Cl	GL:DMC: 1:2 80°C, 1 h	4 mol %	94.1	98.2/92.5	5 (91.4)	[130]
Zn4La1	GL:DMC: 1:6 150°C, 2 h	0.5 wt %	98.5	95.7/97.2	4 (63.96)	[125]
K-zeolite	GL:DMC: 1:3;75 °C; 1.5 h	4 wt %	96	96/100	4 (90)	[142]
HTC-Ni	GL:DMC: 1:3; 100 °C; 2 h	10 wt %	55	55/100	5 (45)	[133]
NaOH/γ-Al_2O_3	GL:DMC: 1:2; 78 °C,1 h	3 wt%	97.9	96.9/99	4 (90.3)	[143]
KF/Al_2O_3	GL:DMC: 1:2; 75 °C , 2 h, DMF	5 wt %	96	95.8/99.8	3 (93)	[144]
Mg_3La_1	GL:DMC: 1:2 85°C, 1 h	5 wt %	65	63.7/98	4 (69.1)	[122]
Mg-Al mixed oxides	GL:DMC: 1:5 100°C, 2 h	10 wt %	66	66/100	5 (58)	[145]
Mg/Zr/Sr	GL:DMC: 1:5 90°C, 1.5 h	15 wt %	96	56/58.3	5 (50)	[128]

1.4 Solketal

Considering the ever-increasing dependence of the world on the fuel industry, one of the other alternatives is to consume an excess of the GL by deriving fuel oxygenated additives such as solketal from it. Produced from the acid catalysed nucleophilic addition reaction of glycerol with ketone (acetone (AC) or propanone), solketal not only help in increasing the octane number of the fuels but also has wide applications in the pharmaceutical industry, in the food industry as a flavoring agent, also used as a solvent, plasticizer, and surfactant [146]**.**

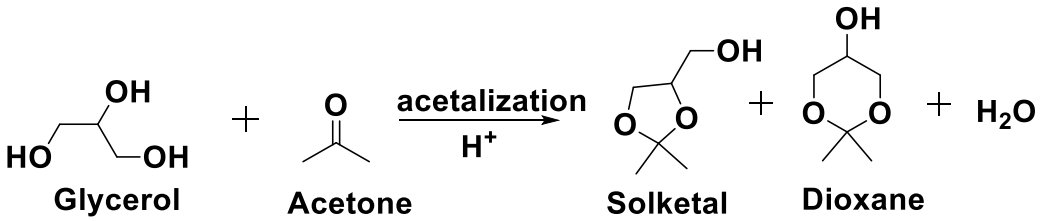

Figure 1.11 Acetalization of glycerol.

Homogeneous acidic catalysts like HCl, *p*TSA, $SnBr_2$, $SnCl_2{\cdot}2H_2O$, SnF_2, [147] employed for the ketalization reactions provided good conversions but reaction neutralization, catalyst separation, and recovery issues associated with them put heterogeneous acid catalysts into the limelight. In order to overcome the thermodynamic as well as kinetic barrier created by the reaction by-product, H_2O [148], acetalization reaction is generally carried out either in excess of the acetone or in the presence of entrainer. Stawicka et al. found that acetalization reaction was carried out more efficiently in the presence of the Bronsted acid [149]. Nonetheless, the formation of H_2O as a side product required the catalyst to be hydrophobic in nature.

Various hydrophobic catalysts like resins, zeolites, silica-supported acid catalysts, transition metal-based catalysts, UiO-66(Hf) MOFs [150], heteropolyacids (HPAs) $HCs_{2.5}H_{0.5}PW_{12}O_{40}$ [151], ($Fe_{4/3}SiW_{12}O_{40}$) [152] mesoporous Ga-silicates [153] are applied for the solketal synthesis, as summarized in **Table 1.4**. Most of the reported catalysts displayed good solketal selectivity. Generally, a high acetone/GL molar ratio and longer reaction time is required for attaining good GL conversion.

Table 1.4 Tabulated view of various catalysts employed for the acetalization and ketalization of glycerol

Catalysts	Conditions	Catalyst (wt%)	Ratio Substrate:GL	GL % Conversion	Selectivity towards solketal (%)	Reusability (cycles)	References
6.8v-MCM-41	60 °C, 1 h	10	6.5:1	95	92	NR	[154]
Nb-HUSY	70 °C, 3 h	2	2:1	58	98	3	[155]
[5%V]Si-ITQ-6	60°C, 2 h	5	3:1	100	99	Activity is retained with acetone washing	[156]
ZrMo-KIT-6	50°C, 4 h	5	8:1	85.8	97.8	5	[157]
SnF_2	25°C, 2 h	1	8:1	96	90	4	[158]
Cu-Mor	100°C, 0.25 h, 500W microwave power	40 mg	3:1	95	98	4	[159]
Nb-Al	50 °C, 6 h	2.7	4:1	84	98	4	[160]
$(C_3H_7)_4N^+$/ PWA	30°C, 2 h	3 wt%	6:1	94	98	3	[161]
$H_3PW_{12}O_{40}$	25°C, 2 h, toulene	1 mol%	20:1	83	98	3	[162]
40 wt%-MoPO	25°C, 2 h	5.4	3:1	100	98	4	[163]
H-Beta Zeolite	25°C,1 h	5	2:1	86	98.5	1	[164]
Amberlyst–36	500psi, 25°C, $2h^{-1}$, ethanol	-	4:1	94	92 (yield)	Decrease in the yield of solketal after each run	[165]
Fe/Al-SBA-15	100°C, 8h	0.1	1:1	58	99	5	[166]
$MSnO_2$	Room temp, 1.5 h	5	1:1	61	96	5	[167]
Nb_2O_5	70°C, 6 h	6.4	1.5:1	80	~92	4	[168]
Hf-TUD-1	80°C, 6 h	3	1:1	52	100	5	[169]
SO_4^{2-}/ZrO_2	25°C, 1.5 h	5	6:1	98	97	NR	[170]
PW_S	70 °C, 3 h	5	6:1	100	97	4	[171]
Nb-SBA-15	25°C, 1 h	100mg	3:1	95	100	4	[172]
$[Cp^*IrCl_2]_2$	40°C, 1 h	Acetone	-	86	98	-	[173]

1.5 DMC-Biodiesel

Besides transforming the excess glycerol into various value-added derivatives, one could put an effort to minimize its production by exploring new methods of glycerol-free biodiesel production [174]. Dimethyl carbonate (DMC) has physical properties similar to methanol and could be used as an alternative to methanol for biodiesel production. Biodiesel (fatty acid methyl esters, FAME) (DMC-BioD) prepared by this method has better fuel properties and oxidation stability because of the miscibility of high oxygen-containing by-products: Fatty acid Glycerol carbonate monoesters (FAGC) and glycerol dicarbonate (GDC) in it [175,176] (**Figure 1.12**).

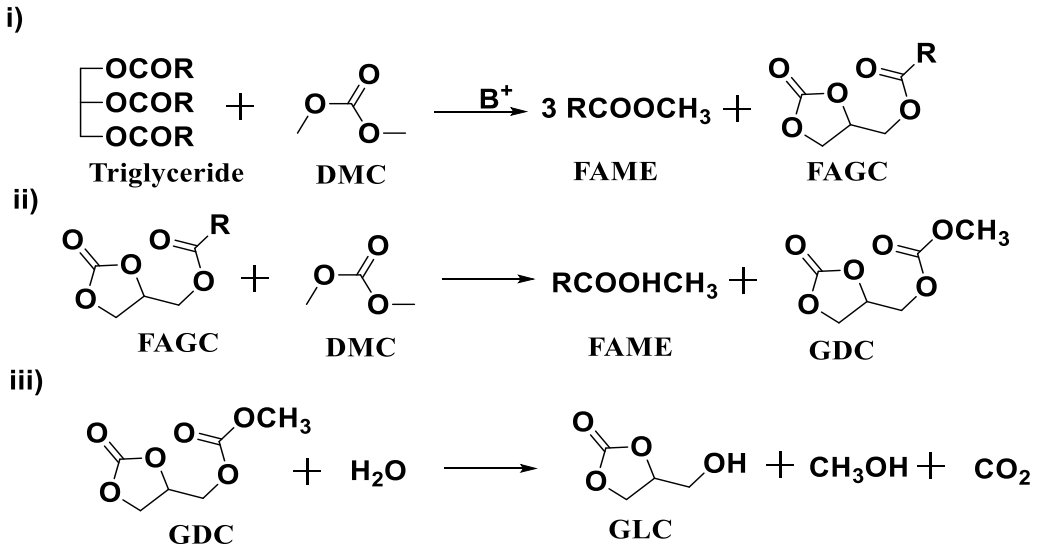

Figure 1.12 Transmethylation of triglyceride with dimethyl carbonate.

Initially, supercritical conditions are applied for DMC-BioD formation, but a prerequisite of high temperature and pressure and partial decomposition of the triglyceride, are few factors of concern [177,178]. In order to make the reaction feasible at moderate conditions, basic and acidic catalysts are employed to carry out DMC-assisted FAME production.

Mostly homogeneous basic catalysts viz., recrystallized $KOCH_3$, K_2CO_3, KOH, NaOH, and $NaOCH_3$ [175,179] are applied to carry out the transesterification reaction, and the difficulty of recovering these catalysts after the reaction is the major obstacle. However, high DMC-BioD yield is obtained from edible and non-edible oils with heterogeneous catalysts viz., Ca-La-Al

mixed metal oxides [180], Mg/Al supported TBD, but with the employment of longer reaction time and high DMC/oil molar ratio. Moreover, reusability studies are less reported and further exploration in this field is required. Few more catalysts employed for the DMC-BioD synthesis are reported in **Table 1.5**.

Table 1.5 Tabulated view of various acidic and basic catalysts employed for the DMC-BioD production.

Catalyst	Oil	Reaction conditions	Catalyst amount (wt %)	Biodiesel yield (%)	Reusability (cycles)	Reference
CaO/KCl	Rapeseed oil	65°C,1 h, Methanol: DMC: Oil 8:1:1	15	96.4	NR	[181]
([IMHPS]x[C18]y	Jatropha curcas oil	80°C, 6 h, DMC: Oil 5:1	260	94	NR	[182]
CaO/NaCl	Rapeseed oil	65°C,1 h, Methanol: DMC: Oil 4:1	15	97.1	6	[183]
[PrSO3HMIM][HSO4]	Rapeseed Oil	110°C , 5 h, DMC: Oil 5:1	25	97.2	NR	[174]
Methane sulphonic acid	Yellow grease oil	70°C, 0.75 h, DMC: Oil 5:1	2	94%	NR	[184]
KF/Al_2O_3	Rapeseed oil	65°C, 2 h, Methanol: DMC: Oil 8:1:1	5	98.8	NR	[185]
Ca-La	Jatropha oil	150°C,2 h, DMC: Oil 4:1	3	99.84	4	[186]
$KOCH_3$	Soyabean oil	200°C, 1 h, DMC: Oil 9:1, 10 bar	5	95.8	NR	[179]
Crystallized $NaOCH_3$	Canola oil	65°C, 1.5 h, DMC: Oil 4:1	1.5	90	NR	[187]
TiO_2/SiO_2	Coconut oil	80°C, 6 h, DMC: Oil 4:1	0.01mmol	88.44	NR	[188]
Triazabicyclodecene	Canola oil	60°C, 2 h, DMC: Oil 3:1	1.5	97.99	NR	[189]

1.6 Conclusions

In the context of deriving new derivatives from the GL, GLC comes out to be one of the promising candidates gaining attention worldwide offering with its wide application in organic synthesis, pharmaceutical, food, and cosmetic industry. Among the three different pathways employed for GLC synthesis, the carboxylation and phosphogenation routes are avoided due to the issue related to the handling of CO_2 and phosgene gases. Transesterification of glycerol with dimethyl carbonate (DMC) is preferred than urea as in glycerolysis; the side product ammonia is formed in large quantity, which limits its industrial implementation. Moreover, conducting the reaction under the reduced pressure, use of solvent or dehydrating agent, and separation of the end products are the other issues related to the carboxylation and glycerolysis pathways. Transesterification, on the other hand, provides good GL conversion under mild reaction conditions. An appropriate basic strength, surface area, and stability of the catalyst play a vital role in elevating the GL conversion. Mostly alkali and alkaline metal-based mixed metal oxides are employed for GLC synthesis due to their strong basic properties. In addition, hydrotalcites with a combination of Lewis and Bronsted basic sites, organo-catalysts, ionic liquids are also practiced for the transesterification reaction providing good results. Despite that, there are still few issues like catalyst reusability, higher reactant ratio and catalyst amount, GLC selectivity that require further attention to develop a more effective and efficient catalyst. Apart from glycerol carbonate, deriving fuel additives from surplus glycerol and minimizing the glycerol production are the other two alternatives that could be opted for attaining sustainability in the supply-demand of glycerol. Fuel additive solketal is derived mainly from the acid-catalyzed acetalization of glycerol. Due to the formation of water as a by-product in the acetalization reaction, catalysts get easily poisoned, thus halting their applicability. Employment of hydrophobic catalyst, a greater amount of acetone, and low reaction temperature are the few prerequisites for attaining maximum glycerol conversion. However, leaching of the catalysts, poor glycerol conversion, high acetone to glycerol molar ratio are few factors that are required to be addressed. Instead of converting excess glycerol to its derivatives, another way is to produce glycerol-free biodiesel by adopting dimethyl carbonate as methylating source instead of methanol. Various alkali and alkaline-based basic catalysts are employed so far for DMC-BioD synthesis, but this area is less explored.

Literature Gaps

Diverse glycerol derivatives have been formed by utilizing the applications of various homogeneous and heterogeneous catalysts. However, certain gaps have been identified based on the literature survey.

a) In most of the reports, employed homogeneous catalysts demonstrate higher catalytic activity and selectivity towards the desired products but causes reactor corrosion and demand extensive product purification steps. Moreover, water cannot be employed to separate glycerol carbonate as later is miscible in water.

b) Most of the reported heterogeneous catalysts provide insufficient conversion levels and GLC selectivity compared to homogeneous catalysts. Very few of the reported catalysts exhibited 100 % selectivity towards glycerol carbonate. Extreme reaction conditions such as higher reactant ratio, temperature, catalyst amount are employed to achieve maximum GL conversion and GLC selectivity.

c) Majority of the employed CaO based heterogeneous catalysts for GLC synthesis suffered from poor reusability and active site poisoning. Catalysts support such as ZrO_2, TiO_2, SiO_2 are less explored for enhancing the stability of the heterogeneous catalysts applied for the GLC formation.

d) Considering the presence of traces of water in the crude glycerol obtained from the biodiesel industry, moisture resistant properties of the applied heterogeneous catalysts are rarely studied.

Objectives

Based on the literature gaps following objectives of the present thesis have been defined.

To prepare a series of mesoporous silica, ZrO_2, TiO_2, and alkaline earth-based solid catalysts by co-precipitation and wet impregnation method.

Application of the prepared catalysts for the preparation of glycerol derivatives such as glycerol carbonate, solketal, and DMC-BioD.

To improve the moisture resistance of the catalysts by modifying the surface functional groups.

To study the stability and reusability of the prepared catalysts.

References

[1] A. Behr, J. Eilting, K. Irawadi, J. Leschinski, F. Lindner, Improved utilisation of renewable resources: New important derivatives of glycerol, Green Chem. 10 (2008) 13–30. https://doi.org/10.1039/b710561d.

[2] N. Rahmat, A.Z. Abdullah, A.R. Mohamed, Recent progress on innovative and potential technologies for glycerol transformation into fuel additives: A critical review, Renew. Sustain. Energy Rev. 14 (2010) 987–1000. https://doi.org/10.1016/j.rser.2009.11.010.

[3] Z. Wang, J. Zhuge, H. Fang, B.A. Prior, Glycerol production by microbial fermentation: A review, Biotechnol. Adv. 19 (2001) 201–223. https://doi.org/10.1016/S0734-9750(01)00060-X.

[4] M.J. Wernke, Glycerol, Encycl. Toxicol. Third Ed. (2014) 754–756. https://doi.org/10.1016/B978-0-12-386454-3.00510-8.

[5] J. Kaur, A.K. Sarma, M.K. Jha, P. Gera, Valorisation of crude glycerol to value-added products: Perspectives of process technology, economics and environmental issues, Biotechnol. Reports 27 (2020) e00487. https://doi.org/10.1016/j.btre.2020.e00487.

[6] N.I.W. Azelee, A.N.M. Ramli, N.H.A. Manas, N. Salamun, R.C. Man, H. El Enshasy, Glycerol in food, cosmetics and pharmaceutical industries: Basics and new applications, Int. J. Sci. Technol. Res. 8 (2019) 553–558.

[7] H.W. Tan, A.R. Abdul Aziz, M.K. Aroua, Glycerol production and its applications as a raw material: A review, Renew. Sustain. Energy Rev. 27 (2013) 118–127. https://doi.org/10.1016/j.rser.2013.06.035.

[8] N. Zoratto, R. Matassa, E. Montanari, G. Familiari, S. Petralito, T. Coviello, C. Di Meo, P. Matricardi, Glycerol as a green solvent for enhancing the formulation of dextran methacrylate and gellan-based semi-interpenetrating polymer networks, J. Mater. Sci. 55 (2020) 9562–9577. https://doi.org/10.1007/s10853-020-04732-1

[9] A. Singhabhandhu, T. Tezuka, A perspective on incorporation of glycerin purification

process in biodiesel plants using waste cooking oil as feedstock, Energy 35 (2010) 2493–2504. https://doi.org/10.1016/j.energy.2010.02.047.

[10] I. Zahid, M. Ayoub, B.B. Abdullah, M.H. Nazir, M. Ameen, Zulqarnain, M.H. Mohd Yusoff, A. Inayat, M. Danish, Production of fuel additive solketal via catalytic conversion of biodiesel-derived glycerol, Ind. Eng. Chem. Res. 59 (2020) 20961–20978. https://doi.org/10.1021/acs.iecr.0c04123.

[11] A. Kazmi, J. Clark, Biomass to chemicals, Elsevier Ltd., 2012. https://doi.org/10.1016/B978-0-08-087872-0.00526-6.

[12] S. Sahani, S.N. Upadhyay, Y.C. Sharma, Critical review on production of glycerol carbonate from bproduct glycerol through transesterification, Ind. Eng. Chem. Res. 60 (2021) 67–88. https://doi.org/10.1021/acs.iecr.0c05011.

[13] I. Ntaikou, I. Koumelis, C. Tsitsilianis, J. Parthenios, G. Lyberatos, Comparison of yields and properties of microbial polyhydroxyalkanoates generated from waste glycerol based substrates, Int. J. Biol. Macromol. 112 (2018) 273–283. https://doi.org/10.1016/j.ijbiomac.2018.01.175.

[14] D. Singh, D. Sharma, S.L. Soni, S. Sharma, P. Kumar Sharma, A. Jhalani, A review on feedstocks, production processes, and yield for different generations of biodiesel, Fuel 262 (2020) 116553. https://doi.org/10.1016/j.fuel.2019.116553.

[15] C. Len, R. Luque, Continuous flow transformations of glycerol to valuable products: an overview, Sustain. Chem. Process. 2 (2014) 1–10. https://doi.org/10.1186/2043-7129-2-1.

[16] N. Vivek, R. Sindhu, A. Madhavan, A.J. Anju, E. Castro, V. Faraco, A. Pandey, P. Binod, Recent advances in the production of value added chemicals and lipids utilizing biodiesel industry generated crude glycerol as a substrate – Metabolic aspects, challenges and possibilities: An overview, Bioresour. Technol. 239 (2017) 507–517. https://doi.org/10.1016/j.biortech.2017.05.056.

[17] M.R. Monteiro, C.L. Kugelmeier, R.S. Pinheiro, M.O. Batalha, A. da Silva César, Glycerol from biodiesel production: Technological paths for sustainability, Renew.

Sustain. Energy Rev. 88 (2018) 109–122. https://doi.org/10.1016/j.rser.2018.02.019.

[18] L.J. Konwar, P. Mäki-Arvela, N. Kumar, J.P. Mikkola, A.K. Sarma, D. Deka, Selective esterification of fatty acids with glycerol to monoglycerides over $–SO_3H$ functionalized carbon catalysts, React. Kinet. Mech. Catal. 119 (2016) 121–138. https://doi.org/10.1007/s11144-016-1040-7.

[19] R.R. Ting, R. Agapay, A.E. Angkawijaya, P.L. Tran Nguyen, C.T. Truong, Y.H. Ju, Diglyceride production via noncatalyzed esterification of glycerol and oleic acid, Asia-Pacific J. Chem. Eng. 14 (2019). https://doi.org/10.1002/apj.2383.

[20] M. Bindea, B. Rusu, A. Rusu, M. Trif, L.F. Leopold, F. Dulf, D.C. Vodnar, Valorification of crude glycerol for pure fractions of docosahexaenoic acid and β-carotene production by using Schizochytrium limacinum and Blakeslea trispora, Microb. Cell Fact. 17 (2018) 1–13. https://doi.org/10.1186/s12934-018-0945-4.

[21] X. Luo, X. Ge, S. Cui, Y. Li, Value-added processing of crude glycerol into chemicals and polymers, Bioresour. Technol. 215 (2016) 144–154. https://doi.org/10.1016/j.biortech.2016.03.042.

[22] T. Zhan, W. Liu, J. Teng, C. Yue, D. Li, S. Wang, H. Tan, Selective oxidation of glycerol to tartronic acid over Pt/N-doped mesoporous carbon with extra framework magnesium catalysts under base-free conditions, Chem. Commun. 55 (2019) 2620–2623. https://doi.org/10.1039/c8cc10273b.

[23] F. Yang, M.A. Hanna, R. Sun, Value added use for crude glycerol-a byproduct of biodiesel production, Biotechnol. Biofuels. 5 (2012) 1–10.

[24] M. Ayoub, A.Z. Abdullah, Critical review on the current scenario and significance of crude glycerol resulting from biodiesel industry towards more sustainable renewable energy industry, Renew. Sustain. Energy Rev. 16 (2012) 2671–2686. https://doi.org/10.1016/j.rser.2012.01.054.

[25] N. Galy, R. Nguyen, P. Blach, S. Sambou, D. Luart, C. Len, Glycerol oligomerization in continuous flow reactor, J. Ind. Eng. Chem. 51 (2017) 312–318.

https://doi.org/10.1016/j.jiec.2017.03.020.

[26] J.A. Sullivan, S. Burnham, The selective oxidation of glycerol over model Au/TiO_2 catalysts-The influcence of glycerol purity on conversion and product selectivity, Catal. Commun. 56 (2014) 72-75. https://doi.org/10.1016/j.catcom.2014.06.026.

[27] N.H. Zamzuri, R. Mat, N.A. Saidina Amin, A. Talebian-Kiakalaieh, Hydrogen production from catalytic steam reforming of glycerol over various supported nickel catalysts, Int. J. Hydrogen Energy 42 (2017) 9087–9098. https://doi.org/10.1016/j.ijhydene.2016.05.084.

[28] G.M. Lari, G. Pastore, C. Mondelli, J. Pérez-Ramírez, Towards sustainable manufacture of epichlorohydrin from glycerol using hydrotalcite-derived basic oxides, Green Chem. 20 (2018) 148–159. https://doi.org/10.1039/c7gc02610b.

[29] X. Wang, G. Wu, X. Zhang, D. Wang, J. Lan, J. Li, Selective oxidation of glycerol to glyceraldehyde with H_2O_2 catalyzed by CuNiAl hydrotalcites supported BiOCl in neutral media, Catal. Letters 149 (2019) 1046–1056. https://doi.org/10.1007/s10562-019-02689-8.

[30] H. Yan, S. Yao, W. Liang, S. Zhao, X. Jin, X. Feng, Y. Liu, X. Chen, C. Yang, Ni–Co oxide catalysts with lattice distortions for enhanced oxidation of glycerol to glyceric acid, J. Catal. 381 (2020) 248–260. https://doi.org/10.1016/j.jcat.2019.11.001.

[31] T. Jedsukontorn, N. Saito, M. Hunsom, Photocatalytic behavior of metal-decorated TiO_2 and their catalytic activity for transformation of glycerol to value added compounds, Mol. Catal. 432 (2017) 160–171. https://doi.org/10.1016/j.mcat.2017.02.022.

[32] J. Xiberras, M. Klein, E. de Hulster, R. Mans, E. Nevoigt, Engineering Saccharomyces cerevisiae for succinic acid production from glycerol and carbon dioxide, Front. Bioeng. Biotechnol. 8 (2020) 1–13. https://doi.org/10.3389/fbioe.2020.00566.

[33] I.C. Freitas, R.L. Manfro, M.M.V.M. Souza, Hydrogenolysis of glycerol to propylene glycol in continuous system without hydrogen addition over Cu-Ni catalysts, Appl. Catal. B Environ. 220 (2018) 31–41. https://doi.org/10.1016/j.apcatb.2017.08.030.

[34] T.H. Kang, J.H. Choi, Y. Bang, J. Yoo, J.H. Song, W. Joe, J.S. Choi, I.K. Song, Dehydration of glycerin to acrolein over $H_3PW_{12}O_{40}$ heteropolyacid catalyst supported on

silica-alumina, J. Mol. Catal. A Chem. 396 (2015) 282–289. https://doi.org/10.1016/j.molcata.2014.10.015.

[35] A.D. da Silva Ruy, R.M. de Brito Alves, T.L. Reis Hewer, D. de Aguiar Pontes, L.S. Gomes Teixeira, L.A. Magalhães Pontes, Catalysts for glycerol hydrogenolysis to 1,3-propanediol: A review of chemical routes and market, Catal. Today 381 (2021) 243-253. https://doi.org/10.1016/j.cattod.2020.06.035.

[36] S. Bruniaux, R.S. Varma, C. Len, A novel strategy for selective O-methylation of glycerol in subcritical methanol, Front. Chem. 7 (2019) 1–7. https://doi.org/10.3389/fchem.2019.00357.

[37] Y. Ji, R. Recent development of heterogeneous catalysis in the transesterification of glycerol to glycerol carbonate, Catalysts 9 (2019) 581. https://doi.org/10.3390/catal9070581.

[38] A. Kostyniuk, D. Bajec, P. Djinović, B. Likozar, One-step synthesis of glycidol from glycerol in a gas-phase packed-bed continuous flow reactor over HZSM-5 zeolite catalysts modified by $CsNO_3$, Chem. Eng. J. 394 (2020) 124945. https://doi.org/10.1016/j.cej.2020.124945.

[39] G. Pradhan, Y.C. Sharma, Green synthesis of glycerol carbonate by transesterification of bio glycerol with dimethyl carbonate over Mg/ZnO: A highly efficient heterogeneous catalyst, Fuel 284 (2021) 118966. https://doi.org/10.1016/j.fuel.2020.118966.

[40] M. Benoit, Y. Brissonnet, E. Guélou, K. De-Oliveira-Vigier, J. Barrault, F. Jérôme, Acid-catalyzed dehydration of fructose and inulin with glycerol or glycerol carbonate as renewably sourced co-solvent, ChemSusChem. 3 (2010) 1304–1309. https://doi.org/10.1002/cssc.201000162.

[41] S. Christy, A. Noschese, M. Lomelí-Rodriguez, N. Greeves, J.A. Lopez-Sanchez, Recent progress in the synthesis and applications of glycerol carbonate, Curr. Opin. Green Sustain. Chem. 14 (2018) 99–107. https://doi.org/10.1016/j.cogsc.2018.09.003.

[42] P. Moussou, L. Danoux, L. Bailey, V. Gillon, Cosmetic composition comprising a

combination of a sugar fatty acid ester with a plant extract of WALTHERA INDICA or PISUM SATIVUM for skin whitening,United States Patent 9949917B2, 2018.

[43] A. Galadima, O. Muraza, Sustainable production of glycerol carbonate from by-product in biodiesel plant, Waste Biomass Valor. 8 (2017) 141–152. https://doi.org/10.1007/s12649-016-9560-y.

[44] M. Ebrahimi, O.B. Villaflores, E.E. Ordono, A.R. Caparanga, Effects of acidified aqueous glycerol and glycerol carbonate pretreatment of rice husk on the enzymatic digestibility, structural characteristics, and bioethanol production, Bioresour. Technol. 228 (2017) 264–271. https://doi.org/10.1016/j.biortech.2016.12.106.

[45] P. de Caro, M. Bandres, M. Urrutigoïty, C. Cecutti, S. Thiebaud-Roux, Recent progress in synthesis of glycerol carbonate and evaluation of its plasticizing properties, Front. Chem. 7 (2019) 1–13. https://doi.org/10.3389/fchem.2019.00308.

[46] M.O. Sonnati, S. Amigoni, E.P. Taffin De Givenchy, T. Darmanin, O. Choulet, F. Guittard, Glycerol carbonate as a versatile building block for tomorrow: Synthesis, reactivity, properties and applications, Green Chem. 15 (2013) 283–306. https://doi.org/10.1039/c2gc36525a.

[47] C.W. Chang, Z.J. Gong, N.C. Huang, C.Y. Wang, W.Y. Yu, MgO nanoparticles confined in ZIF-8 as acid-base bifunctional catalysts for enhanced glycerol carbonate production from transesterification of glycerol and dimethyl carbonate, Catal. Today 351 (2020) 21–29. https://doi.org/10.1016/j.cattod.2019.03.007.

[48] M. Kargar, R. Hekmatshoar, M. Ghandi, A. Mostashari, Use of glycerol carbonate in an efficient, one-pot and solvent free synthesis of 1,3-sn-Diglycerides, J. Am. Oil Chem. Soc. 90 (2013) 259-264. https://doi.org/10.1007/s11746-012-2165-0.

[49] A. Zanoni, G. Gardoni, M. Sponchioni, D. Moscatelli, Valorisation of glycerol and CO_2 to produce biodegradable polymer nanoparticles with a high percentage of bio-based components, J. CO_2 Util. 40 (2020) 101192. https://doi.org/10.1016/j.jcou.2020.101192.

[50] J.R. Ochoa-Gómez, O. Gómez-Jiménez-Aberasturi, C.A. Ramírez-López, J. Nieto-Mestre,

B. Maestro-Madurga, M. Belsué, Synthesis of glycerol carbonate from 3-chloro-1,2-propanediol and carbon dioxide using triethylamine as both solvent and CO2 fixation-activation agent, Chem. Eng. J. 175 (2011) 505–511. https://doi.org/10.1016/j.cej.2011.09.081.

[51] S. Dabral, T. Schaub, The Use of Carbon Dioxide (CO_2) as a Building Block in Organic Synthesis from an Industrial Perspective, Adv. Synth. Catal. 361 (2019) 223–246. https://doi.org/10.1002/adsc.201801215.

[52] J. Li, T. Wang, Chemical equilibrium of glycerol carbonate synthesis from glycerol, J. Chem. Thermodyn. 43 (2011) 731–736. https://doi.org/10.1016/j.jct.2010.12.013.

[53] J. Ma, J. Song, H. Liu, J. Liu, Z. Zhang, T. Jiang, H. Fan, B. Han, One-pot conversion of CO_2 and glycerol to value-added products using propylene oxide as the coupling agent, Green Chem. 14 (2012) 1743–1748. https://doi.org/10.1039/c2gc35150a.

[54] J. Liu, Y. Li, J. Zhang, D. He, Glycerol carbonylation with CO_2 to glycerol carbonate over CeO_2 catalyst and the influence of CeO_2 preparation methods and reaction parameters, Appl. Catal. A Gen. 513 (2016) 9–18. https://doi.org/10.1016/j.apcata.2015.12.030.

[55] J. Liu, Y. Li, H. Liu, D. He, Transformation of CO_2 and glycerol to glycerol carbonate over CeO_2–ZrO_2 solid solution —— effect of Zr doping, Biomass Bioenergy 118 (2018) 74–83. https://doi.org/10.1016/j.biombioe.2018.08.004.

[56] Q. Zhang, H.Y. Yuan, X.T. Lin, N. Fukaya, T. Fujitani, K. Sato, J.C. Choi, Calcium carbide as a dehydrating agent for the synthesis of carbamates, glycerol carbonate, and cyclic carbonates from carbon dioxide, Green Chem. 22 (2020) 4231–4239. https://doi.org/10.1039/d0gc01402h.

[57] X. Su, W. Lin, H. Cheng, C. Zhang, Y. Wang, X. Yu, Z. Wu, F. Zhao, Metal-free catalytic conversion of CO_2 and glycerol to glycerol carbonate, Green Chem. 19 (2017) 1775–1781. https://doi.org/10.1039/c7gc00260b.

[58] C. Collett, O. Mašek, N. Razali, J. McGregor, Influence of biochar composition and source material on catalytic performance: the carboxylation of glycerol with CO_2 as a case

study, Catalysts10 (2020) 1–20. https://doi.org/10.3390/catal10091067.

[59] X. Song, Y. Wu, D. Pan, J. Zhang, S. Xu, L. Gao, R. Wei, G. Xiao, Functionalized DVB-based polymer catalysts for glycerol and CO_2 catalytic conversion, J. CO_2 Util. 28 (2018) 326–334. https://doi.org/10.1016/j.jcou.2018.10.015.

[60] O. Gómez-Jiménez-Aberasturi, J.R. Ochoa-Gómez, A. Pesquera-Rodríguez, C. Ramírez-López, A. Alonso-Vicario, J. Torrecilla-Soria, Solvent-free synthesis of glycerol carbonate and glycidol from 3-chloro-1,2-propanediol and potassium (hydrogen) carbonate, J. Chem. Technol. Biotechnol. 85 (2010) 1663–1670. https://doi.org/10.1002/jctb.2478.

[61] M. Thommes, K. Kaneko, A. V. Neimark, J.P. Olivier, F. Rodriguez-Reinoso, J. Rouquerol, K.S.W. Sing, Physisorption of gases, with special reference to the evaluation of surface area and pore size distribution (IUPAC Technical Report), Pure Appl. Chem. 87 (2015) 1051–1069. https://doi.org/10.1515/pac-2014-1117.

[62] J. George, Y. Patel, S.M. Pillai, P. Munshi, Methanol assisted selective formation of 1,2-glycerol carbonate from glycerol and carbon dioxide using nBu_2SnO as a catalyst, J. Mol. Catal. A Chem. 304 (2009) 1–7. https://doi.org/10.1016/j.molcata.2009.01.010.

[63] M. Aresta, A. Dibenedetto, F. Nocito, C. Pastore, A study on the carboxylation of glycerol to glycerol carbonate with carbon dioxide: The role of the catalyst, solvent and reaction conditions, J. Mol. Catal. A Chem. 257 (2006) 149–153. https://doi.org/10.1016/j.molcata.2006.05.021.

[64] J. Zhang, D. He, Synthesis of glycerol carbonate and monoacetin from glycerol and carbon dioxide over Cu catalysts: The role of supports, J. Chem. Technol. Biotechnol. 90 (2015) 1077–1085. https://doi.org/10.1002/jctb.4414.

[65] J. Zhang, D. He, Surface properties of Cu/La_2O_3 and its catalytic performance in the synthesis of glycerol carbonate and monoacetin from glycerol and carbon dioxide, J. Colloid Interface Sci. 419 (2014) 31–38. https://doi.org/10.1016/j.jcis.2013.12.049.

[66] J. Liu, D. He, Transformation of CO_2 with glycerol to glycerol carbonate by a novel ZnWO4-ZnO catalyst, J. CO_2 Util. 26 (2018) 370–379.

https://doi.org/10.1016/j.jcou.2018.05.025.

[67] H. Li, X. Jiao, L. Li, N. Zhao, F. Xiao, W. Wei, Y. Sun, B. Zhang, Synthesis of glycerol carbonate by direct carbonylation of glycerol with CO_2 over solid catalysts derived from Zn/Al/La and Zn/Al/La/M (M = Li, Mg and Zr) hydrotalcites, Catal. Sci. Technol. 5 (2015) 989–1005. https://doi.org/10.1039/c4cy01237b.

[68] H. Li, C. Xin, X. Jiao, N. Zhao, F. Xiao, L. Li, W. Wei, Y. Sun, Direct carbonylation of glycerol with CO_2 to glycerol carbonate over Zn/Al/La/X (X = F, Cl, Br) catalysts: The influence of the interlayer anion, J. Mol. Catal. A Chem. 402 (2015) 71–78. https://doi.org/10.1016/j.molcata.2015.03.012.

[69] J.H. Park, J.S. Choi, S.K. Woo, S.D. Lee, M. Cheong, H.S. Kim, H. Lee, Isolation and characterization of intermediate catalytic species in the Zn-catalyzed glycerolysis of urea, Appl. Catal. A Gen. 433–434 (2012) 35–40. https://doi.org/10.1016/j.apcata.2012.04.031.

[70] S.E. Kondawar, R.B. Mane, A. Vasishta, S.B. More, S.D. Dhengale, C. V. Rode, Carbonylation of glycerol with urea to glycerol carbonate over supported Zn catalysts, Appl. Petrochemical Res. 7 (2017) 41–53. https://doi.org/10.1007/s13203-017-0177-2.

[71] F. Rubio-Marcos, V. Calvino-Casilda, M.A. Bañares, J.F. Fernandez, Novel hierarchical Co_3O_4/ZnO mixtures by dry nanodispersion and their catalytic application in the carbonylation of glycerol, J. Catal. 275 (2010) 288–293. https://doi.org/10.1016/j.jcat.2010.08.009.

[72] F. Rubio-Marcos, V. Calvino-Casilda, M.A. Bañares, J.F. Fernandez, Control of the interphases formation degree in Co_3O_4/ZnO Catalysts, ChemCatChem. 5 (2013) 1431–1440. https://doi.org/10.1002/cctc.201200620.

[73] Y. Lü, Y. Jiang, Q. Zhou, Y. Li, L. Chen, Q. Kuang, Z. Xie, L. Zheng, Heterometallic metal-organic framework-templated synthesis of porous Co_3O_4/ZnO nanocage catalysts for the carbonylation of glycerol, J. Solid State Chem. 256 (2017) 93–100. https://doi.org/10.1016/j.jssc.2017.08.035.

[74] D. Wang, X. Zhang, X. Cong, S. Liu, D. Zhou, Influence of Zr on the performance of Mg-

Al catalysts via hydrotalcite-like precursors for the synthesis of glycerol carbonate from urea and glycerol, Appl. Catal. A Gen. 555 (2018) 36–46. https://doi.org/10.1016/j.apcata.2018.02.009.

[75] M. Sharath Babu, A. Srivani, G. Parameswaram, G. Veerabhadram, N. Lingaiah, Understanding the role of tantalum in heteropoly tungstate catalysts for the synthesis of glycerol carbonate from glycerol and urea, Catal. Letters 145 (2015) 1784–1791. https://doi.org/10.1007/s10562-015-1582-8.

[76] A. Srikanth, B. Viswanadham, V.P. Kumar, N.R. Anipindi, K.V.R. Chary, Synthesis and characterization of Cs-exchanged heteropolyacid catalysts functionalized with Sn for carbonolysis of glycerol to glycerol carbonate, Appl. Petrochemical Res. 6 (2016) 145–153. https://doi.org/10.1007/s13203-015-0140-z.

[77] K. Jagadeeswaraiah, C.R. Kumar, P.S.S. Prasad, N. Lingaiah, Incorporation of Zn^{2+} ions into the secondary structure of heteropoly tungstate: Catalytic efficiency for synthesis of glycerol carbonate from glycerol and urea, Catal. Sci. Technol. 4 (2014) 2969–2977. https://doi.org/10.1039/c4cy00253a.

[78] C.R. Kumar, K. Jagadeeswaraiah, P.S.S. Prasad, N. Lingaiah, Samarium-exchanged heteropoly tungstate: An efficient solid acid catalyst for the synthesis of glycerol carbonate from glycerol and benzylation of anisole, ChemCatChem. 4 (2012) 1360–1367. https://doi.org/10.1002/cctc.201200110.

[79] H. Zhang, H. Li, A. Wang, C. (Charles) Xu, S. Yang, Progress of catalytic valorization of bio-glycerol with urea into glycerol carbonate as a monomer for polymeric materials, Adv. Polym. Technol. 2020 (2020) 1–17. https://doi.org/10.1155/2020/7207068.

[80] D.W. Kim, M.S. Park, M. Selvaraj, G.A. Park, S. Do Lee, D.W. Park, Catalytic performance of polymer-supported ionic liquids in the synthesis of glycerol carbonate from glycerol and urea, Res. Chem. Intermed. 37 (2011) 1305–1312. https://doi.org/10.1007/s11164-011-0398-4.

[81] D.W. Kim, K.A. Park, M.J. Kim, D.H. Kang, J.G. Yang, D.W. Park, Synthesis of glycerol carbonate from urea and glycerol using polymer-supported metal containing ionic liquid

catalysts, Appl. Catal. A Gen. 473 (2014) 31–40. https://doi.org/10.1016/j.apcata.2013.12.032.

[82] B. Mallesham, A. Rangaswamy, B.G. Rao, T.V. Rao, B.M. Reddy, Solvent-free production of glycerol carbonate from bioglycerol with urea over nanostructured promoted SnO_2 Catalysts, Catal. Letters 150 (2020) 3626–3641. https://doi.org/10.1007/s10562-020-03241-9.

[83] H. Nguyen-Phu, L.T. Do, E.W. Shin, Investigation of glycerolysis of urea over various ZnMeO (Me = Co, Cr, and Fe) mixed oxide catalysts, Catal. Today 352 (2020) 80–87. https://doi.org/10.1016/j.cattod.2019.09.017.

[84] D.M. Chaves, M.J. Da Silva, A selective synthesis of glycerol carbonate from glycerol and urea over $Sn(OH)_2$: A solid and recyclable: In situ generated catalyst, New J. Chem. 43 (2019) 3698–3706. https://doi.org/10.1039/c8nj05635h.

[85] K. Jagadeeswaraiah, C. Ramesh Kumar, A. Rajashekar, A. Srivani, N. Lingaiah, The role of tungsten oxide species supported on titania catalysts for the synthesis of glycerol carbonate from glycerol and urea, Catal. Letters 146 (2016) 692–700. https://doi.org/10.1007/s10562-016-1694-9.

[86] D. Wang, X. Zhang, C. Liu, T. Cheng, Synthesis of glycerol carbonate from glycerol and urea over lanthanum compounds, React. Kinet. Mech. Catal. 115 (2015) 597–609. https://doi.org/10.1007/s11144-015-0858-8.

[87] S. Do Lee, G.A. Park, D.W. Kim, D.W. Park, Catalytic performance of functionalized IRMOF-3 for the synthesis of glycerol carbonate from glycerol and urea, J. Nanosci. Nanotechnol. 14 (2014) 4551–4556. https://doi.org/10.1166/jnn.2014.8255.

[88] K. Jagadeeswaraiah, C.R. Kumar, P.S.S. Prasad, S. Loridant, N. Lingaiah, Synthesis of glycerol carbonate from glycerol and urea over tin-tungsten mixed oxide catalysts, Appl. Catal. A Gen. 469 (2014) 165–172. https://doi.org/10.1016/j.apcata.2013.09.041.

[89] J. Zhang, D. He, Lanthanum-based mixed oxides for the synthesis of glycerol carbonate from glycerol and urea, React. Kinet. Mech. Catal. 113 (2014) 375–392.

https://doi.org/10.1007/s11144-014-0739-6.

[90] M. Hasbi Ab Rahim, Q. He, J.A. Lopez-Sanchez, C. Hammond, N. Dimitratos, M. Sankar, A.F. Carley, C.J. Kiely, D.W. Knight, G.J. Hutchings, Gold, palladium and gold-palladium supported nanoparticles for the synthesis of glycerol carbonate from glycerol and urea, Catal. Sci. Technol. 2 (2012) 1914–1924. https://doi.org/10.1039/c2cy20288c.

[91] C. Hammond, J.A. Lopez-Sanchez, M.H. Ab Rahim, N. Dimitratos, R.L. Jenkins, A.F. Carley, Q. He, C.J. Kiely, D.W. Knight, G.J. Hutchings, Synthesis of glycerol carbonate from glycerol and urea with gold-based catalysts, Dalt. Trans. 40 (2011) 3927-3937. https://doi.org/10.1039/C0DT01389G.

[92] M. Aresta, A. Dibenedetto, F. Nocito, C. Ferragina, Valorization of bio-glycerol: New catalytic materials for the synthesis of glycerol carbonate via glycerolysis of urea, J. Catal. 268 (2009) 106–114. https://doi.org/10.1016/j.jcat.2009.09.008.

[93] W.K. Teng, G.C. Ngoh, R. Yusoff, M.K. Aroua, A review on the performance of glycerol carbonate production via catalytic transesterification: Effects of influencing parameters, Energy Convers. Manag. 88 (2014) 484–497. https://doi.org/10.1016/j.enconman.2014.08.036.

[94] J.R. Ochoa-Gómez, O. Gómez-Jiménez-Aberasturi, B. Maestro-Madurga, A. Pesquera-Rodríguez, C. Ramírez-López, L. Lorenzo-Ibarreta, J. Torrecilla-Soria, M.C. Villarán-Velasco, Synthesis of glycerol carbonate from glycerol and dimethyl carbonate by transesterification: Catalyst screening and reaction optimization, Appl. Catal. A Gen. 366 (2009) 315–324. https://doi.org/10.1016/j.apcata.2009.07.020.

[95] P. Devi, U. Das, A.K. Dalai, Production of glycerol carbonate using a novel Ti-SBA-15 catalyst, Chem. Eng. J. 346 (2018) 477–488. https://doi.org/10.1016/j.cej.2018.04.030.

[96] X. Song, D. Pan, Y. Wu, P. Cheng, R. Wei, L. Gao, J. Zhang, G. Xiao, Synthesis of glycerol carbonate over porous La-Zr based catalysts: The role of strong and super basic sites, J. Alloys Compd. 750 (2018) 828–837. https://doi.org/10.1016/j.jallcom.2018.03.392.

[97] J. Li, T. Wang, On the deactivation of alkali solid catalysts for the synthesis of glycerol carbonate from glycerol and dimethyl carbonate, React. Kinet. Mech. Catal. 102 (2011) 113–126. https://doi.org/10.1007/s11144-010-0259-y.

[98] F.S.H. Simanjuntak, T.K. Kim, S.D. Lee, B.S. Ahn, H.S. Kim, H. Lee, CaO-catalyzed synthesis of glycerol carbonate from glycerol and dimethyl carbonate: Isolation and characterization of an active Ca species, Appl. Catal. A Gen. 401 (2011) 220–225. https://doi.org/10.1016/j.apcata.2011.05.024.

[99] P. Kumar, P. With, V.C. Srivastava, R. Gläser, I.M. Mishra, Glycerol carbonate synthesis by hierarchically structured catalysts: Catalytic activity and characterization, Ind. Eng. Chem. Res. 54 (2015) 12543–12552. https://doi.org/10.1021/acs.iecr.5b03644.

[100] K. Hu, H. Wang, Y. Liu, C. Yang, KNO_3/CaO as cost-effective heterogeneous catalyst for the synthesis of glycerol carbonate from glycerol and dimethyl carbonate, J. Ind. Eng. Chem. 28 (2015) 334–343. https://doi.org/10.1016/J.JIEC.2015.03.012.

[101] P. Lu, H. Wang, K. Hu, Synthesis of glycerol carbonate from glycerol and dimethyl carbonate over the extruded CaO-based catalyst, Chem. Eng. J. 228 (2013) 147–154. https://doi.org/10.1016/j.cej.2013.04.109.

[102] A. Kaur, A. Ali, Surface-modified CaO catalyst for the production of glycerol carbonate, ChemistrySelect 6 (2021) 6102-6114.

[103] W. Roschat, S. Phewphong, T. Kaewpuang, V. Promarak, Synthesis of glycerol carbonate from transesterification of glycerol with dimethyl carbonate catalyzed by CaO from natural sources as green and economical catalyst, Mater. Today Proc. 5 (2018) 13909–13915. https://doi.org/10.1016/j.matpr.2018.02.039.

[104] Y.T. Algoufi, G. Kabir, B.H. Hameed, Synthesis of glycerol carbonate from biodiesel by-product glycerol over calcined dolomite, J. Taiwan Inst. Chem. Eng. 70 (2017) 179–187. https://doi.org/10.1016/j.jtice.2016.10.039.

[105] M. Manikandan, P. Sangeetha, Optimizing the surface properties of MgO nanoparticles towards the transesterification of glycerol to glycerol carbonate, ChemistrySelect. 4

(2019) 6672–6678. https://doi.org/10.1002/slct.201901298.

[106] Z. Bai, Y. Zheng, W. Han, Y. Ji, T. Yan, Y. Tang, G. Chen, Z. Zhang, Development of a trapezoidal MgO catalyst for highly-efficient transesterification of glycerol and dimethyl carbonate, CrystEngComm. 20 (2018) 4090-4098. https://doi.org/10.1039/C8CE00808F.

[107] E.A.R. Assirey, Perovskite synthesis, properties and their related biochemical and industrial application, Saudi Pharm. J. 27 (2019) 817–829. https://doi.org/10.1016/j.jsps.2019.05.003.

[108] N. Labhasetwar, G. Saravanan, S. Kumar Megarajan, N. Manwar, R. Khobragade, P. Doggali, F. Grasset, Perovskite-type catalytic materials for environmental applications, Sci. Technol. Adv. Mater. 16 (2015) 1–13. https://doi.org/10.1088/1468-6996/16/3/036002.

[109] D. Phadtare, S. Kondawar, A. Athawale, C. Rode, Crystalline $LaCoO_3$ perovskite as a novel catalyst for glycerol transesterification, Mol. Catal. 475 (2019) 110496. https://doi.org/10.1016/j.mcat.2019.110496.

[110] P.P. Pattanaik, P.M. Kumar, N. Raju, N. Lingaiah, Continuous synthesis of glycerol carbonate by transesterification of glycerol with dimethyl carbonate over Fe–La mixed oxide catalysts, Catal. Letters 151 (2021) 1433-1443. https://doi.org/10.1007/s10562-020-03397-4.

[111] P.D.L. Mercera, J.G. Van Ommen, E.B.M. Doesburg, A.J. Burggraaf, J.R.H. Ross, Zirconia as a support for catalysts. Evolution of the texture and structure on calcination in air, Appl. Catal. 57 (1990) 127–148. https://doi.org/10.1016/S0166-9834(00)80728-9.

[112] X. Zhang, S. Wei, X. Zhao, Z. Chen, H. Wu, P. Rong, Y. Sun, Y. Li, H. Yu, D. Wang, Preparation of mesoporous CaO-ZrO_2 catalysts without template for the continuous synthesis of glycerol carbonate in a fixed-bed reactor, Appl. Catal. A Gen. 590 (2020) 117313. https://doi.org/10.1016/j.apcata.2019.117313.

[113] M. Varkolu, D.R. Burri, S.R.R. Kamaraju, S.B. Jonnalagadda, W.E. Van Zyl, Transesterification of glycerol with dimethyl carbonate over nanocrystalline ordered

mesoporous MgO–ZrO_2 solid base catalyst, J. Porous Mater. 23 (2016) 185–193. https://doi.org/10.1007/s10934-015-0069-8.

[114] A. Kaur, A. Ali, Lithium zirconate as a selective and cost-effective mixed metal oxide catalyst for glycerol carbonate production, Ind. Eng. Chem. Res. 59 (2020) 2667–2679. https://doi.org/10.1021/acs.iecr.9b05747.

[115] A. Kaur, R. Prakash, A. Ali, ^{1}H NMR assisted quantification of glycerol carbonate in the mixture of glycerol and glycerol carbonate, Talanta 178 (2018) 1001–1005. https://doi.org/10.1016/j.talanta.2017.08.103.

[116] B. Das, K. Mohanty, A green and facile production of catalysts from waste red mud for the one-pot synthesis of glycerol carbonate from glycerol, J. Environ. Chem. Eng. 7 (2019) 102888. https://doi.org/10.1016/j.jece.2019.102888.

[117] B. Das, K. Mohanty, Exploring the promotional effects of K, Sr, and Mg on the catalytic stability of red mud for the synthesis of glycerol carbonate from renewable glycerol, Ind. Eng. Chem. Res. 58 (2019) 15803–15817. https://doi.org/10.1021/acs.iecr.9b00420.

[118] S. Wang, P. Hao, S. Li, A. Zhang, Y. Guan, L. Zhang, Synthesis of glycerol carbonate from glycerol and dimethyl carbonate catalyzed by calcined silicates, Appl. Catal. A Gen. 542 (2017) 174–181. https://doi.org/10.1016/j.apcata.2017.05.021.

[119] J. Granados-Reyes, P. Salagre, Y. Cesteros, CaAl-layered double hydroxides as active catalysts for the transesterification of glycerol to glycerol carbonate, Appl. Clay Sci. 132–133 (2016) 216–222. https://doi.org/10.1016/j.clay.2016.06.008.

[120] E.E. Sann, Y. Pan, Z. Gao, S. Zhan, F. Xia, Highly hydrophobic ZIF-8 particles and application for oil-water separation, Sep. Purif. Technol. 206 (2018) 186–191. https://doi.org/10.1016/j.seppur.2018.04.027.

[121] Y. Wang, C. Liu, J. Sun, R. Yang, W. Dong, Ordered mesoporous $BaCO_3$/C-catalyzed synthesis of glycerol carbonate from glycerol and dimethyl carbonate, Sci. China Chem. 58 (2015) 708–715. https://doi.org/10.1007/s11426-014-5173-0.

[122] F.S.H. Simanjuntak, V.T. Widyaya, C.S. Kim, B.S. Ahn, Y.J. Kim, H. Lee, Synthesis of

glycerol carbonate from glycerol and dimethyl carbonate using magnesium-lanthanum mixed oxide catalyst, Chem. Eng. Sci. 94 (2013) 265–270. https://doi.org/10.1016/j.ces.2013.01.070.

[123] R. Bai, S. Wang, F. Mei, T. Li, G. Li, Synthesis of glycerol carbonate from glycerol and dimethyl carbonate catalyzed by KF modified hydroxyapatite, J. Ind. Eng. Chem. 17 (2011) 777–781. https://doi.org/10.1016/j.jiec.2011.05.027.

[124] M. Du, Q. Li, W. Dong, T. Geng, Y. Jiang, Synthesis of glycerol carbonate from glycerol and dimethyl carbonate catalyzed by K_2CO_3/MgO, Res. Chem. Intermed. 38 (2012) 1069–1077. https://doi.org/10.1007/s11164-011-0443-3.

[125] D. Singh, B. Reddy, A. Ganesh, S. Mahajani, Zinc/lanthanum mixed-oxide catalyst for the synthesis of glycerol carbonate by transesterification of glycerol, Ind. Eng. Chem. Res. 53 (2014) 18786–18795. https://doi.org/10.1021/ie5011564.

[126] M.S. Khayoon, B.H. Hameed, $Mg_{1+x}Ca_{1-x}O_2$ as reusable and efficient heterogeneous catalyst for the synthesis of glycerol carbonate via the transesterification of glycerol with dimethyl carbonate, Appl. Catal. A Gen. 466 (2013) 272–281. https://doi.org/10.1016/j.apcata.2013.06.044.

[127] M. Malyaadri, K. Jagadeeswaraiah, P.S. Sai Prasad, N. Lingaiah, Synthesis of glycerol carbonate by transesterification of glycerol with dimethyl carbonate over Mg/Al/Zr catalysts, Appl. Catal. A Gen. 401 (2011) 153–157. https://doi.org/10.1016/J.APCATA.2011.05.011.

[128] G. Parameswaram, M. Srinivas, B. Hari Babu, P.S. Sai Prasad, N. Lingaiah, Transesterification of glycerol with dimethyl carbonate for the synthesis of glycerol carbonate over Mg/Zr/Sr mixed oxide base catalysts, Catal. Sci. Technol. 3 (2013) 3242–3249. https://doi.org/10.1039/c3cy00532a.

[129] H.J. Cho, H.M. Kwon, J. Tharun, D.W. Park, Synthesis of glycerol carbonate from ethylene carbonate and glycerol using immobilized ionic liquid catalysts, J. Ind. Eng. Chem. 16 (2010) 679–683. https://doi.org/10.1016/j.jiec.2010.07.019.

[130] F.S.H. Simanjuntak, J.S. Choi, G. Lee, H.J. Lee, S.D. Lee, M. Cheong, H.S. Kim, H. Lee, Synthesis of glycerol carbonate from the transesterification of dimethyl carbonate with glycerol using DABCO and DABCO-anchored Merrifield resin, Appl. Catal. B Environ. 165 (2015) 642–650. https://doi.org/10.1016/j.apcatb.2014.10.071.

[131] A. Takagaki, K. Iwatani, S. Nishimura, K. Ebitani, Synthesis of glycerol carbonate from glycerol and dialkyl carbonates using hydrotalcite as a reusable heterogeneous base catalyst, Green Chem. 12 (2010) 578–58. https://doi.org/10.1039/b925404h.

[132] M.G. Alvarez, A.M. Segarra, S. Contreras, J.E. Sueiras, F. Medina, F. Figueras, Enhanced use of renewable resources: Transesterification of glycerol catalyzed by hydrotalcite-like compounds, Chem. Eng. J. 161 (2010) 340–345. https://doi.org/10.1016/j.cej.2009.12.036.

[133] P. Liu, M. Derchi, E.J.M. Hensen, Promotional effect of transition metal doping on the basicity and activity of calcined hydrotalcite catalysts for glycerol carbonate synthesis, Appl. Catal. B Environ. 144 (2014) 135–143. https://doi.org/10.1016/j.apcatb.2013.07.010.

[134] Z. Liu, J. Wang, M. Kang, N. Yin, X. Wang, Y. Tan, Y. Zhu, Structure-activity correlations of $LiNO_3/Mg_4AlO_{5.5}$ catalysts for glycerol carbonate synthesis from glycerol and dimethyl carbonate, J. Ind. Eng. Chem. 21 (2015) 394–399. https://doi.org/10.1016/j.jiec.2014.02.051.

[135] P. Kumar, R.C. Korošec, U.L. Štangar, Highly active and efficient Cu-based hydrotalcite-like structured materials as reusable heterogeneous catalysts used for transcarbonation reaction, J. Colloid Interface Sci. 585 (2021) 549–559. https://doi.org/10.1016/j.jcis.2020.10.035.

[136] P. Rittiron, C. Niamnuy, W. Donphai, M. Chareonpanich, A. Seubsai, Production of glycerol carbonate from glycerol over templated-sodium-aluminate catalysts prepared using a spray-drying method, ACS Omega 4 (2019) 9001–9009. https://doi.org/10.1021/acsomega.9b00805.

[137] Y. Li, J. Liu, D. He, Catalytic synthesis of glycerol carbonate from biomass-based glycerol and dimethyl carbonate over Li-La_2O_3 catalysts, Appl. Catal. A Gen. 564 (2018)

234–242. https://doi.org/10.1016/j.apcata.2018.07.032.

[138] S.E. Kondawar, C.R. Patil, C. V. Rode, Tandem synthesis of glycidol via transesterification of glycerol with DMC over Ba-mixed metal oxide catalysts, ACS Sustain. Chem. Eng. 5 (2017) 1763–1774. https://doi.org/10.1021/acssuschemeng.6b02520.

[139] Y.T. Algoufi, U.G. Akpan, G. Kabir, M. Asif, B.H. Hameed, Upgrading of glycerol from biodiesel synthesis with dimethyl carbonate on reusable Sr–Al mixed oxide catalysts, Energy Convers. Manag. 138 (2017) 183–189. https://doi.org/10.1016/j.enconman.2017.01.078.

[140] X. Song, Y. Wu, F. Cai, D. Pan, G. Xiao, High-efficiency and low-cost Li / ZnO catalysts for synthesis of glycerol carbonate from glycerol transesterification : The role of Li and ZnO interaction, Appl. Catal. A Gen. 532 (2017) 77–85. https://doi.org/10.1016/j.apcata.2016.12.019.

[141] P.U. Okoye, A.Z. Abdullah, B.H. Hameed, Glycerol carbonate synthesis from glycerol and dimethyl carbonate using trisodium phosphate, J. Taiwan Inst. Chem. Eng. 68 (2016) 51–58. https://doi.org/10.1016/j.jtice.2016.09.011.

[142] Y.T. Algoufi, B.H. Hameed, Synthesis of glycerol carbonate by transesterification of glycerol with dimethyl carbonate over K-zeolite derived from coal fly ash, Fuel Process. Technol. 126 (2014) 5–11. https://doi.org/10.1016/j.fuproc.2014.04.004.

[143] R. Bai, Y. Wang, S. Wang, F. Mei, T. Li, G. Li, Synthesis of glycerol carbonate from glycerol and dimethyl carbonate catalyzed by NaOH/γ-Al_2O_3, Fuel Process. Technol. 106 (2013) 209–214. https://doi.org/10.1016/j.fuproc.2012.07.027.

[144] S. Sandesh, G. V. Shanbhag, A.B. Halgeri, Transesterification of glycerol to glycerol carbonate using KF/Al_2O_3 catalyst: The role of support and basicity, Catal. Letters 143 (2013) 1226–1234. https://doi.org/10.1007/s10562-013-1043-1.

[145] P. Liu, M. Derchi, E.J.M. Hensen, Synthesis of glycerol carbonate by transesterification of glycerol with dimethyl carbonate over MgAl mixed oxide catalysts, Appl. Catal. A Gen.

467 (2013) 124–131. https://doi.org/10.1016/j.apcata.2013.07.020.

[146] J.A. Vannucci, N.N. Nichio, F. Pompeo, Solketal synthesis from ketalization of glycerol with acetone: A kinetic study over a sulfated zirconia catalyst, Catal. Today (2020). https://doi.org/10.1016/j.cattod.2020.10.005.

[147] F.D.L. Menezes, M.D.O. Guimaraes, M.J. Da Silva, Highly selective $SnCl_2$-catalyzed solketal synthesis at room temperature, Ind. Eng. Chem. Res. 52 (2013) 16709–16713. https://doi.org/10.1021/ie402240j.

[148] M.R. Nanda, Y. Zhang, Z. Yuan, W. Qin, H.S. Ghaziaskar, C. Xu, Catalytic conversion of glycerol for sustainable production of solketal as a fuel additive: A review, Renew. Sustain. Energy Rev. 56 (2016) 1022–1031. https://doi.org/10.1016/j.rser.2015.12.008.

[149] K. Stawicka, A.E. Díaz-Álvarez, V. Calvino-Casilda, M. Trejda, M.A. Bañares, M. Ziolek, The role of Brønsted and Lewis acid sites in acetalization of glycerol over modified mesoporous cellular foams, J. Phys. Chem. C. 120 (2016) 16699–16711. https://doi.org/10.1021/acs.jpcc.6b04229.

[150] V.R. Bakuru, S.R. Churipard, S.P. Maradur, S.B. Kalidindi, Exploring the Brønsted acidity of UiO-66 (Zr, Ce, Hf) metal-organic frameworks for efficient solketal synthesis from glycerol acetalization, Dalt. Trans. 48 (2019) 843–847. https://doi.org/10.1039/c8dt03512a.

[151] L. Chen, B. Nohair, D. Zhao, S. Kaliaguine, Highly efficient glycerol acetalization over supported heteropoly acid catalysts, ChemCatChem. 10 (2018) 1918–1925. https://doi.org/10.1002/cctc.201701656.

[152] M.J. Da Silva, A.A. Rodrigues, M.G. Teixeira, Iron (III) silicotungstate: An efficient and recyclable catalyst for converting glycerol to solketal, Energy Fuels 34 (2020) 9664–9673. https://doi.org/10.1021/acs.energyfuels.0c01446.

[153] A. Vivian, L. Soumoy, L. Fusaro, S. Fiorilli, D.P. Debecker, C. Aprile, Surface functionalized mesoporous gallosillicate catalysts for the efficient and sustainable upgrading of glycerol to solketal, Green Chem. 23 (2021) 354-366.

(https://doi.org/10.1039/D0GC02562C

[154] T.H. Abreu, C.I. Meyer, C. Padró, L. Martins, Acidic V-MCM-41 catalysts for the liquid-phase ketalization of glycerol with acetone, Microporous Mesoporous Mater. 273 (2019) 219–225. https://doi.org/10.1016/j.micromeso.2018.07.006.

[155] C. Ferreira, A. Araujo, V. Calvino-Casilda, M.G. Cutrufello, E. Rombi, A.M. Fonseca, M.A. Bañares, I.C. Neves, Y zeolite-supported niobium pentoxide catalysts for the glycerol acetalization reaction, Microporous Mesoporous Mater. 271 (2018) 243–251. https://doi.org/10.1016/j.micromeso.2018.06.010.

[156] L.H. Vieira, L.G. Possato, T.F. Chaves, S.H. Pulcinelli, C. V. Santilli, L. Martins, Studies on dispersion and reactivity of vanadium oxides deposited on lamellar ferrierite zeolites for condensation of glycerol into bulky products, Mol. Catal. 458 (2018) 161–170. https://doi.org/10.1016/j.mcat.2017.11.027.

[157] Z. Li, Z. Miao, X. Wang, J. Zhao, J. Zhou, W. Si, S. Zhuo, One-pot synthesis of ZrMo-KIT-6 solid acid catalyst for solvent-free conversion of glycerol to solketal, Fuel 233 (2018) 377–387. https://doi.org/10.1016/j.fuel.2018.06.081.

[158] M.J. da Silva, F. de Ávila Rodrigues, A.A. Júlio, SnF_2-catalyzed glycerol ketalization: A friendly environmentally process to synthesize solketal at room temperature over on solid and reusable Lewis acid, Chem. Eng. J. 307 (2017) 828–835. https://doi.org/10.1016/j.cej.2016.09.002.

[159] S.S. Priya, P.R. Selvakannan, K.V.R. Chary, M.L. Kantam, S.K. Bhargava, Solvent-free microwave-assisted synthesis of solketal from glycerol using transition metal ions promoted mordenite solid acid catalysts, Mol. Catal. 434 (2017) 184–193. https://doi.org/10.1016/j.mcat.2017.03.001.

[160] R. Rodrigues, D. Mandelli, N.S. Gonçalves, P.P. Pescarmona, W.A. Carvalho, Acetalization of acetone with glycerol catalyzed by niobium-aluminum mixed oxides synthesized by a sol–gel process, J. Mol. Catal. A Chem. 422 (2016) 122–130. https://doi.org/10.1016/j.molcata.2016.02.002.

[161] S. Sandesh, A.B. Halgeri, G. V. Shanbhag, Utilization of renewable resources: Condensation of glycerol with acetone at room temperature catalyzed by organic-inorganic hybrid catalyst, J. Mol. Catal. A Chem. 401 (2015) 73–80. https://doi.org/10.1016/j.molcata.2015.02.015.

[162] M.J. Da Silva, A.A. Julio, F.C.S. Dorigetto, Solvent-free heteropolyacid-catalyzed glycerol ketalization at room temperature, RSC Adv. 5 (2015) 44499–44506. https://doi.org/10.1039/c4ra17090c.

[163] S. Gadamsetti, N.P. Rajan, G.S. Rao, K.V.R. Chary, Acetalization of glycerol with acetone to bio fuel additives over supported molybdenum phosphate catalysts, J. Mol. Catal. A Chem. 410 (2015) 49–57. https://doi.org/10.1016/j.molcata.2015.09.006.

[164] P. Manjunathan, S.P. Maradur, A.B. Halgeri, G. V. Shanbhag, Room temperature synthesis of solketal from acetalization of glycerol with acetone: Effect of crystallite size and the role of acidity of beta zeolite, J. Mol. Catal. A Chem. 396 (2015) 47–54. https://doi.org/10.1016/j.molcata.2014.09.028.

[165] M.R. Nanda, Z. Yuan, W. Qin, H.S. Ghaziaskar, M.A. Poirier, C. Xu, Catalytic conversion of glycerol to oxygenated fuel additive in a continuous flow reactor: Process optimization, Fuel 128 (2014) 113–119. https://doi.org/10.1016/j.fuel.2014.02.068.

[166] C. Gonzalez-Arellano, S. De, R. Luque, Selective glycerol transformations to high value-added products catalysed by aluminosilicate-supported iron oxide nanoparticles, Catal. Sci. Technol. 4 (2014) 4242–4249. https://doi.org/10.1039/c4cy00714j.

[167] B. Mallesham, P. Sudarsanam, G. Raju, B.M. Reddy, Design of highly efficient Mo and W-promoted SnO_2 solid acids for heterogeneous catalysis: Acetalization of bio-glycerol, Green Chem. 15 (2013) 478–489. https://doi.org/10.1039/c2gc36152c.

[168] G.S. Nair, E. Adrijanto, A. Alsalme, I. V. Kozhevnikov, D.J. Cooke, D.R. Brown, N.R. Shiju, Glycerol utilization: Solvent-free acetalisation over niobia catalysts, Catal. Sci. Technol. 2 (2012) 1173–1179. https://doi.org/10.1039/c2cy00335j.

[169] L. Li, T.I. Korányi, B.F. Sels, P.P. Pescarmona, Highly-efficient conversion of glycerol to

solketal over heterogeneous Lewis acid catalysts, Green Chem. 14 (2012) 1611–1619. https://doi.org/10.1039/c2gc16619d.

[170] P.S. Reddy, P. Sudarsanam, B. Mallesham, G. Raju, B.M. Reddy, Acetalisation of glycerol with acetone over zirconia and promoted zirconia catalysts under mild reaction conditions, J. Ind. Eng. Chem. 17 (2011) 377–381. https://doi.org/10.1016/j.jiec.2011.05.008.

[171] P. Ferreira, I.M. Fonseca, A.M. Ramos, J. Vital, J.E. Castanheiro, Valorisation of glycerol by condensation with acetone over silica-included heteropolyacids, Appl. Catal. B Environ. 98 (2010) 94–99. https://doi.org/10.1016/j.apcatb.2010.05.018.

[172] S. Ammaji, G.S. Rao, K.V.R. Chary, Acetalization of glycerol with acetone over various metal-modified SBA-15 catalysts, Appl. Petrochemical Res. 8 (2018) 107–118. https://doi.org/10.1007/s13203-018-0197-6.

[173] C. Crotti, E. Farnetti, N. Guidolin, Alternative intermediates for glycerol valorization: Iridium-catalyzed formation of acetals and ketals, Green Chem. 12 (2010) 2225–2231. https://doi.org/10.1039/c0gc00096e.

[174] P. Fan, J. Wang, S. Xing, L. Yang, G. Yang, J. Fu, C. Miao, P. Lv, Synthesis of glycerol-free biodiesel with dimethyl carbonate over sulfonated imidazolium ionic liquid, Energy Fuels 31 (2017) 4090–4095. https://doi.org/10.1021/acs.energyfuels.7b00115.

[175] D. Celante, J.V.D. Schenkel, F. de Castilhos, Biodiesel production from soybean oil and dimethyl carbonate catalyzed by potassium methoxide, Fuel 212 (2018) 101–107. https://doi.org/10.1016/j.fuel.2017.10.040.

[176] A.O. Esan, A.D. Adeyemi, S. Ganesan, A review on the recent application of dimethyl carbonate in sustainable biodiesel production, J. Clean. Prod. 257 (2020) 120561. https://doi.org/10.1016/j.jclepro.2020.120561.

[177] Z. Ilham, S. Saka, Two-step supercritical dimethyl carbonate method for biodiesel production from Jatropha curcas oil, Bioresour. Technol. 101 (2010) 2735–2740. https://doi.org/10.1016/j.biortech.2009.10.053.

[178] Z. Ilham, S. Saka, Dimethyl carbonate as potential reactant in non-catalytic biodiesel production by supercritical method, Bioresour. Technol. 100 (2009) 1793–1796. https://doi.org/10.1016/j.biortech.2008.09.050.

[179] F.A. Dawodu, O.O. Ayodele, J. Xin, S. Zhang, Dimethyl carbonate mediated production of biodiesel at different reaction temperatures, Renew. Energy. 68 (2014) 581–587. https://doi.org/10.1016/j.renene.2014.02.036.

[180] Y. Syamsuddin, M.N. Murat, B.H. Hameed, Transesterification of Jatropha oil with dimethyl carbonate to produce fatty acid methyl ester over reusable Ca-La-Al mixed-oxide catalyst, Energy Convers. Manag. 106 (2015) 1356–1361. https://doi.org/10.1016/j.enconman.2015.10.057.

[181] Y. Tang, H. Liu, H. Ren, Q. Cheng, Y. Cui, J. Zhang, Development KCl/CaO as a catalyst for biodiesel production by tri-component coupling transesterification, Environ. Prog. Sustain. Energy 38 (2019) 647–653. https://doi.org/10.1002/ep.12977.

[182] B. Panchal, T. Chang, S. Qin, Y. Sun, J. Wang, K. Bian, Process optimization using novel acidic ionic liquids and the kinetics modeling of methyl esters using Jatropha curcas oil with dimethyl carbonate, Fuel 258 (2019) 116165. https://doi.org/10.1016/j.fuel.2019.116165.

[183] Y. Tang, S. Li, J. Dong, M. Meng, J. Zhang, An efficient CaO-based catalyst for rapid production of biodiesel without glycerol as a by-product using a tri-component reaction, J. Am. Oil Chem. Soc. 95 (2018) 1487–1496. https://doi.org/10.1002/aocs.12143.

[184] B.M. Panchal, S.A. Deshmukh, M.R. Sharma, Production and kinetic transesterification of biodiesel from yellow grease with dimethyl carbonate using methanesulfonic acid as a catalyst, Environ. Prog. Sustain. Energy 36 (2017) 802-807. https://doi.org/10.1002/ep.12559.

[185] Y. Tang, H. Ren, F. Chang, X. Gu, J. Zhang, Nano KF/Al_2O_3 particles as an efficient catalyst for no-glycerol biodiesel production by coupling transesterification, RSC Adv. 7 (2017) 5694–5700. https://doi.org/10.1039/c6ra25782h.

[186] Y. Syamsuddin, B.H. Hameed, Synthesis of glycerol free-fatty acid methyl esters from Jatropha oil over Ca-La mixed-oxide catalyst, J. Taiwan Inst. Chem. Eng. 58 (2016) 181–188. https://doi.org/10.1016/j.jtice.2015.06.041.

[187] T. Kai, G.L. Mak, S. Wada, T. Nakazato, H. Takanashi, Y. Uemura, Production of biodiesel fuel from canola oil with dimethyl carbonate using an active sodium methoxide catalyst prepared by crystallization, Bioresour. Technol. 163 (2014) 360–363. https://doi.org/10.1016/j.biortech.2014.04.030.

[188] K.D. Pandiangan, W. Simanjuntak, Transesterification of coconut oil using dimethyl carbonate and TiO_2/SiO_2 heterogeneous catalyst, Indones. J. Chem. 13 (2013) 47–52. https://doi.org/10.22146/ijc.21325.

[189] M.R. Islam, Y.M. Kurle, J.L. Gossage, T.J. Benson, Kinetics of triazabicyclodecene-catalyzed canola oil conversion to glycerol-free biofuel using dimethyl carbonate, Energy Fuels 27 (2013) 1564–1569. https://doi.org/10.1021/ef400048v.

Material and Methods

2.1 Chemicals

Zirconium oxide (ZrO_2), lithium zirconate (Li_2ZrO_3), and zirconium oxychloride octahydrate ($ZrOCl_2.8H_2O$) are purchased from Sigma Aldrich (USA). Lithium nitrate ($LiNO_3$), sodium nitrate ($NaNO_3$), potassium nitrate (KNO_3), calcium oxide (CaO), calcium nitrate ($Ca(NO_3)_2$), potassium hydroxide (KOH), magnesium nitrate ($Mg(NO_3)_2$), zinc nitrate ($Zn(NO_3)_2.6H_2O$), glycerol, 2-methylimmidazole, ethyl acetate, methanol, ammonium hydroxide solution (25% v/v) (all chemicals of analytical grade purity) were obtained from Loba Chemie Ltd. (India) and are used as such without further purification. Methanol, dimethyl carbonate, ethyl bromide, propyl bromide, butyl bromide, pentyl bromide, benzyl bromide, bromobenzene (all chemicals of analytical grade purity) are purchased from Spectrochem Pvt. Ltd. (India). Deuterium oxide D_2O and Dimethyl sulfoxide-d_6 have been procured from Sigma-Aldrich, India. Glycerol 1,2 dicarbonate is purchased from TCI Chemicals, JAPAN. HPLC grade hexane and isopropanol solvents are also purchased from Spectrochem, INDIA.

2.2 Reaction kinetics and thermodynamics

The transesterification reaction of DMC with GL, in literature, has been reported to follow the second-order kinetic model [1]. It is observed that both the liquids, which otherwise have limited immiscibility, become miscible as the reaction is progressed with the generation of GLC along with methanol [2]. Thus during the course of the reaction, a biphasic system (solid-liquid) exists in the reaction mixture.

The second-order rate constant as well as the activation energy was determined from the linear graph obtained by fitting the appropriate values in the **equation (2.1)** [3] and **equation (2.2)** [4] mentioned below

$$\frac{1}{1-X_{glc}} = \frac{1}{X} + kt \qquad \textbf{(2.1)}$$

$$\ln K = \ln A - \frac{E_a}{RT} \qquad \textbf{(2.2)}$$

where k is the second-order rate constant of reaction in $M^{-1}s^{-1}$, X_{glc} is the GLC yield at time t, X is the initial amount of GL, E_a is the activation energy (kJ mol^{-1}), A is the pre-exponential factor (min^{-1}), R is the gas constant (8.314 J $K^{-1}mol^{-1}$) and T is the reaction temperature (K).

Eyring–Polanyi equation (**equation 2.3**) was employed [4] to calculate thermodynamic parameters such as enthalpy and entropy of the activation.

$$\ln(k/T) = -\Delta H^{\ddagger}/RT + \ln(k_B/h) + \Delta S^{\ddagger}/R \quad \textbf{(2.3)}$$

Where *k* is the reaction rate constant, T is the temperature (K), R is gas constant (8.314 J $K^{-1}mol^{-1}$), $\Delta H^{\ddagger}$ and $\Delta S^{\ddagger}$ is the enthalpy and entropy of activation, k_B and h are the Boltzmann (1.38×10^{-23} J K^{-1}) and Planck (6.63×10^{-34} Js) constants, respectively. Gibb's free energy is calculated by incorporating the enthalpy and entropy values in **equation (2.4)** [4].

$$\Delta G^{\ddagger} = \Delta H^{\ddagger} - T\Delta S^{\ddagger} \quad \textbf{(2.4)}$$

2.3 Turn over frequency (TOF)

The turnover frequency (TOF) [5] of the prepared catalysts was determined using **equation 2.5**

$$TOF = \frac{mol_{actual}}{f_m \times m_{cat} \times t} \quad \textbf{(2.5)}$$

where mol_{actual} is the moles of GLC at 30 % GLC conversion; m_{cat} is the mass of catalyst; t is the reaction time, and f_m is active sites (basic) of catalyst (in mmol g^{-1}) as calculated by TPD.

2.4 Instruments

2.4.1 Powder X-ray diffraction (XRD)

Powder X-ray diffraction (XRD) patterns of the prepared catalysts were recorded on a PANalytical's X'Pert Pro using monochromatic Cu Kα radiation (λ= 1.54060 ˚A) as the X-ray source over a scanning 2θ range of 15–80°. The obtained XRD diffraction patterns were identified by the use of database files provided by the Joint Committee on Powder Diffraction Standards (JCPDS).

2.4.2 X-ray photoelectron spectroscopy (XPS)

The surface elemental electronic state, as well as binding energy of the elements existing in the catalysts, were calculated by X-ray photoelectron spectroscopy using ESCA X-ray Photoelectron Spectrometer instrument (Kratos Analytical, UK) equipped with monochromatized alumina

source (Al Kα radiation; $h\nu$ = 1486.7 eV). The instrument was operated at 15 kV and 20 mA. For calibration purposes, C 1s binding energy of 285.3 eV is taken as a reference. The charging issue is overcome by applying a charge neutralizer of 2 eV. Before analysis, air contamination is minimized by degassing the powdered samples in the XPS chamber for 2 h.

2.4.3 Fourier transformation infrared spectroscopy (FT-IR)

For the detection of surface functional groups present on the prepared catalyst, Fourier-transform infrared spectroscopy (FTIR) was carried out using Perkin Elmer-Spectrum RX-I having a scan range of 4000 cm^{-1} to 250 cm^{-1}. Prior to analysis, the sample is grinded thoroughly before KBr addition. Afterward, the sample is mixed with KBr and is placed onto a pellet die, pressed using Qwick Handi-Press to form a pellet. The pellet is then placed onto the sample holder for FTIR analysis**.**

2.4.4 Fourier transform-nuclear magnetic resonance (FT-NMR)

Fourier transform-nuclear magnetic resonance (FT-NMR) spectra of glycerol and glycerol carbonate were recorded on a JEOL ECS-400 (400 MHz) spectrophotometer with tertramethyl silane (TMS) used as an internal reference. The chemical shifts (δ) of the NMR spectra were indicated in parts per million (ppm). ^{1}H-NMR spectra were recorded in either D_2O or DMSO-d_6 with the following acquisition parameters: 45° pulse angle of 4.87 μs pulse width; transmitter frequency offset (O1P) of 5 ppm; acquisition time 2.18 s; 64 scans; spectral acquisition temperature 291-298 K. All spectra were processed by the MestReNova package (6.0.2-5475). The relaxation time of the protons employed for the quantitative analysis was determined by the inversion recovery experiment at a 90° pulse angle, using the Delta NMR software supplied with the JEOL equipment.

2.4.5 Thin-layer chromatography (TLC)

To monitor the progress of the reaction, a little fraction of the reaction mixture was withdrawn from the reaction flask with the help of a glass capillary and diluted with ethyl acetate. The diluted reaction mixture was subjected to thin-layer chromatography (TLC), over silica-packed aluminum plates using ethyl acetate as an eluent. The TLC plates were initially exposed to the $KMnO_4$ solution and then heated with a hot air blower to develop the spots. Now the spots on the

TLC plates are visible as yellow dots against a purple background.

2.4.6 High-performance liquid chromatography (HPLC)

The normal phase High-performance Liquid Chromatography (HPLC) was conducted on Agilent 1260 infinity series instrument equipped with refractive index (RI) detector, RX–SIL column (4.6 mm inner diameter × 250 mm, 5 μm particles) as a stationary phase, and the mixture of isopropyl alcohol: hexane (80:20, v/v) as a mobile phase. Solutions (0.01M) for the analysis were prepared by dissolving the appropriate amount of the reaction mixture in a hexane/isopropanol (20/80, v/v) solvent system and the solutions thus prepared were passed through the syringe filters to remove any undissolved particles. A fixed volume (20 μL) of the sample solution was injected into the HPLC column, and a steady solvent flow rate (0.3 mL/min) was maintained throughout the analysis. The product has been quantified by calculating the %age of the peak area related to the GL and GLC with respect to the total area of the chromatogram.

2.4.7 Scanning electron microscopy-Energy Dispersive X-ray Analysis (SEM-EDS)

The surface morphology and the elemental ratio of the elements present in the catalysts were determined by conducting Scanning electron microscopy along with energy dispersive X-ray spectrometry on JEOL JSM 7600 F instrument. The sample dissolved in ethanol was initially ultrasonicated for 1 h. Further, a drop of this prepared suspension was mounted onto the sample holder with the help of carbon adhesive. The samples are then analyzed under the instrument after making it conductive by sputtering it with gold.

2.4.8 High resolution transmission electron microscopy (HRTEM)

Transmission electron microscopy images of the sample were recorded on the JEOL JEM 2100 plus instrument. Initially, the sample was mixed in ethanol, ultrasonicated for 1 h to obtain a well-dispersed suspension. Prior to administering the sample for analysis, a drop of the prepared suspension is dispersed onto the copper grid and dried for evaporating the solvent.

2.4.9 Brunauer-Emmett-Teller (BET) surface area

The surface properties of the prepared catalysts were determined by applying Standard Brunauer-Emmett-Teller (BET) method using Microtec Belsorp Miniell equipment. Before analysis, pretreatment of the sample to remove the physically adsorbed species was conducted under a nitrogen atmosphere at 200 °C for 2 h.

2.4.10 CO_2-Temperature programmed desorption (CO_2-TPD)

For the determination of the basic strength of the catalysts, CO_2-temperature programmed desorption (TPD) was conducted using the BELCAT II instrument of MicrotracBEL Corporation. Initially, the catalyst (0.05 g) was loaded into the glass tube and was flushed with He gas at 300 $^{\circ}$C to remove the physically adsorbed gases and moisture for 1 h. Afterward, CO_2 gas was adsorbed onto the catalyst surface by purging with the pure CO_2 gas at 100 $^{\circ}$C for 0.5 h. To remove the physically adsorbed CO_2, from the sample, He gas is purged. Afterward, the same sample was heated up to the desired temperature with a ramp of 10 °C/min under the He atmosphere, and the desorbed CO_2 was quantified using a thermal conductivity detector (TCD).

2.4.11 Microwave plasma -Atomic emission spectrometry (MP-AES)

The metal concentration in GLC was estimated through Microwave plasma-Atomic emission spectroscopic 4100 instrument of Agilent technologies. For analysis, 50 mg of the sample was taken in a beaker, and 5 mL of concentrated HNO_3 (16 M) was added to it. For digesting all the organic matter; the resultant mixture was first heated to obtain a clear solution which was then cooled down. The later was transferred to the 50 mL volumetric flask and the solution was made up to the volume mark with the de-ionized water.

2.4.12 Carbon hydrogen nitrogen sulfur analyzer (CHNS)

The carbon content in the catalyst was analyzed by the FLASH 2000 series CHNS-O analyzer of Thermo Scientific.

References

[1] Z. Herseczki, G. Marton, Synthesis of glycerol carbonate from glycerol , a by-product of biodiesel production, Int. J. Reactor Eng. 7 (2009). doi: 10.2202/1542-6580.2168

[2] J. Esteban, E. Domínguez, M. Ladero, F. Garcia-Ochoa, Kinetics of the production of glycerol carbonate by transesterification of glycerol with dimethyl and ethylene carbonate using potassium methoxide, a highly active catalyst, Fuel Process. Technol. 138 (2015) 243–251. doi:10.1016/j.fuproc.2015.06.012.

[3] L. Arnaut, S. Formosinho, H. Burrows, Reaction order and rate constants, In Chemical Kinetics, 1st ed, Elsevier Science: The Netherlands, 77 (2007) 77–113. ISBN 9780444521866**.**

[4] N. Kaur, A. Ali, Biodiesel production via ethanolysis of jatropha oil using molybdenum impregnated calcium oxide as solid catalyst, RSC Adv. 5 (2015) 13285–13295. doi:10.1039/c4ra14786c.

[5] N. Kaur, A. Ali, Lithium zirconate as solid catalyst for simultaneous esterification and transesterification of low quality triglycerides, Appl. Catal. A Gen. 489 (2015) 193–202. doi:10.1016/j.apcata.2014.10.013.

^{1}H-NMR Assisted Quantification of Glycerol Carbonate in the Mixture of Glycerol and Glycerol Carbonate

Abstract

This chapter discussed the techniques adopted for quantifying the GLC formed from the transesterification reaction of the DMC with GL. The demerits of the widely used chromatographic techniques viz., Gas chromatography (GC) and High performance liquid chromatography (HPLC) for GLC quantification has been reviewed. A quick and simple method for quantifying GLC synthesized via DMC-assisted transesterification with GL has been proposed for the first time. A simple, accurate, and non-destructive quantitative proton nuclear magnetic resonance (qHNMR) method has been applied to determine GLC in the mixture of GL and GLC. Based upon the study, two different equations were proposed to calculate the GLC employing the data obtained from the ^{1}H-NMR spectra. qHNMR results are also validated by preparing the standard mixtures of varying concentrations of GL and GLC. Further, to confirm the developed method for a real application, GLC concentration was also estimated during DMC transesterification with GL. The qHNMR assisted GLC quantification was consistent with those obtained from high-performance liquid chromatography analysis (R^2 =0.99).

3.1 Introduction

^{1}H-NMR, a non-destructive analytical technique being used widely for determining the structure of molecules, has also emerged as an analytical tool for quantifying the molecules due to its accuracy, specificity, and selectivity [1,2]. The driving principle of quantitative NMR analysis has emerged from the fact that the integrated peak area of each ^{1}H-NMR signal provided directly corresponds to the equal number of equivalent nuclei/nucleus responsible for that signal [10]. To calculate the molar ratios in a mixture of two compounds, the integration value of the baseline separated signals and the number of participating nuclei are considered [3].

In literature, two chromatographic methods, viz., GC [4] and HPLC [5] has been widely employed for GLC quantification. However, out of these two techniques, GC is destructive in nature and required a complicated operational procedure, volatile component, and mass

spectroscopy for product confirmation [6]. At the same time, HPLC is a time-consuming technique demanding costly HPLC grade solvents, set of standards, equilibration of the columns and derivatization of the analyte [7] and also has no universal detector.

On the other hand, qHNMR does not require any complicated sample preparation method or high purity sample, longer analysis time, or sample reference. The amount of deuterated solvent needed for qHNMR analysis is minimal (~ 0.5 ml or less) than the larger solvent volume used in HPLC or the large volume of high purity gases required for GC analysis. Thus, the higher costs for deuterated solvents could be easily compensated.

To the best of our knowledge, qHNMR technique was not explored for the GLC quantification in the literature. Herein, we have proposed qHNMR spectroscopic method to determine the composition of samples obtained from the transesterification of DMC with GL to produce GLC without any requirement of sample derivatization.

3.2. Experimental section

3.2.1 GL and GLC sample preparation

To test the linearity and reproducibility of the qHNMR technique, different samples were prepared by mixing the known amount of GL and GLC in various molar ratios as described in **Table 3.1**. A known amount (8 mg) was weighed from these prepared mixtures, which were finally diluted with 0.6 mL of D_2O or DMSO and subjected to ^{1}H-NMR analysis.

3.2.2 ^{1}H-NMR analysis-Inversion Recovery Experiment

Relaxation delay (d1), for the proton signal employed in quantification, must be ≥ 5 times the value of the longest relaxation time (T1) [2]. During the inversion recovery experiments (Chapter 2), a maximum value of the T1 was found to be 2.8 s; hence, d1 was fixed at 14 s for quantification experiments. Two different relaxation delay (d1) times, 4 s (by default) and 14 s (obtained from the inversion recovery experiment), were opted for carrying out the qHNMR analysis. Spectra obtained at both the relaxation delay were compared for finding out the accuracy of the ^{1}H-NMR signals. Each ^{1}H-NMR spectrum was normalized by assigning a value of 1 to one of the methylene proton (c1) of glycerol carbonate molecule to obtain the reference integration value.

3.2.3 HPLC analysis

For HPLC analysis, different samples were prepared by mixing the known amount of GL and GLC in varied molar ratios using hexane/isopropanol (20/80, v/v) solvent system as described in **Table 3.1**.

3.2.4 Transesterification of dimethyl carbonate with glycerol

To quantify the GLC in a reaction mixture, transesterification of dimethyl carbonate with glycerol in the presence of CaO was conducted, as shown in **Scheme 3.1**. In a typical reaction, GL (21.7 mmol, 2 g), DMC (43.4 mmol, 3.9 g), and CaO (100 mg) were added to the 25 mL two-necked round-bottomed flask equipped with an oil bath, magnetic stirrer, and reflux condenser. The mixture was heated with continuous stirring at 85 $^{\circ}$C temperature for 1 h. After the stipulated time, the reaction mixture was filtered to remove the solid catalyst, and the liquid phase was rotary evaporated at 65 $^{\circ}$C to remove the excess DMC and methanol. The reaction mixture thus obtained was analyzed by ^{1}H-NMR and HPLC techniques.

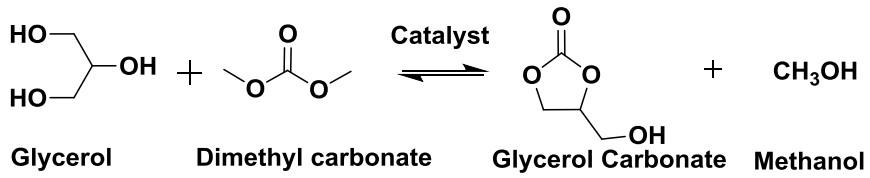

Scheme 3.1 Catalyst assisted transesterification of dimethyl carbonate with glycerol.

3.3 Results and Discussion

3.3.1 Choice of solvent for NMR (DMSO versus D_2O)

In literature, ^{1}H-NMR spectra of GLC, recorded in deuterated DMSO, were primarily used to determine the molecule's chemical structure [8,9] but not for quantitative purpose. ^{1}H-NMR spectrum of a mixture of GL and GLC in DMSO-d_6 shows **d**, $\mathbf{e_1}$, and $\mathbf{e_2}$ proton signals of GL superimposed with $\mathbf{a_1}$ protons of GLC in the region of 4.33-4.48 ppm and H_2O peak of DMSO-d_6 in the range of 3.273-3.412 ppm, as shown in **Figure 3.1**. This difficulty could be overcome by recording the ^{1}H-NMR spectra of GL as well GLC in D_2O. As shown in **Figure**

3.1, each GL and GLC proton signal is well resolved and could be easily assigned to the respective protons without having the issue of D_2O signal overlapping with sample proton signals. In D_2O, the comparison of ^{1}H-NMR spectra of GL with GLC (**Figure 3.1**) showed that signals $\mathbf{a_1}$, $\mathbf{a_2}$, **b**, $\mathbf{c_1}$, and $\mathbf{c_2}$ are observed only for GLC and signal **d**, $\mathbf{e_1}$, and $\mathbf{e_2}$ observed for GL. **Table B.1** provided descriptions of all the signals observed in the ^{1}H-NMR spectrum of both the molecules, and overlapping signals (used for quantification purpose) are shown in italics.

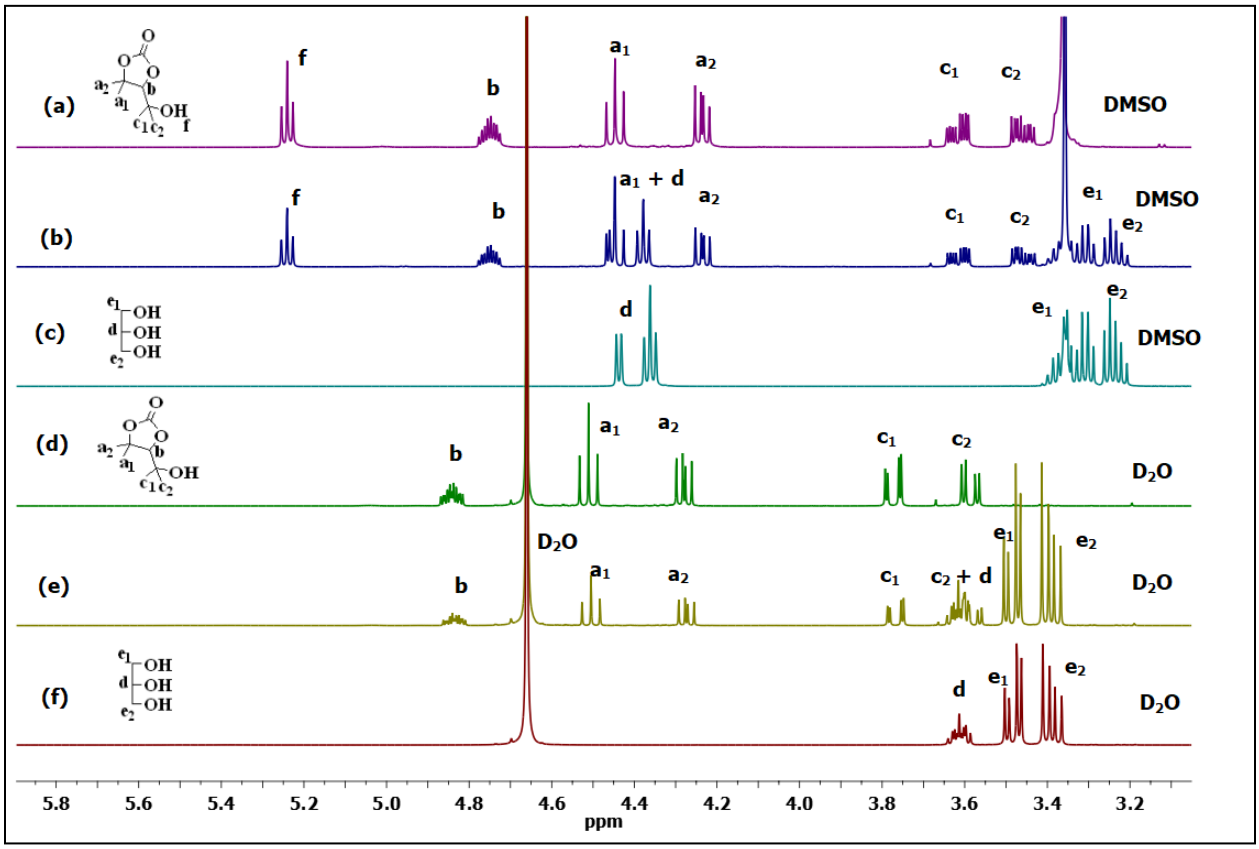

Figure 3.1 ^{1}H-NMR spectra of standard (a) GLC (b) 30:70 (m/m) mixture of GL/GLC and (c) GL in DMSO; standard (d) GLC (e) 40:60 (m/m) mixture of GL/GLC and (f) GL in D_2O respectively.

In a ^{1}H-NMR spectrum of a mixture of GL and GLC in D_2O, **d** proton signal of GL overlaps with one of the doublets of $\mathbf{c_2}$ proton signal (3.557-3.640 ppm) of GLC as shown in **Figure 3.2**. In this overlapping zone, the peak area corresponding to GLC proton ($\mathbf{c_2}$) would be equal to the peak area of non-overlapping GLC proton ($\mathbf{c_1}$, $\mathbf{a_1}$, **and** $\mathbf{a_2}$). This analogy is used while

deriving the **Equation 3.1** and **3.2** for calculating the molar %age of GLC in a mixture of GL and GLC.

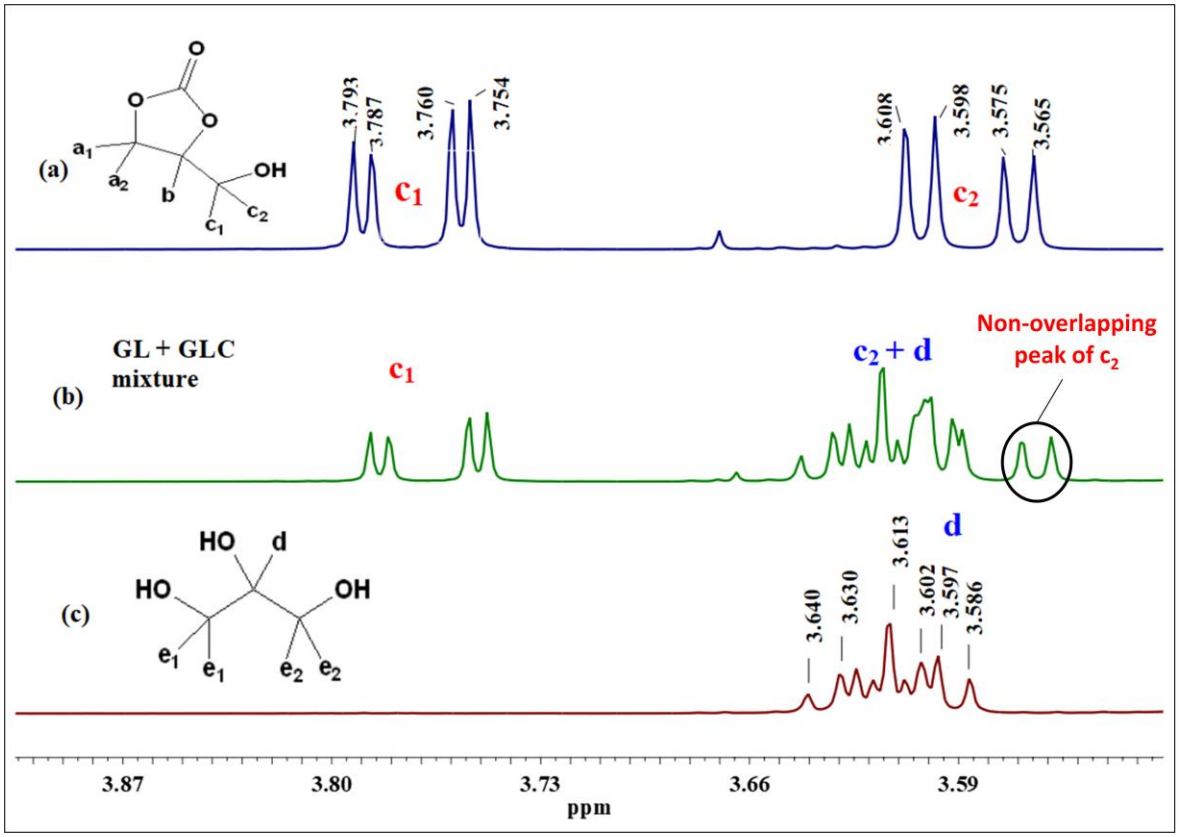

Figure 3.2 Expanded region (3.53 to 3.91 ppm) of ^{1}H-NMR spectra in D_2O; (a) pure GLC, (b) 40/60 (m/m) GL/GLC mixture and (c) pure GL.

3.3.2 Selection of relaxation delay (d1)

Besides selecting a suitable solvent, instrumental parameters like relaxation delay (d1) need to be optimized to develop an accurate qHNMR method as it may influence the appearance and intensity of the peaks in the ^{1}H-NMR spectra. T1 values for the protons employed for the quantitative analysis were found 2.8 s, 2.3 s, 1.8 s for GLC, GL and a mixture of GL/GLC, respectively. In order to satisfy the underlying principle of qHNMR technique (d1 ≥ 5T1), a d1 value of 14 s was used.

In few reports, shorter relaxation times were also employed during the qHNMR experiments [10]. Even in the present study, at shorter relaxation delay (4 s), ~ 90% signal

recovery was observed, as given in **Figure A.1,** Appendix A. Further, quantification results obtained by qHNMR either at 14 s or 4 s relaxation delay yielded comparable results, as shown in **Table 3.1**. Hence, to save the analysis time, qHNMR experiments were performed at 4 s of relaxation delay.

Table 3.1 Comparison of the actual glycerol carbonate concentrations and those predicted by the qHNMR at different relaxation delays.

S. No.	Mole % taken		Predicted % C_{GLC} by ^{1}H-NMR	
	GLC	GL	**d1= 4 s**	**d1= 14 s**
1	90	10	87.71	87.28
2	80	20	78.70	79.50
3	70	30	69.44	68.75
4	60	40	62.10	62.65
5	50	50	49.26	45.02
6	40	60	41.49	40.39
7	30	70	30.21	28.97
8	20	80	20.07	19.20
9	10	90	10.01	10

GLC = Glycerol carbonate, GL = Glycerol, C_{GLC} = % Molar concentration of glycerol carbonate, d1 = Relaxation delay

3.3.3 Quantifying the GLC and GL in a mixture with qHNMR

In the mixture of GLC and GL, which is practically observed during the GL transformation into GLC, both the molecules could be quantified by comparing the integration of proton signals corresponding to $\mathbf{c_1}$ of GLC and **d** of GL. With the progress of the reaction, the integration value of GL peaks would decrease while the integration value corresponding to GLC signals would increase. The equation is derived by considering that the integrated peak area in the ^{1}H-NMR spectra of a molecule is directly proportional to the number of protons, which was dependent on the molar concentration of that molecule [11].

In ^{1}H-NMR spectra of GLC, protons $\mathbf{c_1}$, $\mathbf{c_2}$ and $\mathbf{a_1}$, $\mathbf{a_2}$ appears as a doublet of doublets having equivalent areas as they correspond to one proton, as shown in **Figure A.2** (Appendix A).

Thus, % molar concentration of GLC (C_{GLC}) in a mixture of GL and GLC could be calculated by substituting the integrated peak areas corresponding to either **c_1**, **a_1**, or **a_2** protons of GLC and **d** proton of GL in either equation **3.1** or **3.2**.

$$\%C_{GLC} = 100 \times \left(\frac{I_{c_1}}{I_d + I_{c_2}}\right) \quad (\mathbf{3.1})$$

Another formula employing the integrated peaks areas $I_{a_1} or\ I_{a_2}$ of GLC could be used for the quantification purpose.

$$\%C_{GLC} = 100 \times \left(\frac{I_{a_1} or\ I_{a_2}}{I_d + I_{c_2}}\right) \quad (\mathbf{3.2})$$

Similarly, the unconverted amount of glycerol ($\%C_{GL}$) could also be calculated by substituting the peak areas corresponding to **c_1** protons of GLC and **d** protons of GL in equation **3.3**.

$$\%C_{GL} = 100 \times \left\{\frac{(I_d + I_{c_2}) - I_{c_1}}{I_d + I_{c_2}}\right\} \quad (\mathbf{3.3})$$

Where i) $\%C_{GLC}$ = percentage glycerol carbonate; (ii) I_{c_1}= integration of **c_1** of GLC at 3.736-3.793 ppm; (iii) I_{a_1}= integration of **a_1** of GLC at 4.534-4.470 ppm; (iv) I_{a_2}= integration of **a_2** of GLC at 4.242-4.303 ppm (v) $I_d + I_{c_2}$= total integration of **d** proton of GL and **c_2** proton of GLC superimposed at 3.557-3.640 ppm.

A comparison between actual GLC concentrations and those predicted by the equation **3.1** and **3.2** following the NMR method (**Table 3.2**), showed the acceptable agreements with a standard deviation value of up to ± 2 %. Thus, either of these two equations could be engaged to quantify the GLC present in a reaction mixture. It is due to the fact that integration values corresponding to the GLC protons employed in both the equations, *viz.*, I_{a_1}, I_{a_2} and I_{c_2}, correspond to one proton each, and the integration value corresponding to the GL proton *viz.*, I_d, was constant in both the equations. The linearity of the proposed qHNMR technique was also evaluated for both the equations (**Figure 3.3**), which demonstrated a correlation coefficient of > 0.99.

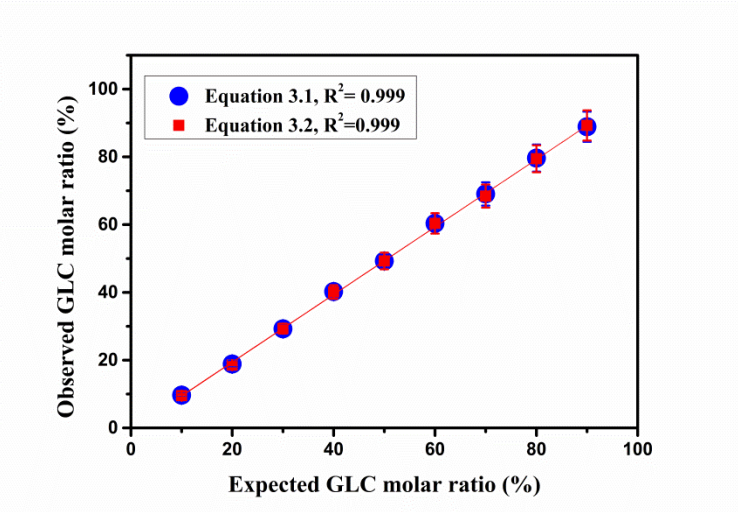

Figure 3.3 Linearity curve of the observed GLC molar ratio versus expected GLC ratio for the signal $\mathbf{c_1}$ (equation 3.1) and $\mathbf{a_1}$or $\mathbf{a_2}$ (equation 3.2) obtained in the ^{1}H-NMR spectrum of GLC.

Finally, the reproducibility of the method was tested by 3 different students using the same experimental conditions and employing equations **3.1** and **3.2**. The obtained results showed the acceptable agreement with the actual concentrations, as shown in **Table B.2** (Appendix B)**.** To demonstrate the application of these equations for the actual samples, GLC produced from the CaO assisted transesterification reaction was also quantified employing equation **3.1** and **3.2** and obtained results were given in **Table 3.2**. As evident from **Table 3.2**, the GLC quantification by qHNMR technique demonstrated the acceptable agreements with those obtained by the HPLC technique.

Table 3.2 Comparison of the actual glycerol carbonate concentrations and those predicted by the qHNMR and HPLC techniques.

S. No.	Mole % taken		Predicted % C_{GLC} by ^{1}H-NMR		Predicted % C_{GLC} by HPLC
	GLC	GL	Equation 3.1(± S.D.)	Equation 3.2(± S.D.)	
1	90	10	88.9 ± 1.05	89.28 ± 0.81	89.58
2	80	20	79.66 ± 0.97	79.45 ± 0.40	80.53
3	70	30	69.07 ± 1.59	68.44 ± 1.54	70.87
4	60	40	60.38 ± 1.64	60.38 ± 1.64	59.87
5	50	50	49.28 ± 0.21	49.28 ± 0.21	49.7
6	40	60	40.26 ± 1.08	40.12 ± 1.24	41.34
7	30	70	29.24 ± 0.88	29.32 ± 1.81	30.57
8	20	80	18.86 ± 1.96	18.52 ± 2.09	21.1
9	10	90	9.67 ± 0.42	9.5 ± 0.52	10.87
10	CaO based reaction		75.01	75.0	78.44

Values predicted by qHNMR technique are average of three measurements, S.D. = Standard Deviation, GLC = Glycerol carbonate, GL = Glycerol, C_{GLC} = % Molar concentration of glycerol carbonate

3.3.4 GLC quantification with HPLC

The prepared standard samples containing different molar ratios of GL and GLC were analyzed by HPLC technique to compare the results obtained by the qHNMR technique for GLC quantification. In HPLC chromatogram, GL and GLC retention times were found to be 14.176 and 15.30 min, respectively, using a mixture of hexane: isopropanol [20:80 (v/v)] as mobile phase. In the HPLC chromatogram of standard combinations of GL/GLC, %age peak area values were found directly proportional to the %age molar concentration of respective compounds (**Figure A.5-A.8**, Appendix A**)**. The results obtained by HPLC are comparable to those obtained by qHNMR technique, as shown in **Figure 3.4**.

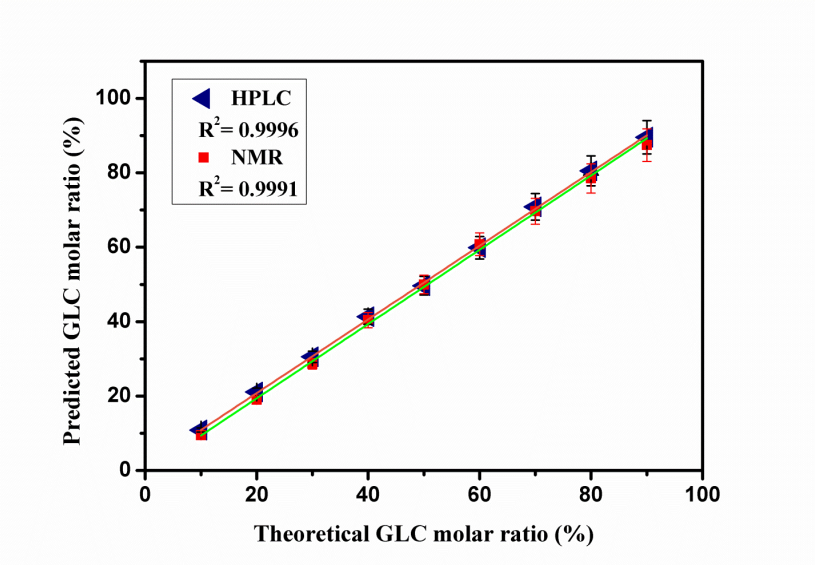

Figure 3.4 Plot showing the comparison of HPLC and ^{1}H-NMR predicted GLC molar values versus theoretical GLC molar ratios in standard GL/GLC mixtures (R^2= 0.999, 0.996 respectively).

3.4 Conclusions

For the first time, the present study purposes a straightforward equation for GLC quantification based on qHNMR technique. No significant difference in the GLC quantification values were obtained when the method was employed either at 14 s or 4 s of relaxation delay. The method proposed in the present study is simple, fast, non-destructive and accurate compared to those reported based on GC and HPLC techniques. GLC quantification values obtained by qHNMR method were found to show an acceptable correlation with those obtained by HPLC technique. Therefore, qHNMR could be employed as a quick and cost-effective alternative for GLC quantification in a mixture of GLC and GL.

References

[1] Q. Yang, H. Qiu, W. Guo, D. Wang, X. Zhou, D. Xue, J. Zhang, S. Wu, Y. Wang, Quantitative ^{1}H-NMR method for the determination of tadalafil in bulk drugs and its tablets, Molecules 20 (2015) 12114–12124. doi:10.3390/molecules200712114.

[2] G.F. Pauli, B.U. Jaki, D.C. Lankin, Quantitative ^{1}H NMR: Development and potential of a method for natural products analysis, J. Nat. Prod. 68 (2005) 133–149. doi:10.1021/np0497301.

[3] U. Holzgrabe, Quantitative NMR spectroscopy in pharmaceutical applications, Prog. Nucl. Magn. Reson. Spectrosc. 57 (2010) 229–240. doi:10.1016/j.pnmrs.2010.05.001.

[4] L. Wang, Y. Ma, Y. Wang, S. Liu, Y. Deng, Efficient synthesis of glycerol carbonate from glycerol and urea with lanthanum oxide as a solid base catalyst, Catal. Commun. 12 (2011) 1458–1462. doi:10.1016/j.catcom.2011.05.027.

[5] C.Hammond, J.A.Lopez-Sanchez, M.H. Ab Rahim, N.Dimitratos, R.L.Jenkins, A.F. Carley, Q. He, C.J. Kiely, D.W. Knight, G.J. Hutchings, Synthesis of glycerol carbonate from glycerol and urea with gold-based catalysts, Dalton Trans. 40 (2011) 3927-3937.

[6] H.M. McNair, J.M. Miller, Basic Gas Chromatography, second ed., John Wiley & Sons, Inc., Hoboken, New Jersey, 2009.

[7] U. Holzgrabe, R. Deubner, C. Schollmayer, B. Waibel, Quantitative NMR spectroscopy - Applications in drug analysis, J. Pharm. Biomed. Anal. 38 (2005) 806–812. doi:10.1016/j.jpba.2005.01.050.

[8] G. Rokicki, P. Rakoczy, P. Parzuchowski, M. Sobiecki, Hyperbranched aliphatic polyethers obtained from environmentally benign monomer: Glycerol carbonate, Green Chem. 7 (2005) 529–539. doi:10.1039/b501597a.

[9] D.O. Nogueira, S.P. De Souza, R.A.C. Leão, L.S.M. Miranda, R.O.M.A. De Souza, Process intensification for tertiary amine catalyzed glycerol carbonate production: Translating microwave irradiation to a continuous-flow process, RSC Adv. 5 (2015) 20945–20950. doi:10.1039/c5ra02117k.

[10] Z.W. Wang, J.S. Wang, M.H. Yang, J.G. Luo, L.Y. Kong, Developmental changes in the composition of five anthraquinones from rheum palmatum as quantified by ^{1}H-NMR, Phytochem. Anal. 24 (2013) 329–335. doi:10.1002/pca.2414.

[11] S.K. Bharti, R. Roy, Quantitative ^{1}H NMR spectroscopy, Trends Anal. Chem. 35 (2012)

5–26. doi:10.1016/j.trac.2012.02.007.

Lithium zirconate as a selective and cost-effective mixed metal oxide catalyst for glycerol carbonate production

Abstract

Alkali and alkaline metal (Li, Na, K, Ca, and Mg) loaded zirconium oxide catalysts were prepared by the wet impregnation method. All the prepared catalysts were employed as active heterogeneous catalysts for the transesterification of dimethyl carbonate (DMC) with glycerol (GL) producing glycerol carbonate (GLC). The catalyst with 20 wt% loading of Li on ZrO_2 showed maximum catalytic activity with 100 % selectivity towards GLC. The structure and basic properties of the prepared catalysts were studied by XRD, HRTEM, XPS, and CO_2-TPD techniques. The effect of various reaction parameters like catalyst concentration, reaction temperature, the molar ratio of reactants on the GLC yield was also studied. For the first time, the reaction product was quantified using the ^{1}H-NMR technique. The kinetics of dimethyl carbonate transesterification with glycerol is rarely reported in the literature, and hence, kinetic parameters of the reaction were also studied. The Li/ZrO_2 catalyzed transesterification reaction followed second-order kinetics with activation energy (Ea) of 93.7 kJ mol^{-1}. Thermodynamic parameters like enthalpy ($\Delta H^{\ddagger}$), entropy ($\Delta S^{\ddagger}$), and Gibbs free energy ($\Delta G^{\ddagger}$) of the activation were also determined.

4.1. Introduction

The performance of the heterogeneous catalyst was decided by its catalytic activity as well as stability [1]. An appropriate selection of the support would enhance the catalytic properties of the catalyst to a considerable extent. Owing to the high thermal stability and surface area [2] of zirconium oxide (ZrO_2), the same was utilized as a matrix for catalyst preparation. Various alkali (Li, Na, and K) and alkaline earth (Ca and Mg) metal-loaded ZrO_2 catalysts were prepared via the wet impregnation method and employed for the transesterification of DMC with GL to furnish GLC. ^{1}H-NMR technique was utilized for the first time for GLC quantification. Moreover, the kinetics of DMC transesterification was also studied under the optimized reaction conditions.

4.2. Experimental section

4.2.1 Catalyst preparation-wet impregnation method

Alkali and alkaline metal-doped zirconia catalysts, employed for the transesterification reaction, were prepared *via* the simple wet impregnation method. In a typical preparation, 10 g of zirconium oxide was suspended in 50 mL of deionized water, and to this 30 mL aqueous solution of lithium nitrate of desired concentration was added, and the resulting mixture was stirred for 4 h. After the stipulated time, the reaction mixture was filtered to obtain the off-white solid which was dried at 120 $^{\circ}$C for 12 h and then calcined at the desired temperature (500–800 $^{\circ}$C) for 4 h to get the corresponding catalyst. Similarly, ZrO_2 impregnated with Na or K or Ca or Mg were also prepared following the same experimental procedure as provided for Li/ZrO_2, but employing the appropriate nitrate salts of the metal. Prepared M/ZrO_2 catalysts were named as x-M/ZrO_2-T, where M, x, and T represent the impregnated metal, its content (wt%), and calcination temperature ($^{\circ}$C), respectively.

4.2.2 Preparation of the Li/ZrO_2 catalyst by the co-precipitation method

To access the impact of the catalyst preparation over the catalyst activity, Li/ZrO_2 catalyst having lithium and zirconium in an atomic ratio of 3:1 (Li/Zr) was also prepared by the co-precipitation method. In a typical preparation, 5 g of $ZrOCl_2.8H_2O$ and an appropriate amount of $LiNO_3$ were mixed in 50 mL distilled water. To this 25 wt% ammonium hydroxide solution was added to attain the pH of 10 in the reaction mixture. The resulting mixture was stirred for 4 h, filtered, and washed with distilled water to get rid of the residual nitrates and neutralizing the pH. The resulting white solid was then dried at 120 $^{\circ}$C for 24 h and calcined at 700 $^{\circ}$C for 3 h to activate the catalyst.

4.2.3 Catalytic activity test

The transesterification of DMC with GL was carried out in a 50 mL round-bottomed flask equipped with a magnetic stirrer, condenser, and oil bath. In a typical experiment, 54 mmol (5 g) of GL and 162 mmol (14.6 g) of DMC were placed into the flask, followed by the addition of 0.25 g (5 wt%) of the desired catalyst with continuous stirring. Subsequently, the reaction system was heated to the desired temperature for a designed time. The progress of the reaction

was monitored by thin-layer chromatography as per the method described in Chapter 2. After the stipulated reaction time, the catalyst was separated from the reaction mixture by filtration. Left out DMC and methanol present in the resulting reaction mixture were separated from the reaction mixture using a rotary-evaporator as they both form a lower boiling azeotropic mixture [3]. In order to ascertain that Li plays an important role in catalyzing the transesterification reaction, a blank reaction with bare ZrO_2 has also been performed. The GLC thus produced was characterized and quantified by ^{1}H-NMR spectroscopy (**Figure 4.1**) following the **equation (3.1)** derived in Chapter 3.

The reaction kinetics and the turnover frequency (TOF) of the prepared catalysts were determined using the method discussed in Chapter 2.

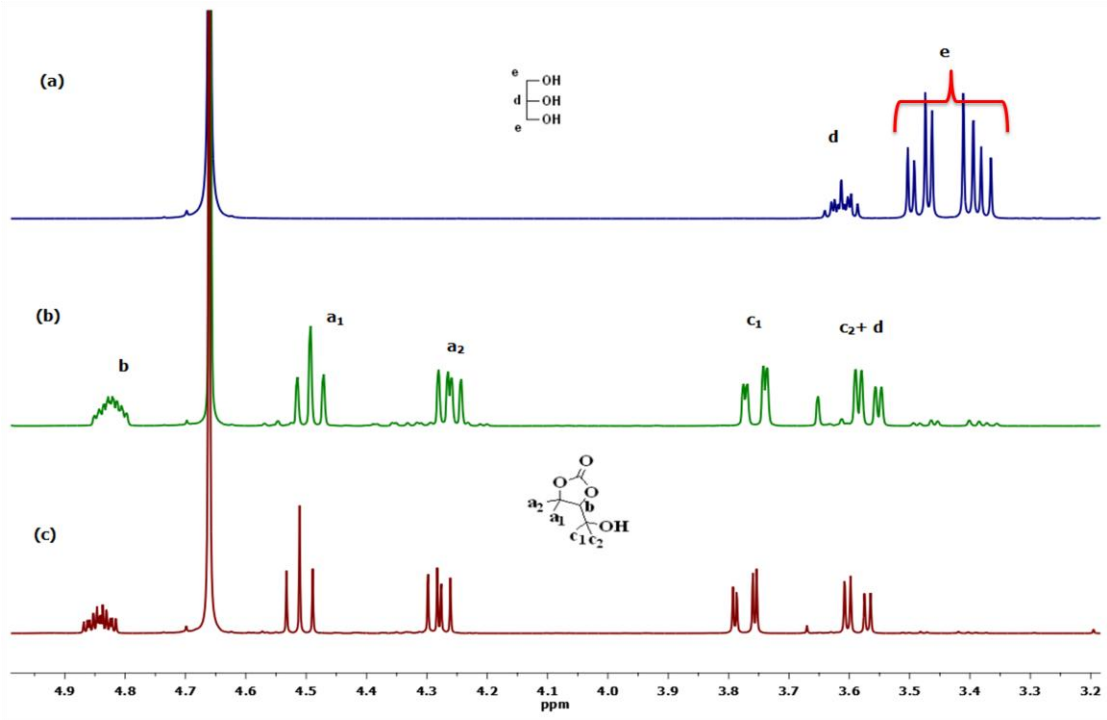

Figure 4.1 ^{1}H NMR spectra of (**a**) standard GL, (**b**) 20-Li/ZrO_2-700 catalyzed transesterification reaction, and (**c**) standard GLC.

4.3. Results and discussion

4.3.1 Catalyst Characterization

4.3.1.1 X-ray diffraction studies (XRD)

The XRD patterns of 20-Li/ZrO_2 calcined at various temperatures are shown in **Figure 4.2a**. At 500-600 $^{\circ}$C, characteristic reflections corresponding to a monoclinic phase of LiOH (JCPDS card no. 32-0564) and Li_2ZrO_3 (JCPDS card no. 76-1150) has been observed. As the temperature is further raised to 700 $^{\circ}$C, intense diffraction peaks consisting of a monoclinic phase of lithium zirconate (Li_2ZrO_3 and Li_4ZrO_4) (JCPDS card no. 76-1150 and 20-0645) were observed. The observed trend is in line with the studies conducted by Ida and coworkers [4] as they also observed an increase in peak intensity related to the monoclinic Li_2ZrO_3 phase with the increase in the calcination temperature due to a solid-state reaction between LiOH and ZrO_2. Senso et al. [5] also studied the effect of calcination temperature on ZrO_2 based catalyst and found the calcination under various environment leads to an increase in the monoclinic phase of zirconia. Minor traces of Li_2CO_3 found in the sample could be attributed to the reaction of formed Li_2ZrO_3 with atmospheric CO_2. A similar explanation has been given by Narasimharao et al. [6] for the formation of the Li_2CO_3 phase in the lithium zirconate sample. Comparison of XRD patterns of the samples with varying (5–25 wt%) lithium content (**Figure 4.2b**) also showed that at lower metal loading mixed monoclinic phases of ZrO_2, Li_2ZrO_3, and tetragonal ZrO_2 were formed. As the Li loading is increased gradually up to 25 wt%, the amount of monoclinic Li_2ZrO_3 and Li_4ZrO_4 phases was also found to increase. The presence of this secondary monoclinic phase of lithium zirconate (Li_4ZrO_4) could be attributed to the high amount of Li used during the synthesis stage [7].

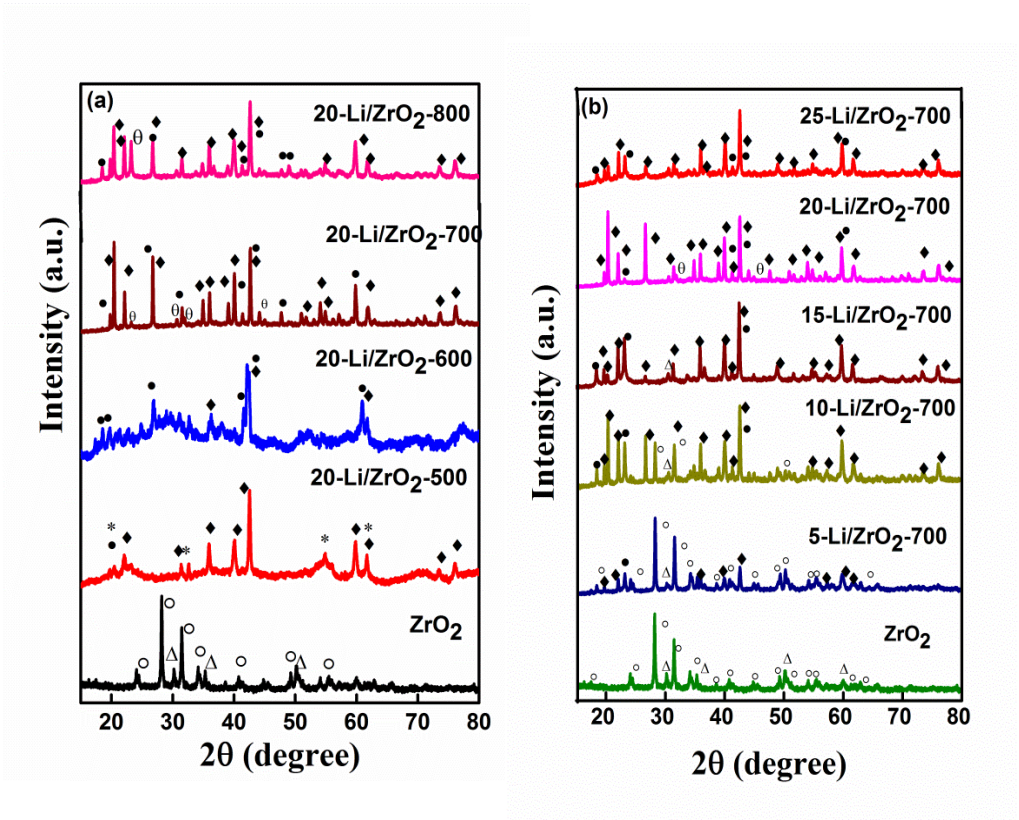

Figure 4.2 Comparison of XRD patterns of Li/ZrO_2 catalyst prepared by (**a**) varying calcination temperature, (**b**) varying lithium loadings [♦= monoclinic Li_2ZrO_3 (JCPDS card no. 76-1150), •= monoclinic Li_4ZrO_4 (JCPDS card no. 20-0645), *= tetragonal LiOH, (JCPDS card no. 32-0564), ◦= monoclinic ZrO_2, (JCPDS card no. 37-1484), θ = monoclinic Li_2CO_3 (JCPDS card no. 22-1141), Δ= tetragonal ZrO_2 (JCPDS card no. 50-1089)].

4.3.1.2 High resolution electronic microscopic study (HRTEM)

HRTEM images of the 20-Li/ZrO_2-700 catalyst are shown in **Figure 4.3a**. The prepared catalyst was found to possess particles of varied sizes. It is due to the agglomeration of the Li/ZrO_2 crystallites fused to form particles of bigger size having a somewhat cuboidal shape. The average particle size was found to be ~67 nm which is in close resemblance to the particle size depicted by XRD employing the Scherrer formula (~69 nm). Fauth et al. [8] also found the Li_2ZrO_3 particle in the agglomerated form with irregular shape. Narasimharao and Ali [6] has prepared Li_2ZrO_3 employing different organic and inorganic routes. They have found that depending on the preparation method, the crystallite size of the Li_2ZrO_3 particles varied between

50 and 100 nm. Lattice fringes of the catalyst particles are aligned in a parallel fashion with a lattice spacing of 0.34 and 0.28 nm (**Figure 4.3b,c**) correlating to the (112) and (111) planes of Li_4ZrO_4 and Li_2ZrO_3 phases, respectively. The corresponding SAED indexing pattern (**Figure 4.3d**) of 20-Li/ZrO_2-700 confirms the presence of the crystalline monoclinic planes (-223) (-513) (-511) of Li_4ZrO_4, (-131) (-311) of Li_2ZrO_3, and (231) of ZrO_2 phase as also supported by the powder XRD analysis.

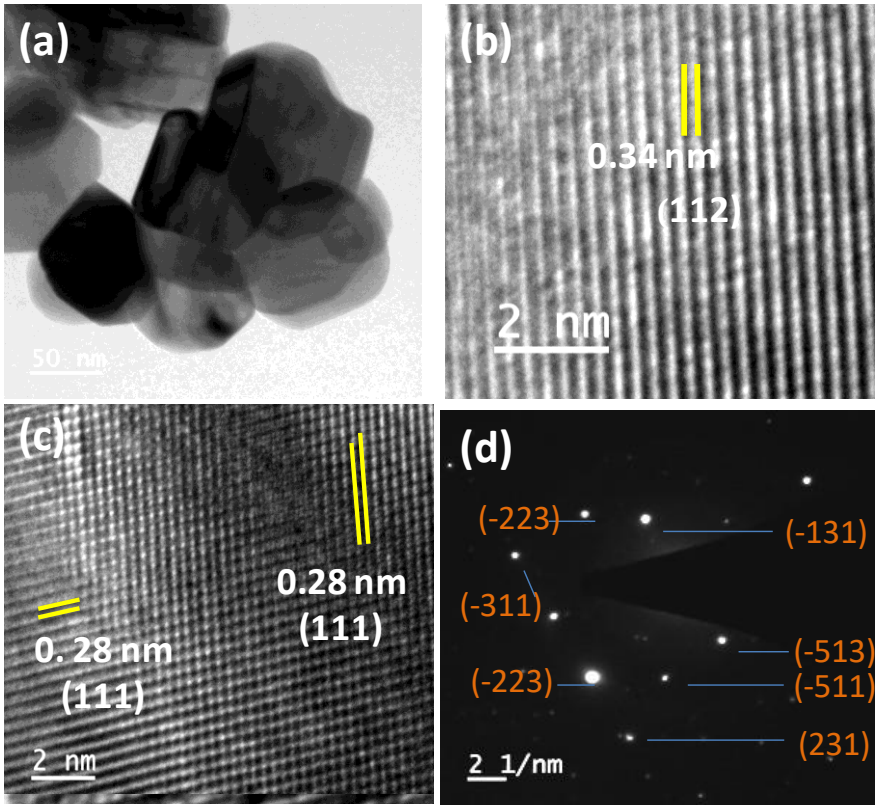

Figure 4.3 HR-TEM images of (**a**) aggregates of 20-Li/ZrO_2-700 particles; (**b,c**) lattice fringes corresponding to (112) plane of Li_4ZrO_4 and (111) plane of Li_2ZrO_3 and (**d**) SAED pattern of 20-Li/ZrO_2-700 catalyst.

4.3.1.3 X-Ray Photoelectron Spectroscopy (XPS)

The oxidation state of the elements present as well as the surface composition of the prepared 20-Li/ZrO_2-700 catalyst, was determined by XPS spectroscopy. The full scan spectra of the catalyst revealing the presence of Zr, Li, and O elements over the catalyst surface is shown in **Figure 4.4a**. The deconvoluted Li 1s spectra (**Figure 4b**) showed a minor peak at 55.11 eV and

another major peak at 55.99 eV. The minor peak at 55.11 eV could be attributed to the presence of Li bonded to C=O in Li_2CO_3 formed by the reaction of Li_2ZrO_3 with CO_2 (see **Scheme 4.1**). In literature also it has been found that with the capture of CO_2, Li 1s peak in Li_2ZrO_3 emerged at 55.1 eV [9]. Another Li 1s peak observed at 55.99 eV could be assigned to Li—O bond in the Li_2ZrO_3 phase. The result is in accordance with the XRD analysis as monoclinic Li_2ZrO_3 is the primary species observed in the 20-Li/ZrO_2-700 catalyst. Yuan and coworkers have also found the binding energy (B.E.) at 55.42 eV for the Li 1s in Li_2ZrO_3 nanofibers treated at 900 °C [10].

$$Li_2ZrO_3 + CO_2 \longrightarrow Li_2CO_3 + ZrO_2$$

Scheme 4.1 Decomposition of lithium zirconate by the reaction with atmospheric carbon dioxide.

Deconvoluted Zr 3d spectra showed intense doublet at 182.73 and 185.12 eV binding energies (**Figure 4.4c**) which could be ascribed to Zr $3d_{5/2}$ and Zr $3d_{3/2}$ peaks, respectively, formed due to spin-orbit coupling [11]. The separation between the two Zr 3d doublet peaks is 2.39 eV which is in agreement with the distinct separation of peaks corresponding to the compounds where zirconium is present in the +4 oxidation state [12]. The comparison of XPS spectra of the catalyst with that of native ZrO_2 (**Figure A.11,** Appendix A) indicates no significant change in the B.E. of the Zr 3d peaks. The observation further supports that the oxidation state and coordination environment of the Zr remains intact even upon the Li loading.
The O 1s peak, in the case of native ZrO_2, was observed at B.E. of 530.52 and 532.02 eV (**Figure A.10**, **A.11,** Appendix A), which could be ascribed to the O-Zr and O-H bonds, respectively [13]. However, the same peak in the case of Li/ZrO_2 (**Figure 4.4d**) was found to be positioned at 532.67 and 533.07 eV as major peaks while at 530.82 eV as a minor peak. The minor component observed at 530.82 eV corresponds to the lattice oxygen of lithium zirconate. The peak observed at 530 eV in the literature has been reported due to the lattice oxygen in Li_2ZrO_3 nanofibers [10] prepared by the electrospinning method. In the light of the Li 1s peak recognized at 55.11 eV, the peak observed at 532.67 eV could be assigned to the oxygen of the carbonate group present in the Li_2CO_3 phase. While conducting the CO_2 capture studies of Li_2ZrO_3, Peltzer et al. [9] have also assigned the peak at 532 eV to the carbonate oxygen.

Another, O 1s peak at 533.07 eV could be assigned to the O—Li bond in the Li_2ZrO_3 phase. This position is found to be similar to the peak observed at 533.8 eV for the O—Li bond, formed by loading the Li:Zr over silica to create Li-$ZrSiO_4$ [14]. Thus, upon lithium loading over ZrO_2, the environment around oxygen ions changes to support the interaction of Li with ZrO_2.

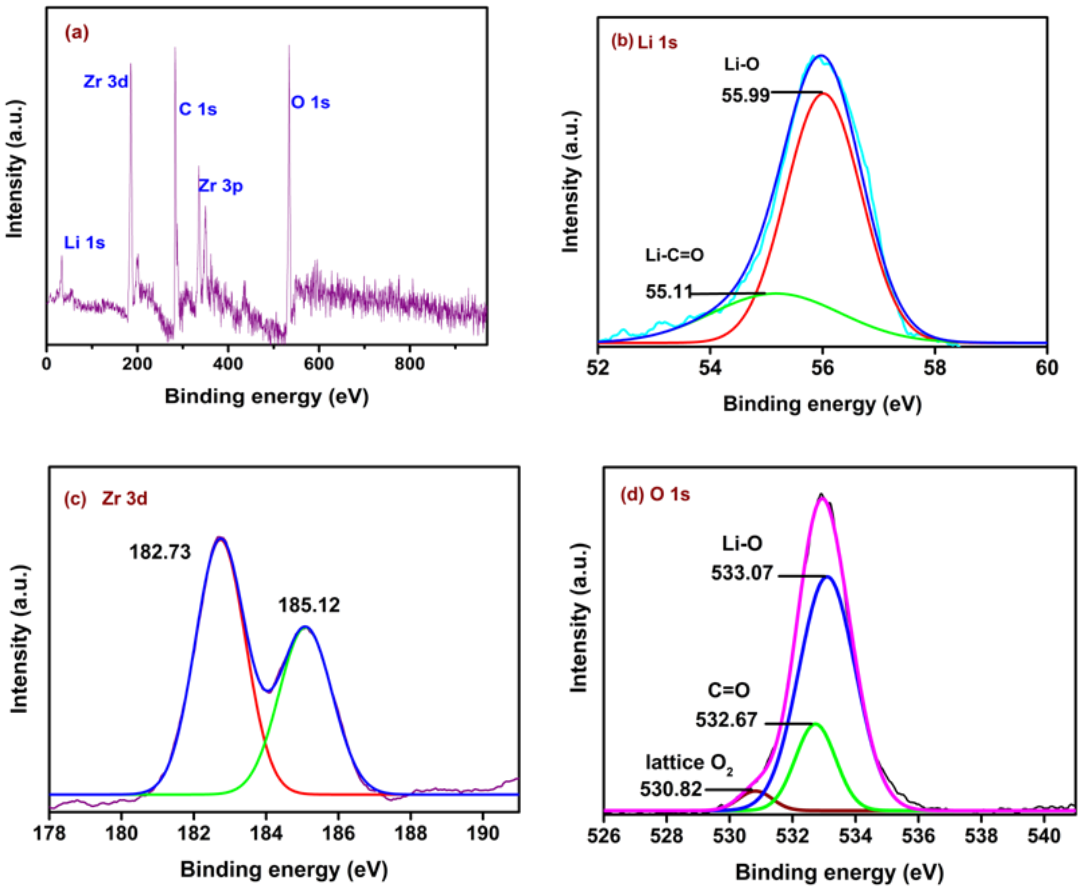

Figure 4.4 XPS spectra of (a) 20-Li/ZrO_2-700 catalyst full scan, and of the individual elements (**b**) Li, (**c**) Zr, and (**d**) O present in it.

4.3.1.4 CO_2- Temperature Programmed Desorption (CO_2-TPD)

The CO_2-TPD technique has been employed for the determination of the total basic sites present in the catalyst. In the present study, the CO_2-TPD has been performed up to 600 °C (**Figure 4.5**) to understand the basic strength of the 20-Li/ZrO_2-700 catalyst. The study suggested two different types of basic sites, namely, moderate (278 °C) and very strong (584 °C)

in the catalyst. The presence of desorption peaks at two distinct temperatures could be attributed to the two different modes of interactions of the CO_2 with the prepared catalyst, *viz.*, physisorption and chemisorption. The desorption peak at elevated temperature (not evolved completely) depicts that CO_2 has reacted with Li_2ZrO_3 to form the Li_2CO_3, which have been reported to have a decomposition temperature of higher than 1400 °C [13]. In the present study, complete CO_2 desorption is not achieved till 1000 °C for the 20-Li/ZrO_2 catalyst (Figure A.12, Appendix A) due to the high decomposition temperature of the Li_2CO_3. The total basicity calculated from the CO_2-TPD profile of 20-Li/ZrO_2-700 catalyst, up to 1000 °C, was found to be 2.01 mmol/g having a minimal contribution from the moderate basic sites (0.007 mmol/g).

In order to study the effect of Li content on the basic strength of the catalyst, the CO_2-TPD profile of the Li/ZrO_2 having the lithium contents in the range of 15-25 wt%, has been compared (**Figure 4.5**). The strong basic sites (~ 590 °C) were found to be maximum for the catalyst prepared with 20 wt% Li content, and hence, the same was selected for further study to optimize the reaction parameters for the GLC synthesis.

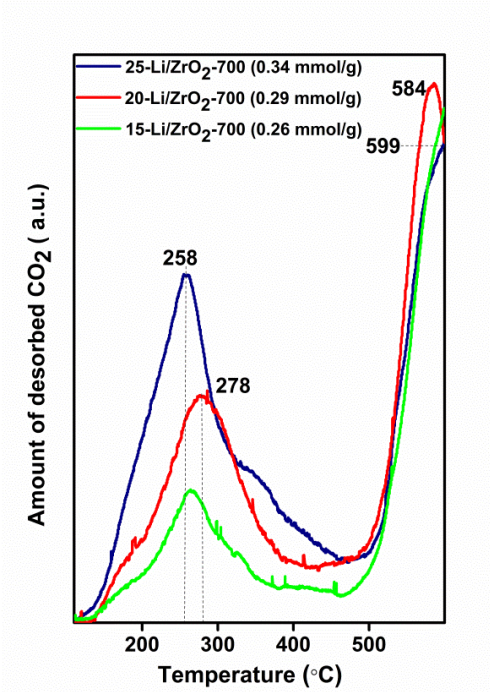

Figure 4.5 CO_2-TPD profile of Li/ZrO_2 catalysts with varying Li contents

To support the hypothesis that Li_2ZrO_3 constitutes the active sites of the catalyst, the CO_2-TPD of the catalyst has been compared with that of the commercially available Li_2ZrO_3 up to 750 °C. The comparison demonstrates almost similar desorption patterns (**Figure A.13,** Appendix A) to support that Li_2ZrO_3 is the major phase constituting the active sites of the catalyst. The basicity of the pure Li_2ZrO_3 (0.44 mmol/g) also comes similar to that obtained for the 20-Li/ZrO_2-700 catalyst (0.47 mmol/g).

Further, in order to ascertain that Li_2CO_3 has formed while performing the CO_2-TPD experiment, in a blank run, of TPD of 20-Li/ZrO_2-700 catalyst without CO_2 adsorption has also been performed (**Figure 4.6**). It is evident from the comparison that negligible desorption of gases was observed in the sample which was not exposed to the CO_2. Thus it is safe to assume now that Li_2CO_3 has formed when the catalyst is exposed to CO_2 while performing the CO_2-TPD.

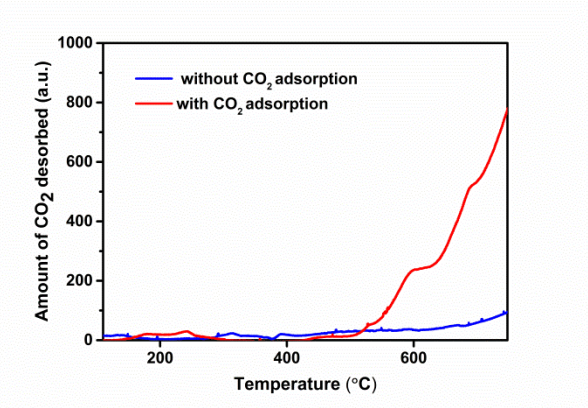

Figure 4.6 Comparative study of the CO_2-TPD profile of the 20-Li/ZrO_2-700 catalyst with and without CO_2 adsorption.

The powder XRD analysis also supported the presence of Li_2ZrO_3 as a major phase in the catalyst, which could be associated with the Lewis basic sites due to the presence of oxide ions [6]. The CO_2-TPD profile could also be used to distinguish between Bronsted, and Lewis basic sites [6] as Lewis sites demonstrates the desorption at higher temperatures in comparison to the Bronsted sites. In the case of KF/La-Zr catalyst, Song et al. [15] have assigned the lower temperature (150 °C) desorption of CO_2 to the Bronsted sites (surface hydroxyl groups) and that of a higher temperature (560 and 630 °C) to the Lewis basic sites. Because in the present study,

no desorption peak was observed at less than 250 °C, hence, all basic sites could be associated with the Lewis one.

4.3.2. Catalytic activities

4.3.2.1 Screening of alkali and alkaline metals loaded ZrO_2 catalysts

ZrO_2 is a typical acid-base bifunctional oxide that has offered its catalytic properties for the synthesis of olefins, 1-butene, allyl alcohols, and so forth. ZrO_2 has also been employed as catalyst support, and the addition of alkali metals was found to enhance the basic properties of the resultant catalyst [2]. Based on this analogy, a series of different alkali and alkaline metals (Li, Na, K, Ca, and Mg) impregnated ZrO_2 catalysts were prepared in the present study. The catalytic activities of the prepared catalysts were compared by carrying out the transesterification reaction of DMC with GL (GL: DMC molar ratio 1:3) at 95 °C for 2 h (**Figure 4.7a**). All the prepared catalysts were found to be 100 % selective towards the GLC as no other side product was obtained during the transesterification reaction. Among the catalysts, prepared by varying the impregnated metals, Li and K one demonstrated the higher activity in comparison to the rest of the catalysts. However, when the stability of the Li/ZrO_2 and K/ZrO_2 was compared former was found to be more stable based on metal content analysis in the reaction mixture (**Table B.3,** Appendix B). Consequently, Li/ZrO_2 was selected for the detailed study owing to its higher stability. In order to correlate the activity with the structure of the catalyst, the powder XRD plots for the Li or K or Na containing ZrO_2 catalysts (**Figure A.14,** Appendix A) had also been compared, which revealed the formation of multi phases in case of later two while a major phase of lithium zirconate in case of Li impregnated one. For the Li/ZrO_2 catalyst, due to the size similarity of Li^+ and Zr^{4+} (0.76 and 0.72 °A, respectively), both the ions were expected to exchange their positions readily to form the Li_2ZrO_3 as a major phase [16]. This was further supported by another report where Zn^{2+} (0.74°A) have been substituted with Li^+ (0.76 °A) from the lattice because of their comparable ionic radii while preparing the Li/ZnO catalyst, *via* wet impregnation method, for the transesterification of the DMC with GL [17]. Thus among all the prepared catalysts, Li/ZrO_2 was found to have greater stability as well as better activity for the GL conversion (91 %) (**Figure 4.7b**), and hence, it was opted for the detailed study.

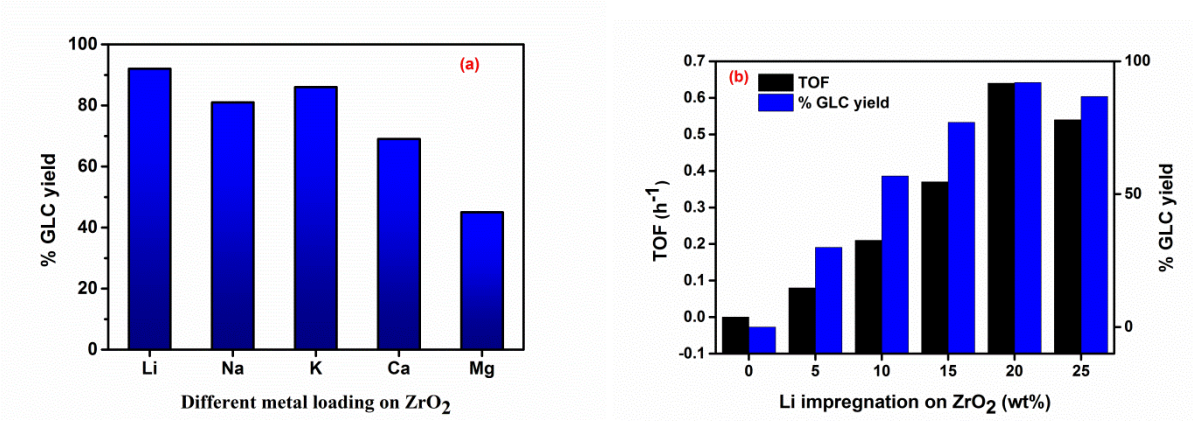

Figure 4.7 Graphs showing the effect of (**a**) variation of metal and (**b**) Li wt% loading on the GLC yield under optimized reaction conditions. (Reaction conditions: DMC/GL molar ratio 3:1, catalyst amount= 5 wt% of the catalyst concerning GL, temperature 95 $^{\circ}$C, time 2 h).

4.3.2.2 Selection of the preparation method

In the literature, wet impregnation and co-precipitation are the two methods that have been widely employed for the preparation of the heterogeneous catalyst. However, both the methods have their advantages as well disadvantages. In the present study, the wet impregnation method is employed as it is faster, simple, and generates lesser wastes [18]. The main drawback of this method is the formation of the catalyst with relatively lesser surface area; however, this method allowed the homogeneous distribution of the active species over the catalyst surface owing to the similarity in the matrix (Zr^{4+}) and impregnated metal (Li^{+}) ions size [19].

To study the influence of the preparation method upon the catalytic activity, two different preparation methods *viz.*, co-precipitation and wet impregnation methods, have been employed for the preparation of Li/ZrO_2 catalyst. The comparison of the catalytic activities of Li/ZrO_2 catalysts prepared by these two methods revealed that higher GLC yield (91 %) was obtained by Li/ZrO_2 catalyst prepared by wet impregnation method as compared to the one prepared by co-precipitation method (68 %). In order to correlate the catalyst activity with its structure, the XRD data of the catalysts, prepared by both the preparation methods have also been compared (**Figure 4.8**). The catalyst prepared *via* the wet impregnation method supported the formation of monoclinic Li_2ZrO_3 as major a phase. However, in the case of the co-precipitation method, the diffraction patterns suggest the minimal interaction between Li and ZrO_2 to yield the bare ZrO_2

as a major phase and tetragonal Li_2ZrO_3 as a minor phase. Thus, the formation of monoclinic Li_2ZrO_3 is required for better catalytic activity, and the same is achieved in the case of the wet impregnation method. Thus, the wet impregnation method is preferred over the co-precipitation method for the catalyst preparation in the present study.

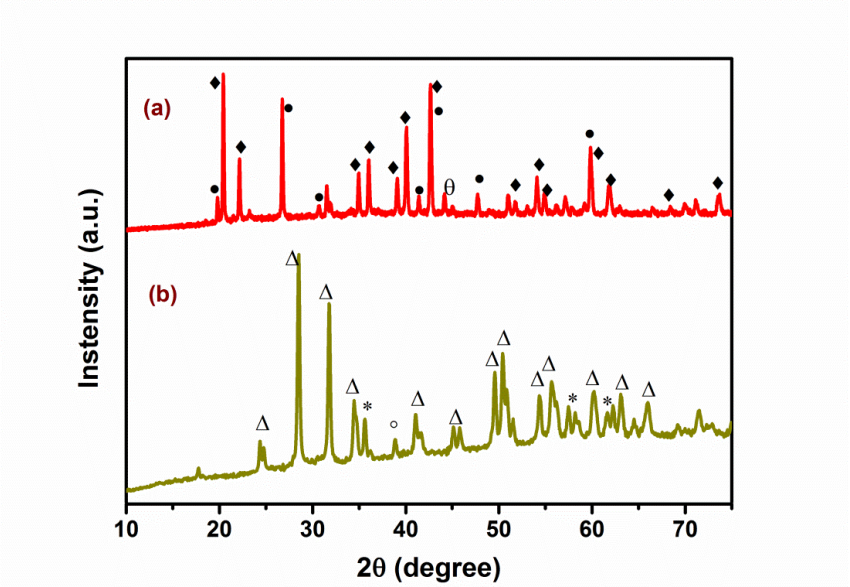

Figure 4.8 Comparative study of the XRD pattern of the Li/ZrO_2 catalyst prepared by the (**a**) wet impregnation method (**b**) and co-precipitation method [♦= monoclinic Li_2ZrO_3 (JCPDS card no. 33-0843), •= monoclinic Li_4ZrO_4 (JCPDS card no. 20-0645), *= tetragonal Li_2ZrO_3 (JCPDS card no. 041-0324), ◦= cubic Li_2O, (JCPDS card no. 065-2972), θ = monoclinic Li_2CO_3 (JCPDS card no. 22-1141), Δ= monoclinic ZrO_2 (JCPDS card no. 013-0307)].

4.3.3. Optimization of influencing reaction parameters

From the economic point of view, it is vital to determine the parameters which are optimum to make the GLC production cost-effective. The prime objective for the optimization is to achieve maximum GLC yield in the lesser possible time. For the determination of the optimized reaction conditions, a series of transesterification reactions were carried out using Li impregnated ZrO_2 catalyst varying one parameter at a time out of the following: (i) Li content on ZrO_2 (ii) catalyst amount with respect to GL, (iii) DMC to GL molar ratio, and (iv) reaction

temperature. The reusability of the catalyst was also evaluated under the optimized reaction conditions.

4.3.3.1 Effect of Li metal concentration on the catalyst activity

The transesterification reaction of DMC with GL is generally relying on the basic strength of the catalyst [2]. Higher catalyst basicity is usually found to catalyze the reaction to a greater extent. The basicity of the prepared catalysts was found to a function of alkali metal contents along with the calcination temperature opted for the catalyst preparation. In order to study the effect of the Li metal loading on the catalytic activity of the catalyst, a series of the catalyst with varying Li concentrations (0-25 wt%) was prepared, and the transesterification reaction was performed at 95 °C employing DMC to GL molar ratio of 3. The GL conversion was found to increase with Li loading up to 20 wt%, after which no significant increase in GLC yield was observed with a further increase in Li loading **Figure 4.7b**. It has also been observed in XRD analysis that 20 wt% Li loaded catalyst has more intense peaks of monoclinic Li_2ZrO_3 phase than in 25 wt% Li loading. No significant conversion is obtained in the absence of Li in ZrO_2 to ascertain that lithium ions are acting as the catalytic center and ZrO_2 is playing the role of the matrix for the immobilization of the active species. Moreover, the TOF calculation supports that the 20-Li/ZrO_2 catalyst showed maximum turnover (0.64 h^{-1}) as compared to the 15 wt% (0.37 h^{-1}) and 25 wt% (0.54 h^{-1}) loaded Li/ZrO_2 catalyst (**Figure 4.7b**). Hence, 20-Li/ZrO_2 was employed further for optimizing the other reaction parameters to achieve maximum GL conversion.

4.3.3.2 Effect of calcination temperature

In order to enhance the catalytic activity of the catalysts, the obtained metal hydroxides were calcined beyond their decomposition temperature, forming their respective metal oxides having a higher number of lewis basic sites (O^{2-}) [16]. High-temperature treatment may also promote the solid-state interaction among the catalyst component providing more stability to the catalyst. The calcination temperature was optimized by calcining the 20-Li/ZrO_2 catalyst in the range of 500–800 °C. The catalytic activity was found to increase with the increase in the calcination temperature as shown in **Figure 4.9a**. The highest activity was observed for 20-Li/ZrO_2-700. The XRD study has also supported the solid-state reaction between LiOH and ZrO_2

to form the Li_2ZrO_3 phase at 700 °C calcination temperature. Further increase in the calcination temperature (800 °C) has a minimal effect on the catalytic activity of the catalyst; thus 700 °C temperature has been selected for carrying out the calcination of the prepared 20-Li/ZrO_2 catalyst.

4.3.3.3 Effect of catalyst amount

In order to find out the optimum catalyst concentration for achieving maximum GLC yield, transesterification reactions were performed, varying the catalyst amount with respect to GL from 1 to 7 wt%. Higher is the catalyst amount, more will be the accessibility of the active sites present on the catalyst surface to the substrate, and accordingly greater will be the conversion levels. The same trend has been observed in the case of DMC transesterification reaction as GLC yield was found to increase with the increase in the catalyst concentration from 1 to 5 wt% as shown in **Figure 4.9b**. However, when the catalyst loading was further increased to 7 wt%, no significant increase in the GLC yield was observed. This could be due to the increase in the viscosity of the reaction mixture, causing the improper mixing to cause the reduced interactions between the reactants and the catalyst. Thus 5 wt% catalyst amount was selected for further transesterification reaction.

4.3.3.4 Effect of reactants molar ratio

Theoretically, equimolar ratios of reactants are required for carrying out the complete transesterification of DMC. However, to drive the reversible transesterification reaction in the forward direction, to obtain the maximum GLC yield, an excess amount of the carbonate source is required [20]. In order to determine the optimal DMC/GL molar ratio, a string of transesterification reactions was performed with 5 wt% of 20-Li/ZrO_2-700 at 95 °C with varying DMC/GL molar ratio from 1:1 to 5:1. It was found that GLC yield increases as the DMC/GL molar ratio was raised from 1:1 to 3:1. As evident from **Figure 4.9c**, GLC yield reached the maximum at GL/DMC molar ratio 3. Further, increase in the DMC/GL molar ratio leads to a drop in the GLC yield as it decreases the glycerol concentration in the reaction mixture resulting in a lower reaction rate [20]. This observation has also been supported in the literature by Simanjuntak et al. [21] while studying the Mg/La catalyzed transesterification reaction of the DMC with GL. They have studied the impact of the increase in DMC to GL molar ratio (up to

10) on the reaction rate. During the study, maximum GL conversion is obtained at a DMC/GL molar ratio of 4 and a further increase in the DMC/GL molar ratio was found to decrease the GLC yield. From the study, it has been concluded that the decrease in the GL conversion is due to the lesser interaction of the catalyst with GL on increasing the DMC molar ratio.

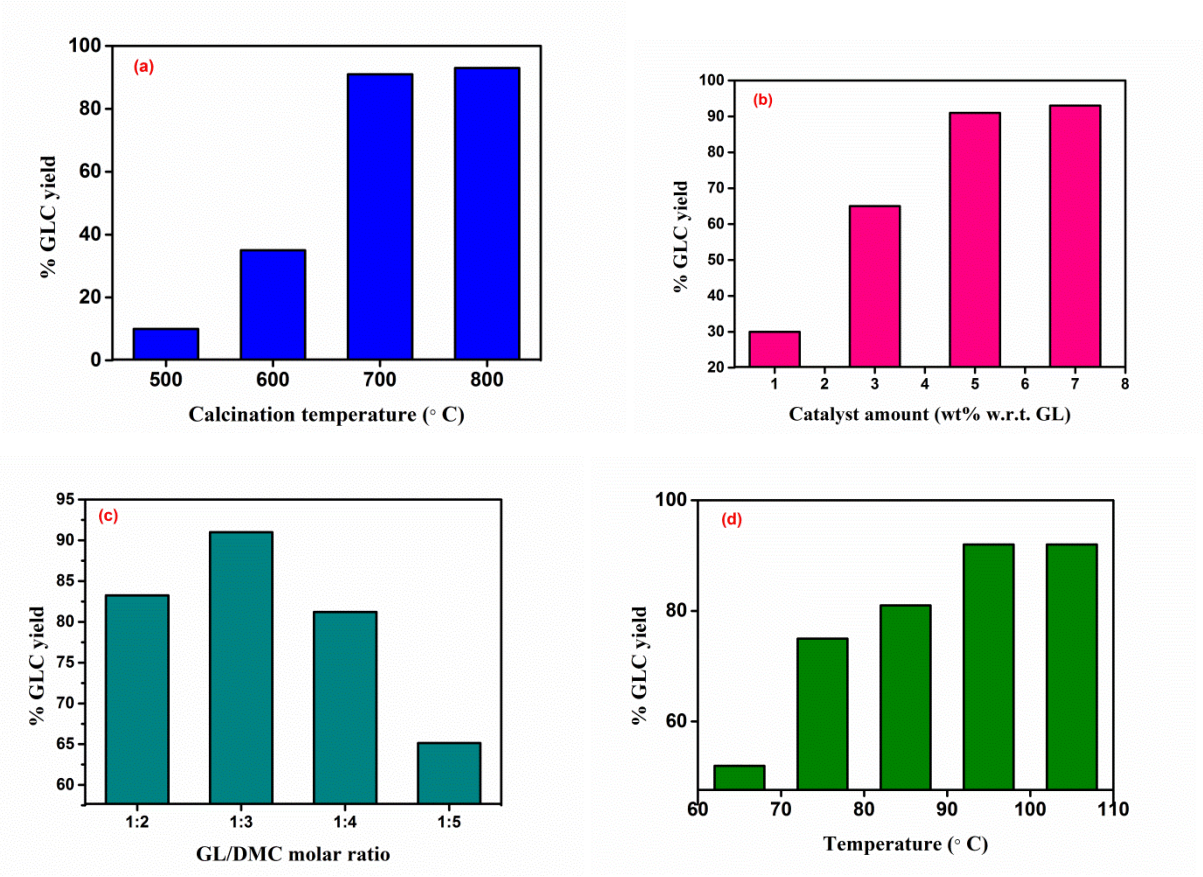

Figure 4.9 Effect of (**a**) catalyst calcination temperature (Reaction conditions: DMC/GL molar ratio 3:1, catalyst amount= 5 wt% of catalyst with respect to GL, temperature 95 °C, time 2 h); (**b**) catalyst concentration with respect to GL (Reaction conditions: DMC/GL molar ratio 3:1, temperature 95 °C, time 2 h); (**c**) GL/DMC molar ratio (Reaction conditions: catalyst amount= 5 wt% of catalyst with respect to GL, temperature 95 °C, time 2 h) and (**d**) reaction temperature on the transesterification of DMC yielding GLC (Reaction conditions: DMC/GL molar ratio 3:1, catalyst amount= 5 wt% of catalyst with respect to GL, time 2 h).

4.3.3.5 Effect of reaction temperature

As the transesterification reaction of DMC with GL is reversible in nature, the reaction temperature is one of the prime factors determining the fate of the reaction. Generally, an increase in the temperature will lead to an increase in the collisions of the reactants and the catalyst and thus results in higher product yield [20]. In order to determine the effect of the reaction temperature on GLC yield, transesterification reactions were performed in the range of 65-105 °C employing a 3:1 DMC/GL molar ratio 5 wt% of 20-Li/ZrO_2-700 catalyst. It has been observed that an increase in the temperature up to 95 °C has pushed the reaction in the forward direction resulting in higher GLC yield (**Figure 4.9d**). However further increase in the temperature has not enhanced the GLC yield to a considerable extent. A similar trend has been found in the literature for Mg/Zr/Sr catalyst where 90 °C has been optimized for obtaining maximum GLC yield [22]. In most of the literature reported DMC-assisted synthesis of GLC, a temperature range of 70-100 °C has been opted to obtain the maximum GLC yield [20, 43]. Thus 95 °C has been optimized for the DMC transesterification reaction in the present chapter.

4.3.4 Regeneration of the used catalyst

Reusability is one of the important aspects of heterogeneous catalysts as it enhances its utility at an industrial level by reducing the production cost of the desired chemical. The reusability of the 20-Li/ZrO_2-700 catalyst was studied for the transesterification reaction of DMC with GL under the optimized reaction conditions (catalyst 5 wt%, DMC/GL molar ratio 3:1, 95 °C, and 2 h of reaction duration). Prior to reuse, the recovered catalyst has been regenerated under two different conditions *viz.*, (i) simple washing of the recovered catalyst with methanol followed by drying (120 °C), and (ii) methanol washing of the recovered catalyst, drying (120 °C), and recalcination at 700 °C. The catalyst regenerated by methods (i), and (ii) upon first reuse was found to give 56 % and 80 % GLC yield, respectively. In order to understand the reason behind the difference in activity, the XRD patterns of the regenerated catalyst, under both the methods, have been compared with the fresh catalyst, as shown in **Figure 4.10**. As evident from the comparison, major structural changes have occurred during the catalyst usage and washing. However, these changes could be reversed upon recalcination. Thus, the recalcination

method was employed for catalyst regeneration to achieve better catalyst reusability as well as stability.

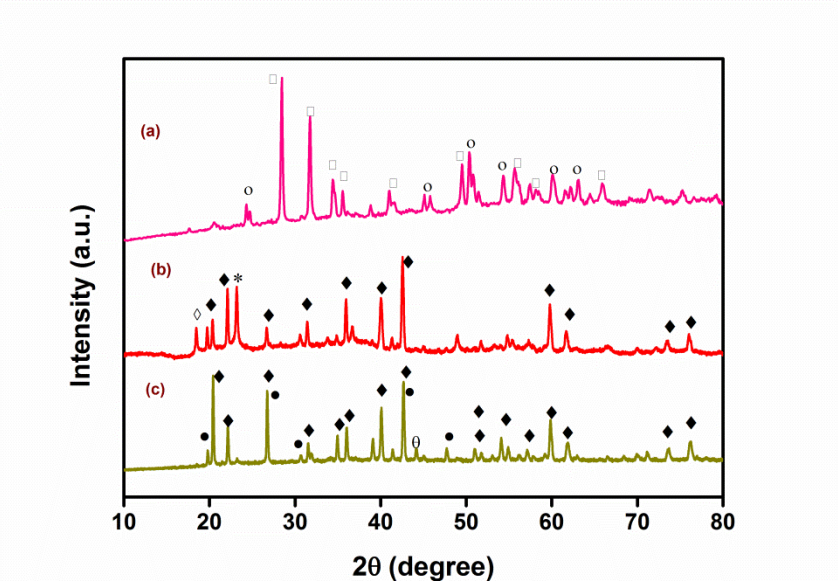

Figure 4.10 Comparison of the XRD pattern of the 20-Li/ZrO_2-700 catalyst recovered by (**a**) method (i) and (**b**) method (ii) with that of (**c**) fresh catalyst. [♦= monoclinic Li_2ZrO_3 (JCPDS card no. 33-0843), •= monoclinic Li_4ZrO_4 (JCPDS card no. 20-0645), * = Li_4ZrO_4 (JCPDS card no. 036-0121], θ = monoclinic Li_2CO_3 (JCPDS card no. 22-1141), ◊ = monoclinic $Li_6Zr_2O_7$ (JCPDS card no. 81-2375), □ = monoclinic ZrO_2 (JCPDS card no. 013-0307), ○ =monoclinic Li_2ZrO_3 (JCPDS card no. 076-1150)]

4.3.5 Recyclability of the catalyst

The catalyst regenerated by method (ii) was reused under the optimized reaction conditions during four successive runs by following the identical experimental and regeneration conditions. The catalyst reused during the first run was found to yield the 81 % GLC yield, which gradually decreases to 52 % during the last run, as shown in **Figure 4.11**. On the other hand, it is worth mentioning, GLC selectivity is maintained during all the catalytic cycles as shown in **Figure 4.11**. The product mixture was found to have GLC and unreacted GL without forming any other side product (**Figure A.15**, Appendix A).

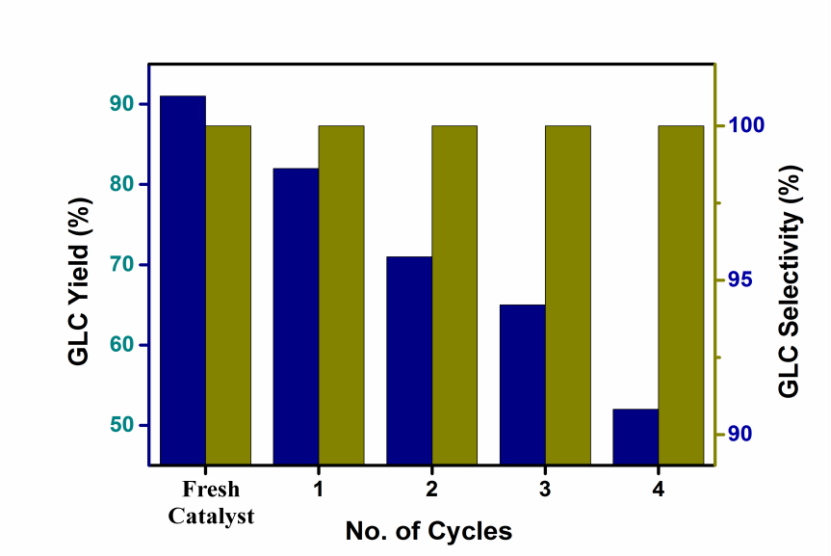

Figure 4.11 Reusability study of 20-Li/ZrO_2-700 catalyst (Reaction conditions: GL/DMC molar ratio = 1:3; Catalyst amount = 5 wt% with respect to GL; Temperature = 95 °C, time 2 h).

In order to understand the decline in catalyst activity, the XRD patterns of the fresh and reused catalyst have been compared as shown in **Figure 4.12**. The XRD analysis showed the formation of tetragonal Li_2ZrO_3 as a major phase and another minor phase of $Li_6Zr_2O_7$ in the reused catalyst (**Figure 4.12**). Thus structural changes have occurred upon the repeated use of the catalyst and the same could be the reason behind the decline in catalytic activity.

Since XRD analysis of the reused catalyst indicated the structural changes which might results in the partial dissolution of the catalyst into the reaction mixture. In order to evaluate the metal contents into the reaction mixture, the organic phase obtained after the 4^{th} cycle was analyzed for the Zr and Li contents. While Zr contents could not be detected in the reaction mixture, a negligible Li content (1.61 ppm) was observed to support the highly stable nature of the catalyst (**Table B.3**, Appendix B). The Li^+ dissolved into the reaction mixture could catalyze the reaction similar to a homogeneous catalyst. Therefore, a hot filtration test has been employed to establish the homogeneous contribution in the catalytic activity. The transesterification reaction was performed under optimized reaction conditions employing 20-Li/ZrO_2-700 as a catalyst. The catalyst was removed after 60 min by filtration, and filtrate was again allowed to react for another 1.5 h. After the stipulated time, only 8 % gain in the GLC yield was obtained to rule out any significant homogeneous contribution in catalytic activity (**Figure A.16**, Appendix A). In order to confirm the catalyst stability, the Li content in the fresh and reused catalyst has

been determined. The analysis reveals that the Li content in the recovered catalyst (131 ppm) was found almost similar to that of the fresh catalyst (134 ppm). The observation supported the catalyst stability and also further eradicates the possibility of the presence of lithium in the reaction mixture due to the catalyst leaching.

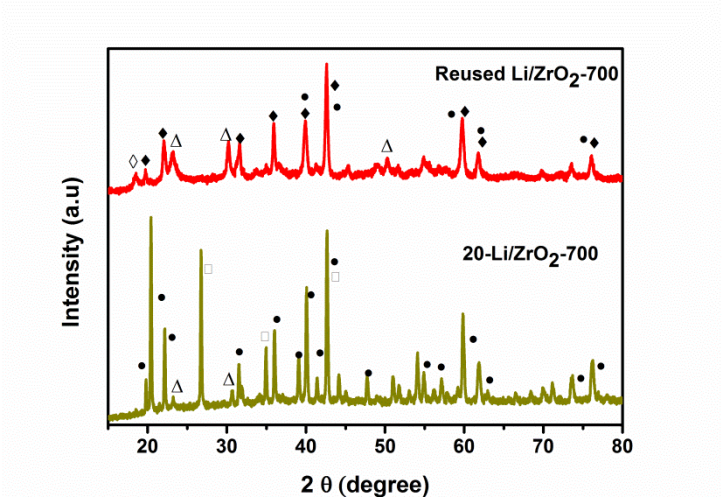

Figure 4.12 Comparison of XRD patterns of fresh and reused 20-Li/ZrO_2-700 catalyst. ([♦=tetragonal Li_2ZrO_3 (JCPDS card no. 20-0647), •= monoclinic Li_2ZrO_3 (JCPDS card no. 76-1150), □= monoclinic Li_4ZrO_4 (JCPDS card no. 20-0645), ◊= monoclinic $Li_6Zr_2O_7$ (JCPDS card no. 81-2375), Δ = monoclinic Li_2CO_3 (JCPDS card no 22-1141)].

4.3.6 Reaction Kinetics

There has been a scarcity of data related to the kinetics study of the transesterification of DMC forming GLC. In order to study the reaction kinetics of the reaction, transesterification of the DMC with GL was performed in the presence of 20-Li/ZrO_2-700 catalyst at various reaction temperatures (65-95 $^{\circ}$C) employing a DMC/GL molar ratio of 1:3 for 2 h. The order of the reaction was determined by fitting the appropriate values in zero, first and second-order rate equations provided in Chapter 2. Among all the plotted graphs, the linear nature of ($1/1-X_{glc}$) versus *t* plot was obtained with second-order rate law (**Figure 4.13c**). The apparent second-order rate constant from the plot has been found to be 0.07 $M^{-1}s^{-1}$ at 95 $^{\circ}$C.

This observation is expected as in the present study GL and DMC have been used in 1:3 molar ratios under optimized reaction conditions. In literature similar observations were

reported, for example, Singh et al. have purposed a second-order kinetic model for the Zn/La catalyzed synthesis of GLC from GL. They have performed the reaction in a batch autoclave utilizing a 1:4 molar ratio of GL and DMC [23]. Yadav et al. have applied the Langmuir–Hinshelwood–Hougen–Watson (LHHW) model for studying the kinetics of the GLC formation employing the silica-supported hydrotalcites as a heterogeneous catalyst and employing GL: DMC molar ratio of 1:3. On the basis of the study, they have also concluded that the reaction is a kinetically controlled one following a second-order rate law [24].

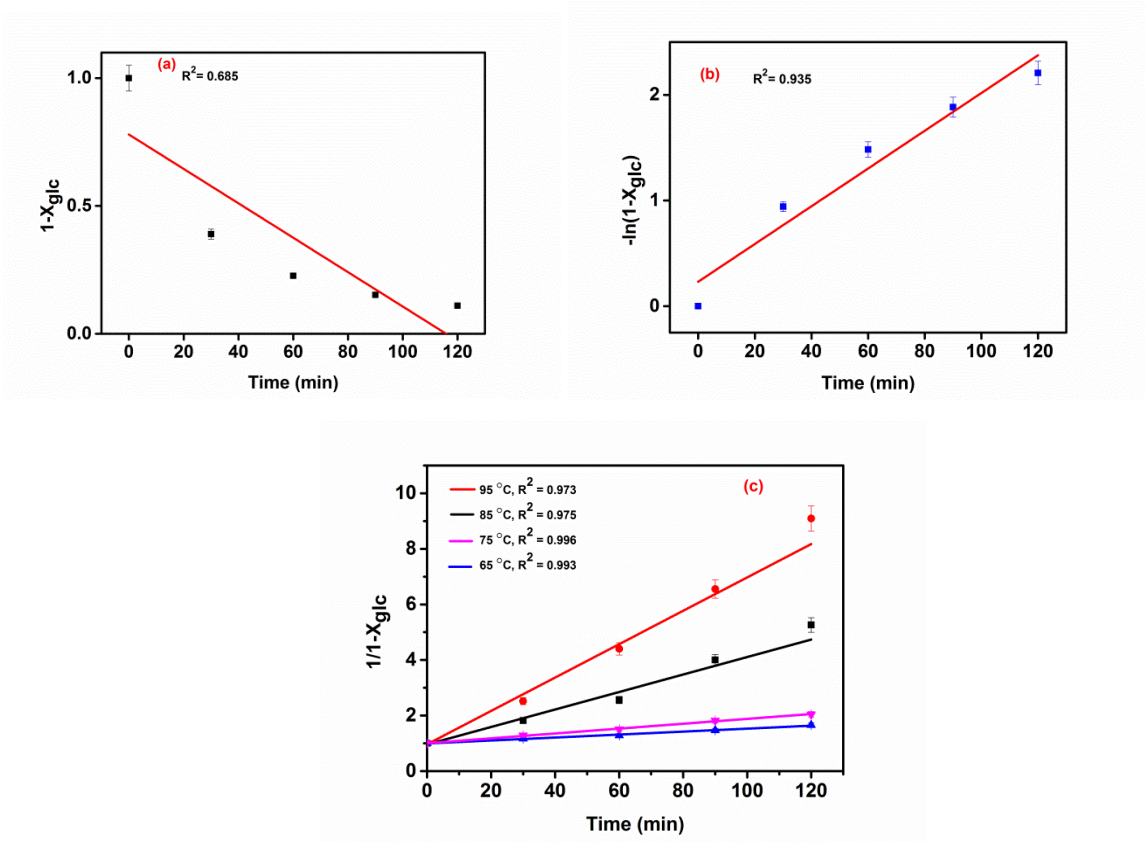

Figure 4.13 A plot of (**a**) l-X_{glc} ; (**b**) –ln(1–X_{glc}) and (**c**) 1/1-X_{glc} *versus* reaction time (t) at different temperatures (Reaction conditions: GL/DMC molar ratio = 1:3 ; catalyst amount = 5 wt% with respect to GL, time 2 h).

The Arrhenius model was employed to estimate the activation energy (E_a) of the reaction following the **equation (2.2)** (provided in Chapter 2) and the corresponding plot between ln k vs. 1/T was shown in **Figure 4.14a**. The value of E_a from the same plot was found to be 93.7 kJ mol^{-1}. In literature, activation energies for the transesterification of dialkyl or cyclic organic

carbonates with GL have been reported in the range of 55.5 - 87.9 kJ mol^{-1} [24–27]. The enthalpy (ΔH‡) and entropy (ΔS‡) of activation calculated from the linear plot between ln (k/T) and 1/T (**Figure 4.14b)** were found to be 90.68 kJ mol^{-1} and -0.02 kJ mol^{-1} $K^{-1,}$ respectively. By substituting the values of ΔH‡ and ΔS‡ in **equation (2.4)** (Chapter 2), Gibbs free energy (ΔG‡) of the activation was found to be 98.7 kJ mol^{-1}. All the values reported for rate constant and thermodynamic activation parameters are apparent. The positive value of ΔG‡ confirmed that the transesterification reaction of DMC with GL is not spontaneous in nature. An external force in the form of heat, catalyst, and so forth is required for pushing the reaction in the forward direction. Further, a positive value of ΔH‡ indicates the endothermic nature of the reaction [28].

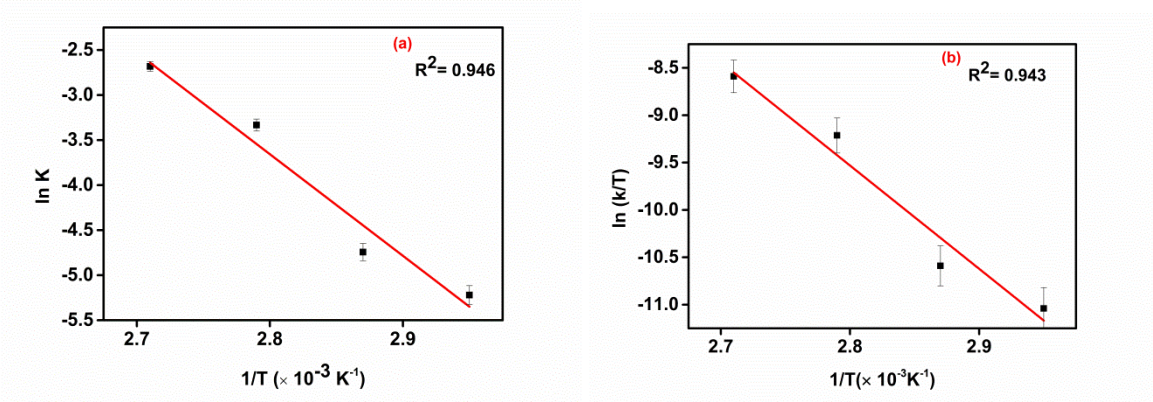

Figure 4.14 (a) Arrhenius plot for transesterification of DMC in presence of 20-Li/ZrO_2-700 and (**b**) plot of ln (k/T) *versus* 1/T.

4.4 Plausible mechanism

The Li/ZrO_2 assisted transesterification reaction of DMC with GL to afford GLC involves the steps, as shown in **Scheme 4.2**. Depending upon the catalyst characterization results, a plausible reaction mechanism was proposed. Both the reactants come in close proximity over the surface of the catalyst (I). In the first step, the basic sites of the catalyst abstract the proton from the primary hydroxyl group of GL (II) [29]. Meanwhile, DMC is activated by the Lewis acid sites of Zr present in the catalyst [15]. The activated primary hydroxyl group of GL (II) then undergoes nucleophilic attack on the carbonyl group of DMC,

followed by the elimination of one molecule of methanol to give an intermediate (III) [22]. The intermediate III then undergoes intramolecular nucleophilic substitution to yield the final product GLC (IV) along with the elimination of another methanol molecule.

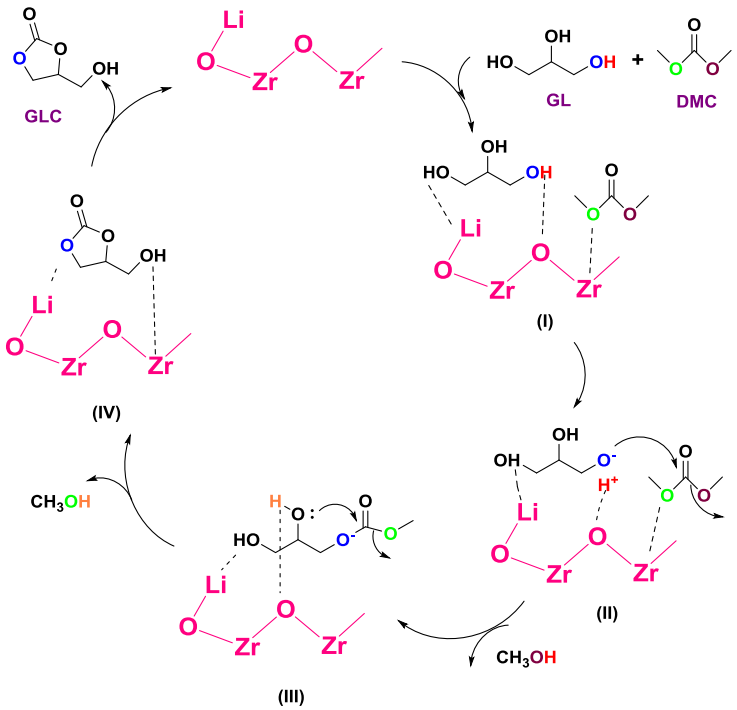

Scheme 4.2 Proposed reaction mechanism for Li/ZrO_2 assisted tranesterification of DMC with GL.

4.5 Comparison of the catalyst with reported catalysts

The pioneer results of heterogeneously catalyzed transesterification of DMC with GL have been compared with that of the present 20-Li/ZrO_2-700 catalytic system and the results are presented in **Table 4.1.** Although Zr-based tri-metallic mixed oxide (Mg/Sr/Zr) showed good GL conversion but has poor selectivity towards GLC [22]. Mg impregnated ZrO_2 offered good selectivity towards GLC at the expense of a higher DMC/GL molar ratio [48]. On the other hand, Li metal-loaded ZnO required a longer time to make the reaction more selective towards GLC [9]. HTC-Ni catalyst has been reported to yield 100 % GLC selectivity, however, in the presence of 1,4-butanediol solvent and higher catalyst amount (10 wt%). To overcome the issues related to the reported catalysts, to make the reaction more selective towards GLC we have prepared Li impregnated ZrO_2 catalyst and utilized the same for the transesterification reaction of DMC with

GL. The reusability of the Li/ZrO_2 catalyst is found to be comparable with most of the reported work, however, the catalyst reported in the present study achieved 100 % GLC selectivity with 91 % GLC yield under mild reaction conditions of DMC to GL molar ratio of 3, catalyst amount of 5 wt%, reaction temperature of 95 $^{\circ}$C and in 2 h of reaction duration.

Table 4.1 Comparison of previously reported catalysts with present catalyst employed for the transesterification of DMC with GL.

S.No.	Catalyst	Reaction parameters Glycerol:DMC/Temp ($^{\circ}$C)//Time (h)/Catalyst wt%	GL conversion/ GLC Yield/ GLC selectivity (%)	Reusability (cycle)/ GL conversion in last cycle (%)	Reference
1.	CaO/Al_2O_3 (polyamide)	1:3/80 / **5**/ 1.6	95.39/ 90.57/94.95	5 /62.5	[13]
2.	$Li/Mg_4AlO_{5.5}$	1:3/80 /1.5/ 4	100/96.28/96.28	**NR**	[30]
3.	Ti-SBA-15	**1:5**/ 87.5 /**4**/ 5.5	94/82/87	3 (Selectivity towards GLC decreases considerably)	[31]
4.	CaAl -LDHs	1:3.5/90/ 3 / 0.7 **N_2 atmosphere**	79/NR/60	4 /51	[32]
5.	Mg/ZrO_2	1:5/ 70/ 2.5/ **15**	96/88/NR	5/84	[33]
6	KF/La-Zr	1:2/90/1.5/ 3	NR/91/99	5/54.14	[15]
7	Mg/Zr/Sr	1:5/90/1.5/**15**	96/56/NR	4/85	[22]
8	Li/ZnO	1:3/95/**4**/ **5**	96.1/93.7/97.5	4/60.57	[17]
9.	$NaAlO_2$ with glycerol as template	1:4/ 70/ 2/ **30 wt% glycerol template**	85/85/100	5 /69	[34]
10.	HTC-Ni	1:3/100 /2/10 **Solvent :1,4-butanediol**	55/55/100	4 /45	[35]
11.	20-Li/ZrO_2-700	1:3/ 95/ 2/ 5	91/91/100	4/ 52	Present study

Y= yield of glycerol carbonate, C= conversion of glycerol, S= selectivity of glycerol carbonate, NR = not reported

4.6 Conclusions

In the present chapter, 20-Li/ZrO_2-700 catalyst prepared by wet impregnation method was found to be an effective catalyst for the transesterification of DMC with GL yielding GLC as an exclusive product. The catalyst characterization by powder XRD, XPS, and HRTEM techniques supports the complete dispersion of lithium on the surface as a single phase of lithium zirconate was formed. Under optimized reaction conditions (catalyst concentration 5 wt%, GL to DMC molar ratio of 1:3 at 95 $^{\circ}$C for 2 h), the transesterification of the DMC was found to follow second-order rate law. The activation energy for the reaction was found to be 93.7 kJ mol^{-1}. The positive value of enthalpy $\Delta H^{\ddagger}$ (90.68 kJ mol^{-1}) supported the endothermic nature of the reaction. The Gibbs free energy of activation $\Delta G^{\ddagger}$ (98.7 kJ mol^{-1}) predicts the non-spontaneous nature of the reaction. The catalyst has been recovered and recycled with a gradual decrease in its catalytic activity after each run owing to the change in the catalyst structure. The leaching study supported the negligible homogeneous contribution in catalytic activity. Thus Li/ZrO_2 has emerged as a simple, cost-efficient, and highly active catalyst with 100 % selectivity towards glycerol carbonate.

References

[1] P.D.L. Mercera, J.G. Van Ommen, E.B.M. Doesburg, A.J. Burggraaf, J.R.H. Ross, Zirconia as a support for catalysts. Evolution of the texture and structure on calcination in air, Appl. Catal. 57 (1990) 127–148. doi:10.1016/S0166-9834(00)80728-9.

[2] T. Yamaguchi, Application of ZrO_2 as a catalyst and a catalyst support, Catal. Today 20 (1994) 199–217. doi:10.1016/0920-5861(94)80003-0.

[3] J. Ochoa-Gómez, O. Gómez-Jiménez-Aberasturi, C. Ramírez-López, M. Belsué, A brief review on industrial alternatives for the manufacturing of glycerol carbonate, Green Chem. 16 (2012) 389–399. doi:10.1016/S0168-583X(03)01665-3.

[4] J. ichi Ida, R. Xiong, Y.S. Lin, Synthesis and CO_2 sorption properties of pure and modified lithium zirconate, Sep. Purif. Technol. 36 (2004) 41–51. doi:10.1016/S1383-5866(03)00151-5.

[5] N. Senso, B. Jongsomjit, P. Praserthdam, Effect of calcination treatment of zirconia on W/ZrO_2 catalysts for transesterification, Fuel Process. Technol. 92 (2011) 1537–1542. doi:10.1016/j.fuproc.2011.03.016.

[6] K. Narasimharao, T.T. Ali, Effect of preparation conditions on structural and catalytic properties of lithium zirconate, Ceram. Int. 42 (2016) 1318–1331. doi:10.1016/j.ceramint.2015.09.068.

[7] J.A. Mendoza-Nieto, Y. Duan, H. Pfeiffer, Alkaline zirconates as effective materials for hydrogen production through consecutive carbon dioxide capture and conversion in methane dry reforming, Appl. Catal. B Environ. 238 (2018) 576–585. doi:10.1016/j.apcatb.2018.07.065.

[8] D.J. Fauth, E.A. Frommell, J.S. Hoffman, R.P. Reasbeck, H.W. Pennline, Eutectic salt promoted lithium zirconate: Novel high temperature sorbent for CO_2 capture, Fuel Process. Technol. 86 (2005) 1503–1521. doi:10.1016/j.fuproc.2005.01.012.

[9] D. Peltzer, J. Múnera, L. Cornaglia, Operando Raman spectroscopic studies of lithium

zirconates during CO_2 capture at high temperature, RSC Adv. 6 (2016) 8222–8231. doi:10.1039/c5ra21970a.

[10] K. Yuan, X. Jin, C. Xu, X. Wang, G. Zhang, L. Zhu, D. Xu, Fabrication of dense and porous Li_2ZrO_3 nanofibers with electrospinning method, Appl. Phys. A 124 (2018) 1-10. doi:10.1007/s00339-018-1821-0.

[11] L. Kumar, D.D. Sarma, S. Krummacher, XPS study of the room temperature surface oxidation of zirconium and its binary alloys with tin, chromium and iron, Appl. Surf. Sci. 32 (1988) 309–319. doi:10.1016/0169-4332(88)90016-5.

[12] J.L. Colón, D.S. Thakur, C.Y. Yang, A. Clearfield, C.R. Martini, X-ray photoelectron spectroscopy and catalytic activity of α-zirconium phosphate and zirconium phosphate sulfophenylphosphonate, J. Catal. 124 (1990) 148–159. doi:10.1016/0021-9517(90)90111-V.

[13] J. Liu, M. Liao, M. Imura, A. Tanaka, H. Iwai, Y. Koide, Low on-resistance diamond field effect transistor with high-k ZrO_2 as dielectric, Sci. Rep. 4 (2014) 2–6. doi:10.1038/srep06395.

[14] H. Pfeiffer, P. Bosch, J.A. Odriozola, A. Lopez, J.A. Ascencio, S. Bulbulian, Sol-gel synthesis of Li-$ZrSiO_4$, J. Mater. Res. 15 (2000) 1490–1495. doi:10.1557/JMR.2000.0214.

[15] X. Song, D. Pan, Y. Wu, P. Cheng, R. Wei, L. Gao, J. Zhang, G. Xiao, Synthesis of glycerol carbonate over porous La-Zr based catalysts: The role of strong and super basic sites, J. Alloys Compd. 750 (2018) 828–837. doi:10.1016/j.jallcom.2018.03.392.

[16] N. Kaur, A. Ali, Lithium zirconate as solid catalyst for simultaneous esterification and transesterification of low quality triglycerides, Appl. Catal. A Gen. 489 (2015) 193–202. doi:10.1016/j.apcata.2014.10.013.

[17] X. Song, Y. Wu, F. Cai, D. Pan, G. Xiao, High-efficiency and low-cost Li / ZnO catalysts for synthesis of glycerol carbonate from glycerol transesterification : The role of Li and ZnO interaction, Appl. Catal. A Gen. 532 (2017) 77–85. doi:10.1016/j.apcata.2016.12.019.

[18] N.M. Deraz, The comparative jurisprudence of catalysts preparation methods: I. precipitation and impregnation methods., J. Ind. Environ. Chem. 2 (2018) 1–3.

[19] J. Haber, J.H. Block, B. Delmon, Manual of methods and procedures for catalyst characterization (Technical Report), Pure Appl. Chem. 67 (1995) 1257-1306.

[20] W.K. Teng, G.C. Ngoh, R. Yusoff, M.K. Aroua, A review on the performance of glycerol carbonate production via catalytic transesterification: Effects of influencing parameters, Energy Convers. Manag. 88 (2014) 484–497. doi:10.1016/j.enconman.2014.08.036.

[21] F.S.H. Simanjuntak, V.T. Widyaya, C.S. Kim, B.S. Ahn, Y.J. Kim, H. Lee, Synthesis of glycerol carbonate from glycerol and dimethyl carbonate using magnesium-lanthanum mixed oxide catalyst, Chem. Eng. Sci. 94 (2013) 265–270. doi:10.1016/j.ces.2013.01.070.

[22] G. Parameswaram, M. Srinivas, B. Hari Babu, P.S. Sai Prasad, N. Lingaiah, Transesterification of glycerol with dimethyl carbonate for the synthesis of glycerol carbonate over Mg/Zr/Sr mixed oxide base catalysts, Catal. Sci. Technol. 3 (2013) 3242–3249. doi:10.1039/c3cy00532a.

[23] D. Singh, B. Reddy, A. Ganesh, S. Mahajani, Zinc/lanthanum mixed-oxide catalyst for the synthesis of glycerol carbonate by transesterification of glycerol, Ind. Eng. Chem. Res. 53 (2014) 18786–18795. doi:10.1021/ie5011564.

[24] G.D. Yadav, P.A. Chandan, A green process for glycerol valorization to glycerol carbonate over heterogeneous hydrotalcite catalyst, Catal. Today 237 (2014) 47–53. doi:10.1016/j.cattod.2014.01.043.

[25] J. Esteban, E. Domínguez, M. Ladero, F. Garcia-Ochoa, Kinetics of the production of glycerol carbonate by transesterification of glycerol with dimethyl and ethylene carbonate using potassium methoxide, a highly active catalyst, Fuel Process. Technol. 138 (2015) 243–251. doi:10.1016/j.fuproc.2015.06.012.

[26] J. Zhang, Y. Wu, X. Song, S. Xu, S. Li, Y. Zhu, L. Gao, J. Zhang, G. Xiao, Thermodynamic and kinetic studies for synthesis of glycerol carbonate from glycerol and diethyl carbonate over Ce–NiO catalyst, Chem. Pap. 72 (2018) 2909–2919.

doi:10.1007/s11696-018-0518-3.

[27] J. Esteban, A.J. Vorholt, Obtaining glycerol carbonate and glycols using thermomorphic systems based on glycerol and cyclic organic carbonates: Kinetic studies, J. Ind. Eng. Chem. 63 (2018) 124–132. doi:10.1016/j.jiec.2018.02.008.

[28] D. Galvan, J.R. Orives, R.L. Coppo, E.T. Silva, K.G. Angilelli, D. Borsato, Determination of the kinetics and thermodynamics parameters of biodiesel oxidation reaction obtained from an optimized mixture of vegetable oil and animal fat, Energy Fuels 27 (2013) 6866–6871. doi:10.1021/ef401927x.

[29] J.R. Ochoa-Gómez, O. Gómez-Jiménez-Aberasturi, B. Maestro-Madurga, A. Pesquera-Rodríguez, C. Ramírez-López, L. Lorenzo-Ibarreta, J. Torrecilla-Soria, M.C. Villarán-Velasco, Synthesis of glycerol carbonate from glycerol and dimethyl carbonate by transesterification: Catalyst screening and reaction optimization, Appl. Catal. A Gen. 366 (2009) 315–324. doi:10.1016/j.apcata.2009.07.020.

[30] Z. Liu, J. Wang, M. Kang, N. Yin, X. Wang, Y. Tan, Y. Zhu, Structure-activity correlations of $LiNO_3/Mg_4AlO_{5.5}$ catalysts for glycerol carbonate synthesis from glycerol and dimethyl carbonate, J. Ind. Eng. Chem. 21 (2015) 394–399. doi:10.1016/J.JIEC.2014.02.051.

[31] P. Lu, H. Wang, K. Hu, Synthesis of glycerol carbonate from glycerol and dimethyl carbonate over the extruded CaO-based catalyst, Chem. Eng. J. 228 (2013) 147–154. doi:10.1016/j.cej.2013.04.109.

[32] J. Granados-Reyes, P. Salagre, Y. Cesteros, CaAl-layered double hydroxides as active catalysts for the transesterification of glycerol to glycerol carbonate, Appl. Clay Sci. 132–133 (2016) 216–222. doi:10.1016/j.clay.2016.06.008.

[33] M. Varkolu, D.R. Burri, S.R.R. Kamaraju, S.B. Jonnalagadda, W.E. Van Zyl, Transesterification of glycerol with dimethyl carbonate over nanocrystalline ordered mesoporous $MgO–ZrO_2$ solid base catalyst, J. Porous Mater. 23 (2016) 185–193. doi:10.1007/s10934-015-0069-8.

[34] P. Devi, U. Das, A.K. Dalai, Production of glycerol carbonate using a novel Ti-SBA-15 catalyst, Chem. Eng. J. 346 (2018) 477–488. doi:10.1016/j.cej.2018.04.030.

[35] P. Liu, M. Derchi, E.J.M. Hensen, Promotional effect of transition metal doping on the basicity and activity of calcined hydrotalcite catalysts for glycerol carbonate synthesis, Appl. Catal. B Environ. 144 (2014) 135–143. doi:10.1016/j.apcatb.2013.07.010.

Surface-Modified CaO Catalyst for the Production of Glycerol Carbonate

Abstract

For enhancing the moisture resistance properties of the commercial CaO, the surface of the CaO was modified using various aliphatic and aromatic groups as modifiers. The binding of the modifiers onto the surface of the CaO was confirmed through the FTIR and XPS techniques. For the first time, these modified CaO catalysts were employed to carry out the transesterification reaction of glycerol and dimethyl carbonate forming glycerol carbonate. Under the optimized reaction conditions, benzyl modified CaO catalyst showed better catalytic activity yielding 82 % glycerol carbonate with 100 % selectivity. The 0.5-Ben/CaO catalyst was found to resist the presence of 5 wt% H_2O content in the reaction due to the presence of the hydrophobic layer formed by the benzyl functionalization over the CaO surface. The humidity test also revealed that the modified CaO showed better resistance to moisture adsorption than its native counterpart.

5.1. Introduction

The GL procured from the biodiesel industry contains traces of water, and hence the catalyst employed for the chemical transformation of such GL must not be sensitive towards moisture. The easy availability of CaO has made it an eligible candidate to utilize it for carrying out the GL transformation. However, the catalyst poisoning via atmospheric moisture remained an issue. To strengthen the chemical stability and boost up water-resistance of CaO, the surface of the commercially available CaO was modified using various aliphatic and aromatic bromides. For the first time, these modified catalysts were applied for the synthesis of GLC. The moisture resistance ability of the modified CaO was compared with the native CaO for the transesterification reaction of DMC with GL.

5.2. Experimental

5.2.1 Modification of CaO

A series of modified CaO catalysts were prepared by employing various aliphatic and aromatic bromides viz., ethyl bromide (Eth), propyl bromide (Pro), butyl bromide (But), pentyl bromide (Pen), benzyl bromide (Ben), and bromobenzene (Bro) as a modifier. In a typical experiment, commercial CaO (5 g) was added to the methanolic solution (60 mL) of ethyl bromide of varying concentration (0.3- 0.9 %) in a 100-mL beaker to get the desired modifier to CaO ratio. The resulting mixture underwent stirring for 8 h at room temperature with the help of a magnetic stirrer. After 8 h, the resultant mixture was separated from the mother liquor through centrifugation and washed using methanol to eliminate the unreacted alkyl bromide. The solid thus obtained was dried at 80 $^{\circ}$C for 10 h and calcined in the temperature range of 150-550 $^{\circ}$C to obtain the ethyl modified CaO. A similar experimental procedure has been opted for the preparation of other aliphatic and aromatic group modified CaO. The modified catalyst has been named x-Aaa/CaO-y, where x is the weight percent of the modifier grafting. Aaa is three initial letters of the aliphatic or aromatic bromide taken, and y is the calcination temperature of the preparation process. For instance, a catalyst with 0.3 wt% grafting of the ethyl bromide prepared at 250 $^{\circ}$C has been named 0.3-Eth/CaO-250.

5.2.2 Humidity test

To calculate the extent of the hydrophobic stability, the modified CaO was exposed to the moisture and adsorbed moisture content was determined. For this, both commercial and modified CaO catalysts were retained in a humid environment for 5 days to accelerate the adsorption process. To ensure that both the catalyst samples would experience a similar humid environment, before the humidity test, a desiccator was partially filled with a fixed amount of water and sealed with a parafilm wrap for 24 hours to form a humid atmosphere. Both the catalysts (CaO and modified one) were weighed separately, transferred in separate Petri dishes, and kept in the same desiccator which was sealed with a parafilm wrap. After the stipulated time, both the samples were taken out together, weighed, and kept again in the sealed desiccator. A pictorial representation of the experimental setup has been given in **Figure A.17**, Appendix A.

The weight % of moisture adsorption (%) was determined by equation **5.1**.

$$\text{Weight \% age of moisture adsorbed} = \frac{\Delta m}{m_o} \times 100 \quad \textbf{(5.1)}$$

Where Δm is the increase in the weight and m_o is the initial weight of the sample.

5.2.3 Catalytic activity test

The transesterification reaction of DMC with GL was performed as per the method described in Chapter 4 but utilizing modified CaO as a catalyst. The product was analyzed and quantified via ^{1}H-NMR and HPLC techniques following the procedure described in Chapters 2 and 3.

5.3 Result and discussion

5.3.1 Catalyst Characterization

5.3.1.1 X-Ray diffraction (XRD)

X-ray diffraction (XRD) patterns of the commercial CaO and 0.5-Ben/CaO-250 were compared as shown in **Figure 5.1**. It is evident from the comparison that diffraction patterns of commercial CaO show the peaks associated with the cubic phase (JCPDS card no 077-2376). However, upon modification with a benzyl group, cubic CaO, and rhombohedral $CaCO_3$ (JCPDS card no. 086-2334) were the major phases along with hexagonal $Ca(OH)_2$ (JCPDS card no. 087-0674) as a minor phase. The reduced intensity of the diffraction peaks, corresponding to the CaO, could be attributed to the extensive dispersion of the CaO in $CaCO_3$ and $Ca(OH)_2$ phases during the modification step. Moreover, the intense diffraction peaks of $CaCO_3$ depict the CaO poisoning with CO_2 during the modification step, but it seldom affects the catalytic activity. Xue et al.[1] have also observed the formation of $CaCO_3$ while modifying the CaO with ethyl bromide. As discussed in the subsequent section, the interaction of the CaO with the organic group was found responsible for imparting the hydrophobic nature to the catalyst.

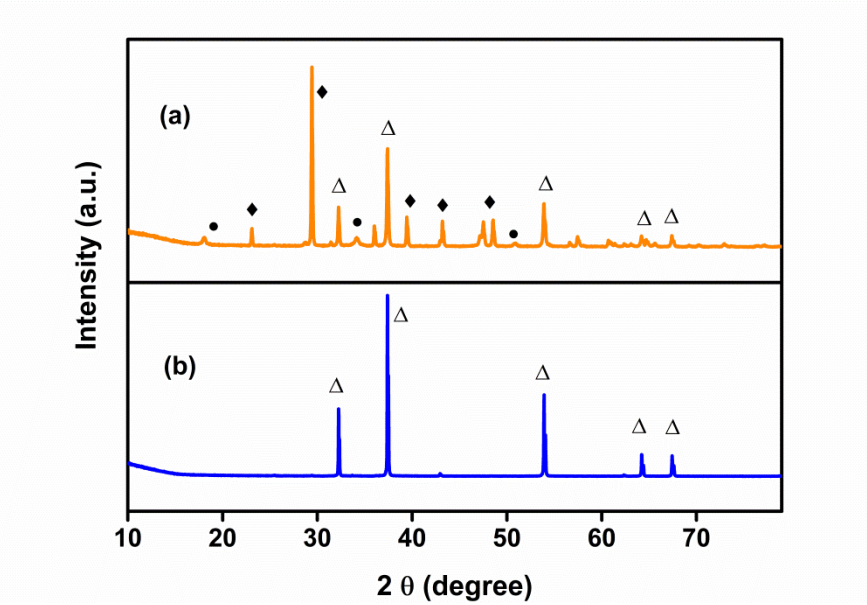

Figure 5.1 Comparison of the XRD pattern of the (a) commercial CaO (Δ cubic CaO) and (b) 0.5-Ben/CaO-250 (Δ cubic CaO , ♦ rhombohedral $CaCO_3$, • hexagonal $Ca(OH)_2$).

5.3.1.2 Fourier Transformer Infrared Spectroscopy (FT-IR)

The comparison of FTIR spectra of CaO and 0.5-Ben/CaO prepared at various calcination temperatures (150-550 °C) is shown in **Figure 5.2**. The –C–H stretching band in the range of 2700–2900 cm^{-1}, in the modified catalyst (calcined up to 250 °C), supported the interaction of the hydrocarbon chain with the CaO surface. The appearance of new stretching vibration of -C-O- bonding around 1074 cm^{-1} in the spectra of modified CaO (calcined at 250 °C) depicts the interaction of the modifier with the hydroxyl groups of the CaO surface. These observations are in accordance with the FTIR results obtained by Wang et al. [2] and Tang et al.[3] for the bromobenzene and benzyl bromide modified CaO catalysts, utilized to carry out the aldol condensation. However, while looking at the impact of the calcination temperature upon the modified CaO catalyst, it is evident that the characteristic –C–H band disappear for the samples calcined at 350 °C. This observation indicates the thermal decomposition of the organic group from the catalyst at a temperature higher than 350 °C. Furthermore, the elemental analysis also revealed the presence of 10 % carbon in the 0.5-Ben/CaO-250, further supporting the anchoring of organic moiety over the CaO surface.

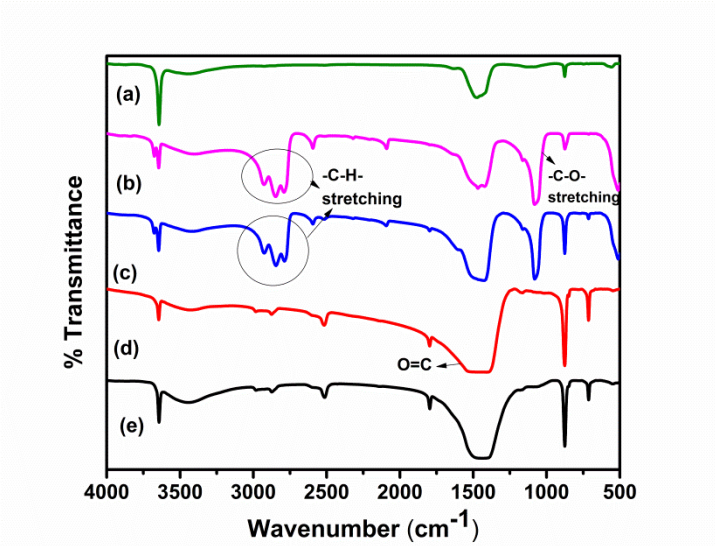

Figure 5.2 Comparison of the FTIR spectra of (a) commercial CaO with that 0.5-Ben/CaO calcined at (b) 150°C (c) 250°C (d) 350°C and (e) 550°C.

5.3.1.3 X-Ray Photoelectron Spectroscopy

The surface elemental oxidation state of 0.5-Ben/CaO-250 has been analyzed by the XPS technique (**Figure 5.3a**). The doublet of Ca 2p spectra could be deconvoluted into four sub-peaks forming two sets of Ca $2p_{3/2}$ and Ca $2p_{1/2}$ peaks representing the presence of Ca in different states in the prepared catalyst as shown in **Figure 5.3b**. The peaks detected at 346.89 and 350.35 eV correspond to $2p_{3/2}$ and $2p_{1/2}$ states of Ca^{2+} bonded to O^{2-} in the CaO phase. Hanawa et al. [4] have also reported the peak corresponding to the 347.1 eV to Ca $2p_{3/2}$ in CaO while comparing the changes in the binding energy (B.E.) of the calcium phosphate found on the surface films of titanium. The spin-orbit coupling splitting separation (Ca $2p_{3/2}$ – Ca $2p_{1/2}$) of 3.46 eV closely resembles that of reported (3.5 ± 0.2 eV) in literature for the different CaO compounds [5]. The peaks observed at B.E. of 347.76 and 351.26 eV (spin-orbit coupling splitting 3.5 eV) could be attributed to $2p_{3/2}$ and $2p_{1/2}$ states of Ca^{2+} bonded to CO_3^{2-} in the $CaCO_3$ phase. This is in accordance with the B.E. assigned for calcite in literature at 347.7 and 351.2 eV while determining the bonding environment at the calcite structure [6]. Moreover, the results determined by the XPS study are in accordance with the results of XRD analysis in which $CaCO_3$ and CaO have been observed as major phases. The deconvoluted O 1s spectra revealed three peaks at B.E. of 531.17, 531.99, and 532.97 eV (**Figure 5.3c**). The peak corresponding to 531.17 eV could be assigned to the O^{2-} bonded to Ca^{2+} in CaO. Demri et al. [5] have also

assigned the B.E. of 531.2 eV to the O 1s present in CaO while conducting the XPS study of the various calcium compounds *viz.*, CaO, $CaHPO_4$, $Ca(HCOO)_2$, $Ca(NO_3)_2$, etc. The peak with B.E. of 531.99 eV could be assigned to O^{2-} bonded to CO_3^{2-} in the $CaCO_3$ phase. Stipp et al. [6] have also found that the O 1s peak observed at B.E. of 531.9 eV is due to the presence of O^{2-} in the form of CO_3^{2-} in the calcite structure. The O 1s peak at 532.97 has been assigned to the O^{2-} bonded to the modifier (O-C). Lopez et al. [7] have analyzed the B.E. of O 1s for the polymers possessing different organic groups *viz.*, esters, ethers, hydroxyl, and ketone and concluded that the B.E. of O 1s in alcohol and ether exist in the range of 532.7 to 533.1 eV. A doublet for C 1s at B.E. of 285.31 and 290.12 eV (**Figure 5.3d**) is observed. The B.E. of 285.31 eV could be attributed to the organic carbon present in the modified catalyst. While analyzing the XPS of the benzene doped C_3N_4 nanosheets, Liu et al.[8] also mentioned that the C1s peak observed at B.E. 284.8 eV corresponds to the sp^2 hybridized carbon originating from the benzene ring. The B.E. of 290.12 eV could be ascribed to the carbon present in the form of $CaCO_3$ in the modified catalyst. Stipp et al. [6] also reported that the peak found at B.E. of 290.1 eV was due to the carbon present in carbonate group in case of calcite structure.

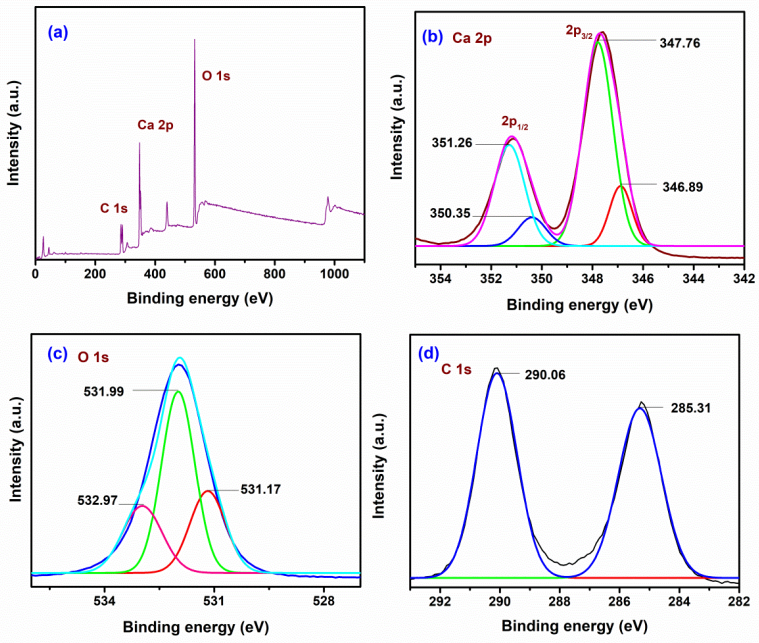

Figure 5.3 XPS spectra of (a) 0.5- Ben/CaO catalyst full scan and of the individual elements (b) Ca, (c) O, and (d) C present in it.

5.3.1.4 SEM and HRTEM

The effect of modifier grafting on the morphology of the commercial CaO has been studied using the SEM technique. The SEM study illustrates that commercial CaO exhibits irregular cluster-shaped particles (**Figure 5.4a**). The modifier grafting over CaO presents an exfoliated morphology as a more diffused aggregate of particles, as shown in **Figure 5.4b**. Tang et al. [9] have also observed that the modification process of CaO with ethyl bromoacetate causes exfoliation of CaO, resulting in better dispersion of the smaller CaO particles.

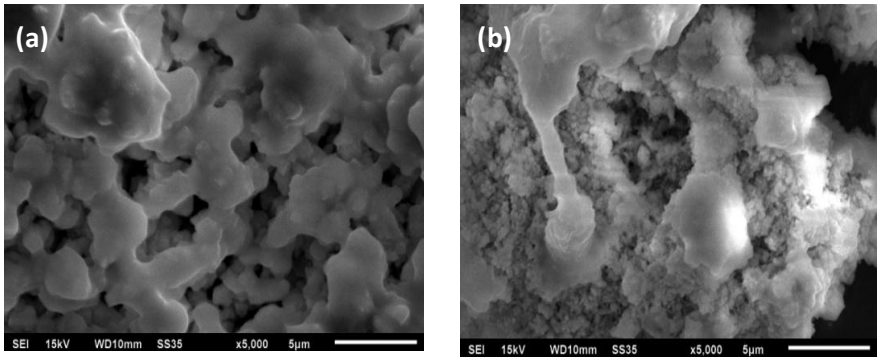

Figure 5.4 SEM images of (a) Commercial CaO and (b) 0.5-Ben/CaO-250.

Comparison of the TEM images of commercial and 0.5-Ben/CaO-250 revealed that scattered particles of CaO have become aggregated upon the modification and found encapsulated by the hydrophobic layer of the benzyl group (**Figure 5.5b**). The average particle size is found to be 95 nm compared to the crystallite size of 70 nm depicted by the XRD study.

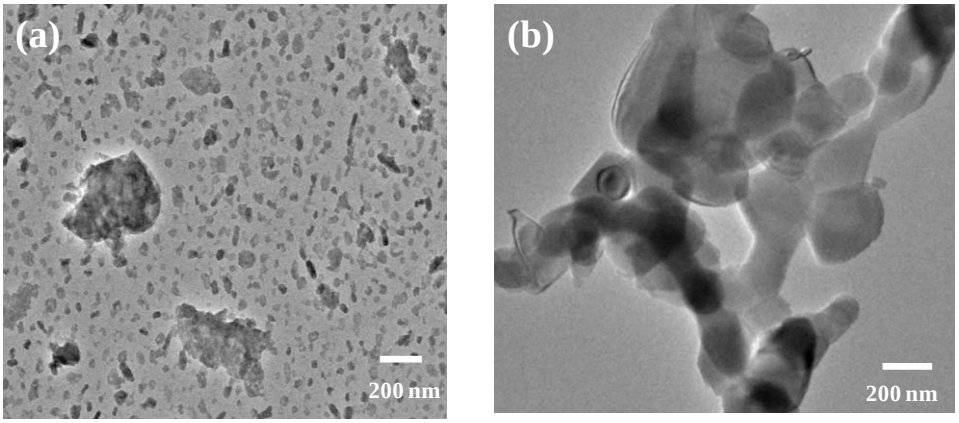

Figure 5.5 TEM micrographs of (a) Commercial CaO and (b) 0.5-Ben/CaO-250.

HRTEM study of commercial CaO revealed the presence of lattice fringes with a lattice spacing of 0.16 and 0.14 nm corresponding to the (220) and (311) planes, respectively, of the cubic CaO phase (**Figure 5.6a**). Benzyl group modified CaO, along with (220) plane of CaO, also demonstrates the lattice spacing of 0.18 and 0.19 nm corresponding to the (116) and (018) plane, respectively, of rhombohedral $CaCO_3$ phase (**Figure 5.6b**). Similarly, in the SAED indexing pattern (**Figure 5.6d**) of modified CaO (220) plane corresponding to the cubic phase of CaO and (012), (116), and (018) planes of $CaCO_3$ phase has also been observed. This observation supported that $CaCO_3$ has formed during the CaO modification step, and a similar finding is found while analyzing the sample by powder XRD analysis.

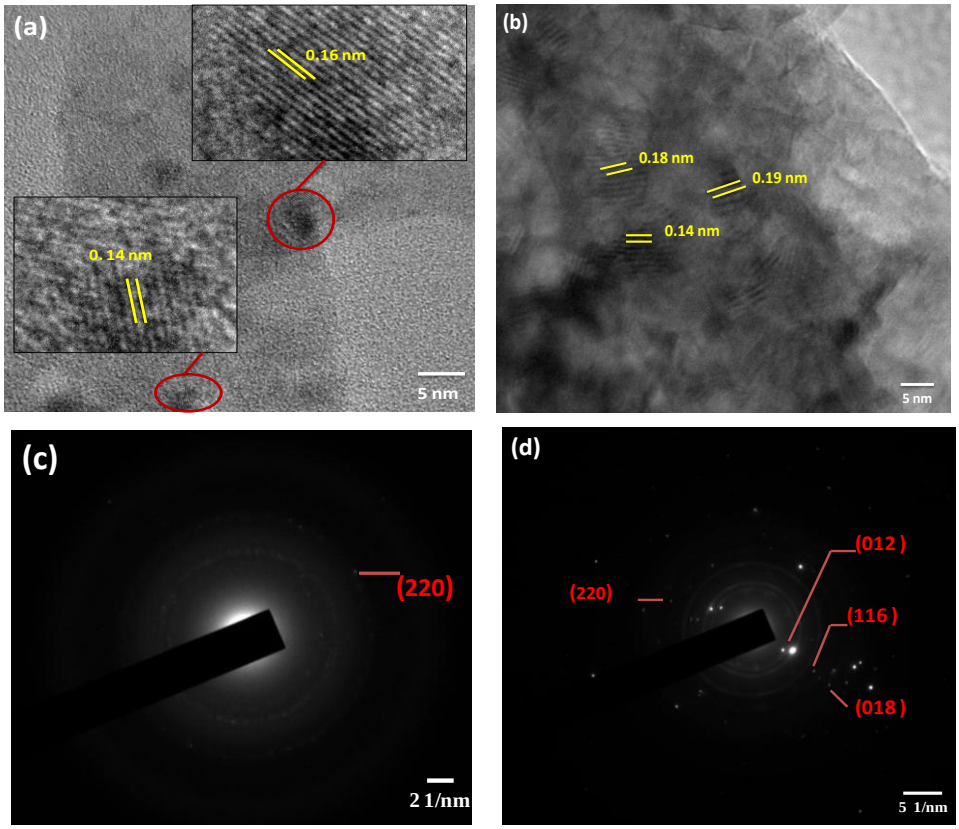

Figure 5.6 Lattice fringes of (a) commercial CaO and (b) 0.5-Ben/CaO-250 and SAED pattern of (c) commercial CaO and (d) 0.5-Ben/CaO-250 catalyst, respectively.

5.3.1.5 BET

The impact of the modifier grafting upon surface properties of CaO has been studied by conducting the N_2 adsorption-desorption experiments, as shown in **Figure 5.7**. It is evident from the figure that both commercial CaO, as well as 0.5-Ben/CaO-250, follow the type IV isotherm curve indicating the mesoporous nature of the modified CaO material [10]. Roschat et al. [11] have also found, based on BET analysis, that commercial as well as lime-derived CaO exhibit characteristic type IV adsorption isotherm.

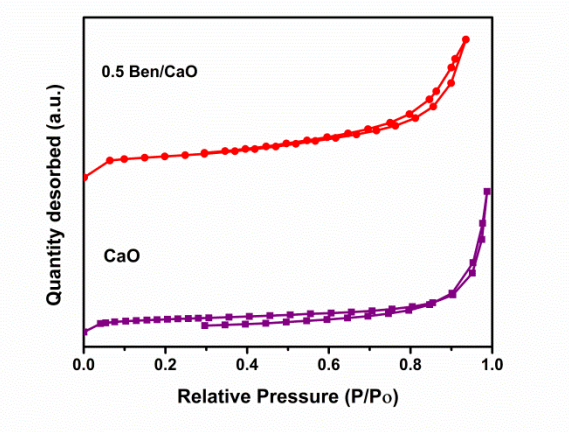

Figure 5.7 N_2 adsorption-desorption isotherms of commercial CaO and 0.5-Ben/CaO catalyst.

It has been observed that grafting of the modifier (benzyl bromide) on the CaO increases the specific surface area (5.89 m^2/g) of the commercial CaO (3.96 m^2/g) (**Table 5.1**). This increase in the surface area upon modification is further supported by the SEM analysis, showing the change in morphology. Pore volume CaO was found to decrease marginally (1.63 nm) upon its modification. However, a significant decrease in the pore diameter of the modified CaO (11.10 nm) in comparison to the commercial CaO (16.86 nm) could be due to the impregnation of the modifier over the catalyst surface. Xue et al. [1] have also explained the increase in the surface area of the ethyl bromide modified CaO due to the surface reaction. They also observed a little decrease in the pore diameter of commercial CaO upon its modification with 0.5 wt% ethyl bromide. The pore size distribution determined by the BJH method indicates non-uniform pore size in the range of 2-11 nm (**Figure A.18,** Appendix A), which falls under the mesoporous range [10].

Table 5.1 Comparison of the surface properties of the commercial CaO with that of the modified CaO catalyst.

S. No.	Catalysts	Average pore volume ($cm^3/g \times 10^{-2}$)	Average pore diameter (nm)	Surface area (m^2/g)
1	CaO	1.67	16.8	3.96
2	0.5-Benzyl-CaO	1.63	11.1	5.89

5.3.1.6 CO_2-Temperature Programmed Desorption

The effect of modification upon the basicity of the commercial CaO has been studied by conducting the CO_2-TPD experiment. The comparative study of the CO_2-TPD profile of the commercial CaO and Ben/CaO-250 catalyst with different modifier grafting amounts is shown in **Figure 5.8**. From the study, it has been observed that the increase in the modifier grafting was found to decrease the basicity of the CaO. This could be due to the partial coverage of the CaO surface basic sites by the benzyl group of the modifier. However, this decrease has minimal effect on the catalytic activity up to 0.5 wt% modifier grafting, as described in the subsequent section.

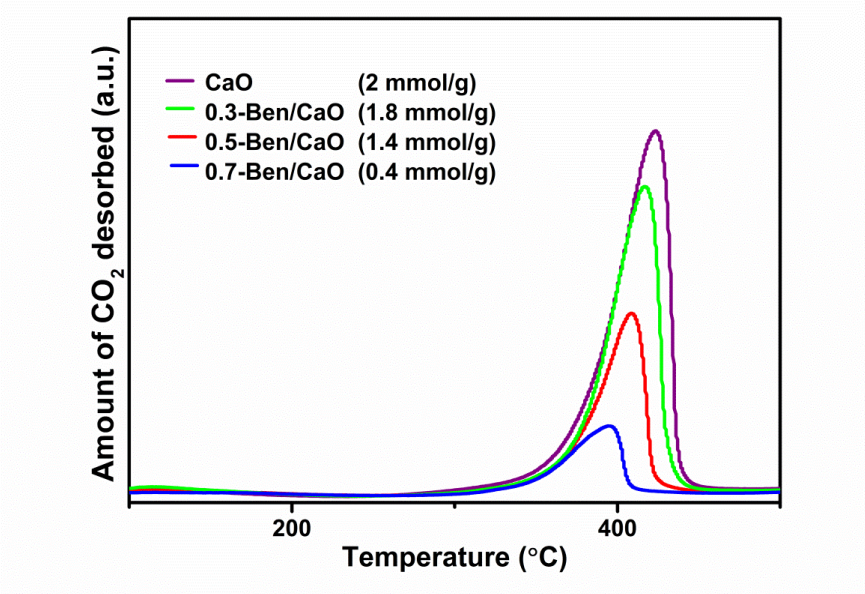

Figure 5.8 Comparison of the CO_2-TPD profile of the commercial CaO with that of Ben/CaO catalysts having varied amounts of the modifier grafting.

5.3.2 Catalytic activity

5.3.2.1 Selection of the modifier

A variety of modifiers *viz.*, ethyl, propyl, butyl, pentyl, and benzyl bromides and bromobenzene, have been employed for the surface modification of CaO. The purpose of the modification was to impart the water resistance to the CaO to make it more stable. To single out the better modifier for the said purpose, the transesterification reaction of DMC with GL has been performed employing the modified CaO catalysts under similar reaction conditions (GL: DMC 1:5 at 95 $^{\circ}$C for 2 h with 5 wt% catalyst). To evaluate the effect of modifier over the moisture resistance of the catalyst, after the first use, the catalysts were exposed to the atmosphere for 24 h. After the stipulated duration, the exposed catalysts were again employed for the transesterification reactions under similar conditions as described earlier. As evident from **Table 5.2**, (i) The optimum amount of the modifier grafting to obtain the better catalyst activity varies with the nature of the modifier, (ii) 0.5 wt% benzyl functionalization of CaO provides the best activity among all modified catalysts (**Figure A. 19-22**, Appendix A**)** (iii) with lower benzyl grafting (0.3 wt%) the activity was also found to be lesser, may be due to the deactivation of catalyst active sites owing to their frequent exposure to the atmospheric H_2O as well as CO_2, and (iv) a higher benzyl grafting (0.7 wt%) also was not found to improve the activity to the significant extent, due to the more coverage of the active sites by the modifier. Thus, the 0.5-Ben/CaO catalyst has demonstrated the best activity and better moisture resistance and, consequently, employed for detailed studies.

Table 5.2 Comparison of the catalytic activity of the CaO catalyst modified with various aliphatic and aromatic groups.

S.No.	Catalysts[a]	GLC yield (%) with fresh catalyst/exposed catalyst to the atmosphere (24 h)[b]
1	0.3-Eth/CaO	47/29
	0.5-Eth/CaO	63/52
	0.7 Eth/CaO	77/76
2	0.3-Pro/CaO	60/33
	0.5-Pro/CaO	53/48
	0.7-Pro/CaO	82/53
3	0.3-But/CaO	58/47
	0.5-But/CaO	54/53
	0.7-But/CaO	83/67
4	0.3-Pen/CaO	56/35
	0.5-Pen/CaO	53/53
	0.7-Pen/CaO	78/67
5	0.3-Bro/CaO	54/52
	0.5-Bro/CaO	56/44
	0.7-Bro/CaO	81/64
6	0.3-Ben/CaO	73/62
	0.5-Ben/CaO	82/75
	0.7-Ben/CaO	81/62
7	CaO	70/52

[a] calcined at 250 °C

[b]Reaction conditions: GL: DMC 1:5; temperature= 95 °C; reaction time= 2h; catalyst amount= 5 wt% catalyst

5.3.2.2 Humidity test

The poisoning of the CaO surface by the adsorption of the moisture causes a decline in its activity [2]. In order to study the impact of the modification on moisture resistance of the 0.5-Ben/CaO-250 catalyst, a humidity test has been conducted. The extent of moisture adsorption ability as a function of time has been compared in **Figure 5.9**. It is evident from **Figure 5.9** that moisture adsorption was found to increase gradually with time for bare CaO as well as modified one. However, after 100 h of exposure, better moisture resistance was demonstrated by benzyl group modified CaO (15.1 % moisture adsorption) compared to bare CaO (29.6 % moisture adsorption). In the modified CaO, organic functional groups were found to form a hydrophobic layer over the catalyst surface, thereby improving its ability to resist moisture adsorption. Elsewhere, a similar observation was also made while carrying out the humidity test of the bromobenzene modified CaO due to the partial coverage of the CaO surface by the hydrophobic benzyl group [2].

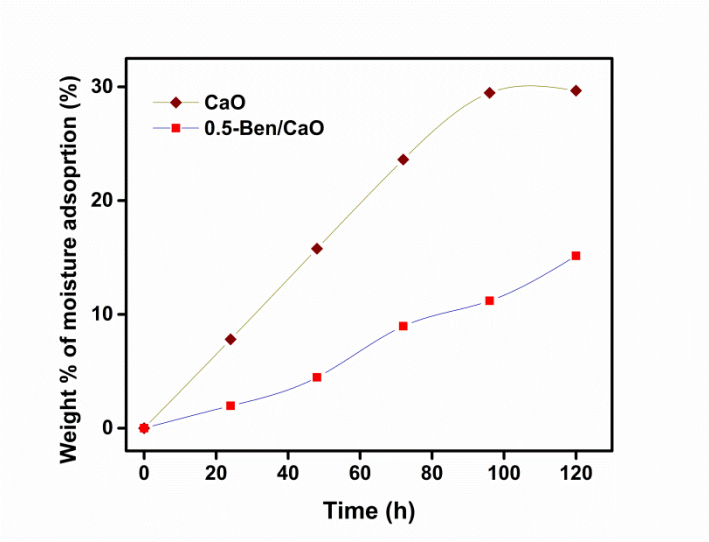

Figure 5.9 Comparison of the moisture adsorbing rates of the commercial CaO with 0.5-Ben/CaO catalyst.

5.3.3 Optimization of the Reaction Variables

5.3.3.1 Calcination Temperature

For enhancing the activity of the catalyst, a high-temperature treatment is given to facilitate the interaction amongst the various catalyst components to achieve stable catalyst formation. To optimize the calcination temperature, for attaining better catalytic activity the 0.5-Ben/CaO catalysts were prepared at 150-350 °C calcination temperature. An increase in the catalytic activity is observed upon raising the calcination temperature to 250 °C, as shown in **Figure 5.10a**. However, a further increase in the calcination temperature leads to a decline in the GLC yield due to the atmospheric poisoning by atmospheric CO_2 and H_2O and decomposition of the organic modifier present over the CaO surface. This observance is in accordance with the FTIR results, which depict modifier decomposition at 350 $^{\circ}$C. Based on the experiments, 250 $^{\circ}$C calcination temperature has been selected to attain the maximum GLC yield.

5.3.3.2 Catalyst Amount

The effect of the catalyst amount (0.5-Ben/CaO-250) on the progress of the reaction has been illustrated in **Figure 5.10b**. The catalyst concentration is varied from 1-7 wt% concerning

GL. As the catalyst amount is increased in the reaction (up to 5 wt%), the reaction is accelerated in the forward direction, resulting in a steady increase in the GLC yield. It could be simply explained due to the availability of more active sites for interaction with the reactant molecules. However, a further increase in catalyst grafting, up to 7 wt% was not found to demonstrate any notable increase in the GLC yield. An increased catalyst amount made the reaction mixture more viscous, which could be accounted for the limited interaction between the reactants and the active site of the catalyst [12]. Thus catalyst concentration of 5 wt% has been selected for carrying out the transesterification reaction.

5.3.3.3 Reactant ratio

Considering the stoichiometry of the transesterification reaction, both GL and DMC reactants are required in a 1: 1 molar ratio. However, due to the limited miscibility of both the reactants and due to the reversible nature of the reaction, generally, an excess amount of the DMC is employed during the reaction [13]. To select the appropriate reactant molar ratios for the transesterification reaction, a series of experiments with a varied amount of GL: DMC molar ratio (1:1 to 1:7) has been performed, taking 5 wt% of 0.5-Ben/CaO-250 catalyst. It has been noticed that on increasing the GL to DMC molar ratio up to 5, GLC yield was also found to enhance. However, a further rise in the GL/DMC molar ratio showed no significant effect on the GLC yield, as evident from **Figure 5.10c**. Thus maximum GLC yield is attained with GL: DMC molar ratio of 1:5, and the same has been selected for executing the transesterification reaction. Malyaadri et al. [14] and Kumar et al. [15] also reported that GL/DMC molar ratio of 1:5 was optimum for obtaining maximum GLC yield employing Mg/Al/Zr and CaLa mixed oxides as catalysts, respectively.

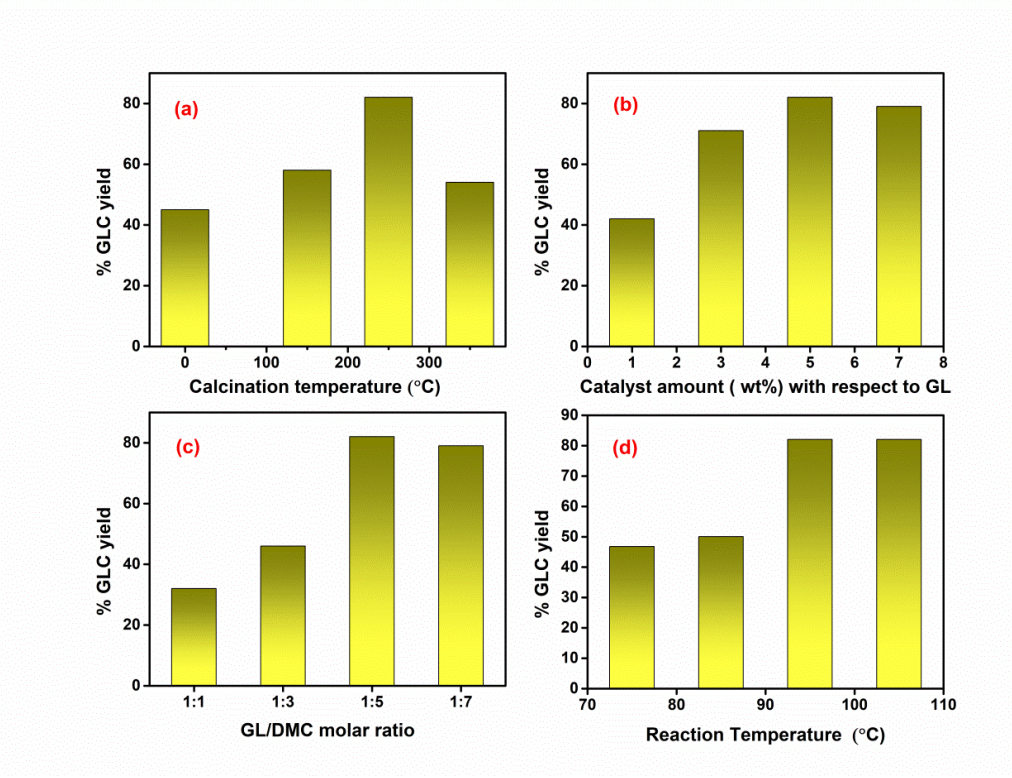

Figure 5.10 Effect of **(a)** calcination temperature (Reaction conditions: DMC/GL molar ratio 5:1, temperature 95 °C, catalyst amount= 5 wt% of catalyst with respect to GL, time 2 h) (**b**) catalyst amount with respect to GL (Reaction conditions: DMC/GL molar ratio 5:1, temperature 95 °C, time 2 h); (**c**) GL/DMC molar ratio (Reaction conditions: catalyst amount= 5 wt% of catalyst with respect to GL, temperature 95 °C, time 2 h) and (**d**) reaction temperature on the transesterification of DMC yielding GLC (Reaction conditions: DMC/GL molar ratio 5:1, catalyst amount= 5 wt% of catalyst with respect to GL, time 2 h).

5.3.3.4 Reaction temperature

Considering the reversibility of the transesterification reaction, temperature plays a crucial role in accelerating the reaction in the forward direction. For finding out the optimum reaction temperature, 0.5-Ben/CaO-250 catalyzed transesterification reaction for GLC production has been conducted at different temperatures as shown in **Figure 5.10d**. It has been observed that raising the reaction temperature up to 95 °C causes a positive impact on the GL conversion due to more collisions between the reactant molecules. Algoufi and Hameed also mentioned that the higher input of the energy in terms of heat facilitates the miscibility of the

DMC in GL, resulting in the greater interaction among the reactants to form GLC [16]. However, beyond 95 $^{\circ}$C, no significant increase in the GL conversion is observed as a majority of DMC above 95 $^{\circ}$C is transformed into the vapor phase, thus reducing the contact between the two reagents. Accordingly, 95 $^{\circ}$C reaction temperature has been selected for achieving a higher GLC yield. In literature reports, the reaction temperature in the range of 70-100 $^{\circ}$C has also been preferred for attaining maximum GLC yield [15,17,18].

5.3.4 Comparison of the water tolerance over commercial and modified CaO

The purpose of the development of the modified CaO is to utilize it as a catalyst for the transformation of GL which is coming from the biodiesel industry. Such GL usually acquires high moisture contents during the biodiesel purification step [19,20]. Thus it is inevitable for the catalyst to be effective towards the GL transesterification reaction that it must not be sensitive towards the presence of water. The effect of water content, present in GL, upon the catalytic activity of the bare CaO and 0.5-Ben/CaO-250 catalysts, has been investigated by carrying out the transesterification reactions under the optimized reaction conditions. During such reactions calculated amount of water (1-7 wt%; with respect to GL) has been added to the reaction media. As evident from **Figure 5.11**, the presence of up to 3 wt% of H_2O caused a considerable decrease in GLC yield (70 % to 58 %) in the case of bare CaO catalyzed reaction. On the other hand, in the presence of a similar amount of moisture, 0.5-Ben/CaO-250 catalyst was found to give 77 % GLC yield. Furthermore, as the water content is increased to 5 wt%, GLC yield over modified CaO and bare CaO was found to be 72 and 54 %, respectively. However, further addition of H_2O (up to 7 wt%) causes a significant decline in the catalytic activity of the modified CaO; it may be due to the dissociation of the organic group from the catalyst surface. Thus the modified CaO can tolerate the presence of up to 5 wt% moisture in the reaction mixture and exhibits the potential to convert the left out GL of the biodiesel industry into a valuable derivative (GLC). In literature, CaO/Al_2O_3 and KNO_3/CaO catalysts employed for GLC production were also found to resist the presence of up to 2 wt% and 5wt% water in GL, respectively [21,22], during the transesterification reaction of DMC.

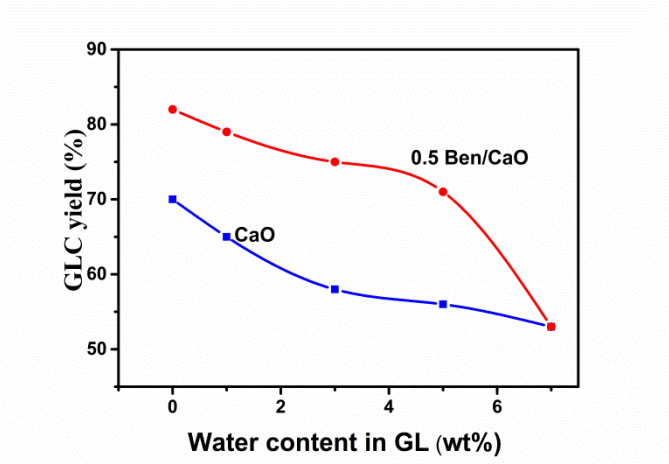

Figure 5.11 Effect of the water content present in GL upon the catalytic activity of the commercial CaO and 0.5-Ben/CaO catalysts calcined at 250 °C(Reaction conditions: DMC/GL molar ratio 5:1, temperature 95 °C, time 2 h; catalyst amount= 5 wt% of catalyst with respect to GL).

5.3.5 Catalyst Reusability

Another critical aspect of the heterogeneous catalyst is its reusability which increases its economic utility. In order to demonstrate the reusability of the benzyl modified CaO catalyst, DMC transesterification has been conducted under optimized reaction conditions. After the stipulated reaction time, the catalyst was separated from the reaction mixture and washed with methanol, and then dried at 120 °C before reuse. The catalyst thus recovered was reused in 4 successive reaction cycles under a similar experimental and regeneration method. As could be seen from **Figure 5.12**, a gradual decline in the GLC yield was obtained after reuse while maintaining 53 % GLC yield with 100 % selectivity in the 4^{th} run. On the other hand, GLC yield during the bare CaO catalyzed reaction was lower in every matching reusability experiment, as evident from **Figure 5.12**. Ochoa-Gomez et al. [23] have also observed a decrease in the catalytic activity of CaO while performing the transesterification reaction of DMC with GL after the first run due to the agglomeration of the catalyst particles. Nevertheless, as far as we know, organic group functionalized CaO has not been applied so far for the GLC synthesis.

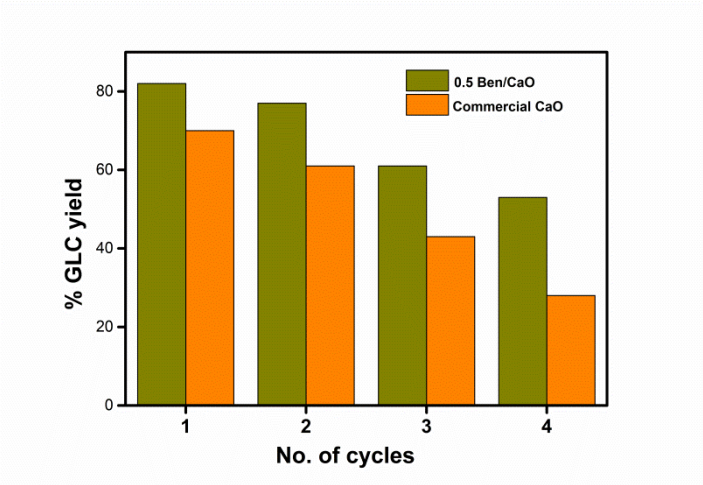

Figure 5.12 Comparison of the reusability study of the commercial CaO and 0.5-Ben/CaO-250 catalysts employed for the GLC synthesis (Reaction conditions: DMC/GL molar ratio 5:1, temperature 95 $^{\circ}$C, catalyst amount= 5 wt% of catalyst with respect to GL; time 2 h).

To assess the cause of the decrease in the catalytic activity during its reusability, the amount of metal dissolution in the reaction mixture has been analyzed. The leaching of Ca^{2+} from the modified CaO was found to be less (2.50 ppm) as compared to the commercial CaO (3.02 ppm). However, to ascertain the homogeneous contribution of the leached-out Ca^{2+} in the catalytic activity, a hot filtration test has also been performed. For this test, the transesterification reaction was performed using 0.5-Ben/CaO catalyst according to the optimized reaction parameters. After 40 minutes, the catalyst was removed from the reaction mixture *via* simple filtration, and the reaction was allowed to proceed with the obtained filtrate for another 1 h (**Figure A.23**, Appendix A). After the catalyst removal, a minimal increase of 4 % GLC yield is observed, which confirmed that the leached catalyst content had not imparted any significant homogeneous contribution towards the catalytic activity. Thus, modification has enhanced the catalyst moisture tolerance and its stability compared to the bare CaO. However, the partial catalyst dissolution of CaO into the reaction mixture could be one reason for the decline in the catalytic activity of the modified CaO.

Moreover, the comparison of the XRD spectra of fresh and the reused catalyst revealed that in the recovered catalyst, mostly the $CaCO_3$ phase has formed, while in the case of fresh catalyst CaO, as well as $CaCO_3$, were detected (**Figure 5.13**). Considering the susceptibility of

the CaO towards the atmospheric CO_2, the formation of $CaCO_3$ could be attributed to the interaction of the catalytic active sites with the atmospheric CO_2 during the catalyst recovery process. Therefore the change in catalyst structure during repeated regeneration could be responsible for the decline in its activity. While conducting the recyclability experiment of KNO_3/CaO for GLC formation, Hu et al. [22] have also found that $CaCO_3$ is present as a major species which could inhibit the proper interaction of the substrate molecule with the active sites of CaO. Lu et al. [21] have also found that generation of the $CaCO_3$ as a major phase in the recovered CaO/Al_2O_3 catalyst is the main reason for its deactivation towards the transesterification reaction of DMC to form GLC.

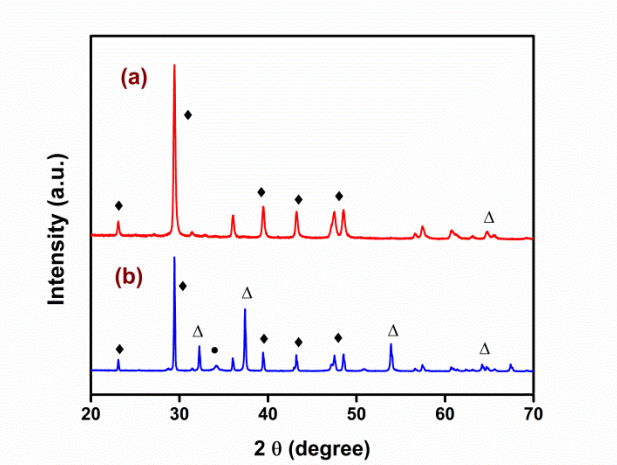

Figure 5.13 Comparison of the XRD pattern of the (a) fresh and (b) reused 0.5-Ben/CaO-250 catalyst (♦ rhombohedral $CaCO_3$, Δ cubic CaO • hexagonal $Ca(OH)_2$).

As evident from FTIR analysis of the reused catalyst (**Figure 5.14**) the intensity of the –C–H stretching band (~2900 cm^{-1}) in the reused catalyst was found to reduce. Nevertheless, the presence of the same band also depicts that the modifier remained intact on the CaO surface during the reusability experiment. Broadening of the carbonate band (~1500 cm^{-1}) showed a change in the chemical environment of the catalyst upon its reuse which is in accordance with the XRD analysis. The absence of the –C–O stretching band (~1074 cm^{-1}) in the reused catalyst showed that the interaction of the modifier with the surface of the CaO is affected during the catalyst reusability. Thus the change in the structural properties of the catalyst and metal ions leaching could be jointly accountable for the decline in the catalytic activity.

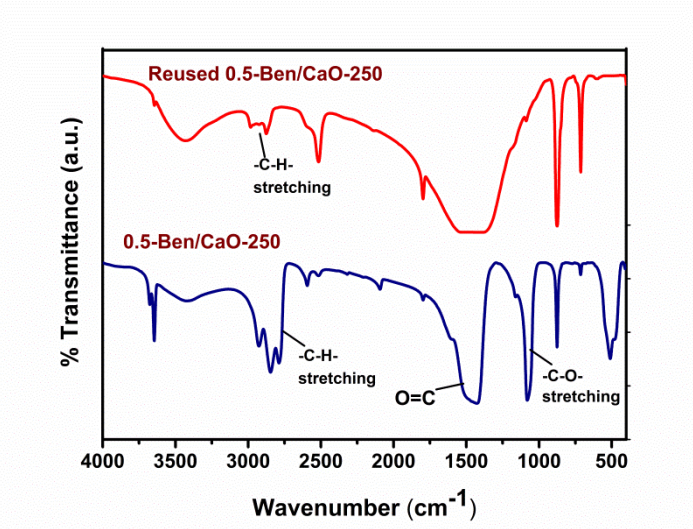

Figure 5.14 Comparison of the FTIR spectra of the fresh and reused 0.5Ben/CaO-250 catalyst.

5.4 Plausible Mechanism

The modified CaO promoted transesterification reaction of DMC with GL producing GLC involves two steps, as shown in **Scheme 5.1.** Based upon the results derived from the catalyst characterization, a plausible reaction mechanism was put forward. Both the reactants approached the surface of the catalyst as indicated in structure (**1**). In the first step, a proton is abstracted from the –OH group of the GL molecule by the [$–O^{2-}–$] sites of the catalyst as indicated in structure (**2**) [23]. Simultaneously, Ca^{2+} sites of the catalyst activate the DMC by interacting with the oxygen of the later. Now, the glyceroxide [$–O^{-}$] group of GL causes a nucleophilic attack on the C=O group of DMC (**2**), eliminating a methanol molecule while forming an intermediate (**3**) [24]. An intramolecular nucleophilic substitution of the intermediate (**3**) yields the final product GLC (**4**) with the removal of one more methanol molecule.

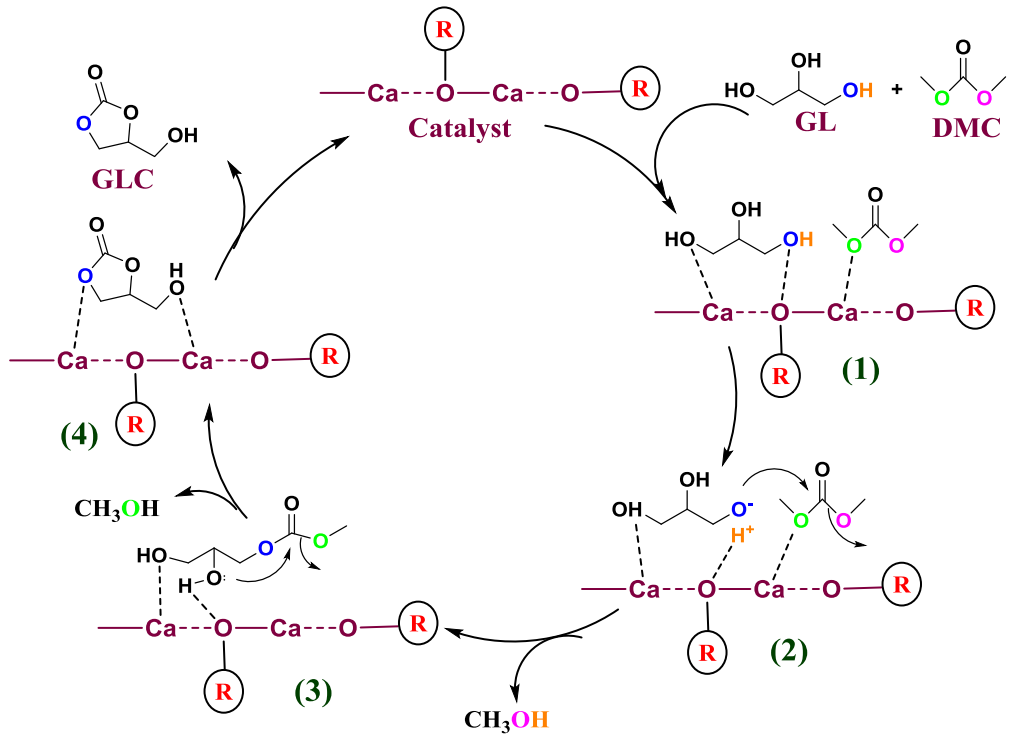

Scheme 5.1 Proposed reaction mechanism of the 0.5-Ben/CaO-250 catalyzed GLC synthesis from GL and DMC (where R= benzyl group).

5.5 Conclusions

In the present study, for the first time, the benzyl group modified CaO has been applied for the preparation of the GLC from GL. The modified catalyst showed a resistance to the presence of up to 5 wt% of the H_2O in the GL and was also reusable in the four reaction cycles. The modified catalyst was found to demonstrate better stability, reusability, and moisture resistance in comparison to the native CaO. A steady decline observed in the catalytic activity could be due to the structural changes and leaching of the catalyst contents into the reaction mixture. However, the selectivity of the catalyst towards GLC remained unaltered during the reusability experiments. The proposed mechanism indicates the attack of ethoxide ion of GL onto the DMC during the formation of the final product. Considering the moisture resistance and the reusability of the benzyl group modified CaO, it can replace the native CaO as a catalyst during GLC synthesis.

References

[1] C. Xue, S. Wang, Z. Zhang, Y. Tang, Novel solid base catalyst for biodiesel production by surface modification CaO with ethyl bromide, Res. Chem. Intermed. 41 (2015) 2697–2707. doi:10.1007/s11164-013-1380-0.

[2] J. Wang, T. Yan, Y. Tang, Y. Miao, High efficient aldol condensation reaction utilizing modified calcium oxide as stable solid base catalyst, Kinet. Catal. 57 (2016) 439–445. doi:10.1134/S0023158416040145.

[3] Y. Tang, G. Chen, Y. Lu, Efficient aldol condensation by using modified CaO as solid-base catalysts, Res. Chem. Intermed. 38 (2012) 937–946. doi:10.1007/s11164-011-0430-8.

[4] T. Hanawa, M. Ota, Calcium phosphate naturally formed on titanium in electrolyte solution, Biomaterials 12 (1991) 767–774. doi:10.1016/0142-9612(91)90028-9.

[5] B. Demri, D. Muster, XPS study of some calcium compounds, J. Mater. Process. Tech. 55 (1995) 311–314. doi:10.1016/0924-0136(95)02023-3.

[6] S.L.S. Stipp, M.F. Hochella, Structure and bonding at the calcite surface as observed with X-ray photoelectron spectroscopy (XPS) and (LEED), Geochim. Cosmochim. Acta. 55 (1991) 1723–1736.

[7] G.P. López, D.G. Castner, B.D. Ratner, XPS O 1s binding energies for polymers containing hydroxyl, ether, ketone and ester groups, Surf. Interface Anal. 17 (1991) 267–272. doi:10.1002/sia.740170508.

[8] J. Liu, Y. Yu, R. Qi, C. Cao, X. Liu, Y. Zheng, W. Song, Enhanced electron separation on in-plane benzene-ring doped g-C_3N_4 nanosheets for visible light photocatalytic hydrogen evolution, Appl. Catal. B Environ. 244 (2019) 459–464. doi:10.1016/j.apcatb.2018.11.070.

[9] Y. Tang, L. Li, S. Wang, Q. Cheng, J. Zhang, Tricomponent coupling production catalyzed by surface modified calcium oxide, Environ. Prog. Sustain. Energy 35 (2016)

257-262. https://doi.org/10.1002/ep.12194

[10] M. Thommes, K. Kaneko, A. V. Neimark, J.P. Olivier, F. Rodriguez-Reinoso, J. Rouquerol, K.S.W. Sing, Physisorption of gases, with special reference to the evaluation of surface area and pore size distribution (IUPAC Technical Report), Pure Appl. Chem. 87 (2015) 1051–1069. doi:10.1515/pac-2014-1117.

[11] W. Roschat, T. Siritanon, B. Yoosuk, V. Promarak, Biodiesel production from palm oil using hydrated lime-derived CaO as a low-cost basic heterogeneous catalyst, Energy Convers. Manag. 108 (2016) 459–467. doi:10.1016/j.enconman.2015.11.036.

[12] F.S.H. Simanjuntak, T.K. Kim, S.D. Lee, B.S. Ahn, H.S. Kim, H. Lee, CaO-catalyzed synthesis of glycerol carbonate from glycerol and dimethyl carbonate: Isolation and characterization of an active Ca species, Appl. Catal. A Gen. 401 (2011) 220–225. doi:10.1016/j.apcata.2011.05.024.

[13] W.K. Teng, G.C. Ngoh, R. Yusoff, M.K. Aroua, A review on the performance of glycerol carbonate production via catalytic transesterification: Effects of influencing parameters, Energy Convers. Manag. 88 (2014) 484–497. doi:10.1016/j.enconman.2014.08.036.

[14] M. Malyaadri, K. Jagadeeswaraiah, P.S. Sai Prasad, N. Lingaiah, Synthesis of glycerol carbonate by transesterification of glycerol with dimethyl carbonate over Mg/Al/Zr catalysts, Appl. Catal. A Gen. 401 (2011) 153–157. doi:10.1016/J.APCATA.2011.05.011.

[15] P. Kumar, P. With, V.C. Srivastava, R. Gläser, I.M. Mishra, Glycerol carbonate synthesis by hierarchically structured catalysts: Catalytic activity and characterization, Ind. Eng. Chem. Res. 54 (2015) 12543–12552. doi:10.1021/acs.iecr.5b03644.

[16] Y.T. Algoufi, B.H. Hameed, Synthesis of glycerol carbonate by transesterification of glycerol with dimethyl carbonate over K-zeolite derived from coal fly ash, Fuel Process. Technol. 126 (2014) 5–11. doi:10.1016/j.fuproc.2014.04.004.

[17] P.U. Naik, L. Petitjean, K. Refes, M. Picquet, L. Plasseraud, Imidazolium-2-carboxylate as an efficient, expeditious and ecofriendly organocatalyst for glycerol carbonate synthesis, Adv. Synth. Catal. 351 (2009) 1753–1756. doi:10.1002/adsc.200900280.

[18] F.S.H. Simanjuntak, V.T. Widyaya, C.S. Kim, B.S. Ahn, Y.J. Kim, H. Lee, Synthesis of glycerol carbonate from glycerol and dimethyl carbonate using magnesium-lanthanum mixed oxide catalyst, Chem. Eng. Sci. 94 (2013) 265–270. doi:10.1016/j.ces.2013.01.070.

[19] M. Hájek, F. Skopal, Treatment of glycerol phase formed by biodiesel production, Bioresour. Technol. 101 (2010) 3242–3245. doi:10.1016/j.biortech.2009.12.094.

[20] M. Carmona, J.L. Valverde, A. Pérez, J. Warchol, J.F. Rodriguez, Purification of glycerol/water solutions from biodiesel synthesis by ion exchange: Sodium removal Part I, J. Chem. Technol. Biotechnol. 84 (2009) 738–744. doi:10.1002/jctb.2106.

[21] P. Lu, H. Wang, K. Hu, Synthesis of glycerol carbonate from glycerol and dimethyl carbonate over the extruded CaO-based catalyst, Chem. Eng. J. 228 (2013) 147–154. doi:10.1016/j.cej.2013.04.109.

[22] K. Hu, H. Wang, Y. Liu, C. Yang, KNO_3/CaO as cost-effective heterogeneous catalyst for the synthesis of glycerol carbonate from glycerol and dimethyl carbonate, J. Ind. Eng. Chem. 28 (2015) 334–343. doi:10.1016/J.JIEC.2015.03.012.

[23] J.R. Ochoa-Gómez, O. Gómez-Jiménez-Aberasturi, B. Maestro-Madurga, A. Pesquera-Rodríguez, C. Ramírez-López, L. Lorenzo-Ibarreta, J. Torrecilla-Soria, M.C. Villarán-Velasco, Synthesis of glycerol carbonate from glycerol and dimethyl carbonate by transesterification: Catalyst screening and reaction optimization, Appl. Catal. A Gen. 366 (2009) 315–324. doi:10.1016/j.apcata.2009.07.020.

[24] X. Song, D. Pan, Y. Wu, P. Cheng, R. Wei, L. Gao, J. Zhang, G. Xiao, Synthesis of glycerol carbonate over porous La-Zr based catalysts: The role of strong and super basic sites, J. Alloys Compd. 750 (2018) 828–837. doi:10.1016/j.jallcom.2018.03.392.

Moisture Resistant K-loaded ZIF-8 Catalyst for Glycerol Carbonate Production

Abstract

Zeolitic imidazolate frameworks (ZIFs) are a new subclass of metal-organic frameworks (MOFs) having structure isomorphic to the aluminosilicate zeolites. ZIF-8 offered greater surface area along with better hydrophobic properties, making it a suitable candidate for catalysis. In the present study, zeolitic imidazolate framework-8 (ZIF-8) was synthesized in an aqueous solution by mixing 2-methylimidazole (mIm) with Zn nitrate hexahydrate (Zn) in deionized water. To enhance the basicity and performance of the ZIF-8 catalyst, a series of K-loaded ZIF-8 catalysts (K/ZIF-8) were prepared having varying amounts (5-10 wt%) of KOH content. Powder XRD, XPS, HRTEM, and TPD techniques have been used for the catalyst characterization. The prepared ZIF-8 and K/ZIF-8 catalysts are employed to carry out the transesterification reaction of GL and DMC to form GLC. The effects of various reaction parameters over the GLC yield, including DMC/GL molar ratio, KOH loading, catalyst amount, and temperature, have been studied. DMC transesterification, employing 10-K/ZIF-8 catalyst, DMC/GL molar ratio of 3:1 over a period of 0.5 h afforded up to 95 % GLC as an exclusive product. Even though K metal is hygroscopic, the prepared catalyst demonstrated better water resistance (up to 5 wt% concerning GL). Moreover, the solid catalyst could be recycled up to three times without any significant decrease in its activity.

6.1 Introduction

The crude glycerol obtained from the biodiesel industry contained traces of water along with methanol and organic impurities. Due to the hygroscopic nature of the glycerol, the water content remained adsorbed in the glycerol layer. These traces of water might cause catalyst poisoning during glycerol carbonate production. In the previous chapter, the hydrophobic nature of the catalyst was achieved by its surface modification, but the catalyst was found to show lesser reusability. In an attempt to further improve the moisture resistance and stability of the catalyst, zeolitic imidazole frameworks (ZIFs) based catalyst were employed for the GLC synthesis. In the present chapter, K impregnated ZIF-8 catalyst was prepared by the simple wet

impregnation method, and its moisture resistance and stability was studied towards the DMC transesterification to yield the GLC.

6.2 Experimental

6.2.1 Preparation of ZIF-8 catalyst

ZIF-8 was prepared in an aqueous medium by adopting the procedure reported in the literature [1]. In a typical experiment, 0.219 g of $Zn(NO_3)_2.6H_2O$ (3.3 mmol) was dissolved in 5 mL deionized water. To this clear solution, 8.2 g of 2-methylimmidazole (mim), dissolved in 60 mL deionized water, was added (Zn:mIm molar ratio = 1:30) to obtain a colorless precipitate. The resulting suspension was stirred for 24 h at room temperature (25 $^{\circ}$C), followed by the centrifugation to obtain the white-colored solid, which was washed with methanol, and dried at 80 $^{\circ}$C for 4 h to get ZIF-8.

6.2.2 Preparation of K/ZIF-8 catalyst

A series of KOH impregnated ZIF-8 catalysts was prepared following the simple wet impregnation method. In a typical setup, 10 mL aqueous KOH solution containing the desired amount of the alkali metal was added to 0.5 g ZIF-8, suspended in 15 mL of deionized water. The resulting mixture was stirred for 4 h at room temperature, filtered, and dried at 100 $^{\circ}$C for 3 h. The obtained off-white solid was then calcined at 150 $^{\circ}$C for 1.5 h to obtain x-K/ZIF-8 catalyst, where x being the K content (wt%).

6.2.3 Transesterification reaction

The transesterification reaction of DMC with GL was carried out utilizing a similar experimental procedure as discussed in chapter 4 but employing K/ZIF-8 as a catalyst. The obtained GLC was characterized by ^{1}H-NMR as well HPLC techniques. The quantification of the GLC was performed by ^{1}H-NMR technique practicing the formula provided in chapter 3.

6.3 Result and discussion

6.3.1 Catalyst characterization

6.3.1.1 X-Ray diffraction (XRD)

Comparison of the X-ray diffraction (XRD) patterns of the prepared ZIF-8 and 10-K/ZIF-8 catalyst revealed that the highly crystalline nature of the ZIF-8 remained intact even after the K loading; however, the intensity of the diffraction peaks was found to decrease (**Figure 6.1**). Both the catalysts showed a characteristic diffraction peak at $2\theta = 7.3^{\circ}$ which is in good accordance with that reported in the literature [2], confirming the formation of crystalline ZIF-8 phase. In diffraction patterns of 10-K/ZIF-8, no peak corresponding to the K_2O phase is identified due to the high dispersion of K in the matrix. Thanh et al. have also observed the absence of the Fe peaks in the XRD spectra of Fe-ZIF-8 catalyst, employed for photocatalytic degradation of Remazol deep black B (RDB) dye, attributed to its existence in the amorphous form [3]. In comparison, Liu et al. have also mentioned the absence of XRD diffractions of NiO in NiO-PTA/ZIF-8 catalyst, employed for hydrocracking of Jatropha oil [4], due to the high NiO dispersion over ZIF-8 and the lower loading amount of NiO.

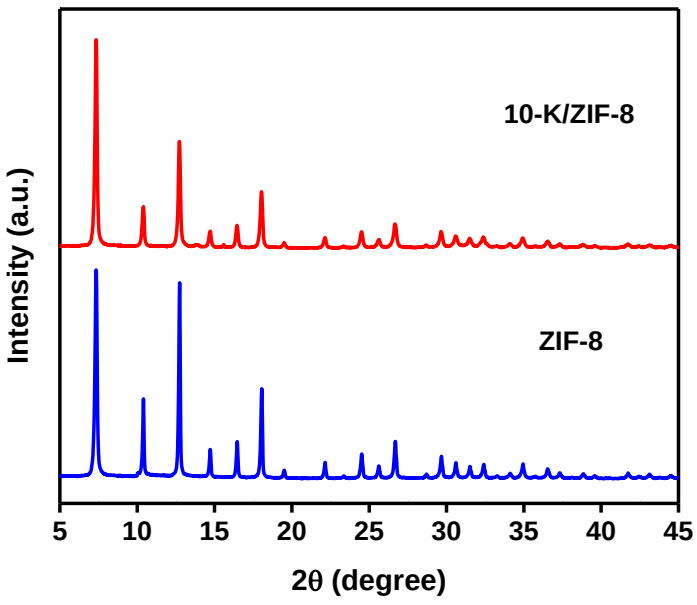

Figure 6.1 Comparison of the XRD pattern of the ZIF-8 and 10-K/ZIF-8 catalysts.

6.3.1.2 X-Ray Photoelectron Spectroscopy

The surface composition and elemental oxidation state of the 10-K/ZIF-8 catalyst was analyzed using the XPS technique. The full scan spectra (**Figure 6.2a**) of the catalyst indicate the presence of Zn, N, K, and O elements over the catalyst surface. The doublet observed at 1022.37, and 1045.51 eV in the Zn 2p spectra could be attributed to the presence of Zn $2p_{3/2}$ and Zn $2p_{1/2}$ states (**Figure 6.2b**). The energy difference of 23.14 eV between the two states reveals the presence of Zn in the +2 oxidation state. This observation is in agreement with reported values for Zn $2p_{3/2}$ and Zn $2p_{1/2}$ peaks at B.E. of 1022.7eV and 1045.9 eV present in ZIF-8 [5,6]. A single peak observed in the O 1s spectra is resolved into a doublet at B.E. values of 532.18 and 532.81 eV representing the bonding of the oxygen in two different forms (**Figure 6.2c**). The peak at 532.18 eV could be assigned to the oxygen present in the form of Zn-O in the ZIF-8 structure. While studying the adsorption performance of ZIF-8 in the water purification process, Ding et al. have assigned the peak at 531.72 eV to the interaction of the hydroxyl group with the zinc ions (Zn-OH) [7]. The peak observed at 532.81 eV could be attributed to the K-O bond present in the form of K_2O. Wang et al. also reported the peak at B.E. of 532.80 eV to the oxygen present in the form of K_2O while conducting the XPS analysis of K_2O-SiO_2 silicate glass [8].

The deconvoluted spectrum of N 1s is resolved into three peaks at B.E. of 398.50, 399.18, and 399.91 eV (**Figure 6.2d**). Peak observed at 398.50 could be assigned to the N bonded to K. Sharma et al. have also mentioned the N 1s peak at 398.66 eV corresponding to the N-K bond present in KN_3 [9]. Peaks observed at 399.18 and 399.91 eV could be assigned to the –N=immidazole and N-H bonding, respectively, present in the imidazole group of ZIF-8. Zhu et al. also reported that in the case of the magnetic MP/ZIF-8 catalyst, employed for Cr(IV) reduction, XPS peak detected at 399.6 and 399.1 eV indicated the presence of -N-H and –N=imidazole present in MP/ZIF-8 [10].

The doublet of K 2p could be deconvoluted into four peaks at B.E. of 292.07, 293.32, 294.23, and 296.56 eV (**Figure 6.2e**). Peaks resolved at B.E. of 293.32 and 296.56 eV represent a set of K $2p_{1/2}$ and K $2p_{3/2}$ peaks corresponding to the K-O bond present in the form of K_2O. Wang et al. have utilized K_2O/C catalyst for the formation of lignocellulosic hydrolysate esters from biomass. While analyzing the catalyst XPS spectra, they assigned the peaks observed at

B.E. of 293.2 and 296.1 eV to set of K $2p_{3/2}$ and K $2p_{1/2}$ peaks of K_2O, respectively [11]. The peak observed at B.E. of 292.07 eV could be attributed to the K-N bond showing the bonding of the loaded K with the imidazole group of ZIF-8. Similarly, during the analysis of the XPS spectra of alkali azides, Sharma et al. have assigned the peak at B.E. of 292.74 to the K-N bond present in KN_3 [9]. The peak resolved at 294.23 eV could be ascribed to the K-C bond representing the linkage of the loaded K species with that of C of the imidazole group of ZIF-8. This observation is supported by literature where the K 2p peak at 294.25 eV was assigned to the K present in the KC_8 compound [12]. Thus, K incorporation with the ZIF-8 has been supported by the XPS study which could not be identified by XRD analysis of the catalyst.

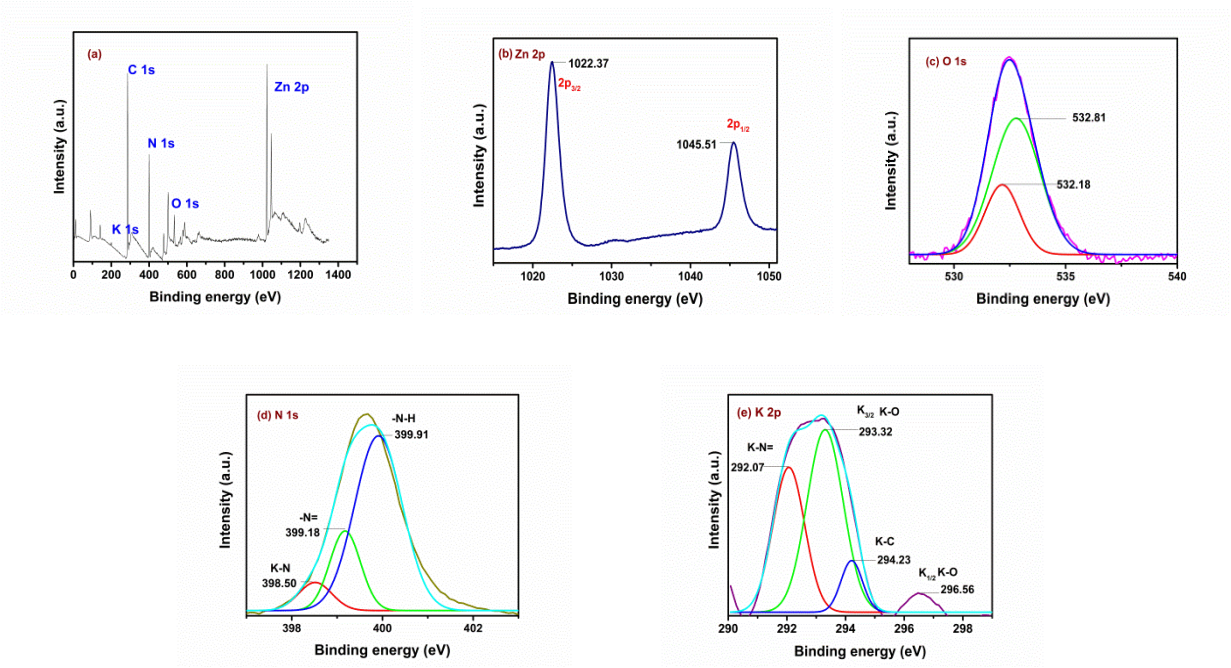

Figure 6.2 XPS spectra of (a) 10-K/ZIF-8 catalyst full scan, and of the individual elements present (b) Zn, (c) O, (d) N and (e) K.

6.3.1.3 SEM-EDX and HRTEM

The SEM images of the ZIF-8 showed the clusters of cubic and rhombic dodecahedral structures of ZIF-8 (**Figure 6.3a, b**). Malekmohammadi et al. also observed that when ZIF-8 was prepared in an aqueous medium, both cubic and truncated rhombic morphology is obtained [13]. Upon KOH loading, the morphology of the obtained K/ZIF-8 catalyst resembles that of the bare ZIF-8 with aggregation of the particles depicting that loading does not have an adverse effect on

the ZIF-8 framework (**Figure 6.3b**). During the SEM analysis of the Fe-ZIF-8 catalyst, Thanh et al. reported the spherical shape of ZIF-8 become irregular upon Fe introduction on it [14]. Furthermore, the elemental composition analysis revealed that the loading of K has been attained over the ZIF-8 surface (**Figure 6.3c, d**).

TEM images also support the well-defined rhombic dodecahedron shaped particles of ZIF-8 with an average particle size of 75 nm (**Figure 6.4a**). TEM analysis of bare ZIF-8, prepared by hydrothermal method employing minimal amount of triethylamine also revealed the formation of rhombic dodecahedron structure [15]. As evident from **Figure 6.4b**, the native shape of the ZIF-8 particles is retained even after K loading, however, with an increase in average particle size (102 nm).

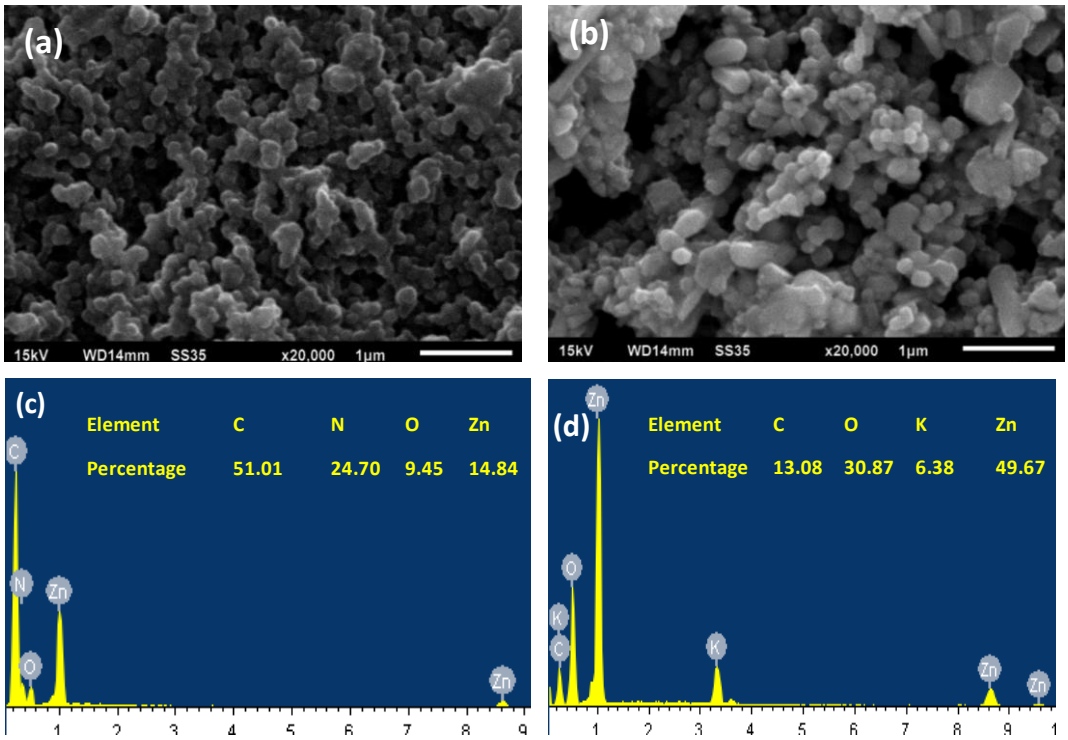

Figure 6.3 SEM images and EDS spectra of (a,c) ZIF-8 and (b,d) 10-K/ZIF-8 catalysts respectively.

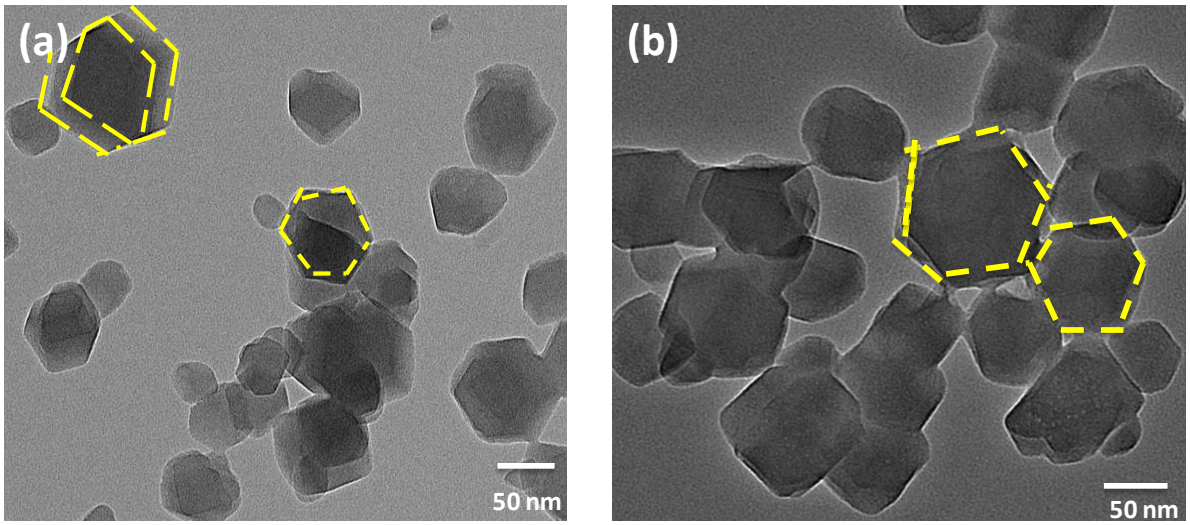

Figure 6.4 HRTEM images of (a) ZIF-8 and (b) 10-K/ZIF-8 catalysts.

6.3.1.4 CO_2-Temperature Programmed Desorption

The effect of K loading over ZIF-8 basicity was studied employing the CO_2-TPD experiment (**Figure 6.5**). A comparison between the CO_2-TPD profile of ZIF-8 and 10-K/ZIF-8 catalysts demonstrated an increase in the basicity of ZIF-8 upon the alkali metal loading. In ZIF-8, the desorption peak positioned at 680 $^{\circ}$C reflects the presence of strong basic sites, corresponding to the total basicity of 4.452 mmol/g. While performing the CO_2-TPD experiment on ZIF-8, Khan et al. also observed that ZIF-8 possess strong basic sites indicated by the CO_2 desorption peak up to 900 $^{\circ}$C [16]. Upon potassium impregnation, the total basicity (5.349 mmol/g), as well as strength of the basic sites present over K/ZIF-8, was found to increase. In K/ZIF-8, the desorption peaks corresponding to the moderate as well as strong basic sites were observed as indicated by the CO_2 desorption at 550 $^{\circ}$C and 680 $^{\circ}$C, respectively. The increase in basic sites could be correlated with the increase in catalyst active sites. Strong basic sites over the catalyst have been interrelated with better catalytic activity towards GLC formation in the literature [17].

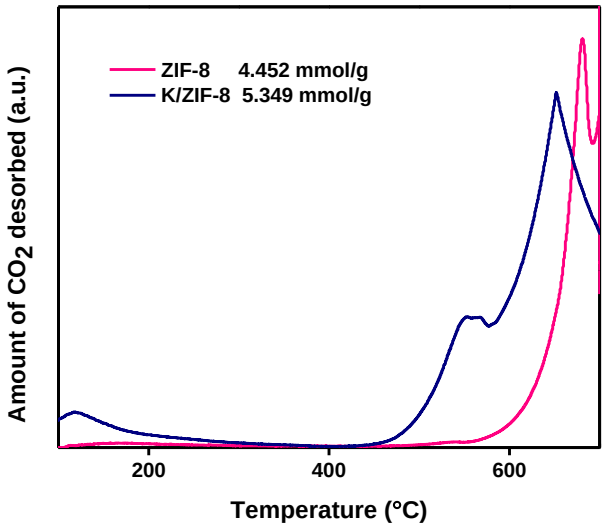

Figure 6.5 Comparison of the CO_2-TPD profile of the ZIF-8 with that of the 10-K/ZIF-8 catalyst.

6.3.2 Optimization of reaction variables

The prepared K/ZIF-8 catalysts were applied for carrying out the synthesis of GLC from GL and DMC. Intending to achieve maximum GLC yield by utilizing minimum resources, all the reaction parameters such as KOH loading, reaction time, reaction temperature, catalyst amount, and reactant ratio were optimized by varying one parameter at a time, as described in subsequent sections.

6.3.2.1 KOH loading

The catalytic activity of the ZIF-8 catalysts impregnated with a varied amount of KOH were compared towards the transesterification reaction employing similar experimental conditions (DMC: GL 3:1 (m/m), 5 wt% catalyst (concerning GL), reaction temp 95 $^{\circ}$C and reaction duration of 0.5 h). As shown in **Figure 6.6a**, bare ZIF-8 demonstrates less than 20 % GLC yield, which upon KOH loading is increased significantly. This is attributed to the increase in catalyst active sites, as also confirmed by the TPD analysis. The entire series of the prepared catalysts has shown 100 % selectivity towards the GLC. However, maximum GL conversion of 95 % is attained with 10 wt% K loaded ZIF-8 catalyst (Figure 6.6a). K loading higher than 10 wt% showed no significant effect on the GLC yield. Thus, in the present study, a minimal amount of the KOH loading can achieve maximum GL conversion than the other literature

reported ZIF-8 based catalyst where 50 wt% MgO loading over ZIF-8 catalyst is required to attain significant (21.2 mmol/g-catalyst) GL conversion levels [18].

6.3.2.2 Catalyst amount

In order to select an appropriate catalyst amount for acquiring maximum GL conversion, transesterification reactions were performed at 95 °C using a varied amount of the catalyst taking DMC/GL molar ratio of 3. As the catalyst amount is increased, more active sites will be available to catalyze the reaction, and accordingly, more GL conversion into the product is obtained. In the present work, maximum GLC yield of 95 % is obtained when 5 wt% of catalyst (concerning GL) is employed. However, further increase in the catalyst amount has no significant effect on the GLC yield due to the limited interaction of the reactant and the catalyst (**Figure 6.6b**). Chang et al. used a catalyst amount of 7.24 wt% for the Mg/ZIF-8 catalyst to attain maximum GL conversion [18]. In literature, generally, the catalyst amount in the range of 1-10 wt% is reported for the potassium-based catalysts (e.g., KF/La-Zr [19], KNO_3/CaO [20], K-zeolite [21] to achieve maximum GLC yield.

6.3.2.3 Reactant ratio

An appropriate amount of reactants is one of the prerequisites to attain a maximum conversion. For selecting the optimum GL/DMC ratio to achieve maximum GLC yield, 10-K/ZIF-8 catalyzed transesterification reactions were performed with varied GL:DMC molar ratios. Due to the reversible nature of the reaction, as the amount of DMC (DMC/GL 3:1) is increased, more GL conversion is obtained. However, upon further increasing the DMC/GL molar ratio to 5, no significant change in conversion level is observed (**Figure 6.6c**). Das et al. [22] also reported that the DMC/GL molar ratio of 3 favours the reaction in the forward direction by reducing the speed of the backward reaction.

6.3.2.4 Reaction temperature

Reaction temperature helps in accelerating the reaction rate by providing sufficient energy to the reactants required for an effective collision. To select an optimum reaction temperature, series of transesterification reactions with varied temperature ranges were

performed utilizing 10-K/ZIF-8 as a catalyst with DMC/GL molar ratio of 3. As the temperature is elevated (95 °C), the reaction is pushed in the forward direction forming more GLC (**Figure 6.6d**). On further increasing the temperature to 105 °C a slight decline in the GLC yield is observed, which could be due to the lesser amount of DMC available for the reaction due to its evaporation at elevated temperature. Likewise Kumar et al. [23] and Song et al. [24] reported reaction temperatures of 90 °C and 95 °C for Cu/Al hydrotalcites and Li/ZnO catalysts, respectively, to achieve maximum GLC yield.

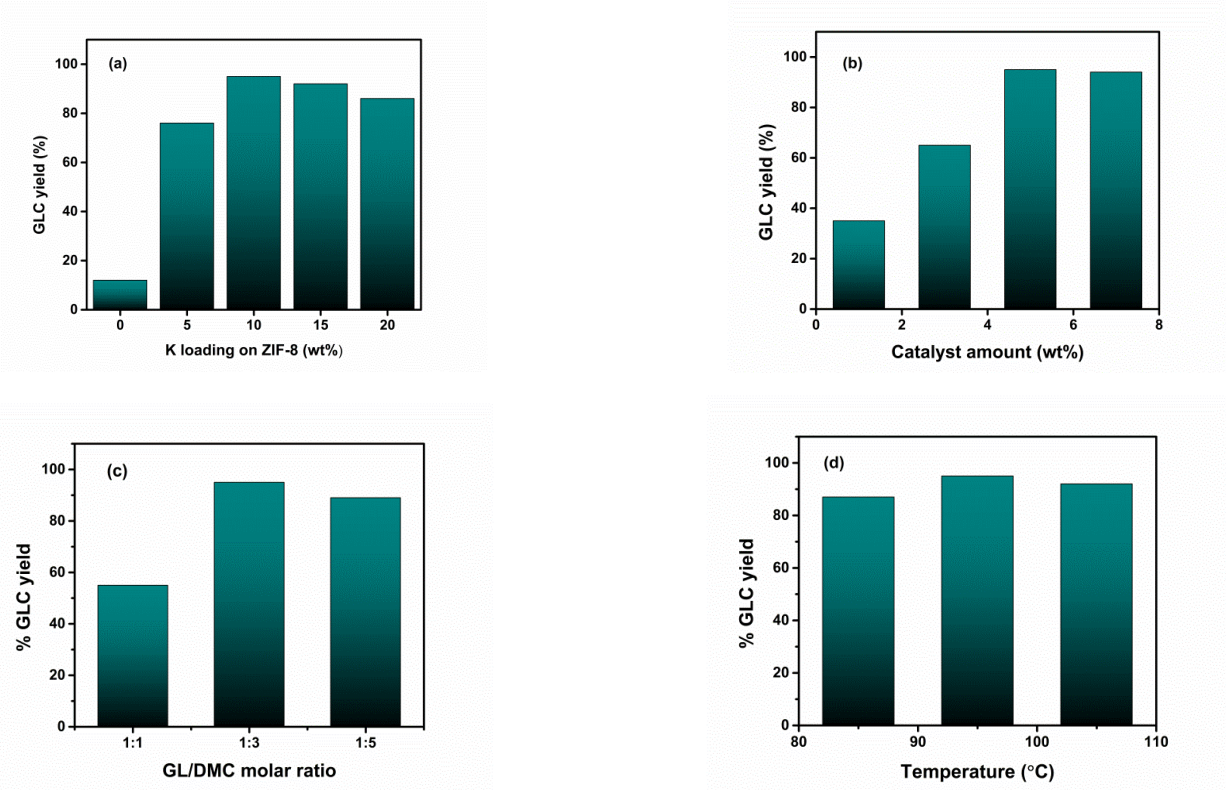

Figure 6.6 Effect of **(a)** KOH loading; (**b**) catalyst amount concerning GL; (**c**) reactant molar ratio and (**d**) reaction temperature on the 10-K/ZIF-8 assisted synthesis of GLC.

6.3.3 Water resistance

The crude GL obtained from the BD industry acquires some amount of water during the refining process. Thus, the catalyst employed for deriving GLC from GL should be resistant to the traces of water present to attain maximum catalytic activity. To check the water resistance of the prepared 10-K/ZIF-8 catalyst, a number of transesterification reactions were conducted by adding a varied amount of water in the reaction mixture (GL+DMC) under the optimized

reaction conditions. As shown in **Figure 6.7**, even in the presence of 4 wt% water (concerning GL), GLC yield does not decline to a significant extent (from 95 % to 88 %). It could be due to the hydrophobic nature of ZIF-8, which was able to repel the water present in the reaction mixture [25]. However, on further addition of water (5 wt%), a drastic decline in the GLC conversion is observed. Although ZIF-8 was found to be stable in water [26], the possible reason for the activity decline could be the hygroscopic nature of the potassium oxide, which upon water adsorption, might block the catalyst active sites. While studying the poisoning of the potassium aluminum oxide catalyst, employed for the biodiesel production from Kusum oil, Yadav et al. have also found that the active sites of the catalyst get poisoned with the adsorption of the water molecules on its surface [27].

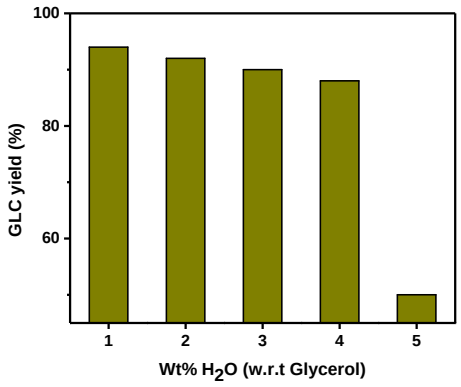

Figure 6.7 Effect of the water content present in the GL upon the catalytic activity of 10-K/ZIF-8 catalyst. (Reaction conditions: DMC/GL molar ratio 3:1, temperature 95 °C, time 0.5 h; catalyst amount= 5 wt% of catalyst concerning GL).

6.3.4 Catalyst reusability

From the economic point of view, the reusability of the catalyst plays a deciding role in ascertaining its implementation on a wider scale. Likewise, the stability of the 10-K/ZIF-8 catalyst was studied under the optimized reaction conditions. Before reuse, the catalyst was separated from the reaction mixture, washed with methanol, and dried at 60 °C for 4 h. A similar experimental procedure is adopted for 3 consecutive cycles. The prepared catalyst exhibits decent reusability as almost comparable GLC yield is obtained during 3 catalytic cycles with 100 % GLC selectivity (**Figure 6.8**).

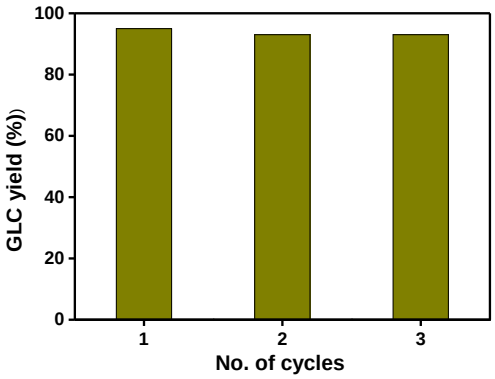

Figure 6.8 Reusability study of the 10-K/ZIF-8 catalyst employed for the GLC synthesis (Reaction conditions: DMC/GL molar ratio 3:1, temperature 95 °C, catalyst amount= 5 wt% of catalyst concerning GL, time 0.5 h).

6.4 Comparison with the reported catalysts

The results obtained with the 10-K/ZIF-8 catalysts were compared with that of the literature reported heterogeneous catalysts applied for the transesterification reaction of GL with DMC (**Table 6.1**). MgO/ZIF-8 catalysts showed 100 % GLC selectivity, but the moisture-resistant property and reusability of the catalyst was not studied. KNO_3/CaO demonstrated good water tolerance and reusability but was not entirely selective to GLC formation. Moreover, a longer reaction duration is required to achieve good GL conversion level (99.23 %). Likewise, CaO/Al_2O_3 catalyst was found to resist the presence of only up to 2 wt% water in the reaction mixture, along with GLC selectivity issue (95 % GLC selectivity). On the other hand, the catalyst developed in the present study demonstrated a better moisture resistance (up to 4 wt%), and was able to achieve more than 95 % GL conversion and 100 % GLC selectivity in just 0.5 h of reaction duration. The reusability studies and other experimental conditions are comparable to those employed for the literature-reported catalysts.

Table 6.1 Comparison of previously reported catalysts with present catalyst employed for the transesterification of DMC with GL.

Catalysts	Reaction conditions	Catalyst amount (wt%)	Water tolerance	GL conversion	GLC selectivity (%)	Reusability (cycles)	Reference
MgO/ZIF-8	DMC/GL 4:1; 75 °C, 2 h	7.24	NR	21.2 mmol/g-catalyst	100	NR	[18]
10-K/ZIF-8	DMC/GL 3:1; 95 °C, 0.5 h	5	4 wt%	95 %	100	3	Present work
KNO_3/CaO	DMC/GL 3:1; 70 °C, 2 h	1.5	5 wt%	99.23 %	86	5	[20]
CaO/Al_2O_3 (polyacrylamide)	DMC/GL 3:1; 80 °C, 2 h	1.6	2 wt%	95.39 %	95	5	[28]

6.5 Conclusions

In the present study, combining the hydrophobic properties of metal-organic framework ZIF-8 and the basic properties of KOH, the catalyst was prepared via a simple wet impregnation method. XRD study revealed that even after the impregnation, the framework of ZIF-8 remained intact. The catalytic activity of the prepared catalyst was tested against the transesterification reaction of GL and DMC. The resultant catalyst, 10-K/ZIF-8 having a higher basic strength than its native counterpart, exhibited better GL conversion providing GLC as a sole product in a short reaction time. Nevertheless, the prepared catalyst demonstrated resistance to the water present in the GL (up to 4 wt%) without significant loss in the activity.

References

[1] K. Kida, M. Okita, K. Fujita, S. Tanaka, Y. Miyake, Formation of high crystalline ZIF-8 in an aqueous solution, Cryst. Eng. Comm. 15 (2013) 1794–1801. doi:10.1039/c2ce26847g.

[2] A. Schejn, L. Balan, V. Falk, L. Aranda, G. Medjahdi, R. Schneider, Controlling ZIF-8 nano- and microcrystal formation and reactivity through zinc salt variations, Cryst. Eng. Comm. 16 (2014) 4493–4500. doi:10.1039/c3ce42485e.

[3] M.T. Thanh, T.V. Thien, P.D. Du, N.P. Hung, D.Q. Khieu, Iron doped zeolitic imidazolate framework (Fe-ZIF-8): synthesis and photocatalytic degradation of RDB dye in Fe-ZIF-8, J. Porous Mater. 25 (2018) 857–869. doi:10.1007/s10934-017-0498-7.

[4] J. Liu, J. He, L. Wang, R. Li, P. Chen, X. Rao, L. Deng, L. Rong, J. Lei, NiO-PTA supported on ZIF-8 as a highly effective catalyst for hydrocracking of Jatropha oil, Sci. Rep. 6 (2016) 1–11. doi:10.1038/srep23667.

[5] D. Muñoz-Gil, F.M.L. Figueiredo, High surface proton conduction in nanostructured ZIF-8, Nanomaterials 9 (2019) 1–14. doi:10.3390/nano9101369.

[6] P.Z. Li, K. Aranishi, Q. Xu, ZIF-8 immobilized nickel nanoparticles: Highly effective catalysts for hydrogen generation from hydrolysis of ammonia borane, Chem. Commun. 48 (2012) 3173–3175. doi:10.1039/c2cc17302f.

[7] Y. Ding, Y. Xu, B. Ding, Z. Li, F. Xie, F. Zhang, H. Wang, J. Liu, X. Wang, Structure induced selective adsorption performance of ZIF-8 nanocrystals in water, Colloids Surfaces A Physicochem. Eng. Asp. 520 (2017) 661–667. doi:10.1016/j.colsurfa.2017.02.012.

[8] R. Sawyer, H.W. Nesbitt, R.A. Secco, High resolution X-ray Photoelectron Spectroscopy (XPS) study of K_2O-SiO_2 glasses: Evidence for three types of O and at least two types of Si, J. Non. Cryst. Solids. 358 (2012) 290–302. doi:10.1016/j.jnoncrysol.2011.09.027.

[9] J. Sharma, T. Gora, J.D. Rimstidt, R. Staley, X-ray photoelectron spectra of the alkali

azides, Chem. Phy. Lett. 15 (1972) 232-235.

[10] K. Zhu, C. Chen, H. Xu, Y. Gao, X. Tan, A. Alsaedi, T. Hayat, Cr(VI) reduction and immobilization by core-double-shell structured magnetic polydopamine@zeolitic idazolate frameworks-8 microspheres, ACS Sustain. Chem. Eng. 5 (2017) 6795–6802. doi:10.1021/acssuschemeng.7b01036.

[11] K. Wang, J. Jiang, X. Liang, Design, synthesis and evaluation of novel glycosyl surfactant—lignocellulosic hydrolysate esters from shrub willow, Ind. Crops Prod. 92 (2016) 127–135. doi:10.1016/j.indcrop.2016.07.036.

[12] H. Estrade-Szwarckopf, B. Rousseau, U.P.S. and X.P.S. studies of alkali-graphite intercalation compounds, Synth. Met. 23 (1988) 191–198.

[13] M. Malekmohammadi, S. Fatemi, M. Razavian, A. Nouralishahi, A comparative study on ZIF-8 synthesis in aqueous and methanolic solutions: Effect of temperature and ligand content, Solid State Sci. 91 (2019) 108–112. doi:10.1016/j.solidstatesciences.2019.03.022.

[14] M. Thi Thanh, T. Vinh Thien, V. Thi Thanh Chau, P. Dinh Du, N. Phi Hung, D. Quang Khieu, Synthesis of iron doped zeolite imidazolate framework-8 and its remazol deep black RGB dye adsorption ability, J. Chem. 2017 (2017). doi:10.1155/2017/5045973.

[15] V. V. Butova, A.P. Budnyk, E.A. Bulanova, C. Lamberti, A. V. Soldatov, Hydrothermal synthesis of high surface area ZIF-8 with minimal use of TEA, Solid State Sci. 69 (2017) 13–21. doi:10.1016/j.solidstatesciences.2017.05.002.

[16] I.U. Khan, M.H.D. Othman, A. Jilani, A.F. Ismail, H. Hashim, J. Jaafar, M.A. Rahman, G.U. Rehman, Economical, environmental friendly synthesis, characterization for the production of zeolitic imidazolate framework-8 (ZIF-8) nanoparticles with enhanced CO_2 adsorption, Arab. J. Chem. 11 (2018) 1072–1083. doi:10.1016/j.arabjc.2018.07.012.

[17] G. Pradhan, Y.C. Sharma, Green synthesis of glycerol carbonate by transesterification of bio glycerol with dimethyl carbonate over Mg/ZnO: A highly efficient heterogeneous catalyst, Fuel 284 (2021) 118966. doi:10.1016/j.fuel.2020.118966.

[18] C.W. Chang, Z.J. Gong, N.C. Huang, C.Y. Wang, W.Y. Yu, MgO nanoparticles confined

in ZIF-8 as acid-base bifunctional catalysts for enhanced glycerol carbonate production from transesterification of glycerol and dimethyl carbonate, Catal. Today 351 (2020) 21–29. doi:10.1016/j.cattod.2019.03.007.

[19] X. Song, D. Pan, Y. Wu, P. Cheng, R. Wei, L. Gao, J. Zhang, G. Xiao, Synthesis of glycerol carbonate over porous La-Zr based catalysts: The role of strong and super basic sites, J. Alloys Compd. 750 (2018) 828–837. doi:10.1016/j.jallcom.2018.03.392.

[20] K. Hu, H. Wang, Y. Liu, C. Yang, KNO_3/CaO as cost-effective heterogeneous catalyst for the synthesis of glycerol carbonate from glycerol and dimethyl carbonate, J. Ind. Eng. Chem. 28 (2015) 334–343. doi:10.1016/j.jiec.2015.03.012.

[21] Y.T. Algoufi, B.H. Hameed, Synthesis of glycerol carbonate by transesterification of glycerol with dimethyl carbonate over K-zeolite derived from coal fly ash, Fuel Process. Technol. 126 (2014) 5–11. doi:10.1016/j.fuproc.2014.04.004.

[22] B. Das, K. Mohanty, Exploring the promotional effects of K, Sr, and Mg on the catalytic stability of Red Mud for the synthesis of gycerol carbonate from renewable glycerol, Ind. Eng. Chem. Res. 58 (2019) 15803–15817. doi:10.1021/acs.iecr.9b00420.

[23] P. Kumar, R.C. Korošec, U.L. Štangar, Highly active and efficient Cu-based hydrotalcite-like structured materials as reusable heterogeneous catalysts used for transcarbonation reaction, J. Colloid Interface Sci. 585 (2021) 549–559. doi:10.1016/j.jcis.2020.10.035.

[24] X. Song, Y. Wu, F. Cai, D. Pan, G. Xiao, High-efficiency and low-cost Li / ZnO catalysts for synthesis of glycerol carbonate from glycerol transesterification : The role of Li and ZnO interaction, Appl. Catal. A, Gen. 532 (2017) 77–85. doi:10.1016/j.apcata.2016.12.019.

[25] E.E. Sann, Y. Pan, Z. Gao, S. Zhan, F. Xia, Highly hydrophobic ZIF-8 particles and application for oil-water separation, Sep. Purif. Technol. 206 (2018) 186–191. doi:10.1016/j.seppur.2018.04.027.

[26] P. Cheng, Y.H. Hu, H_2O-functionalized zeolitic Zn(2-methylimidazole)$_2$ framework (ZIF-8) for H_2 storage, J. Phys. Chem. C. 118 (2014) 21866–21872. doi:10.1021/jp507030g.

[27] M. Yadav, Y.C. Sharma, Process optimization and catalyst poisoning study of biodiesel production from kusum oil using potassium aluminum oxide as efficient and reusable heterogeneous catalyst, J. Clean. Prod. 199 (2018) 593–602. doi:10.1016/j.jclepro.2018.07.052.

[28] P. Lu, H. Wang, K. Hu, Synthesis of glycerol carbonate from glycerol and dimethyl carbonate over the extruded CaO-based catalyst, Chem. Eng. J. 228 (2013) 147–154. doi:10.1016/j.cej.2013.04.109.

Conclusions and Futuristic Aspect

Abstract

The work carried out in Chapters 3-6 has been concluded and compared in this chapter. The future scope of the work has also been discussed.

The conclusion from the present thesis

The present thesis made efforts to transform the surplus GL into a valuable product, glycerol carbonate. The base-catalyzed transesterification route is adopted to synthesize GLC from GL and DMC. The quantitative ^{1}H-NMR technique has been utilized for the first time to quantify the GLC formed from the reaction of GL with DMC. To make the GLC production process more convenient, three different heterogeneous catalysts: 20-Li/ZrO_2-700, modified CaO, and K-loaded ZIF-8 were developed and applied to transform glycerol to glycerol carbonate. The structural and surface properties of the prepared catalysts were studied by different analytical techniques such as powder XRD, BET, XPS, HRTEM, and TPD. In the case of the 20-Li/ZrO_2-700 catalyst, it is observed that the catalyst prepared by the wet impregnation method showed better activity (91 % GLC) than that by the co-precipitation method, indicating that the contribution of the catalyst preparation method is worth noticing. XRD studies depicted that proper interaction between the metal (Li) and the support (ZrO_2) is pivotal for elevating the catalytic activity of the 20-Li/ZrO_2-700 catalyst. The kinetic study revealed that Li/ZrO_2 assisted transesterification reaction of DMC with GL followed second-order rate law with the activation energy of 93.7 kJ mol^{-1}. In another study, to strengthen up the stability of the commercial CaO its surface is made hydrophobic by grafting the benzyl group on its surface through a simple wet impregnation method. It has been observed that besides providing moisture resistance properties (5 wt% of H_2O addition in GL) to the native CaO, the modified CaO catalyst also demonstrated better GL conversion (82 %) than native CaO. However, reusability remains a matter of concern. On the same path, hydrophobic properties of ZIF-8 are also explored towards the GLC synthesis. To make ZIF-8 an eligible candidate for the GL transformation, KOH is loaded on it via a simple wet impregnation method. 10 wt% K loaded ZIF-8 catalyst provided resistance to the presence of 4 wt% of H_2O in the reaction mixture and demonstrated the best activity (95 % GLC) among all the prepared catalysts. The hydrophobic and stable nature of the 10 wt% K loaded ZIF-8 catalyst opened up the way for its industrial implementation.

Table 7.1 Comparison of the reaction conditions and catalytic activity of the prepared catalysts employed for the glycerol carbonate synthesis.

S.No.	Catalyst	Reaction parameters Glycerol:DMC/Temp (°C)//Time (h)/Catalyst wt%	GL conversion/ GLC Yield/ GLC selectivity (%)	Reusability (cycle)/ GL conversion in last cycle (%)	Water resistance (wt% of water with respect to GL)
1.	20-Li/ZrO_2-700	1:3/ 95/ 2/ 5	91/91/100	4/ 52	Not studied
2.	0.5-Ben/CaO-250	1:5/95/2/5	82/82/100	4/53	5
3.	10-K/ZIF-8	1:3/95/0.5/5	95/95/100	3/95	4

All the catalysts prepared in this work showed complete selectivity towards glycerol carbonate. The characteristics feature such as perseverance of the selectivity while reuse, resistance to moisture, and good stability of the prepared catalysts made them an eligible candidate for carrying out the glycerol transformation at a large scale.

Futuristic aspects

Some futuristic proposals related to the present work are enlisted below:

1. To make the separation of the heterogeneous catalysts hassle-free, an attempt would be made to make it magnetic following the procedure reported in the literature.
2. Apart from mixed metal oxides, hydrotalcites, metal-organic framework and mesoporous, basic catalyst would be explored for the transesterification reaction of the GL with DMC.
3. Besides co-precipitation and wet impregnation methods employed for catalyst preparation, effect of other preparation methods such as sol-gel method, hydrothermal method on the catalytic activity towards GLC formation could be studied.
4. To resolve the problem of glycerol management, glycerol-free biodiesel production utilizing dimethyl carbonate as methylating agent would be explored by employing water-resistant basic catalysts.
5. Likewise GLC, an attempt would be made to quantify the GL acetalization product; solketal through ^{1}H-NMR technique.

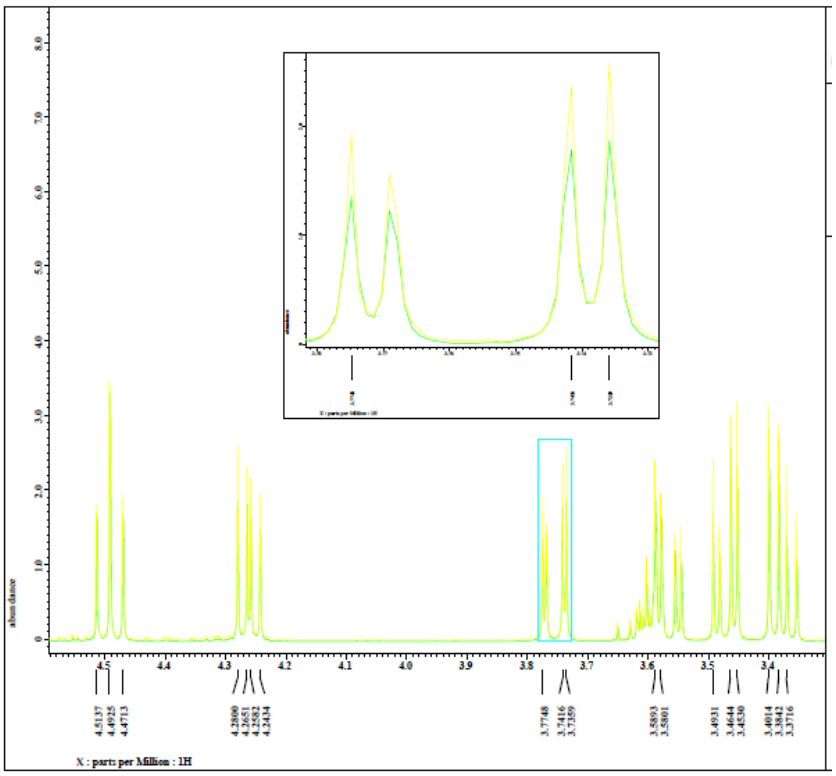

Figure A.1 Influence of d1 values over the ^{1}H-NMR signal areas of the standard GL/GLC mixture.

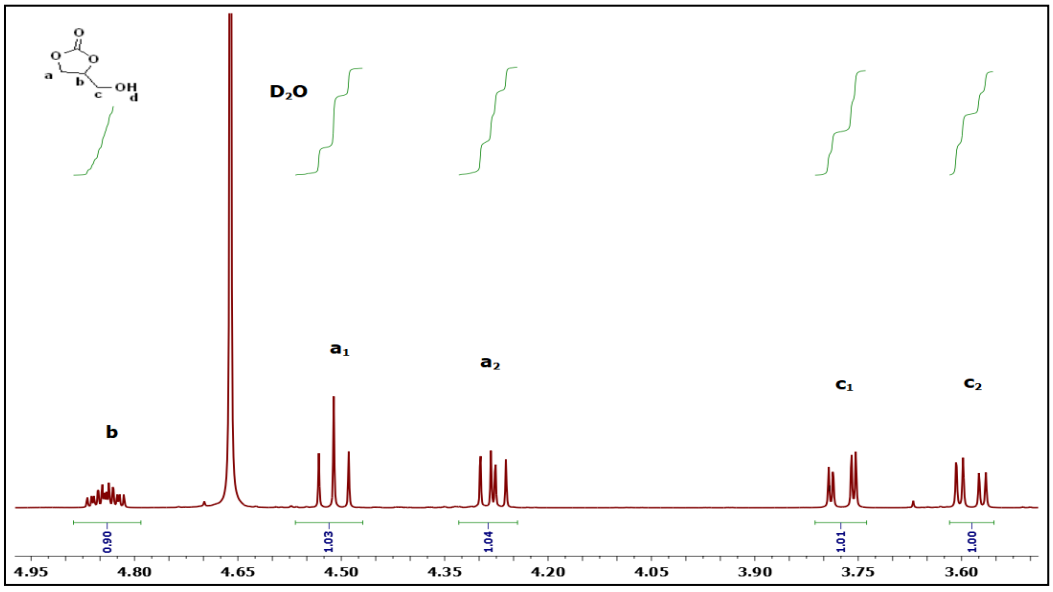

Figure A.2 Integrated ^{1}H-NMR spectra of standard glycerol carbonate.

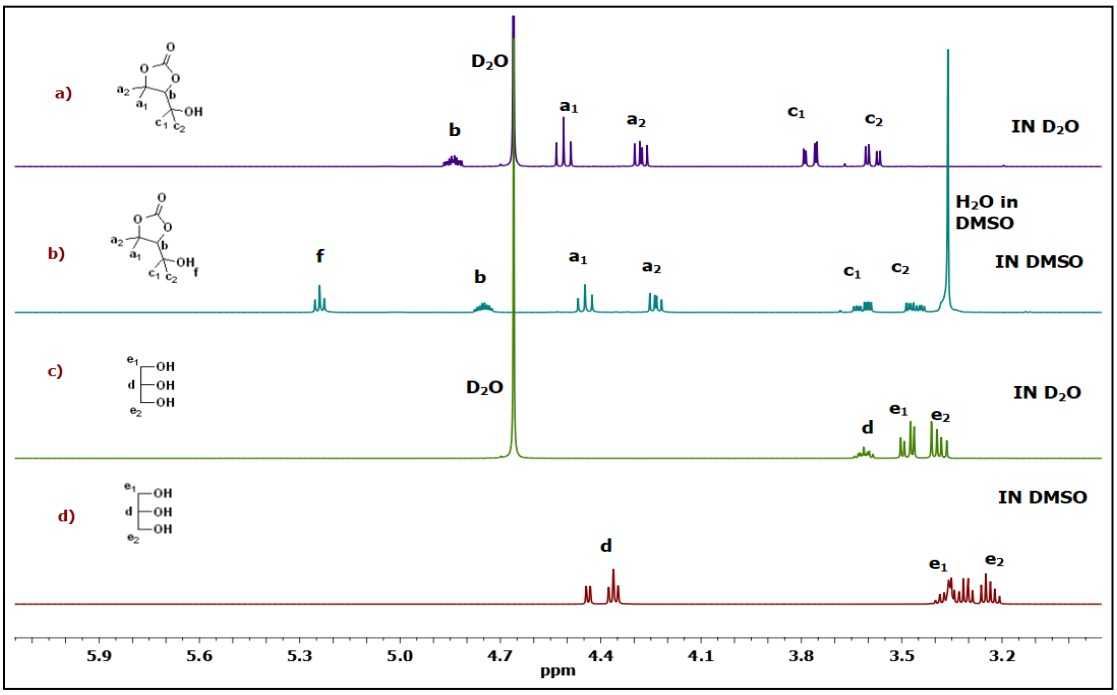

Figure A.3 ^{1}H-NMR spectra of standard GLC (a) D_2O and (b) DMSO; standard GL in (c) D_2O and (d) DMSO

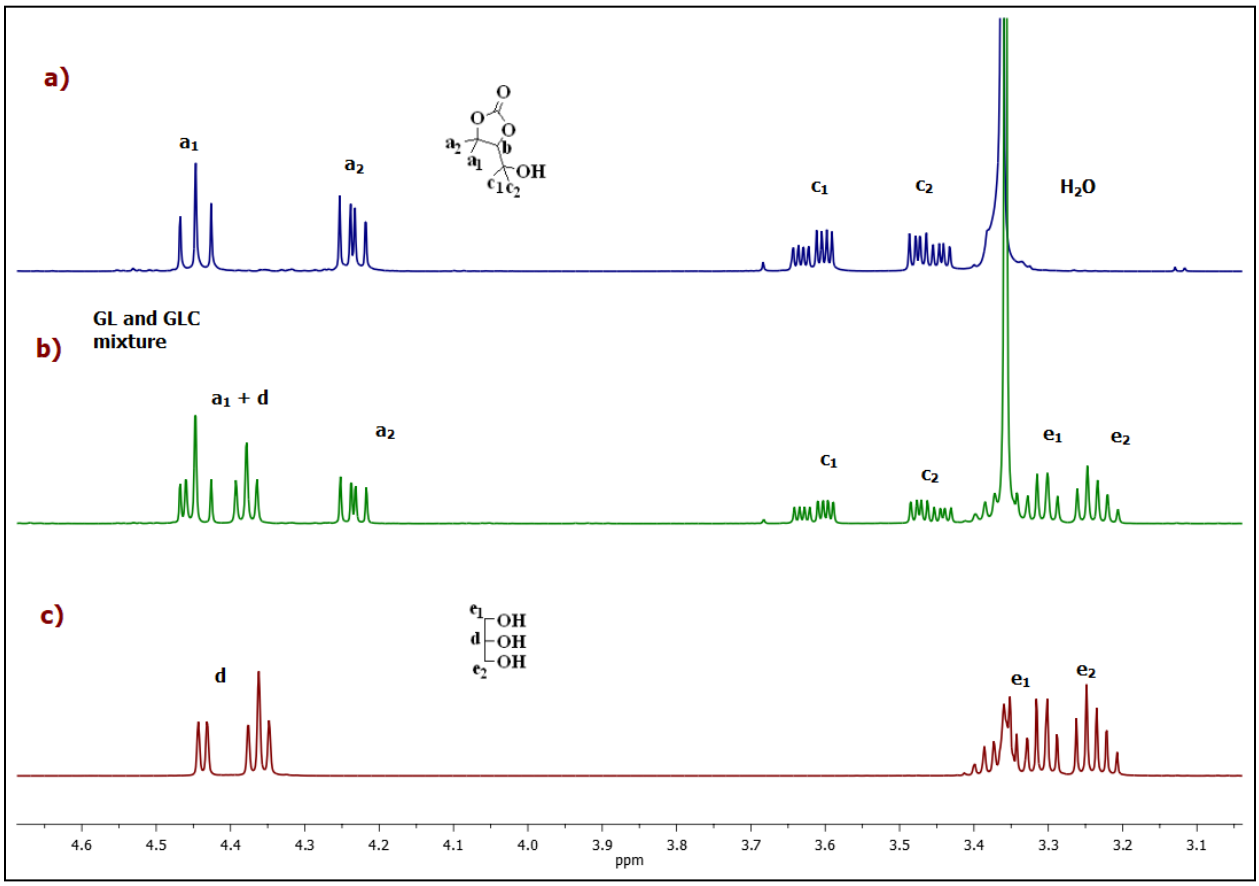

Figure A.4 [1]H-NMR spectra of standard (a) GL, (b) GL/GLC standard mixture 30:70(m/m), and (c) standard GL in DMSO.

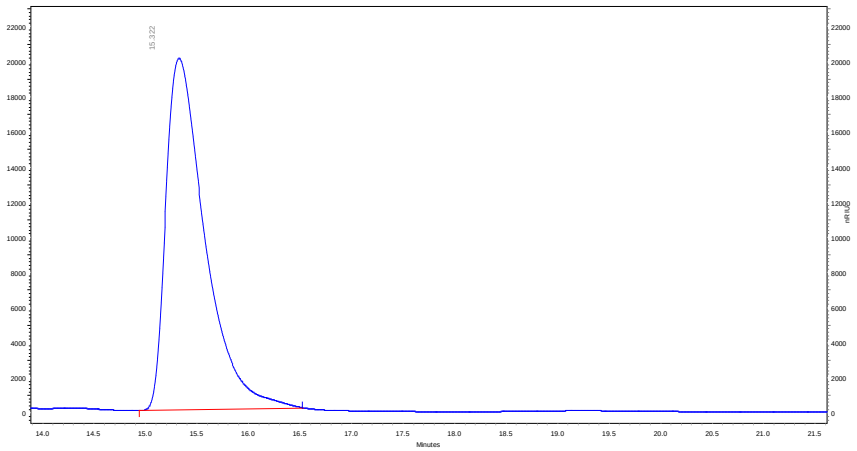

Figure A.5 HPLC chromatogram of standard GLC.

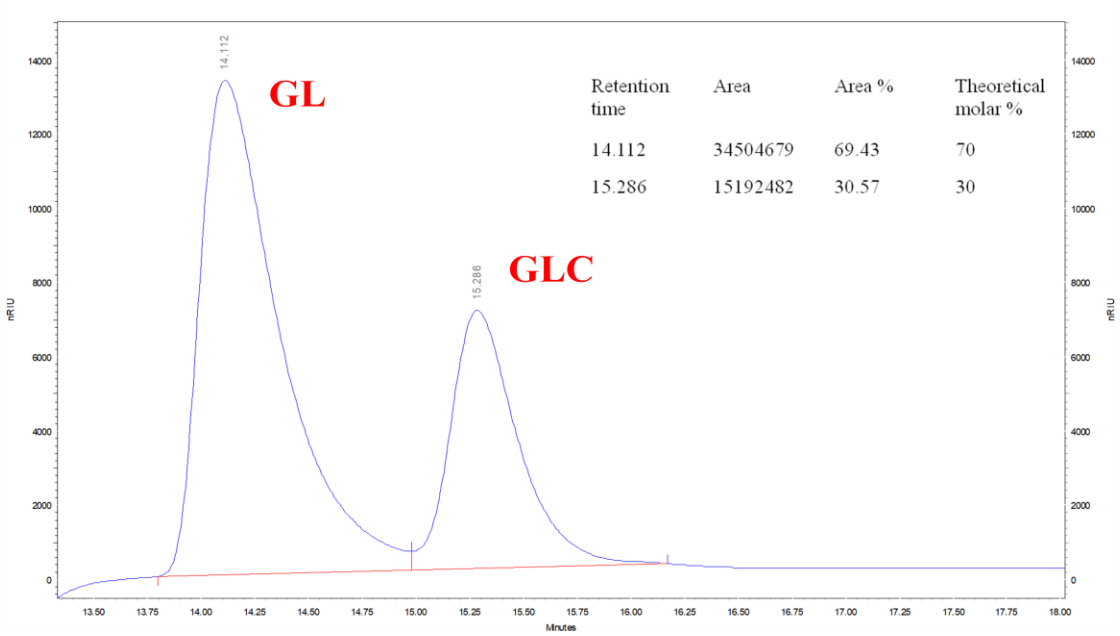

Figure A.6 HPLC chromatogram of GLC/GL mixture (30:70 molar ratio).

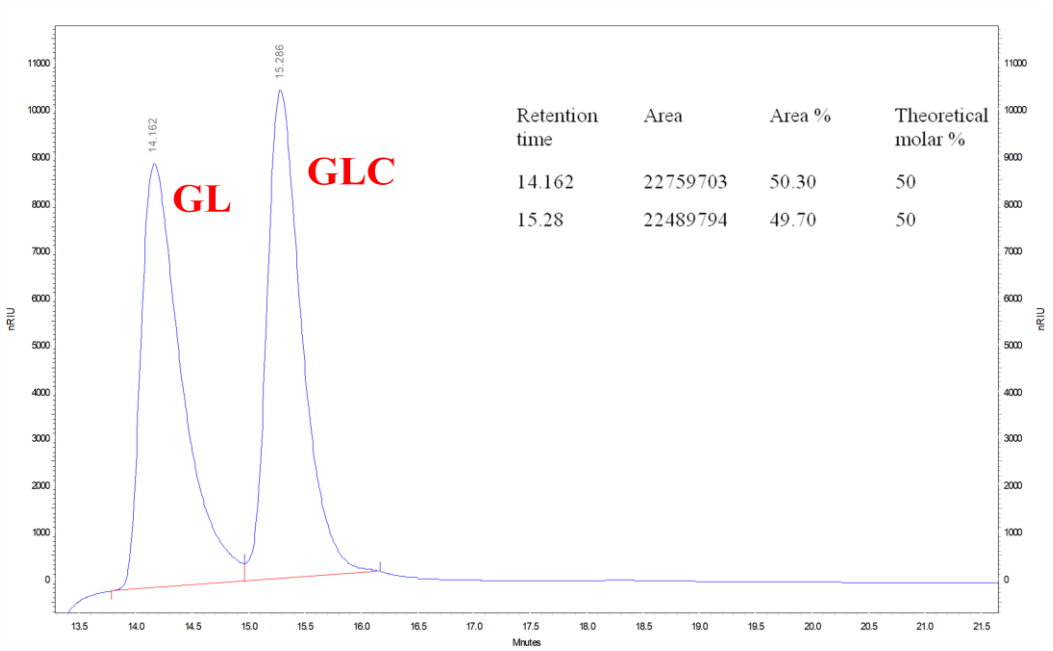

Figure A.7 HPLC chromatogram of GLC/GC mixture of molar ratio 50:50.

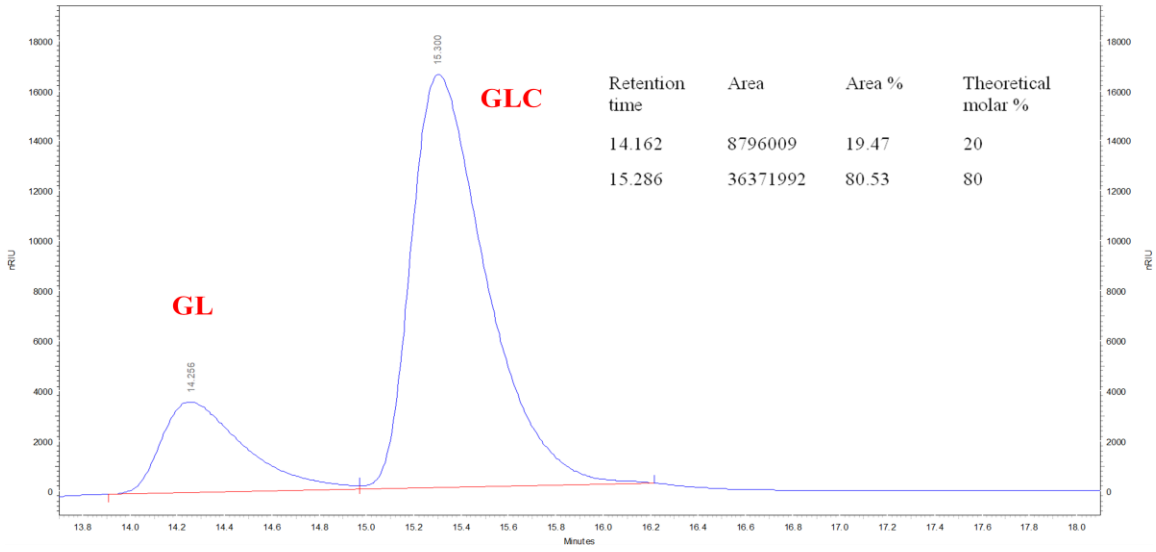

Figure A.8 HPLC chromatogram of GLC/GL mixture (80:20 molar ratio).

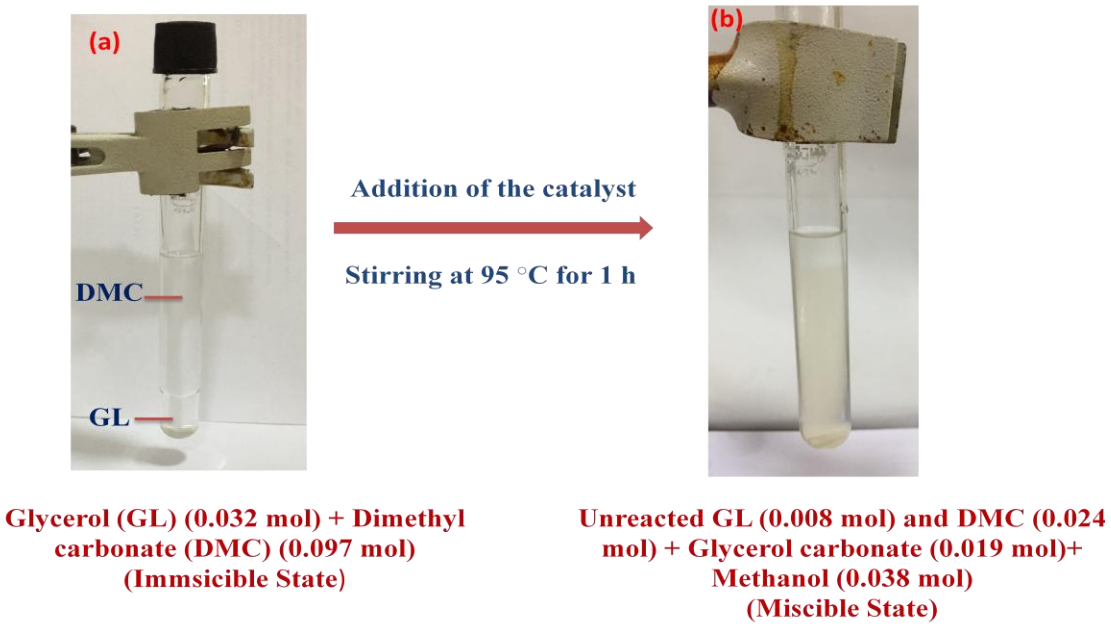

Figure A.9 Demonstration of the miscibility of the GL and DMC before and after the reaction.

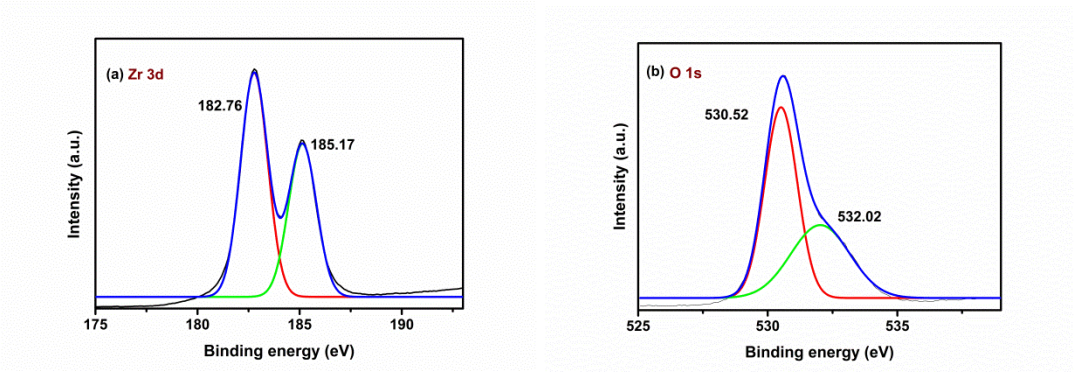

Figure A.10 XPS spectra of (**a**) Zr and (**b**) O present in native ZrO_2.

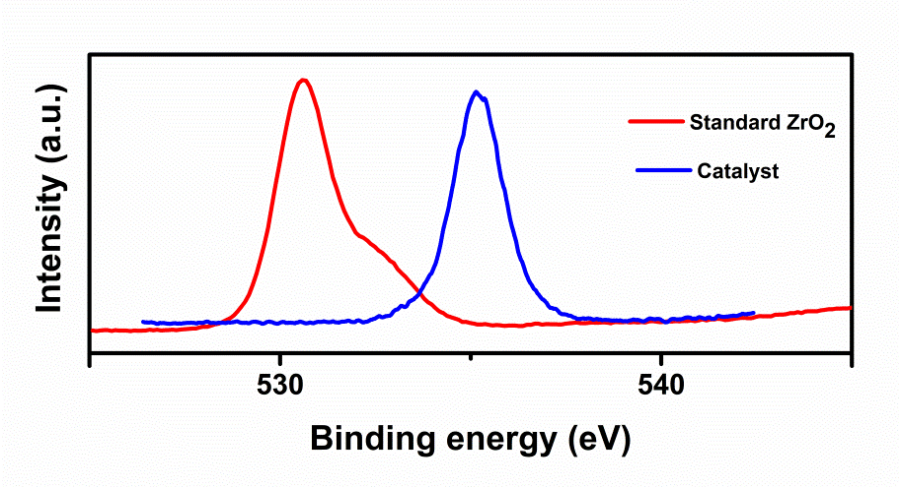

Figure A.11 Comparison of the O 1s XPS spectra of the native ZrO_2 with that of the 20-Li/ZrO_2 catalyst.

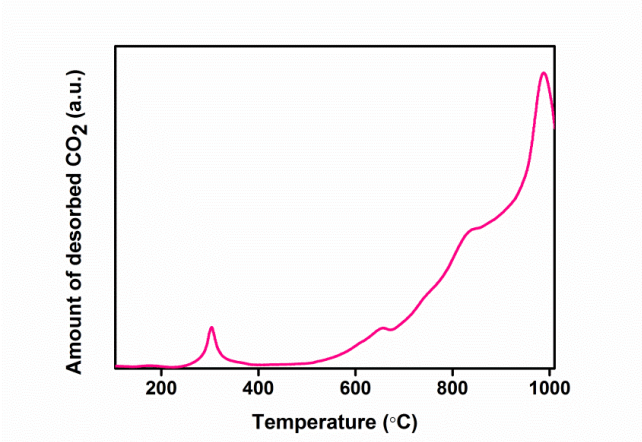

Figure A.12 CO_2-TPD profile of the 20-Li/ZrO_2-700 catalyst

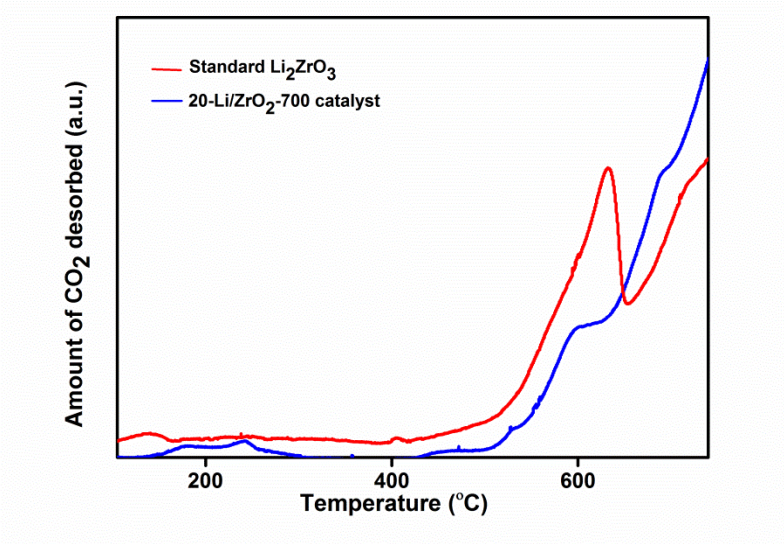

Figure A.13 Comparison of the CO_2-TPD profile of the 20-Li/ZrO_2-700 catalyst with standard Li_2ZrO_3.

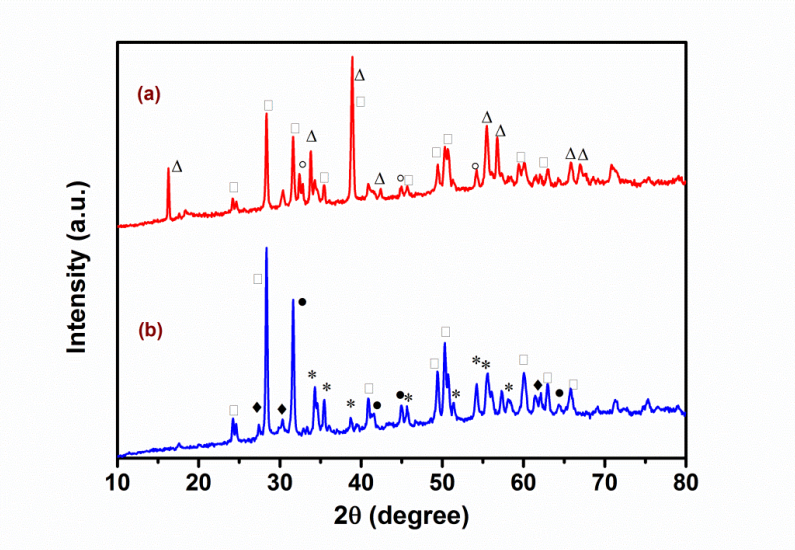

Figure A.14 Comparative study of the XRD spectra of K and Na-loaded ZrO_2 catalyst calcined at 700° C. [•= tetragonal K_2O (JCPDS card no 077-0137), *= orthorhombic K_2ZrO_5 (JCPDS card no.018-1012), Δ= monoclinic Na_2ZrO_3 (JCPDS card no. 008-0242), ◦= orthorhombic NaO_2 (JCPDS card no.089-5953), ♦= orthorhombic ZrO_2 (JCPDS card no. 033-1483), □= monoclinic ZrO_2 (JCPDS card no. 013-0307),].

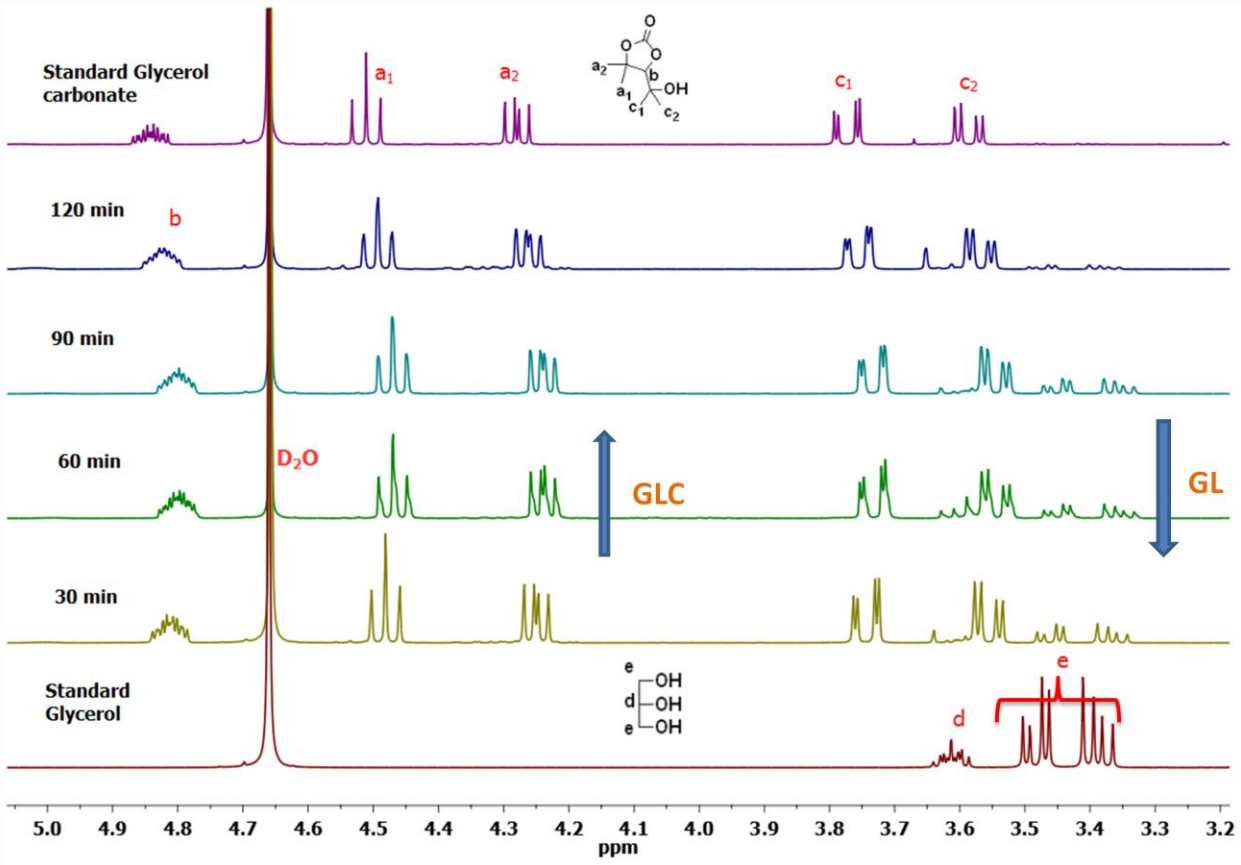

Figure A.15 Comparison of the ^{1}H NMR spectra of the reaction mixture samples of the 20-Li/ZrO_2-700 catalyzed reaction taken at 30, 60, 90, and 120 min of the reaction with that of standard GL and GLC samples

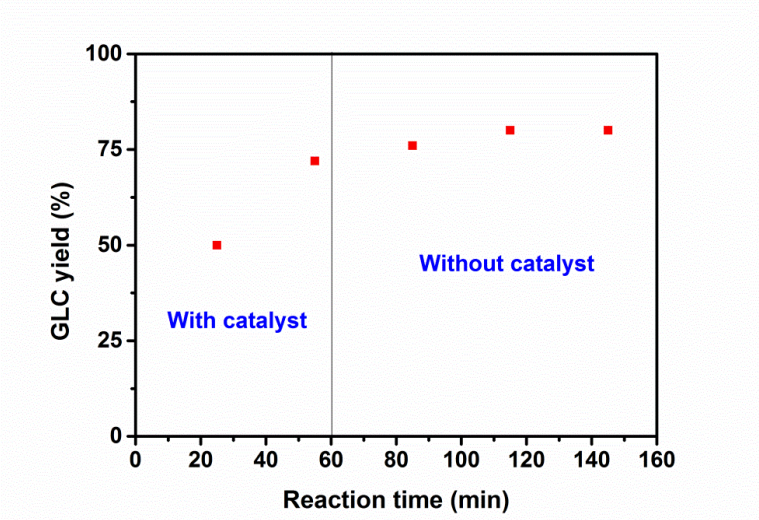

Figure A.16 Hot filtration test for the transesterification of DMC with GL over the 20-Li/ZrO_2-700 catalyst.

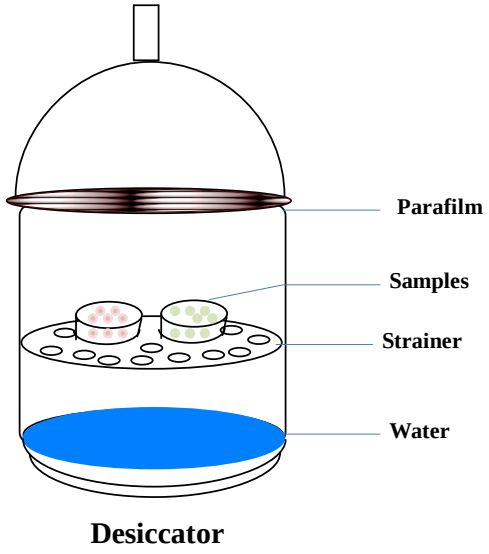

Figure A.17 Pictorial representation of the experimental setup used for the humidity test**.**

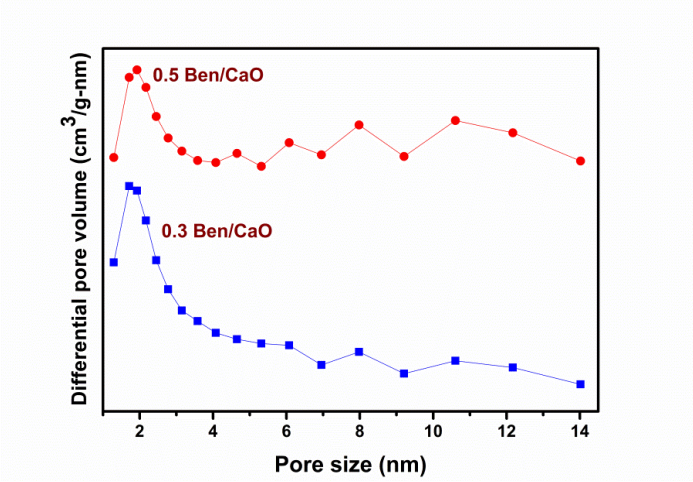

Figure A.18 Comparison of the BJH pore size distribution plot of 0.3-Ben/CaO and 0.5-Ben/CaO catalysts.

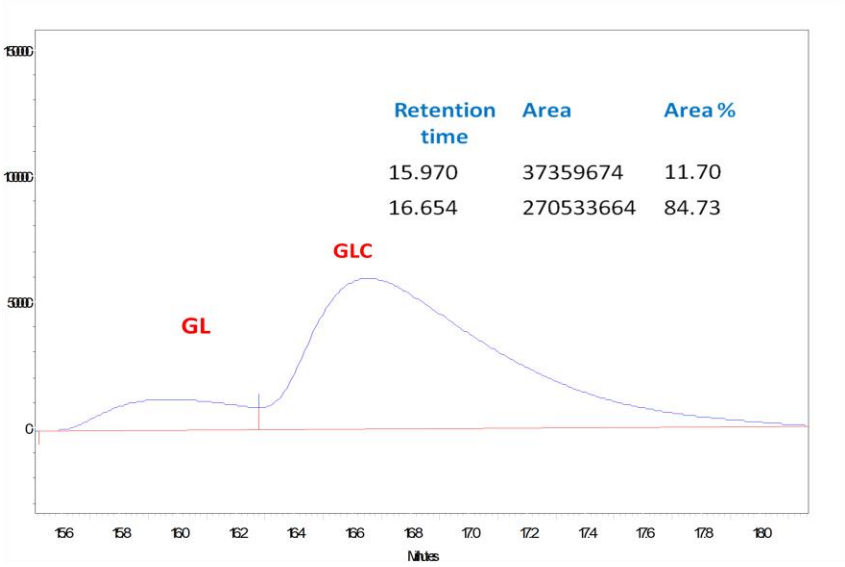

Figure A.19 HPLC chromatogram of the 0.5-Ben/CaO-250 catalyzed transesterification reaction of DMC with GL.

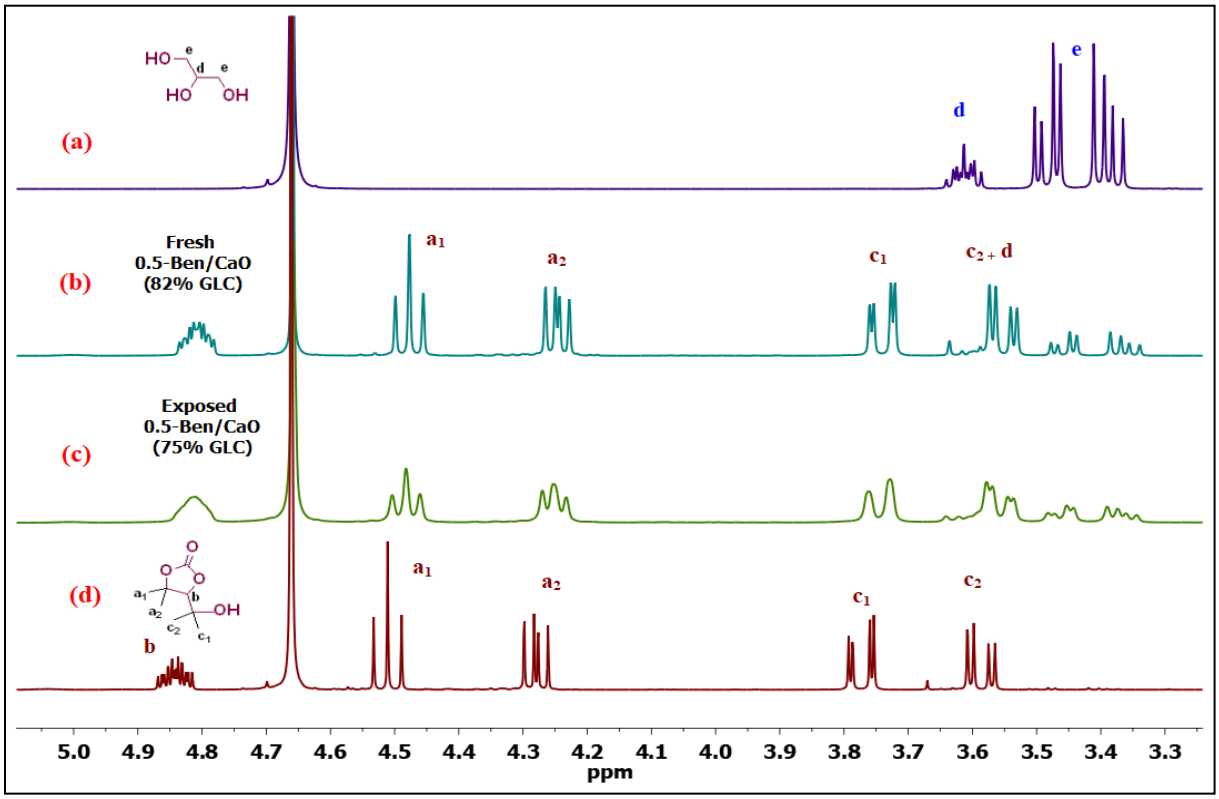

Figure A.20 ^{1}H-NMR spectra of (a) standard GL, (b) fresh, and (c) moisture exposed 0.5-Ben/CaO-250 catalyzed transesterification reaction and (d) standard GLC.

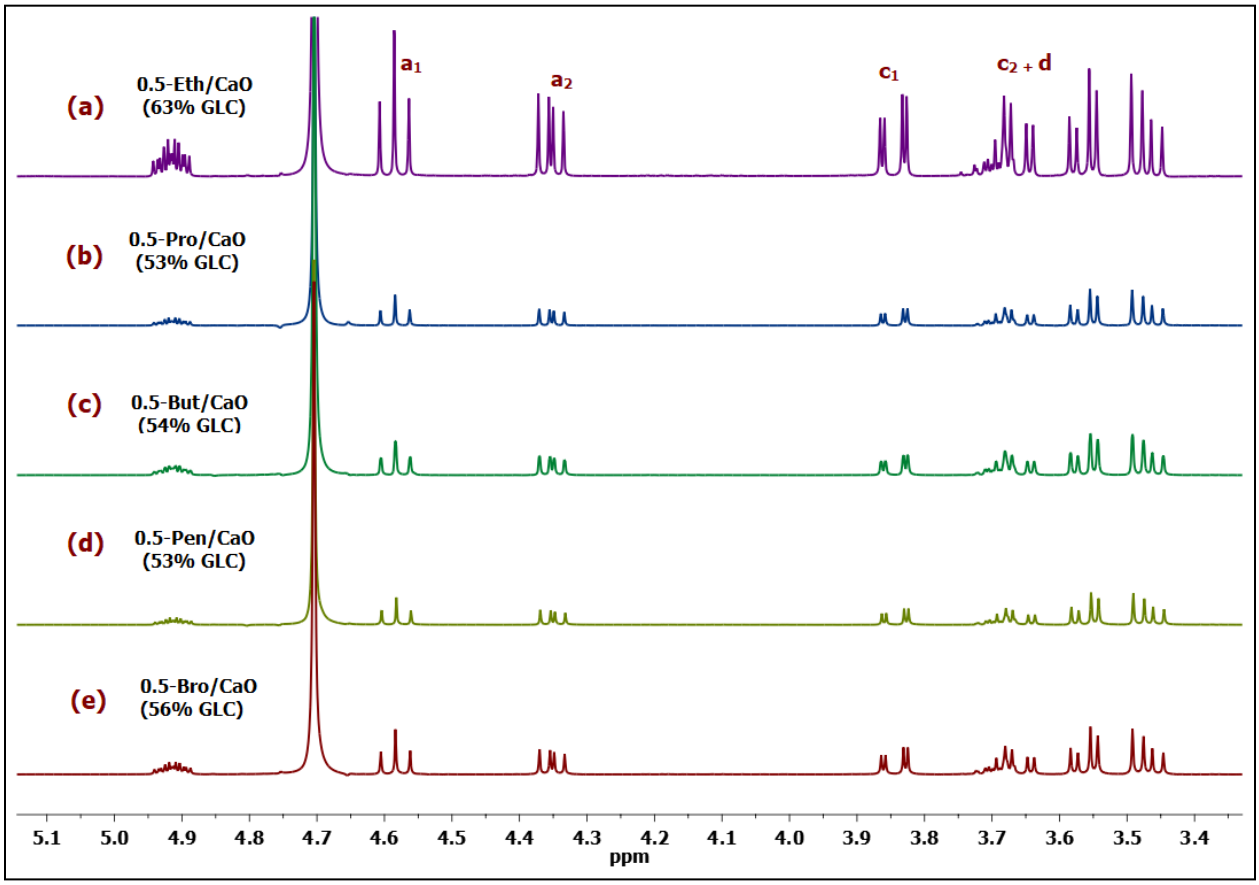

Figure A.21 ^{1}H-NMR spectra of transesterification reactions catalyzed by fresh modified CaO catalyst modified by 0.5 wt% of (a) Ethyl bromide, (b) propyl bromide, (c) butyl bromide, (d) pentyl bromide, and (e) bromobenzene.

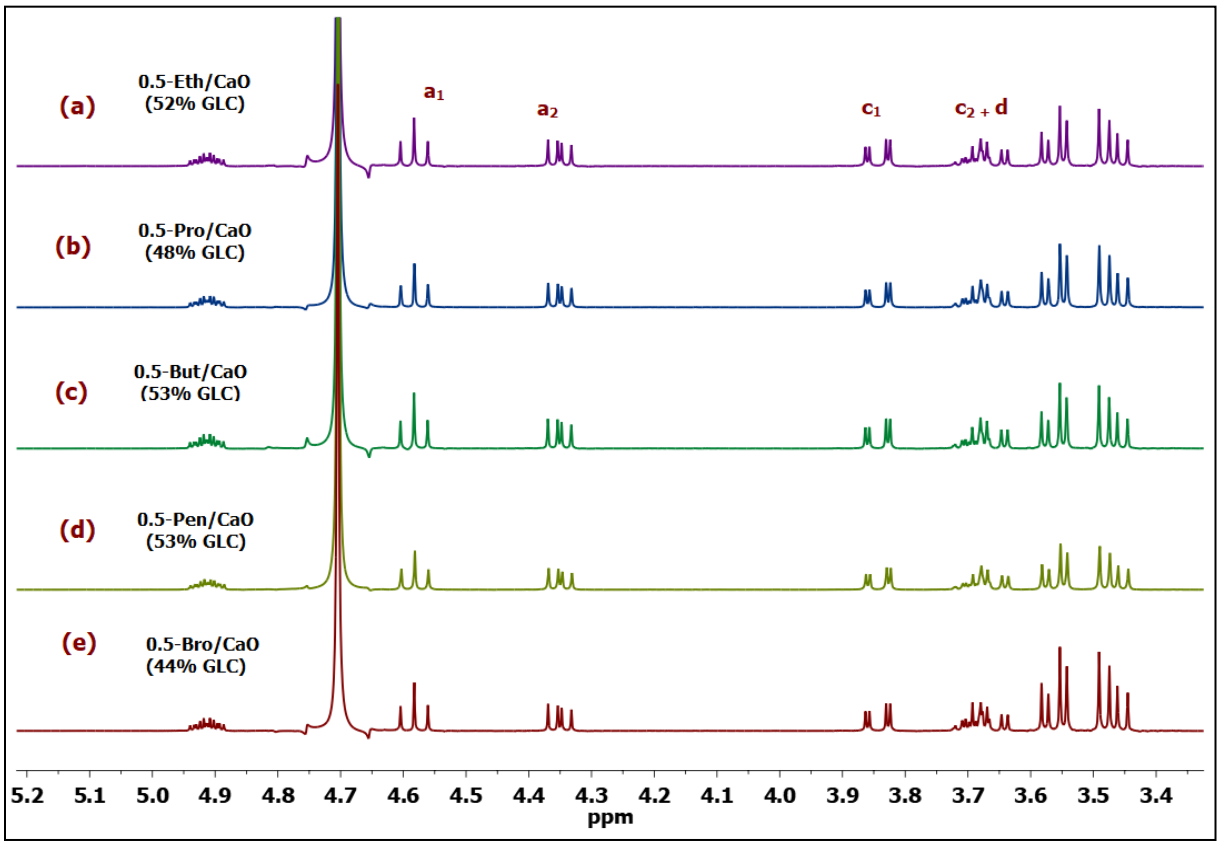

Figure A.22 ^{1}H-NMR spectra of transesterification reactions catalyzed by moisture exposed modified CaO catalyst modified by 0.5 wt% of (a) Ethyl bromide, (b) propyl bromide, (c) butyl bromide, (d) pentyl bromide, and (e) bromobenzene.

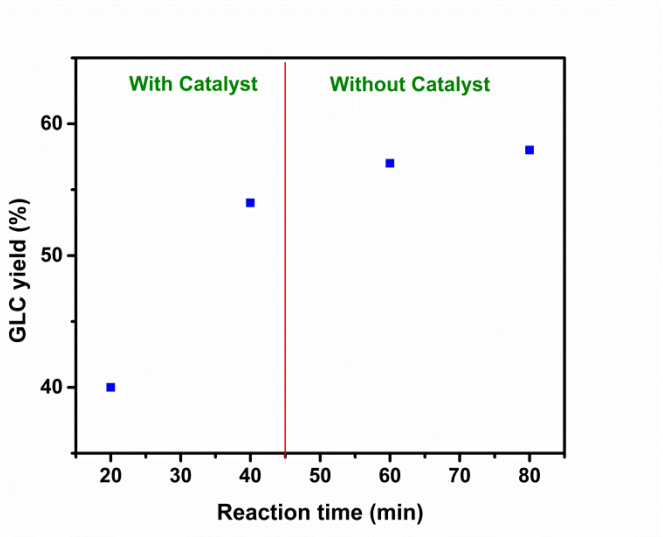

Figure A.23 Hot filtration test for the transesterification of DMC with GL over 0.5-Ben/CaO-250 catalyst.

Table B.1 ^{1}H-NMR chemical shifts of the glycerol carbonate and glycerol in D_2O solvent.

	Glycerol carbonate	**Glycerol**
	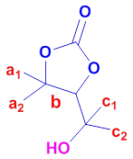	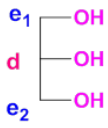

Signal	**δ_H (ppm), J (Hz)**	**Description**
		Glycerol carbonate
b	4.877-4.793 (m)	Methine hydrogen of glycerol carbonate ring
a_1	4.473-4.551 (t)	Ring methyelene proton of glycerol carbonate
	(J_1 4.52 Hz, J_2 4.50 Hz)	
a_2	4.242-4.306 (dd)	Ring methylene proton of glycerol carbonate
	(J_1 4.27 Hz, J_2 4.29 Hz)	
c_1	3.736-3.806 (dd)	One of the outer methylene proton of glycerol carbonate
	(J_1 3.79Hz, J_2 3.76 Hz)	
c_2	*3.549-3.619(dd)*	*One of the outer methylene proton of glycerol carbonate*
	(J_1 3.60Hz, J_2 3.57 Hz)	
		Glycerol
d	*3.577-3.649(m)*	*Methine proton of glycerol*
e_1	3.452-3.511(dd)	Methylene proton of glycerol
e_2	3.355-3.421(dd)	Methylene proton of glycerol

Table B.2 The actual glycerol carbonate concentrations and those predicted by the qHNMR technique.

S. No.	Mole % taken		Predicted mole % of GLC by ^{1}H NMR					
	GLC	GL	Student 1		Student 2		Student 3	
			Eqn. 1	Eqn. 2	Eqn. 1	Eqn. 2	Eqn. 1	Eqn. 2
1	90	10	89.28	90.17	87.71	88.59	89.71	89.08
2	80	20	80.64	79.83	78.7	79.5	79.63	79.03
3	70	30	67.33	66.66	69.44	69.44	70.44	69.21
4	60	40	58.82	58.82	62.10	62.1	60.23	60.23
5	50	50	49.5	49.5	49.26	49.26	49.08	49.08
6	40	60	39.84	39.84	41.49	41.49	39.45	39.04
7	30	70	28.49	28.2	30.21	31.41	29.01	28.34
8	20	80	16.8	16.2	20.07	20.28	19.09	19.09
9	10	90	9.2	8.9	10.01	9.8	9.8	9.8

Table B.3 Estimation of the dissolved metal ion concentration (ppm) in the reaction mixture.

S. No.	Catalyst	Metal	Metal concentration in GLC (ppm)
1	20-Li/ZrO_2-700 (wet impregnation)	Li	1.61
2	20-Li/ZrO_2-700 (co-precipitation)	Li	2.67
3	20-Na/ZrO_2-700	Na	21.8
4	20-K/ZrO_2-700	K	28.3
5	ZrO_2-700	Zr	<0.10

List of Publications

1. A. Kaur, R. Prakash, A. Ali, ^{1}H NMR assisted quantification of glycerol carbonate in the mixture of glycerol and glycerol carbonate, Talanta 178 (2018) 1001–1005.

2. A. Kaur, A. Ali, Lithium zirconate as a selective and cost-effective mixed metal oxide catalyst for glycerol carbonate production, Ind. Eng. Chem. Res. 59 (2020) 2667−2679.

3. A. Kaur, A. Ali, Surface-modified CaO catalyst for the production of glycerol carbonate, ChemistrySelect 6 (2021) 6102– 6114.

4. A. Kaur, N. Bhardwaj, Km Abida, T. P. Nagaraja, A. Ali, R. Prakash, Proton nuclear magnetic resonance-based method for the quantification of epoxidized methyl oleate, J. Am. Oil. Chem. Soc. 98 (2020) 139-147.